Towards improved source apportionment of anthropogenic methane sources

Sabina Assan

université PARIS-SACLAY

NNT : 2017SACLV079

Thèse de doctorat

UNIVERSITÉ DE VERSAILLES ST-QUENTIN-EN-YVELINES

université PARIS-SACLAY

Towards improved source apportionment of anthropogenic methane sources

Thèse de doctorat de l'Université Paris-Saclay
préparée à Université de Versailles – Saint-Quentin-en-Yvelines

École doctorale n°129 Sciences de l'environnement d'Ile-de-France (SEIF)
Spécialité de doctorat: chimie atmosphérique

Soutenance a Gif Sur Yvette, le 18th décembre 2017 .

Sabina Assan

Composition du Jury :

Philippe Bousquet Prof. Des Universites, UVSQ	Président
Martina Schmidt Charge de Recherche, Heidelberg University	Rapporteur
Thomas Roeckmann Professeur, Utrecht University	Rapporteur
Nadine Locoge Professeur, University of Lille Nord	Examinateur
Philippe Ciais Directeur de Recherche, LSCE	Directeur de thèse
Valerie Gros Directeur de Recherche, LSCE	Co-Directeur de thèse
Felix Vogel Charge de Recherche, ECCC	Co-Directeur de thèse

université PARIS-SACLAY | ÉCOLE DOCTORALE Sciences de l'environnement d'île-de-France (SEIF)

Title : Vers une répartition améliorée des sources de méthane anthropique

Keywords : méthane isotopes, COVs, CRDS

Le méthane a la deuxième plus grande contribution à au forçage radiatif global des gaz à effet de serre anthropiques. Après une période de stabilité, son taux de croissance atmosphérique a augmenté rapidement depuis 2007. Les émissions anthropiques de méthane ont un potentiel important d'atténuation ce qui encourage les efforts visant à réduire ses émissions conformément à l'accord de Paris. Toutefois, beaucoup d'incertitudes demeurent concernant la contribution de différentes sources de méthane, les processus et les estimations des émissions, même à une échelle locale ; ce qui entrave la mise en œuvre efficace des stratégies d'atténuation du méthane. Jusqu'à maintenant, de nombreuses études ont été réalisées pour mesurer les flux globaux de méthane, la répartition et la caractérisation des sources de méthane par région mais les processus doivent encore être mieux déterminés.

Cette thèse présente et applique des méthodes pour caractériser les différentes sources de CH_4 présentes dans les mesures de l'air ambiant des sites industriels et développe des outils ciblés pour répondre à cette question. Le premier chapitre traite des améliorations apportées à un instrument CRDS fréquemment déployé pour les mesures de CH_4 et de $\delta^{13}CH_4$. Nous proposons un schéma d'étalonnage pour corriger les interférences C_2H_6 sur $\delta^{13}CH_4$ et permettre des mesures fiables de C_2H_6. Les résultats de ces travaux sont ensuite utilisés pour explorer la valeur ajoutée sur les données de la mise en œuvre de cette méthode sur une station de compresseur de gaz naturel, où une forte corrélation de C_2H_6 et de CH_4 est normalement attendue. Le deuxième chapitre poursuit la caractérisation des sources de CH_4 sur le même site mais porte plus sur l'application et la comparaison des différentes méthodes de répartition des sources. Les contributions des sources de CH_4 et composés organiques volatils (COV) sont explorées selon la méthode de l'analyse isotopique, de l'analyse des séries temporelles multi-espèces à l'aide de modèles source-récepteur (PCA et

PMF), des données météorologiques et des échantillons directs de gaz naturel. Le troisième chapitre présente une utilisation des méthodes de répartition des sources de CH_4 sur les mesures ambiantes des sources de CH_4 biogénique dans la région Ile de France et aide ainsi à compléter l'étude des sources anthropiques de CH_4 les plus pertinentes.

Cette thèse identifie et documente les signatures en $\delta^{13}CH_4$ de différentes sources de CH_4 sur des environnements contrastés à proximité de fermes d'élevage intensif, de stations d'épuration des eaux usées, de décharges d'enfouissement des déchets ou encore de sites de compression du gaz naturel, et étudie leur variabilité spatiale et temporelle pour faciliter la contrainte des émissions. Les résultats obtenus suggèrent que l'identification de différentes sources biogéniques et thermogéniques avec le $\delta^{13}CH_4$ est robuste et adaptable à une grande diversité d'environnements. L'utilisation d'une combinaison d'outils est idéale pour étudier la variabilité à court terme et long terme. Cette thèse présente différentes utilisations de ces nouveaux outils pour diriger les investigations des émissions anthropiques de méthane et sont la base pour de futurs travaux dans ce domaine.

université PARIS-SACLAY | ÉCOLE DOCTORALE Sciences de l'environnement d'île-de-France (SEIF)

Title : Towards improved source apportionment of anthropogenic methane sources

Keywords : Methane isotopes, VOCs, CRDS

Methane has the second largest contribution to the global radiative forcing impact of anthropogenic greenhouse gasses. Since 2007 its atmospheric growth rate, after a period of stability, has again been rising rapidly. Anthropogenic methane emissions hold a large mitigation potential, promoting efforts to curb emissions in accordance with the Paris Agreement. However, the considerable uncertainties regarding methane contributors, drivers and emission estimates even at local scales, hinder the effective implementation of methane mitigation strategies. While many approaches have been established to measure total methane fluxes, the partitioning and characterisation of methane sources by region and processes still need to be better constrained.

This thesis presents practical methods for characterising different CH_4 sources in ambient air measurements at industrial sites, as well as developing more targeted tools. The first chapter focuses on improvements to a CRDS instrument that is commonly deployed for CH_4 and $\delta^{13}CH_4$ field measurements. We propose a calibration scheme to correct for C_2H_6 interference on $\delta^{13}CH_4$, and enable robust C_2H_6 measurements. The results of this work are then used to explore the added value gained when implemented on data from a natural gas compressor station, a site where high correlation of C_2H_6 and CH_4 is expected. The second chapter continues the investigation of CH_4 sources at the same site; with focus shifted towards the application and comparison of different source apportionment methods from time series analysis based on measurements of multiple species, some co-emitted with CH_4. Here the CH_4 and Volatile Organic Compounds (VOC) source contributions are explored through the use of isotopic analysis, receptor model analysis (PCA and PMF), metrological data and direct samples of natural gas. The third chapter applies a selection of the developed CH_4 source apportionment methods to ambient measurements at biogenic CH_4 sites in the Ile de France region and helps complete the survey of the most relevant anthropogenic CH_4 sources.

This thesis identifies and reports local $\delta^{13}CH_4$ source signatures for livestock, wastewater, landfill and natural gas and studies their spatial and temporal variability to aid the constraint of emission inventories. Our findings suggest that source apportionment from $\delta^{13}CH_4$ is robust, and adaptable to the majority of sites. Using a combination of tools is ideal for more specific source determination and for an understanding of long and short term variability. The work presented in this thesis offers example applications of these new tools to directed investigations of anthropogenic methane emissions and lays the foundation for future work in this field.

ACKNOWLEDGMENTS

Firstly, I would like to express my sincere gratitude to Philippe Ciais, Felix Vogel and Valerie Gros for supervising my PhD. Thanks Philippe for your motivation, immense knowledge and constant new ideas of how to take the work forward. Thank you Felix for your continuous support, patience, and all the time you spent explaining, thinking and solving problems with me. Thanks also for all the hard work you put into this PhD, without which it would not be the finished product it is today. I could not have imagined a better advisor and mentor. Thank you Valerie for having followed my PhD, for all your advice, and for always being there when I needed help.

I would like to again thank Nadine Locoge, Thomas Roeckmann, Philippe Bousquet, and Martina Schmidt for accepting to be part of my PhD jury. Thank you also to Rod Robinson, Dave Lowry, and Gabrielle Petron for spending the time to take part in my PhD Committees throughout the years. Your constructive advice helped me to advance the work, and see ideas from a different perspective. Specifically thank you to Rod for your time and advice during field campaigns.

Thank you to Climate-KIC for financing this PhD. A big thank you also to Doug Worthy for welcoming me during my mobility to ECCC, and all the others I met during this exchange.

Thank you equally to Alexia Baudic, Sebastien Ars and Sandy Bsaibes for working with me and helping me throughout the different measurement campaigns. I would also like to say a big thank you to Ali Guemri, Dominique Baisnee and Olivier Laurent for all their technical help and lab measurements throughout the three years. Of course also a big thank you to everyone I met and worked with during my time at LSCE. A particularly massive thank you to Abdel, Xin, Lamia and Jens for all the good times we had, and for keeping me motivated and smiling throughout. It wouldn't have been the same without you.

Finally I thank my friends and coloc-family who always encouraged me and made coming home after work a pleasure every evening.

Contents

Chapter 1 Introduction 12
1.1 The role of Methane in global warming and climate change 12
1.2 The Future of Methane 13
1.3 Uncertainties in Methane emissions estimates 14
1.4 Anthropogenic Methane Source identification 17
1.4.1 Methane Formation 17
1.4.2 VOC Emission Ratios 19
1.4.3 Stable Isotopes of Methane 21
1.5 Thesis 24
1.5.1 Instrumentation 24
1.5.2 Source Apportionment: developments and tests 25
1.5.3 Application to field measurements 26
Chapter 2 Characterisation of interferences to in-situ observations of methane isotopes and C_2H_6 when using a Cavity Ring Down Spectrometer at industrial sites. 27
2.1 Summary of Chapter 2 27
2.2 Introduction 29
2.3 Methods 31
2.3.1 Experimental Setup 31
2.3.2 C_2H_6 calibration setup 35
2.3.3 Determining the correction for isotopes 35
2.3.4 Calibration of isotopes 36
2.4 Results and Discussion 36
2.4.1 Correcting reported C_2H_6 37
2.4.2 C_2H_6 calibration 41
2.4.3 Isotopic correction 42
2.4.4 Isotopic calibration 45
2.4.5 Typical instrumental performance and uncertainties 45
2.4.6 Generalisability of corrections and calibrations 46
2.5 Source Identification at a Natural Gas Compressor Station 48
2.5.1 Description of field campaign 48

2.5.2 Impact of C_2H_6 on isotopic observations at the field site 49
2.5.3 Continuous field measurements of ethane 51
2.5.4 Use of continuous observations of C_2H_6: CH_4 by CRDS 52
2.5.5 Combined method for CH_4 source apportionment 52
2.6 Concluding Remarks 54
Acknowledgements 55
Chapter 3 Can we separate industrial CH_4 emission sources from atmospheric observations? - A test case for carbon isotopes, PMF and enhanced APCA 56
3.1 Introduction 56
3.2 Methods 58
3.2.1 Description of Dataset 58
3.2.2 Methods used for source apportionment 61
3.3 Results & Discussions 66
3.3.1 Observations at the natural gas compressor station 66
3.3.2 Analysing the time-series using isotopic data 69
3.3.3 Analysing the time-series using modified APCA 70
3.3.4 Analysing the time-series using PMF 74
3.4 Conclusions 76
3.5 Supplemental materials: Sensitivity studies 78
S3.1 Creation of pseudo data 78
S3.2 Sensitivity Tests 79
S3.3 Sensitivity Test Results 81
Chapter 4 Fugitive methane source characterisation of biogenic sources in the Ile de France region. 86
4.1 Characterising CH_4 emissions from dairy farming in Ile-de-France 86
4.1.1 Site Description of the Grignon farm 87
4.1.2 Mobile Campaign: 1st May 2017, 9am – Midday 92
4.1.3. Autumn Field Campaign: 19th Oct – 27th Nov 2016 96
4.1.4 Spring Field Campaign: 10th of April until the 1st May 2017 106
4.1.5 Comparison of Autumn & Spring campaigns 114
4.1.6 Grignon farm Conclusion 117
4.2. CH_4 Emissions from the waste management sector 120
4.2.1 Waste Water Treatment Facility: St Thibault-des-Vignes 121

4.2.2 Waste Water Treatment Facility: Cergy Pontoise 126
4.2.3 Landfill: Butte Bellot 132
4.2.4 Waste Management Conclusion 134
4.3 Conclusion 135
Chapter 5 Thesis Conclusions & Outlooks 136
Chapter 6 References 140
Appendix A: Chapter 2 Supplementary Material 151
Appendix B: Chapter 3 Supplementary Material 153
Appendix C: Chapter 4 Supplementary Material 157

Figures

Figure 1.1 AMAP Assessment 2015: Methane as an Artic climate forcer. 14
Figure 1.2 Inventories and emissions factors consistently underestimate actual measured CH_4 emissions across scales. Ratios > 1 indicate measured emissions are larger than expected from EFs or inventories. The main graph compares results to the EF or inventory estimate chosen by each study author. The inset compares results to regionally scaled common denominator, scaled to region of study and the sector under examinations. [Brandt et al., 2014]. 16
Figure 1.3 Methane global emissions from 5 broad categories 19
Figure 1.4 Genetic characterisation of natural gases by compositional and isotopic variations taken from Schoell (1983). 23
Figure 2.1 Flow chart illustrating the steps involved to calibrate C_2H_6, and $\delta^{13}CH_4$. 31
Figure 2.2 Experimental Set-up. The dilution and working gas are connected via two MFCs to two CRDS instruments in parallel. In red is the placement of an optional glass flask used for the C_2H_6 calibration only. The flow is greater than that of the instruments inlets, therefore an open split is included to vent additional gas and retain ambient pressure at the inlets. 32
Figure 2.3 An example of the results from a H_2O interference experiment spanning the range 0-1% H_2O. 38
Figure 2.4 The discontinuity seen for instrument CFIDS 2072 38
Figure 2.5 Relationship between reported C_2H_6 and concentration changes of CO_2 for instrument CFIDS 2072 and 2067 at varying values of H_2O 39
Figure 2.6 Relationship between reported C_2H_6 and concentration changes of CH_4 for both instrument 40
Figure 2.7 (a): Ethane calibration 42
Figure 2.8 During a dilution sequence of ambient gas with C_2H_6, the CH_4 44
Figure 2.9 The effect of C_2H_6 on reported $\delta^{13}CH_4$. 44
Figure 2.10 Ethane and Methane content of two selected peaks. 51
Figure 2.11 Distribution of 16 events according to their C_2H_6: CH_4 ratios and isotopic signature. 53
Figure 2.12 Flow chart illustrating the steps and the corresponding equations to calibrate C_2H_6 and $\delta^{13}CH_4$ as determined from this study. 54
Figure 3.1 Aerial view of the natural gas compressor station and the location of the presumed principle natural gas sources 59
Figure 3.2 Wind data plotted as a windrose for the period of the 25th of June 2014, to 3rd July 2014. 61
Figure 3.3 Monte Carlo simulation of Miller-Tans plots 62
Figure 3.4 Time series of 30min average concentrations of CH_4, $\delta^{13}CH_4$, CO_2, VOCs and wind direction and speed measured at the measurement campaign at the natural gas compressor station 68
Figure 3.5 a) Pollution rose of mean CH_4 concentrations plotted by wind speed and direction bins. 69
Figure 3.6 Temporal results plot. 72
Figure 3.7 Pollution-rose of the reconstructed C_2H_6:CH_4 ratio of PC1 73
Figure 3.8 Modelled factors from the PMF analysis. 75
Figure 4.1 Arial image of Grignon farm and surrounding area. 87
Figure 4-2 (Top) Fluctuation of the expected CH_4 emissions (kg/d) estimated using IPCC Tier 1 method. (Bottom) Weekly measurements of the live weight (metric tonnes) of each ruminant subgroup. 90
Figure 4-3 Wind Rose 91
Figure 4-4 Time series of mobile campaign at Grignon Farm. 93
Figure 4-5 Methane source characterisation plot from mobile campaign at Grignon Farm. 95
Figure 4.7 (left) Methane excess rose at Grignon during the Autumn 2017 campaign. Y-axis signifies the count. (right) Polar plot of mean CH_4 concentration with respect to wind speed and direction. 99

Figure 4.6 Time series data of the variables measured during the Autumn 2017 measurement campaign at Grignon Farm. _____ *100*
Figure 4.8 Isotopic Data from Autumn Campaign at Grignon. _____ *102*
Figure 4.9 Isotopic signatures of CH_4 concentration enhancements _____ *103*
Figure 4.10 10h-mAPCA reconstructed ratios of the Principle Component calculated during the autumn campaign at Grignon Farm. X-axis is the time-series of CH_4. Z-axis is: Top) C_2H_6:CH_4 ratio. Bottom) CH_4: CO_2 ratio. Green dashed line signifies ruminant emissions measured during the mobile field campaign. _____ *104*
Figure 4.11 PMF results for autumn campaign at Grignon: Factor 2 profile [biogenic CH_4 factor. Top) concentration and percentage of species contributing to the factor. Bottom) temporal variation of normalised contributions of factor. _____ *105*
Figure 4.12 (left) Methane pollution rose for spring campaign at Grignon _____ *107*
Figure 4.13 Temporal concentration data of the species measured during the spring measurement campaign __ *108*
Figure 4.14 Isotopic data measured during the spring Grignon field campaign. _____ *109*
Figure 4.15 Variation of $\delta^{13}CH_4$ signatures with respect to wind direction. X-axis represents count number. ____ *110*
Figure 4.16 Temporal variation of (Top) Methane variability (Bottom) Reconstructed components modelled by MC-APCA. _____ *111*
Figure 4.17 10h MC-mAPCA results for the spring campaign. Temporal variation of CH_4 plotted in black on x-axis. _____ *112*
Figure 4.18 Factor 2 profile [CH_4–only factor] _____ *114*
Figure 4.19 Hourly, daily and weekly temporal variation of mean CH_4 concentration for the spring and autumn Grignon campaigns. _____ *115*
Figure 4.20 Methane source characterisation plot. $\delta^{13}CH_4$ signature on the y-axis and CH_4: CO_2 ratios on the x-axis. Methane concentration peaks are plotted in dark and light blue for the spring and autumn campaign respectively. _____ *116*
Figure 4.21 Comparison of $\delta^{13}CH_4$ signatures from ruminants depending on their diet measured in this study and literature _____ *118*
Figure 4.22 St Thibault–des-Vignes WWT site map. Inlet location is marked by a yellow star. _____ *121*
Figure 4.23 Wind rose from wind data at St Thibault WWT _____ *122*
Figure 4.24 Continuous observations of CH_4, CO_2, $\delta^{13}CH_4$ and metrological data at St Thibault WWT plant during the measurement campaign. _____ *124*
Figure 4.26 Methane concentration roses for measurements by NPL at 13 locations surrounding the WWT facility. _____ *125*
Figure 4.25 Methane concentration rose for measurements at inlet. Concentration in ppm. _____ *125*
Figure 4.27 Cergy Pointoise WWT site map _____ *126*
Figure 4.28 Windrose for the duration of the Cergy-Pointoise WWT campaign _____ *127*
Figure 4.29 Continuous observations of CH_4, CO_2, $\delta^{13}CH_4$ and metrological data at Cergy Pointoise WWT during the measurement campaign. Green points are the periods for which isotopic signature was calculated. Blue points are periods for which both the isotopic signature and CH_4:CO_2 ratio was calculated. _____ *128*
Figure 4.30 Mean CH_4 concentrations (ppm) with respect to wind speed and direction. _____ *129*
Figure 4.31 Isotopic signature with respect to wind direction _____ *130*
Figure 4.32 Overview of experimental area of Buttes Bellot mobile measurement campaign. © Google Maps __ *132*
Figure 4.33 Time-series of $\delta^{13}CH_4$ measured downwind of the active landfill (Buttes –Bullot) using mobile measurements. _____ *134*

Tables

Table 1-1 An example of co-emitted VOCs that can be used as tracers to identify specific methane sources. 21
Table 1-2 Anthropogenic Methane sources and their indicative isotopic signatures 24
Table 1-3 Date, location, species measured and instrumentation used for the 6 measurement campaigns undertaken throughout the thesis. 25
Table 2-1 Description of the gas mixtures used to determine the cross sensitives of the interference of CH_4, H_20, CO_2 on C_2H_6 and the interference of C_2H_6 on $\delta^{13}CH_4$. The respective ranges spanned during laboratory test, and the typical range at a natural gas site are noted on the right-hand side. 33
Table 2-2 Summary of C_2H_6 calibration factors calculated for both instruments CFIDS 2072 and 2067. 47
Table 2-3 The various response functions calculated for the $\delta^{13}CH_4$ correction due to C_2H_6. 48
Table 3-1 Summary table specifying the implementation of the 3 identification methods used. 66
Table 3-2 Characteristics of gas taken from the two pipelines at the compressor station, from Assan et al. 2017. ...67
Table 4-1 Results of source signatures from the mobile field campaign at Grignon Farm 95
Table 4-2 Weather conditions on 2.12.2016. 133
Table 5-1 Summary of isotopic source signatures for methane sources in Western Europe, and the values from this thesis. 139

Chapter 1 INTRODUCTION

1.1 THE ROLE OF METHANE IN GLOBAL WARMING AND CLIMATE CHANGE

The Earth's climate system depends on the fine balance between incoming short wave and outgoing longwave solar radiation on the Earth's atmosphere. Approximately half of the solar energy arriving at Earth, roughly 1370Wm^{-2}, is absorbed by its surface, while about 30% is reflected back into space and 20% is absorbed in the atmosphere. The Earth's surface in turn emits energy as longwave (infrared) radiation which is largely absorbed by a number of active gasses (H_2O, CO_2, CH_4, N_2O and other greenhouse gases (GHG)). These re-emit the radiation in all directions; the downward component contributing to the heating of the lower layers of the atmosphere and thus increased global temperatures. As such, greenhouse gasses trap heat in the Earth's atmosphere making them essential for life on earth. Since industrialisation (1750 onwards), global greenhouse gas concentrations within the atmosphere have been strongly increasing due to human activity, and are responsible for an additional radiative forcing of about 2.29Wm-2 [Myhre et al., 2013], thus disrupting the Earth's radiative energy balance. In 1990, IPCC (Intergovernmental Panel on Climate Change) released its first major statement suggesting continued emissions of GHGs would likely result in global temperature and sea level rises. 25 years later, and the IPCC (and many research studies) have concluded that human activities have altered the Earth's mean surface air temperatures over the last 100 years, and that climate change can lead to an increase in the occurrence and strength of extreme weather and climate events.

Being responsible for approximately 20% of all additional radiative forcing produced by GHGs so far, Methane (CH_4) has been identified as one of the most important greenhouse gases. Anthropogenic emissions are those resulting from human activities (IPCC Glossary of Terms) and currently account for 60% of all methane emissions. Predominant sources of anthropogenic emissions include: Agriculture (enteric fermentation and manure being the most important), fossil fuels, and waste decomposition. The impact of greenhouse gases is quantified by their Global Warming Potential (GWP) which is dependent on their radiative forcing and their residence time. Methane has a GWP 28-32 times that of CO_2 on a 100-year time period and even greater on shorter timescales [Etminan, et al., 2016, Allen, 2014]. This is because CH_4 is not only a potent GHG, but also reacts with OH radicals in the atmosphere leading to the production of ozone, stratospheric water vapour and CO_2, all of which continue to drive

global warming. It does, however, have a relatively short lifetime (10 years [Patra et al., 2011]) in comparison to that of CO_2 (50 to 200 years), thus making it an appealing gas to target for efficient, short term climate change mitigation as emission reductions would yield short-term gains in radiative forcing.

1.2 The Future of Methane

Studies show that in recent years, unlike CO_2, CH_4 concentrations have been rising faster than at any time in the past two decades, with a current atmospheric concentration 150% above pre-industrial levels (in 2016, the global annual mean is 1842.72 +/- 0.51 ppb [*Dlugokencky, NOAA/ESRL*]). Since 2007, the atmospheric methane growth has increased substantially (from 0.5 +/-3.1ppb per year for 2000-2006, to 6.9 +/- 2.7 ppb per year for 2007-2015 [Dlugokencky, 2016]), however, the relative methane contributors and drivers remain uncertain. Furthermore, annual anthropogenic CH_4 emissions are predicted to continue rising substantially; between 400 and 500Tg CH_4 in 2030, and between 430 and 680Tg CH_4 in 2050. The upper bar chart in Figure 1.1 shows the regional distribution of estimated annual baseline CH_4 emissions in 2030, by sector and world region in a continue as usual scenario. The projected increase in emissions are greatest for methane from livestock and oil and gas systems as countries with fast growing economies and populations are expected to increase energy and waste consumption [EPA 430-R-12-006, 2012]. For example, China and Latin & Central America are expected to be the dominating emitters due to extensive coal, and cattle & oil industries respectively. These projected trends are in contradiction to the 2016 Paris Agreement wherein 195 countries adopted the action plan to limit the increase of global average temperatures to 1.5degC in order to reduce the risks and impacts of climate change. Given that anthropogenic methane emissions (responsible for over half of global methane emissions) are dominantly industry related suggests a large potential to reduce emissions. Studies suggest that at present, technically feasible mitigation methods hold the potential to prevent a third [USEPA, 2014] or half of future anthropogenic CH_4 emissions by 2030 (reduction potential of about 200 Tg CH_4) [Hoglund-Isaksson, 2012]. Of this mitigation potential, more than 60% can be realised in the fossil fuel industry from reduced venting and leakages. Thus, regions with the largest potential for CH_4 mitigation are those with extensive fossil fuel extraction industries, in particular China, Latin America and Asia (see Figure 1.1). Other large abatement potentials are the separation and treatment of biodegradable waste to replace landfills. As mitigation calculations from these studies are based strictly on technical abatement options, reductions from agricultural sources is limited due to the

requirement of changes in food production and consumption structures which are not deemed feasible on short timescale. To effectively create and implement CH_4 mitigation methods, the sources and sinks must be well characterised and understood. Unfortunately, up until now the sizes of fluxes from individual sources still remain highly uncertain.

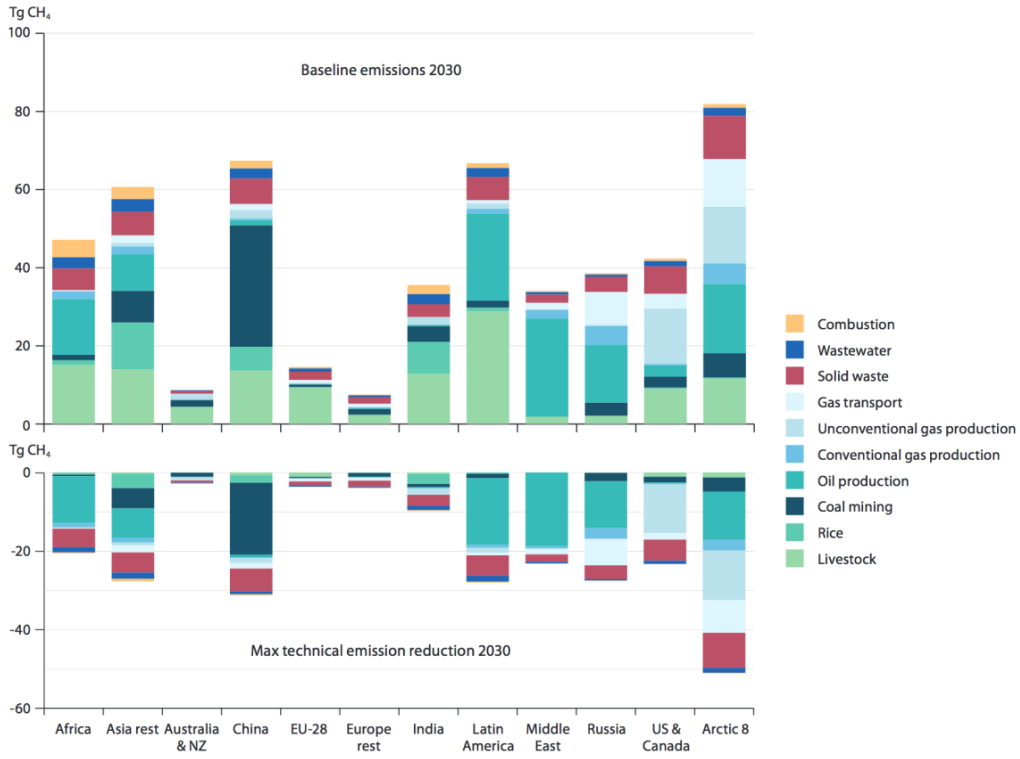

Figure 1.1 AMAP Assessment 2015: Methane as an Artic climate forcer.
Estimates of methane emissions in 2030 by world region from the GAINS model & maximum technically feasible reduction of methane emissions in 2030.

1.3 Uncertainties in Methane emissions estimates

For methane mitigation, it is vital to separate sources to aid planning purposes and green investment. Although methane emissions can now be inferred from inverse modelling as shown by recent studies [Pandey et al., 2016, Alexe et al., 2015, Hein et al., 1997], identifying and attributing contributions from multiple potential sources can be challenging. Hence emission inventories can aid to generate bottom up estimates of sector specific emissions which requires three steps: Identifying the sources of emissions, collecting the activity data and associated emission factors. Currently, existing bottom-up inventories do not well explain top down trends in methane emissions observed in the atmosphere

[Saunois et al., 2016, Hausmann et al, 2016, Kirschke et al. 2013, Nisbet et al 2014.]. Both methods have high uncertainties, as can be seen in the boxplots of Figure 1.3. For bottom-up estimates this may be because although generally sources are very well identified, emissions inventories still have very high uncertainties due to the uncertainties in individual source strength estimates. Brandt et al., (2014) find that inventories and emission factors consistently underestimate actual measured CH_4 emissions in both bottom-up and top-down studies, see Figure 1.2. The study is based on 20 years of literature on natural gas emissions in North America. Top down atmospheric studies (i.e. estimating CH_4 emissions after atmospheric mixing occurs) are plotted with a common baseline in the inset of Figure 1.2 which shows measured CH_4 emissions are systematically higher than predicted by inventories. Results from device and facility scale measurements (generally < 10^9 g CH_4/year) are shown in the main chart of Figure 1.2. While emissions factors were also found to underestimate the bottom up measurements, the results are more scattered than for atmospheric studies. Emission uncertainties are a consequence of the large variations seen in experimental data as emissions from anthropogenic sources can vary across space and time. Often inventories are based on single emissions factors for a given activity and/or from a small number of samples and point sources, e.g. IPCC Tier 1 methods, which do not sufficiently represent the areas and activities which they are applied to. For example, most studies on fugitive methane emissions from oil and gas are based on a limited number of studies specific to certain fields in the USA or Canada, however there are a number of parameters that will be country/site specific or change over time and thus without more systematic measurements their magnitudes will remain largely unknown for most major oil and gas producing countries. It is also possible that substantial sources remain outside of GHG emission inventories, for example abandoned oil & gas wells were found to contribute 5-8% of the estimated annual anthropogenic methane emissions for 2011 in Pennsylvania and are not included in the GHG emission inventory [Kang et al., 2016]. Thus, the requirement to improve current estimates means the partitioning of methane sources by region and processes need to be better constrained. To do this, observations of specific, individual methane sources must be extended.

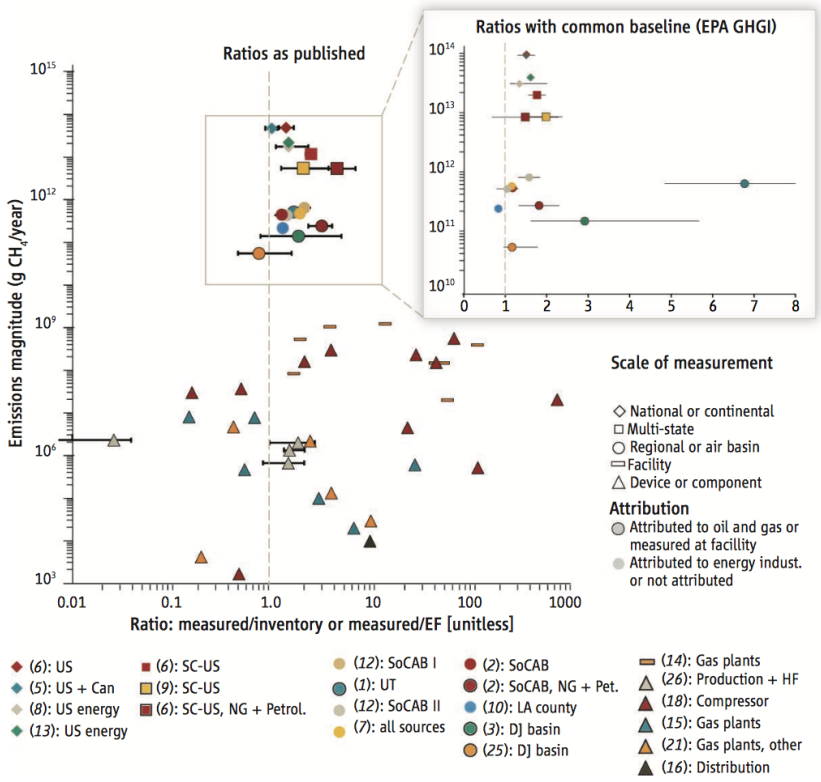

Figure 1.2 Inventories and emissions factors consistently underestimate actual measured CH_4 emissions across scales. Ratios > 1 indicate measured emissions are larger than expected from EFs or inventories. The main graph compares results to the EF or inventory estimate chosen by each study author. The inset compares results to regionally scaled common denominator, scaled to region of study and the sector under examinations. [Brandt et al., 2014].

1.4 ANTHROPOGENIC METHANE SOURCE IDENTIFICATION

Besides dedicated emissions measurements, one important way to reduce uncertainties in methane inventories is by correctly distinguishing between emissions from various methane sources, often occurring in the same region. The formation of methane (either by biogenic, thermogenic or pyrogenic formation) dictates the individual characteristics of each methane source, e.g. their isotopic signature or species co-emitted, and as such an understanding of the processes involved in the creation of methane is particularly important.

1.4.1 METHANE FORMATION

Biologically produced methane arises through the decomposition of organic matter by methanogenic bacteria (archaea) under anaerobic conditions. The major anthropogenic sources arise from agriculture and waste. Agriculture, being the category with the largest contribution to anthropogenic CH_4 releases (approximately 45% [JRC/PBL, 2012]), has two predominant sources; rice paddies and livestock. Rice paddies, the lesser contributor between the two, mainly emit methane during the flooding period when the anaerobic conditions needed for methane production are present. Livestock emissions are estimated as double that of rice emissions globally, and are a result of the microbiological fermentation that breaks down cellulose and other macro molecules in the rumen [Lassey, K. 2006]. The produced CH_4 and CO_2 are released from the rumen mainly through the mouth of multi-stomached ruminants (87% of ruminant emissions) [Saunois et al., 2016], generally cattle but can also be other domestic livestock such as sheep, goats, buffalo and camels. Emissions are strongly influenced by the total weight and diet of the animals. In addition, methane emissions arise when the livestock manure is stored or treated in systems that promote anaerobic conditions. The second biogenic category, waste, accounts for approximately 18% of total anthropogenic emissions [Saunois et al., 2016, Bogner et al. 2008] and includes two sub-sources, namely wastewater and landfill. Wastewater emissions occur when anaerobic conditions exist. This can be deliberately induced (specifically for wastewater with high organic content) or happen by coincidence [Andre et al. 2014]. In landfills, methane is produced as a waste gas due to the decomposition of organic material, and accounts for approximately 5-10% of global anthropogenic methane emissions [Bogner et al. 2008].

Thermogenic methane is typically produced during the decomposition of kerogen at depths below 1000m [Floodgate and Judd, 1991] at high temperature and pressures. In such conditions bacteria

cannot survive and the process takes place without any microbial activity leading to mature gases with higher CH_4 concentrations. Its anthropogenic sources are predominantly fossil fuel methane emissions (hereafter referred to as $ffCH_4$), accounting for approximately 34% of global anthropogenic methane emissions [Saunois et al., 2016]. Fossil fuel CH_4 emissions arise from the production and use of Coal, Oil and in particular, natural gas. Coal-related $FFCH_4$, estimated between 8-12% of anthropogenic methane emissions [Chai et al. 2016] is primarily emitted during the mining process when coal seams are fractured, but emissions can also occur during post mining processing such coal waste piles and abandoned mines [Penman et al., 2000 (IPCC)]. Natural gas is composed of >90% CH_4, thus it is not surprising that its loss to the atmosphere during extraction, processing and transport can represent a significant component of methane emissions. Natural gas is often co-located with petroleum, therefore, although on a lesser scale (in the US oil operations release one quarter as much CH_4 as natural gas systems), trapped methane is also released in large quantities during mining of petroleum (oil itself only contains trace amounts of methane so little is emitted during refinement/transportation [Smith et al., 2010]. It is estimated that emission factors for unconventional gas (gas trapped within shale formations mined via hydraulic fracturing) are larger than conventional oil and gas by 3-17%, due to higher releases in the drilling phase [Caulton, D. et al, 2014, Schneising et al., 2014, Howarth, 2011].

Finally, accounting for approximately 13% of anthropogenic emissions, pyrogenic methane arises from the incomplete combustion of biomass, thus the largest sources can be considered as peat fires, biomass burning and biofuel usage [Saunois et al., 2016]. The fraction of carbon that is released as methane depends on the fuel type and burning conditions, e.g. Burning dry savanna releases relatively small amounts of CH_4 compared with forest fires [Encyclopedia of atmospheric sciences, Volume 3].

Estimates of global and European emissions from 5 broad methane source categories is shown in Figure 1.3, taken from the study Saunois et al. [2016]. Agriculture and waste emissions dominate in Europe.

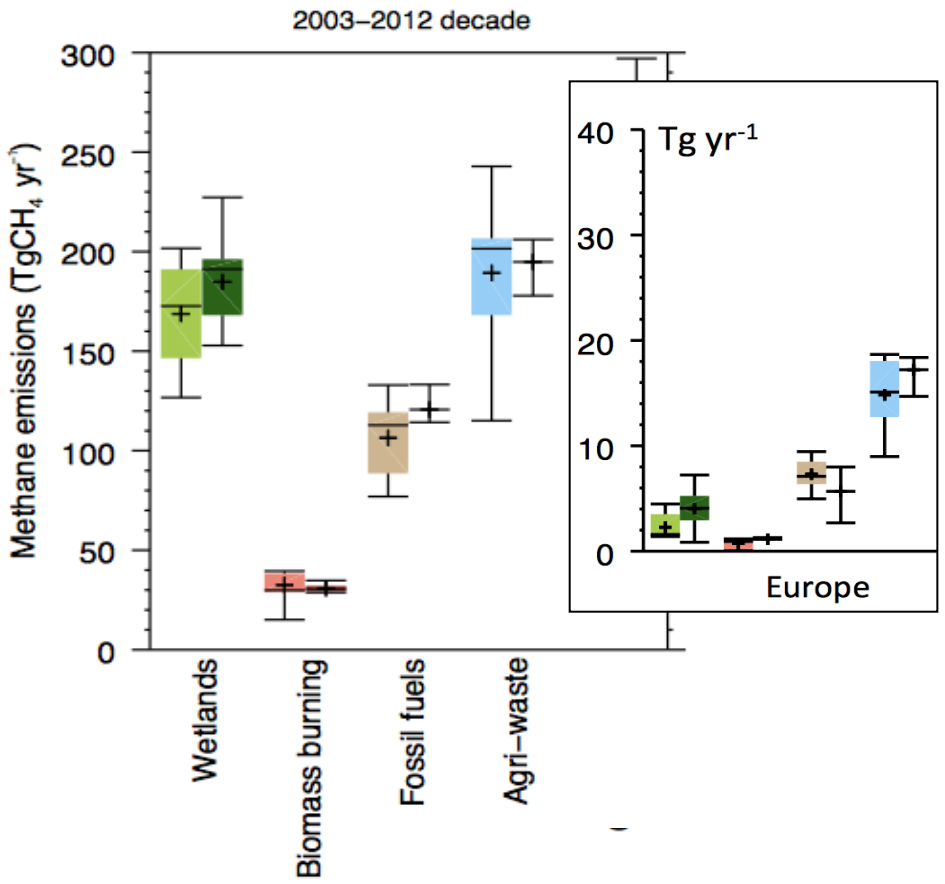

Figure 1.3 Methane global emissions from 5 broad categories (Wetlands, Biomass burning, Fossil fuels, and Agriculture and waste) for the 2003-2012 decade from top down inversion models (left light coloured boxplots) and bottom up models/inventories (right, dark coloured boxplots) in Tg $CH_4 yr^{-1}$ taken from Saunois et al. 2016. The inset plots the regional CH_4 budget for Europe using the same categories. In Europe, anthropogenic methane (in particular Agriculture and Waste) are dominant over natural methane sources.

1.4.2 VOC Emission Ratios

The formation of methane is often accompanied by a number of other compounds, whose abundances depend strongly on the creation conditions. Thus, it is possible to use correlations of co-emitted compounds with methane to distinguish between individual sources.

The term volatile organic compounds (VOCs) is used to denote the entire set of vapour phase atmospheric organics excluding CO and CO_2. Given their short atmospheric lifetimes (fractions of a day to weeks) they have little direct impact on radiative forcing but are central to atmospheric chemistry,

participating in atmospheric photochemical reactions and influencing the air quality and climate through their production of ozone and organic aerosols. Within this thesis, non-methane hydrocarbons (NMHC), which are organic chemical compounds consisting of hydrogen and carbon atoms emitted from both natural and anthropogenic sources are used as complementary tracers for CH_4. Here, the words NMCHs and VOCs are used interchangeably.

The majority of VOC emissions are related to natural sources which originate from nearly exclusively (approximately 90%) vegetation [Guenther et al., 1995]. Nonetheless, global emissions of anthropogenic VOCs is approximately 186 Tg/year [EDGAR 2005], of which a number of sources are shared with methane. The ratio of methane to light VOCs is very high for biologically produced methane because the biochemical mechanism for methanogensis are very specific, whereas in thermogenic reactions substantial amounts of ethane and propane can also be produced. VOCs can be separated into a number of sub-categories which can be used as trace gasses to identify methane sources, namely: alkanes, alkenes, alkynes, aromatics and oxygenated VOCs (OVOCs). The main sources of alkane emissions, such as ethane and propane, are from exploitation and distribution of natural gas, petrochemical industries and biomass burning. Fossil fuels contain only small amounts of alkenes, thus such VOCs (e.g. ethene and propene) are emitted predominantly from vehicle exhaust (due to incomplete combustion), from biofuel combustion and biomass burning. Aromatics, such as benzene, toluene, xylenes (BTEX) are components in fossil fuels, and are predominantly emitted by vehicle exhaust from fuel evaporation and spillage. Distinction between sources can sometimes be difficult as source characteristics vary spatially and temporally. For example, exhaust contribution to VOC levels were found to vary depending on the time of day and day of the week by Rubin et al. [2006]. Furthermore, the composition of the exhaust was found to be dependent on the type of vehicle and fuel used [Verma and des Tombe, 2002, Schuetzle et al., 1994, Zhao et al., 2011].

The use of emissions ratios is a widely-used method for determining source composition and allows for the separation of sources. In literature, this method has been predominantly used to characterise NMHCs [So et al., 2004, Wang et al., 2010]. Nonetheless there has been a recent surge in publications using VOC emissions ratios to identify and distinguish between thermogenic (in particular oil and gas) methane emissions. [Koss et al, 2015, Warneke et al., 2014, Gilman et al, Petron et al., 2014]. Oil and gas sources can be identified using a number of VOC:CH_4 correlations, the predominant being ethane, (C_2H_6) which is the secondary component in natural gas, as well as other light hydrocarbons C1-C5. An example of how the C_2H_6:CH_4 ratio can be used to identify gas of differing origins can be seen in Figure 1.4 from

Schoell [1983]. The plot indicates that thermogenic gasses formed during or directly after the formation of oil (green regions) are much richer in C2+ hydrocarbons than dry gasses formed later (pink regions). Biogenic methane trace gases can be slightly more complex to distinguish; Yuan et al. 2017 found ammonia and ethanol to be good tracers for animal & waste emissions and feed storage & handling emissions respectively. The major co-emitted VOCs for anthropogenic methane sources can be found in *Table 1.1*.

Table 1-1 An example of co-emitted VOCs that can be used as tracers to identify specific methane sources. The VOC:CH_4 ratio can depend on many environmental factors e.g. temperature, location etc., and thus can vary for each individual source and in time.

Anthropogenic Methane Source	Selection of co-emitted VOCs.
Oil and Gas	Light hydrocarbons, in particular Ethane [c]
Animal Operations	Short chained alcohols, e.g. Ethanol, carboxylic acids, ammonia.[a,b] Ethane [c]
Landfill	Dichloroethene, carbon monoxide, hydrogen sulphide, propane, toluene [c]
Biomass Burning	Carbon Monoxide & small oxygenated VOCs[d]

a)Ngwabue Ngwa et al,2007 Volatile organic compound emission and other trace gases from selected animal buildings.

b)Yuan et al., 2017. Emissions of volatile organic compounds from CAFOs

c) David Allen 2016. Atributing atmospheric methane to anthropogenic emissions sources

d)Warneke et al., 2010. VOC identification and inter-comparison from laboratory biomass

1.4.3 Stable Isotopes of Methane

Another consequence of methane formation is that different methane processes result in different isotopic ratios of carbon ($^{13}C/^{12}C$) and hydrogen (D/H). It has been demonstrated that these stable isotope ratios can be used to identify methane sources because the isotopic signatures of different sources and sinks are unique [Schoell, 1983]. Carbon isotopes are the most frequently measured isotope ratios in atmospheric CH_4 and are an integral part of this work, thus in this thesis I will focus on $\delta^{13}C\text{-}CH_4$, which is also commonly abbreviated as $\delta^{13}CH_4$.

Most methane on earth is composed of one atom of ^{12}C and four atoms of ^{1}H, however found in small quantities methane isotopologues containing heaver isotopes of carbon, namely ^{13}C and ^{14}C are also present. The abundance of the heavier isotopologues differs slightly between the land surface and atmosphere due to isotopic fractionation when methane is produced or consumed. Heavier isotopes have lower reaction rates, so emitted methane contains a lower fraction of heavier isotopes than the reaction substrate, while methane sinks lead to enrichment of reservoir CH_4 in atmospheric heavy isotopologues as the reaction consumes preferably $^{12}CH_4$. Thus, the isotopologue abundances of emitted methane depends strongly on the isotopic abundances in the organic matter substrate, which is relatively constant in time. Following this we can use the isotopic ratio to attribute a characteristic isotopic signature to each source process; the isotopic signature is as D and expressed as the relative deviation against the Vienna Peedee belemnite (VPDB) reference material. Because the variations that occur are on the order of one part in a thousand or smaller they are expressed in permil (‰) or parts per thousand:

$$\delta^{13}C\ (‰) = [(^{13}C/^{12}C)_{sample}/(^{13}C/^{12}C)_{standard} - 1] * 1000\ ‰ \qquad \textit{Equation 1.1}$$

The average $\delta^{13}CH_4$ values of the contemporary atmosphere range about -47.5‰ [e.g. Quay et al., 1999] with an annual cycle resulting from the spatio-temporal distribution of sinks and sources and atmospheric transport [Hein et al., 1997, Quay et al., 1999, Stevens & Engelkemeir, 1988].

Using the method described by *Equation 1.1* methane sources can be characterised by source specific isotopic signatures as they reflect different methane production processes. For example, methanogenisis results in emissions that are highly depleted in ^{13}C ($\delta^{13}CH_4$ is in the range of -60‰), whereas methane derived from biomass burning retains the isotopic characteristic of the fuel and is generally highly enriched in ^{13}C compared to background atmospheric methane (ranging from -27‰ to –18‰ depending on C-3 or C-4 plants). The typical ranges of $\delta^{13}C$ of methane sources can be found in *Table 2*. Figure 1.4, taken from Schoell (1983), demonstrates how combining information of the methane isotopic signature and the concentration of hydrocarbons can be used to identify the origins of natural gas and petroleum, thus providing a means to fingerprint such methane sources.

In this way, isotopic measurements can aid in partitioning and identifying sources when measuring site scale emissions thus improving emission inventories, and also provide an additional constraint on the large uncertainties in the present methane budget estimates because the net isotopic composition of methane emissions depends on the balance of these different sources.

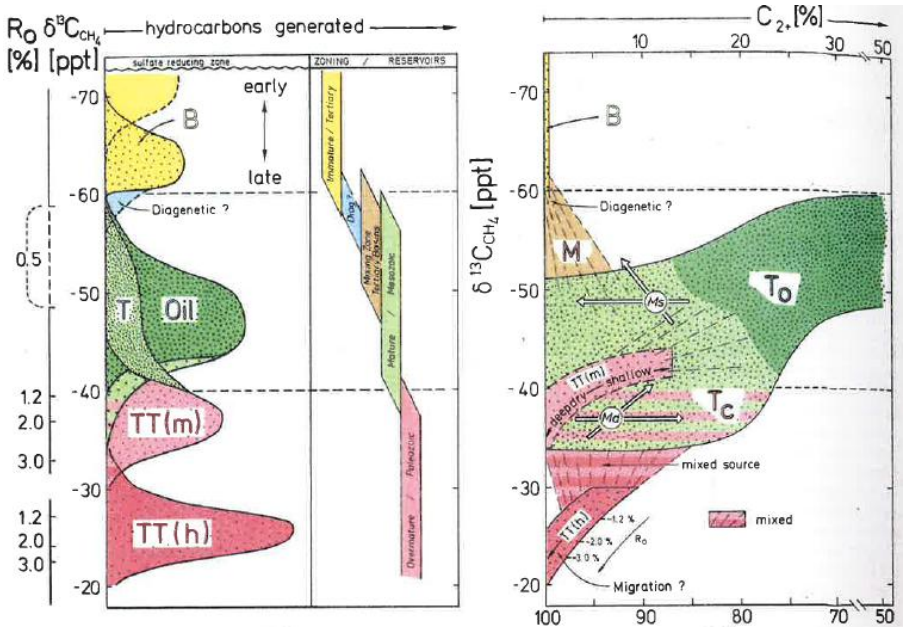

Figure 1.4 Genetic characterisation of natural gases by compositional and isotopic variations taken from Schoell (1983). A) A schematic illustration of the formation of natural gas and petroleum in relation to the maturity of organic matter B) The relative concentration of C2+ hydrocarbons in gases in relation to ^{13}C concentration in methane. Biogenic gas is represented in yellow and by the letter B. There are two stages of thermogenic gas, T in light green which forms during or directly after oil formation, and deep dry gasses TT formed after the principle stages of oil formation (formed by humic, TT(h) and from marine source rocks TT(m) in light and dark pink respectively

Table 1-2 Anthropogenic Methane sources and their indicative isotopic signatures , taken from Denmanm et al., 2007.

Anthropogenic Sources	Indicative $\delta^{13}CH_4$ (‰)
Coal Mining	-37
Gas, oil Industry	-44
Landfills & Waste	-55
Ruminants	-60
Rice Agriculture	-63
Biomass Burning	-25
C3/C4 vegetation	-25/-12

1.5 THESIS

The overall aim of this thesis was to test and further develop the current methods used for anthropogenic methane source identification of site scale measurements. The primary objective was to improve on present source apportionment techniques, whilst the second objective was to apply the developed methods to separate methane sources at industrial sites. Throughout the thesis, a number of measurement field campaigns were undertaken, targeting the major industries contributing to methane emissions, namely: natural gas compressor station, oil extraction, wastewater treatment plants, landfill, and agriculture. The dates, locations and species measured at these sites can be seen in Table 1.3. The aim of such measurement campaigns was to gain an insight into the characteristics of emissions from a variety of industries, and to test different measurement methods to determine the most useful instruments and techniques to measure and separate methane sources for specific sites.

1.5.1 INSTRUMENTATION

Predominantly two instruments were used regularly throughout this thesis; Cavity Ring Down Spectroscopy (CRDS) measuring CH_4, CO_2, H_2O, C_2H_6, $\delta^{13}CH_4$ and $\delta^{13}CO_2$, and Gas Chromatographs (GC) measuring light (C2-C5) VOCs. CRDS uses a single frequency laser diode to measure specific gas-phase

molecules which scatter and absorb light in the near infrared absorption spectrum. By measuring the height of absorption peaks the concentrations of specific species can be determined. The CRDS instrument used throughout this thesis is a G2201-i Picarro. The GCs used in this thesis are based on flame ionisation detectors (FIDs) which measure the concentrations of organic species in a gas stream by detecting the ions formed during the combustion of organic compounds in a hydrogen flame. A manual GC (Chrompack Variean 3400) was used for measurements of flask samples while for continuous, field measurements an automatic GC (Chromatotec) was used. The instruments used and technical developments of CRDS are described in Chapter 2 which is based on the published study Assan et al., (2017).

Table 1-3 Date, location, species measured and instrumentation used for the 6 measurement campaigns undertaken throughout the thesis.

Industry	Dates	Location	Variables Measured	Instruments Used
Natural Gas Compressor Station	25.06.14– 3.07.14	Northern England	CH_4, CO_2, C_2H_6, $\delta^{13}CH_4$, $\delta^{13}CO_2$, C2-C5 VOCs.	CRDS, GC
Wastewater Treatment Plant	24.10.15-7.11.15	Ile de France (Cergy-Pointoise)	CH_4, CO_2, C_2H_6, $\delta^{13}CH_4$, C2-C5 VOCs.	CRDS, GC
Wastewater Treatment Plant	21.07.15-6.08.15	Ile de France (Saint Thibault des Vignes)	CH_4, CO_2, C_2H_6, $\delta^{13}CH_4$	CRDS
Agriculture	19.10.16– 27.11.16 & 10.04.17 – 1.05.17	Ile de France (Grignon)	CH_4, CO_2, C_2H_6, $\delta^{13}CH_4$, C2-C5 VOCs.	CRDS, GC, PTRMS
Landfill	2.12.16	Ile de France	CH_4, CO_2, C_2H_6, $\delta^{13}CH_4$	CRDS

1.5.2 Source Apportionment: developments and tests

The improvement and evaluation of source apportionment techniques specifically for methane source identification is explored in Chapter 3. Three methods are applied to continuous measurements of CH_4 and VOCs taken at a natural gas compressor station campaign, and compared, namely; carbon isotopes in methane, principle component analysis (PCA) and positive matrix factorisation (PMF). PCA and PMF are linear receptor models often used in PM studies to identify contributions of different sources to local concentration enhancements. Source profiles and contributions are calculated on the basis of

correlations within the data, which assumes that highly correlated variables originate from the same source. Chapter 3 describes these models and details developments made to enhance their CH_4 source identification potential. A sensitivity study of PCA and PMF can be found at the end of Chapter 3. All three methods are used to analyse data from a natural gas compressor station, and results compared.

1.5.3 Application to field measurements

In the final Chapter of this thesis, the source apportionment techniques developed are implemented on data taken from 6 measurement campaigns. The sites constitute the major biogenic CH_4 sources in the Ile de France region: livestock, wastewater and landfill. Chapter 4 characterises these sources using isotopic analysis, source ratios of co-emitted species and, receptor models.

Chapter 2 CHARACTERISATION OF INTERFERENCES TO IN-SITU OBSERVATIONS OF METHANE ISOTOPES AND C_2H_6 WHEN USING A CAVITY RING DOWN SPECTROMETER AT INDUSTRIAL SITES.

Sabina Assan[1], Alexia Baudic[1], Ali Guemri[1], Philippe Ciais[1], Valerie Gros[1] and Felix R. Vogel[1]

[1]Laboratoire des Sciences du Climat et de l'Environnement, Chaire BridGES, UMR CNRS-CEA-UVSQ, Gif-sur-Yvette, Ile-de-France, 91191, France

2.1 SUMMARY OF CHAPTER 2

The increase of atmospheric methane (CH_4) is the second largest contributor to the increased radiative forcing since the industrial revolution. Natural gas extraction and distribution is associated with CH_4 leaks of significantly uncertain magnitude that has spurred interest for developing new methods to measure them. Typically, global CH_4 emissions related to the oil and gas industry (up-stream, mid-stream and downstream) are estimated at 69-88TgCH_4 of the total of 340-360Tg CH_4 of anthropogenic CH_4 [Saunois et al. 2017]. This chapter is based on the published study by Assan et al., [2017], [1]which uses a cavity ring-down spectrometer (CRDS), namely a Picarro G2201i, to evaluate its applicability for two methane identification methods commonly used to better constrain emission estimates from natural gas leaks, a) analysis of ^{13}C and ^{12}C ratios, the two most abundant and stable isotopes of carbon, as well, b) the ethane:methane ratio (C_2H_6:CH_4). Initially, the used G2201i instrument is only specified to measure $^{12}CH_4$, $^{13}CH_4$, $^{12}CO_2$, $^{13}CO_2$ and H_2O by the manufacturer. However, during this work it was found that CRDS measurements of $\delta^{13}CH_4$ in the near infrared spectral domain are subject to significant cross sensitivities due to absorption from multiple gases, especially C_2H_6. The study presents extensive laboratory tests to characterize these cross sensitivities and propose corrections for the biases they induce as well as allow to perform calibrated C_2H_6 measurements on all G2201i series instruments. Two G2201i instruments were tested to determine the interference of CO_2, CH_4, and H_2O concentrations on C_2H_6 measurements, and the interference of C_2H_6 on reported $\delta^{13}CH_4$. Methane isotopic measurements

[1] The full article of Assan et al. 2017 was published in the journal of Atmospheric Measurement Techniques, 10, 2077-2091, (Copernicus Publications) on June 7th, 2017, date of submission, August 2nd, 2016. The full text of the peer-reviewed article is included in the appendix of this thesis.

were biased to heavier values due to the interference caused by elevated C_2H_6 concentrations (a secondary component in many natural gas types) by +23.5‰ ppm CH_4 /ppm C_2H_6. The reported C_2H_6 displays a small sensitivity to absorption interferences from CO_2 and CH_4, but the predominant interference results from water vapor (with an average linear sensitivity of 0.9 ppm C_2H_6 per % H_2O in ambient conditions, meaning that the presence of H_2O causes the inference of too high C_2H_6 mixing ratios if no correction is applied). Yet, this sensitivity was found to be discontinuous with a strong hysteresis effect. Throughout the range of C_2H_6 concentrations measured in this study (0-5ppm C_2H_6), which is large enough to reflect concentrations seen at industrial sites, both CRDS instruments consistently measure concentrations double that reported by a calibrated gas chromatograph, thus we have calculated a calibration factor of 0.5. The generalizability of the corrections and calibrations were determined by repeating the experiments in the study multiple times over the course of a year on two instruments. The study found the calibration factors to be stable in time and between instruments if H_2O is kept < 0.16%, to avoid any hysteresis effect. To demonstrate the significance of the corrections, the study tested two source identification methods based on $\delta^{13}CH_4$ and C_2H_6:CH_4 of air measured at a natural gas compressor station. The presence of C_2H_6 in natural gas emissions at an average ambient concentration of 0.3ppm was found to shift the reported isotopic signature by 2.5‰. Furthermore, after correction and calibration the average reported C_2H_6:CH_4 ratio shifts by +0.06. These results indicate that when using such CRDS instruments in conditions of elevated C_2H_6 for CH_4 source determination it is imperative to account for the biases discussed and corrected within this study. Both $\delta^{13}CH_4$ and C_2H_6:CH_4 methods were able to correctly distinguish a biogenic source from the on-site natural gas sources; moreover the study found that combining the two independent methods presented a clearer fingerprint of the sources.

2.2 INTRODUCTION

With increasing efforts to mitigate anthropogenic greenhouse gas emissions, opportunities to reduce leaks from fossil fuel derived methane ($ffCH_4$) is of particular importance as they currently account for approximately 30% of all anthropogenic methane emissions [Kirschke et al., 2013]. At present, technically feasible mitigation methods hold the potential to half future global anthropogenic CH_4 emissions by 2030. Of this mitigation potential more than 60% can be realised in the fossil fuel industry [Hoglund-Isaksson, 2012]. However for effective implementation, sources, locations and magnitudes of emissions must be well known.

The global increase in the production and utilisation of natural gas, of which methane is the primary component, has brought to light questions in regards to its associated fugitive emissions, i.e. leaks. Recent estimates of CH_4 leaks vary widely (1-10% of global production) [Allen et al., 2014] and US inventories of natural gas CH_4 emissions have uncertainties of up to 30% [EPA, 2016]. To address this issue the ability to distinguish between biogenic and different anthropogenic sources is of vital importance. For this reason methane isotopes ($\delta^{13}CH_4$) are commonly used to better understand global and local emissions as demonstrated in a number of studies [Lamb et al., 1995, Lowry et al., 2001, Hiller et al., 2014]. The discrimination of sources with relatively close isotopic composition such as associated-oil gas and natural gas, whose isotopic signatures can be separated by only ~4 ‰ [Stevens et al., 1988], requires precise and reliable $\delta^{13}CH_4$ measurements.

Ethane (C_2H_6) is a secondary component in natural gas and can be used as a marker to distinguish between different CH_4 sources. Use of the C_2H_6:CH_4 ratio provides a robust identifier for the gas of interest. Recent findings in the US found coal bed C_2H_6:CH_4 ratios ranging between 0-0.045, while dry and wet gas sources displayed differing ratios of <0.06 and >0.06 respectively [Yacovitch et al., 2014, Roscioli et al., 2015].

Laser spectrometers, especially based on **C**avity **R**ing **D**own **S**pectroscopy (CRDS) are now a common deployment for site-scale CH_4 measurement campaigns [Yvon-Lewis et al., 2011, Phillips et al., 2013, Subramanian et al., 2015]. However, with the advent of such novel technologies, there lies the risk of unknown interference of laser absorption which can cause biases to measurements. Some examples of which are discussed in Rella et al., (2015) and many others [e.g. K.Malowany et al., 2015, Vogel et al., 2013, Nara et al., 2012]. Using a CRDS instrument we show that the presence of C_2H_6 is causing

significant interference on the measured $^{13}CH_4$ spectral lines thus resulting in shifted reported $\delta^{13}CH_4$ values. We propose a method to correct these interferences, and test it on measurements of natural gas samples performed at an industrial natural gas site.

The CRDS instruments used throughout this study are Picarro G2201-i analysers (Picarro INC, Santa Clara, USA) whose measured gasses include CH_4, CO_2, H_2O, and, although not intended for use by standard users, C_2H_6. This model measures in 3 spectral ranges; lasers measuring spectral lines at roughly 6057cm^{-1}, 6251cm^{-1} and 6029cm^{-1} are used to quantify mole fractions of $^{12}CH_4$, $^{12}CO_2$ and $^{13}CO_2$, and $^{13}CH_4$, H_2O and C_2H_6 respectively. The spectrograms are fit with two non-linear models in order to determine concentrations; the primary fit is performed excluding the model function of C_2H_6 while the second includes this function thus adding the ability to measure C_2H_6 [Rella et al., 2015]. Such a method for measuring C_2H_6 concentrations is crude, thus the uncalibrated C_2H_6 concentration data is stored in private archived files which until now have been used primarily for the detection of sample contamination. The measurements of $\delta^{13}CH_4$ and $\delta^{13}CO_2$ are calculated using the ratios of the concentrations of $^{12}CH_4$, $^{13}CH_4$, $^{12}CO_2$ and $^{13}CO_2$ respectively.

Presented here is an experimental procedure to correct the interference caused by C_2H_6 on the retrieval of $\delta^{13}CH_4$ using such a CRDS instrument for application to in-situ or continuous measurements of $\delta^{13}CH_4$ strongly contaminated by C_2H_6, i.e. in the vicinity of ffCH_4 sources. The step by step procedure of the experimental methods developed to quantify the cross sensitivities and the proposed calibration for $\delta^{13}CH_4$ and C_2H_6 are depicted in Fig. 2.1, and presented in detail in Sect. 2. Section 3 encompasses a discussion of the results, including analysis of the instrumental responses for two spectrometers with an evaluation of the stability and repeatability of the suggested corrections. Finally, field measurements were performed at a natural gas compressor station of which the aim was to identify emissions between two natural gas pipelines. In Sect. 5 the importance of the corrections for field measurements is demonstrated by applying our methods to data retrieved during this period while also revealing the instruments potential to measure C_2H_6.

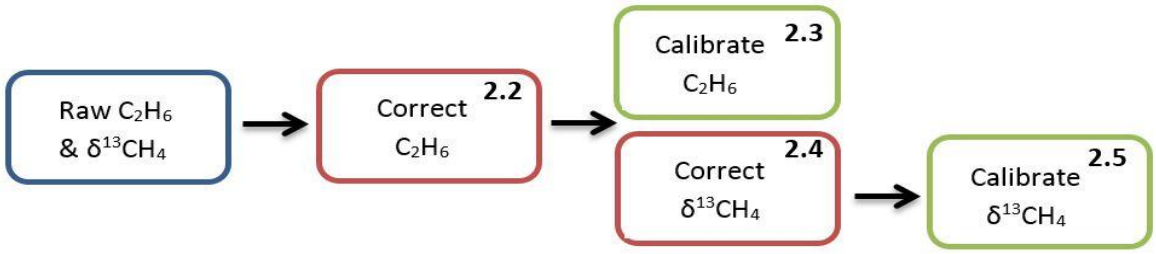

Figure 2.1 Flow chart illustrating the steps involved to calibrate C_2H_6, and $\delta^{13}CH_4$.The number in the top right hand corner corresponds to the subsection in which the methods of each step are explained in detail.

2.3 METHODS

The purpose of laboratory tests was to characterize the instruments response to concentration changes in gasses found at fossil fuel sites (e.g. gas extraction or compressor stations). Specifically, the cross-sensitivities of CO_2, CH_4, and H_2O on C_2H_6 and of C_2H_6 on $\delta^{13}CH_4$. Presumably there are additional gases with the potential for interference; this study focuses on those reported to have a significant effect on C_2H_6 and $\delta^{13}CH_4$ measurements by Rella et al., (2015). We also define and describe a new procedure to calibrate both C_2H_6 and $\delta^{13}CH_4$.

In the following chapter the general setup used for the majority of experiments is described after which we enter a more detailed description of the processes involved in each step individually.

2.3.1 EXPERIMENTAL SETUP

2.3.1.1 Method

Each cross sensitivity is measured by creating a gas dilution series designed to control the concentrations of the gas responsible for the interference in steps while keeping concentrations of the other gas components constant (in particular the component subject to interference). The instrument response was evaluated for a large range of concentrations and different combinations of gas components, an example of such a measurement time series can be seen in Figure S2.1. The experimental set-up used includes two CRDS instruments (Picarro G2201-i) running in parallel in a laboratory at ambient conditions (25°C, 100m above sea level (a.s.l)). The instruments were used in iCO_2-iCH_4 auto switching mode, in which we consider only the 'high precision' mode of $\delta^{13}CH_4$

throughout the study. For the dilution series, a working gas is diluted in steps using a setup of two Mass Flow Controllers (MFC) (El-flow, Bronkhorst, Ruurlu, The Netherlands), as shown in Fig. 2.2. A T-junction splits the gas flow to both instruments; the total flow is greater than the flow drawn into the instruments, hence to maintain an inlet pressure close to ambient, the setup includes an open split to vent additional gas. In order to assess variability and error, each experiment is repeated a minimum of 3 times consecutively. To detect instrumental drift between experiments, a target gas is measured before commencing each dilution sequence. An overview of each cross interference targeted, with information on the gasses used and ranges spanned in laboratory tests can be found in Table 2.1.

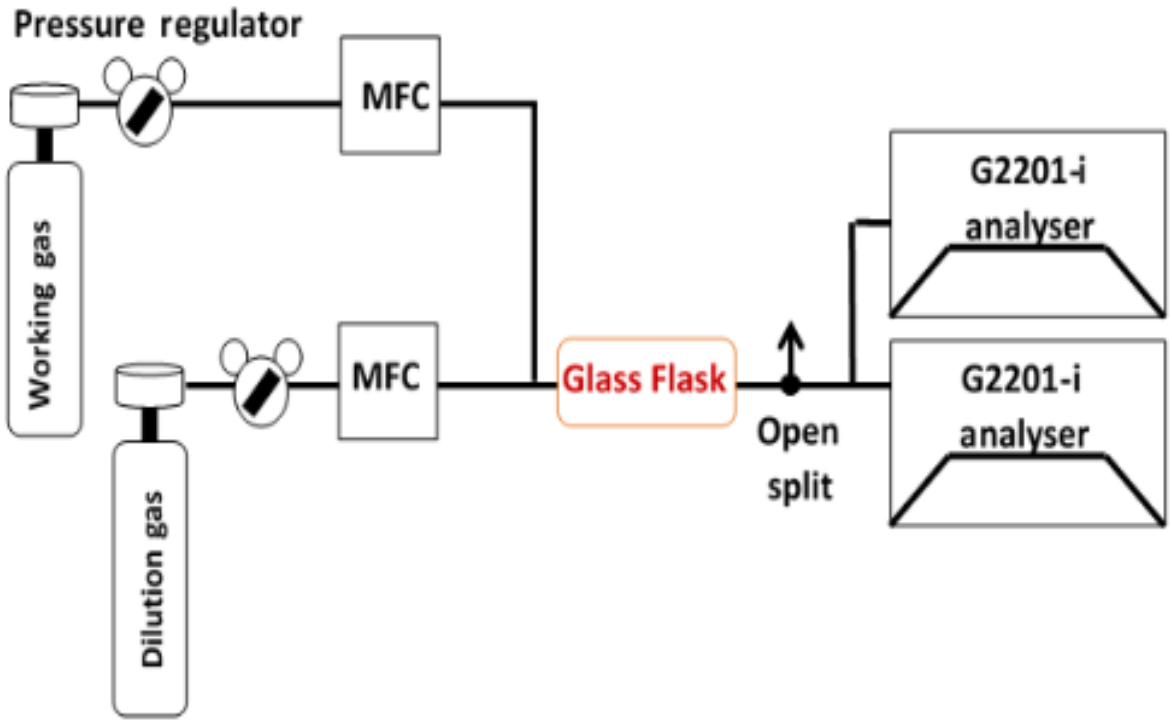

Figure 2.2 Experimental Set-up. The dilution and working gas are connected via two MFCs to two CRDS instruments in parallel. In red is the placement of an optional glass flask used for the C_2H_6 calibration only. The flow is greater than that of the instruments inlets, therefore an open split is included to vent additional gas and retain ambient pressure at the inlets.

Table 2-1 Description of the gas mixtures used to determine the cross sensitives of the interference of CH_4, H_20, CO_2 on C_2H_6 and the interference of C_2H_6 on $\delta^{13}CH_4$. The respective ranges spanned during laboratory test, and the typical range at a natural gas site are noted on the right-hand side.

		Method	Dilution Gas	Working Gas	Lab Concentration Range	Typical Range at NG site
H_2O Interference on C_2H_6	<0.16% (Dry)	Magnesium Perchlorate	N/A	Ambient Air	0-0.5% H_2O	0-2% H_2O
	≥0.16% (Wet)	Dilution Series & Humidifier		Zero Air	0.25-2.5% H_2O	
CO_2 Interference on C_2H_6	<0.16% (Dry)	Dilution Series	Zero Air	2000ppm CO_2, 1.7ppm CH_4, < 1ppb C_2H_6 and 50ppb CO in natural air	0-1500ppm CO_2	400-1000 ppm CO_2
	≥0.16% (Wet)	Dilution Series & Humidifier			0-1500ppm CO_2, 0.5-1.5 % H_2O	
CH_4 Interference on C_2H_6	<0.16% (Dry)	Dilution Series & Ascarite	Zero Air	6ppm CH_4, 360ppm CO_2, 310ppb N_2O, < 1ppb C_2H_6 and 50ppb CO in natural air	0-6ppm CH_4	2-20 ppm CH_4
	≥0.16% (Wet)	Dilution Series, Ascarite & Humidifier			0-6ppm CH4, 1%H_2O	
C_2H_6 Interference on $\delta^{13}CH_4$		Dilution Series (CRDS)	Natural Air Matrix (<1ppb C_2H_6)	C_2H_6 standard of 52ppm in Nitrogen	0-1.5 ppm C_2H_6 /ppm CH_4	0-0.3 ppm C_2H_6/ ppm CH_4
C_2H_6 Calibration		Dilution Series (CRDS & GC)	Natural Air Matrix (<1ppb C_2H_6)	C_2H_6 standard of 52ppm in Nitrogen	0-5ppm C_2H_6	0.3-3 ppm C_2H_6

2.3.1.1 Gases

Throughout the experiments 4 categories of gas were used: a zero air gas with measured residual concentrations of <1ppm CO_2, <30ppb CH_4 , ≈170ppb CO, <1ppb C_2H_6 (Deuste-Steininger,Walldorf, Germany), working gases with variable concentrations of CO_2 and CH_4 in a natural air matrix (Deuste-Steininger,Walldorf, Germany), a C_2H_6 standard of 52 ppm in Nitrogen (National Physics Laboratory (NPL), Teddington, United Kingdom), and dried ambient air in 40L aluminium cylinders filled using an oil-free RIX compressor (RIX industries, Benicia, USA). Details of the gas mixture used in each dilution series depends on the response targeted within the experiment. Information can be found in Table 2.1 and are also discussed in further detail throughout this chapter.

2.3.1.2 Determination of C_2H_6 corrections from H_2O, CH_4 and CO_2 interference

The value of C_2H_6 based on the standard CRDS data processing package (hereafter, the raw value) is biased by cross-sensitivities with H_2O, CO_2 and CH_4. Experiments where conducted at different constant C_2H_6 concentrations so that any shifts in the raw C_2H_6 is due to the cross sensitivity to other components in the measured samples. To alter the water vapour content of a sample, the experimental setup described in Fig. 2.2 was modified by incorporating a humidifier. The humidifier consists of a liquid flow controller (Liqui-flow, Bronkhorst, Ruurlu, The Netherlands) and a mass flow controller (El-flow, Bronkhorst, Ruurlu, The Netherlands) fed into a controlled evaporator mixer (CME) (Bronkhorst, Ruurlu, The Netherlands). The tube departing the CME contains a gas flow of 2L/min and is heated to 40°C to prevent any condensation. A short description and diagram of the humidifying bench can found in Laurent et al., (2015).

The H_2O interference on C_2H_6 was measured by using the humidifier to vary the H_2O content of zero air gas in the range of 0.25%- 2.5% H_2O, representing the range of real world conditions. The humidifier set up cannot reliably reach humidity's below 0.2% H_2O, a range frequently reached when measuring cylinders or dried air. This low range was attained using a H_2O scrubber (Magnesium Perchlorate, Fisher Scientific, Loughborough, UK) connected to the CRDS instrument inlet while measuring ambient air. As the efficiency of the scrubber decreases over time, a slow increase of H_2O spanning low concentrations in the range of 0%-0.5% can be observed.

The CH_4 interference on C_2H_6 was measured by creating a dilution series of variable CH_4 content using zero air and a working gas of 6ppm CH_4, 360ppm CO_2, 310ppb N_2O and 50ppb CO in natural air. Methane concentrations ranged from 0 – 6ppm. To keep other causes of interference at a minimum the gas mixture passed through two scrubbers; the first a CO_2 scrubber (Ascarite(ii), Acros Organics, USA), and

the second a H_2O scrubber (Magnesium Perchlorate, Fisher Scientific, Loughborough, UK). As an independent check on the linearity of the response functions each dilution sequence was repeated at two humidities, (0% H_2O and 1% H_2O), and four C_2H_6 concentrations (between 0-1.5ppm).

The CO_2 interference on C_2H_6 was measured with a dilution series ranging 0-1500ppm CO_2 created by mixing zero air and a working gas of 2000ppm CO_2, 1.7ppm CH_4 and 50ppb CO in natural air. Any interference due to CH_4 was accounted for during data processing. This test was repeated at 4 water vapour levels (0%, 0.5%, 1% and 1.5%), and five C_2H_6 concentrations (between 0-2.5 ppm).

2.3.2 C_2H_6 CALIBRATION SETUP

In order to correctly use the C_2H_6 data from CRDS instruments, the data must be calibrated to an internationally recognised scale. To achieve this, the set up described in Sect. 2.1 was modified to include the filling of removable samples (1L glass flasks) whose concentrations could be independently verified, as shown in Fig. 2.2. A gas mixture using the C_2H_6 standard and an ambient air cylinder was created via two MFCs before passing through the flask on its way to the instruments inlets. Each step in the dilution series requires an individual flask, which was flushed for 20 minutes and then analysed for 10 minutes with an average precision of 0.02ppm C_2H_6 on the CRDS instrument. The flask is subsequently sealed and removed for analysis on a Gas Chromatograph (GC) [Chrompack Varian 3400, Varian Inc, USA] which uses National Physics Laboratory (NPL) standards, and has an uncertainty better than 5%. The system is described in more detail in Bonsang and Kanakidou (2001).

In total 17 flasks were filled with gas mixtures spanning from 0ppm to 5ppm C_2H_6, covering the range expected near a leak of ffCH_4 [Gilman et al., 2013, Jackson et al., 2014]. In order to calibrate the linearity of the response at very high concentrations which may be expected from pure natural gas samples we conducted a measurement at 100% of the C_2H_6 standard (52 ppm ± 1 ppm).

2.3.3 DETERMINING THE CORRECTION FOR ISOTOPES

Measured $\delta^{13}CH_4$ is altered in the presence of C_2H_6. To understand the magnitude of this effect, experiments were conducted using the method described in Sect. 2.1. The dilution series uses the C_2H_6 standard and a cylinder filled with ambient air, i.e. with a negligible C_2H_6 mixing ratio (<1 ppb) to create concentration values spanning from 0-4 ppm C_2H_6. As there is only one source of CH_4 in the experiment,

the addition of C_2H_6 should not affect the value of $\delta^{13}CH_4$, hence any change seen is an apparent shift of $\delta^{13}CH_4$ due to C_2H_6 interference. This concentration range was chosen as it encompasses a C_2H_6:CH_4 ratio of 0 to 1, well within the likely range to be measured from fossil fuel sources [Yacovitch et al., 2014].

2.3.4 Calibration of isotopes

The reported $\delta^{13}CH_4$ was calibrated to Royal Holloway University of London (RHUL) scale using 4 calibration gases spanning -25‰ to -65‰ that were created by different dilutions of pure CH_4 and CO_2 with ambient air of which aliquots were measured multiple times by Isotope Ratio Mass Spectrometry (IRMS) at RHUL. The precision for $\delta^{13}CH_4$ obtainable with this IRMS is reported as 0.05‰, detailed information on the measurement system can be found in Fisher et al. (2006). The calibration factor is determined from a linear regression and calibrations were performed once a day for 3 consecutive days before, and after the laboratory experiments. A target gas was measured regularly to track any drift in $\delta^{13}CH_4$ and as an independent check on the calibration quality.

2.4 Results and Discussion

This study focuses on determining a reliable correction and calibration scheme for a Picarro G2201-i when measuring methane sources with C_2H_6 interference. Findings from the experiments described in Sect. 2 are discussed in detail here.

In order to calibrate $\delta^{13}CH_4$ and C_2H_6 values, there are a series of corrections that must take place beforehand (see Fig. 1.1). The initial correction to be applied is on C_2H_6 due to interference from CH_4, CO_2 and H_2O. Particular emphasis is placed on this correction due to the discovery of significant non-linear behaviour in the presence of H_2O, CH_4 and CO_2 in the sample gas. Once the C_2H_6 has been corrected, the calibration of C_2H_6 using independent GC measurements, the C_2H_6 interference correction on $\delta^{13}CH_4$ and finally the calibration of $\delta^{13}CH_4$ can be effected.

For our results to be applicable to future studies we examine the inter-instrument variability, stability over time, compare our results to current literature and discuss the uncertainties attributed to our results. Throughout this study we refer to raw, uncorrected C_2H_6 and $\delta^{13}CH_4$ concentrations as

"reported" to highlight that they may be influenced by interferences and are uncorrected. Within this section often negative C_2H_6 concentrations are mentioned, we note that this is the "reported" C_2H_6 concentration by the instrument. Unless otherwise stated, the standard deviation reported is calculated from one minute averages and depicted as error bars within figures.

2.4.1 CORRECTING REPORTED C_2H_6

2.4.1.1 H_2O interference on C_2H_6

H_2O content was found to be the dominating source of interference to reported C_2H_6; its presence decreases the reported concentration of C_2H_6 with increasing H_2O concentration. Furthermore, the response function exhibits a hysteresis effect, which, although small, can be considerable when changing from dry to undried air samples (e.g. between dry calibration gas and undried ambient air). There are two distinct instrumental responses, dependant on if measuring dried or undried ambient air during the night preceding the experiment, depicted in Figure 2.3 by light and dark blue markers respectively. When the CRDS instrument measures dry air prior to the experiment, a discontinuity is observed at 0.16% H_2O. Figure 2.4 shows this effect in more detail; prior to 0.16% H_2O the response function exhibits a stable linear response. The correction within this low range was found to be the same for both instruments, 0.44 ± 0.03 ppm C_2H_6/ % H_2O. After passing the 0.16% H_2O threshold the response exhibits a discontinuity whose magnitude and subsequent slope are also dependent on the air moisture beforehand. This is seen in Fig. 2.4 whereby the discontinuity of two repetitions (A and B depicted by dark and light blue markers respectively) differs in magnitude by 0.1ppm reported C_2H_6. The discontinuity occurs when the instrument passes the 0.16% H_2O threshold, both when moving from dry to wet air, or vice versa (see Figure S2.2). If measuring undried air before the experiment, the interference due to H_2O can be described well by a linear response (blue markers in Fig. 2.3), and potentially causes large biases from the true C_2H_6. For example, if measuring at 1% H_2O both instruments display a change in reported C_2H_6 of approximately -0.9ppm. Individually the response function calculated for instruments *CFIDS 2072* and *2067* differed showing -0.72 ± 0.03 ppm C_2H_6/%H_2O and -1.00 ± 0.01 ppm C_2H_6/%H_2O with R^2 values of 0.98 and 0.99 respectively. The hysteresis effect is evident when measuring with undried air; the slope was seen to shift after each repetition, in total by 0.1 ppm C_2H_6/%H_2O.

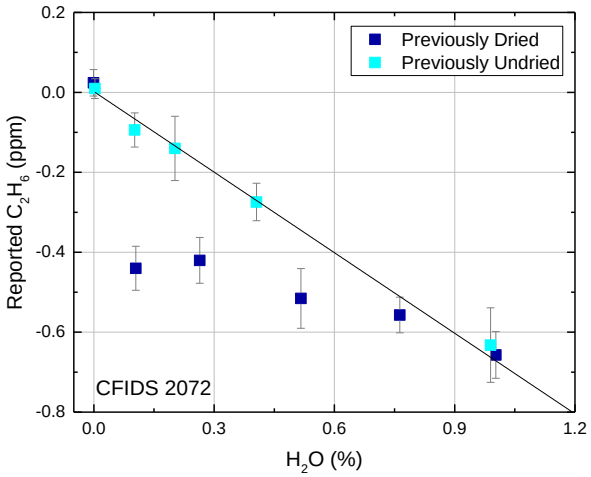

Figure 2.3 An example of the results from a H_2O interference experiment spanning the range 0-1% H_2O. The reported C_2H_6 is altered due to the addition of water vapour when measuring zero air (<1ppb C_2H_6). Dark and light blue markers signify the response when dried and undried ambient air have been measured overnight by the instrument prior to the experiment respectively. Error bars signify the standard deviation of each measurement

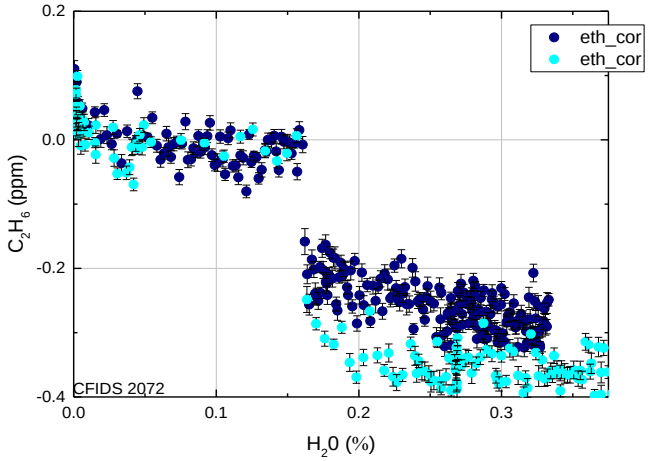

Figure 2.4 The discontinuity seen for instrument CFIDS 2072 for two repetitions denoted by different colours. After the discontinuity at 0.16% the subsequent slope clearly differs between the two repetitions. Both instruments display a discontinuity at 0.16% H_2O. Each point represents a one minute average, the error bars represent the standard deviation of the raw data.

2.4.1.2 CO_2 interference on C_2H_6

For both instruments an increase in the CO_2 concentration results in lower reported values of C_2H_6 and it is furthermore apparent, that the magnitude of this interference is dependent on air humidity. For a dry

sample gas (H_2O <0.16% - demonstrated in the left hand column of Fig. 2.5), the interference for both instruments is found to be highly stable and well characterised by a linear slope of $1x10^{-4} \pm 1x10^{-5}$ $ppmC_2H_6/ppmCO_2$ with a R^2 value of 0.9. There was no measurable difference in slope at any of the C_2H_6 concentrations tested (see Figure S2.3 in Appendix A). In contrast, for water vapour levels ≥ 0.5% H_2O (see right hand column of Fig. 2.5) measurements exhibit a higher scatter between repetitions. This is mainly attributed to a drifting intercept however the experiments also show a smaller R^2 of 0.8. We calculate a characteristic linear slope of $3.8x10^{-4} \pm 1x10^{-5}$ $ppmC_2H_6/ppmCO_2$ and $3.9x10^{-4} \pm 1x10^{-5}$ for ≥0.5% water vapour for instruments *CFIDS 2072* and *2069* respectively. Therefore, when measuring undried ambient air the presence of CO_2 at a level near 400 ppm will induce a shift in the reported C_2H_6 of approximately -0.15 ppm C_2H_6, whereas if the air is dried the reported shift is much smaller, being approximately of -0.04ppm C_2H_6.

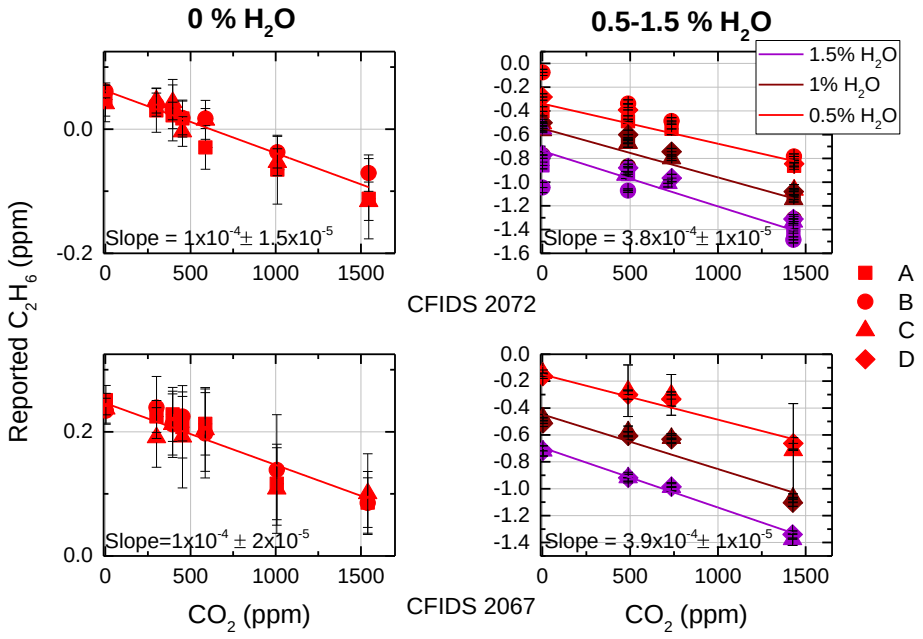

Figure 2.5 Relationship between reported C_2H_6 and concentration changes of CO_2 for instrument CFIDS 2072 and 2067 at varying values of H_2O, at 0ppm C_2H_6 (within our instrumental precision). For each plot the bottom axis indicates the concentration of the targeted gas (CO_2). Plots on the left are at 0% H_2O, on the right are experiments at varying humidities, distinguishable by colour. The legend denotes repetitions of the experiment. The error bars in each plot denote the standard deviation of each measurement. The R^2 value for the experiments at 0% H_2O is 0.9 and 0.8 for all other H_2O experiments for both instruments.

2.4.1.3 CH_4 interference on C_2H_6

The CH_4 effect on C_2H_6, as shown in Fig. 2.6, is less prominent by at least an order of magnitude than both the H_2O and CO_2 interferences. At dried ambient CH_4 concentrations a typical change in reported C_2H_6 of approximately -0.008ppm is observed within both instruments. Dried air experiments show a high scatter of points between repetitions, an R^2 value of 0.4 and 0.6 for instruments *CFIDS 2072* and *2067* respectively is calculated. Despite its large uncertainty the data suggests both instruments display a similar response with a statistically significant slope within the range of C_2H_6 concentrations tested (see Figure S2.3). In light of this we use a weighted mean to calculate a linear response of $9x10^{-3} \pm 2x10^{-3}$ $ppmC_2H_6/ppmCH_4$ for dry air measurements for *CFIDS 2067*, and $7x10^{-3} \pm 5x10^{-3}$ $ppmC_2H_6/ppmCH_4$ for *CFIDS 2072*. The results obtained at 1% H_2O show little correlation (as shown in the right hand column of Fig. 2.6), with both instruments displaying a R^2 value of 0.2. An ANOVA test suggests the slopes are not significantly different from zero, thus we omit a CH_4 correction for this case.

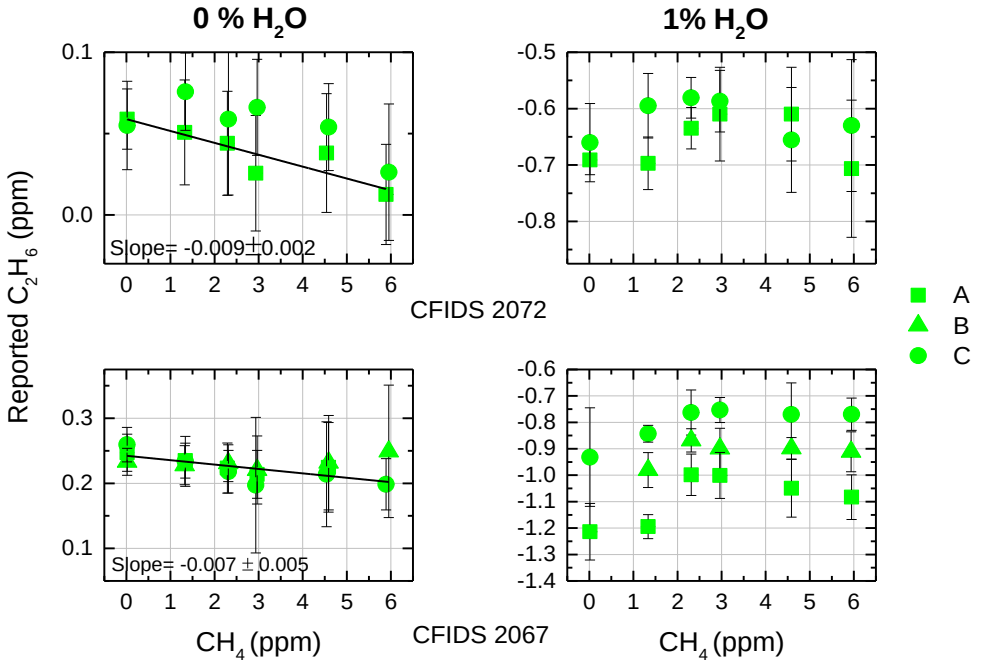

Figure 2.6 Relationship between reported C_2H_6 and concentration changes of CH_4 for both instruments at 0ppm C_2H_6 (within our instrumental precision). For each plot, the bottom axis indicates the increase in concentration of the targeted gas. The vertical bars in each plot denote the standard deviation of each point. The legend denotes repetitions of the experiment. Plots on the left are at 0% H_2O. The R^2 value is 0.4 and 0.6 for instruments CFIDS 2072 and 2067 respectively. Plots on the right show the response at 1% H_2O. These two plots have a R^2 value of 0.2.

2.4.1.4 Combining the CO_2, CH_4 and H_2O correction on C_2H_6

To fully take into account all (known) C_2H_6 cross-sensitivities, the corrections to reported C_2H_6 need to be combined. Due to the non-linearity of the discontinuity in reported C_2H_6 at 0.16% H_2O and its subsequent slope we choose to report correction coefficients for the two found linear regimes, i.e. for continuous measurements with sample humidities below 0.16% and sample humidities above 0.16%. Within each range the proposed correction formula is given as:

$$[C_2H_6]_{CORRECTED} = [C_2H_6]_{RAW} + A^* [H_2O] + B^* [CH_4] + C^* [CO_2] \quad \text{Equation 2-1}$$

If the humidity is limited to **less than** 0.16% before and during measurements, A=0.44 ± 0.03 $ppmC_2H_6/\%H_2O$, B=$8x10^{-3}$ ± $2x10^{-3}$ $ppmC_2H_6/ppmCH_4$, C=$1x10^{-4}$ ± $1x10^{-5}$ $ppmC_2H_6/ppmCO_2$. Both instruments demonstrated good agreement for all the correction factors calculated at <0.16% H_2O.

Corrections for measurements undertaken at concentrations **higher than or equal to** 0.16% H_2O are: A=0.7 ± 0.03 $ppmC_2H_6/\%H_2O$, B=0 $ppmC_2H_6/ppmCH_4$, C=$3.8x10^{-4}$ ± $2x10^{-5}$ $ppmC_2H_6/ppmCO_2$ for *CFIDS 2072* and A=1 ± 0.01 $ppmC_2H_6/\%H_2O$, B=0 $ppmC_2H_6/ppmCH_4$, C=$3.9x10^{-4}$ ± $2x10^{-5}$ $ppmC_2H_6/ppmCO_2$ for *CFIDS 2067*.

2.4.2 C_2H_6 CALIBRATION

To make use of the corrected C_2H_6 it should be calibrated to match an internationally recognised scale. This is achieved by measuring whole-air samples by CRDS and independently on a calibrated Gas Chromatograph, as discussed within Sect. 2. The calibration factor is determined by comparing the corrected C_2H_6 resulting from CRDS and C_2H_6 as confirmed by the GC, plotted in Fig. 2.7a. The relationship was found to be linear throughout the range of 0-5ppm C_2H_6 with a slope of 0.505±0.007 and 0.52 ± 0.01 for instruments *CFIDS 2072* and *2067* respectively. The results are reported in Table 2.2 from which we can see the intercept of the calibration for instrument *CFIDS 2072* shifts between the experiment in February and that in October, while the slope remains constant over long periods of time. The change in the intercept is attributed to a C_2H_6 baseline drift which we have monitored over time using regular target gas measurements, example given in Fig. 2.7b. To account for this drift, and any elevated baselines (such as that of CFIDS 2067 – see Table 2.2) a regular measurement of a working gas is necessary, from which the instrument offset can be calculated. For the full calibration we thus suggest using Eq. (2), where D is the calibration factor (slope) for the instrument, i.e. for *CFIDS 2072* D= 0.505±0.007 and Δ [WGS] the baseline drift determined using the working gas.

$[C_2H_6]_{calibrated}=D*([C_2H_6]_{corrected}-\Delta[WGS])$ Equation 2-2

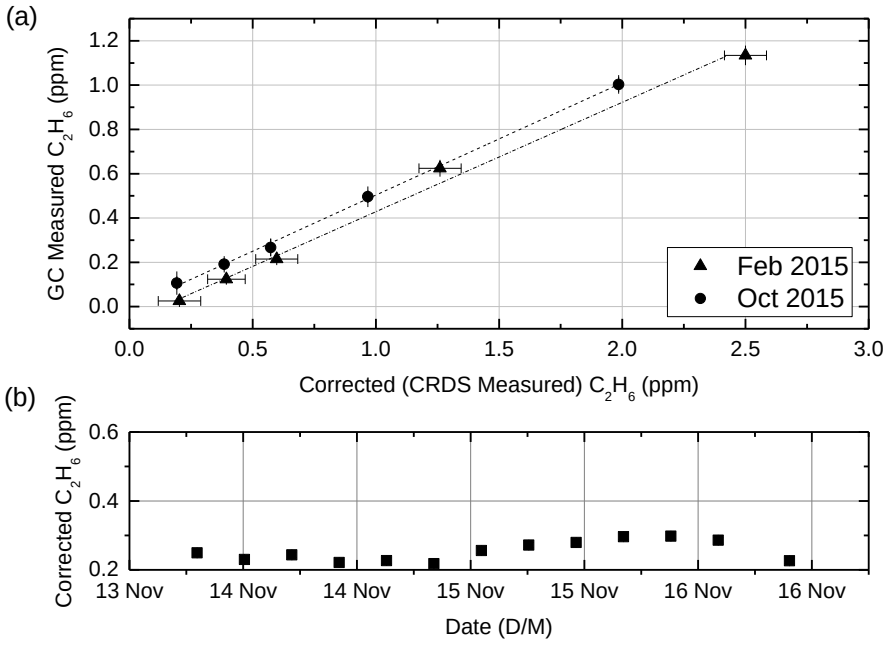

Figure 2.7 (a): Ethane calibration calculated from measurements of flask samples by both the GC and CRDS. The x-axis is the corrected C_2H_6 ($C_2H_{6\ COR}$) using the corrections described previously. The y-axis is the C_2H_6 as measured by a manual GC. The error bars indicate the standard deviation of each flask measurement, for certain flasks error bars are smaller than their respective markers.

(b): 30 minute target measurements over a period of 4 days, from 13th November 2015, to 16th November 2015. The standard error of each target is smaller than the plotted marker. The baseline C_2H_6 is seen to drift with time

2.4.3 ISOTOPIC CORRECTION

By measuring the shift of the reported $\delta^{13}CH_4$ in C_2H_6-contaminated samples, we have observed that the instrument reports heavier values of $\delta^{13}CH_4$ in the presence of C_2H_6. The shift is a result of increased reported $^{13}CH_4$ in samples containing C_2H_6 (see Fig. 2.8). This is most likely caused by the overlapping of spectral lines within the 6029 wavenumber region [Rella et al., 2015]. We calculate the $\delta^{13}CH_4$ correction by taking the slope of $\Delta\delta^{13}CH_4$ (the difference between the reported $\delta^{13}CH_4$ and the initially reported one of the C_2H_6-free gas) and the corrected C_2H_6 to CH_4 ratio. The ratio is used to permit the calculation of the $\delta^{13}CH_4$ response function per ppm CH_4 as the magnitude of interference is dependent on CH_4 concentration [Rella et al., 2015]. The significance of the interference on $\delta^{13}CH_4$ concentrations is

illustrated in Fig. 2.9; as the C_2H_6:CH_4 ratio increases, the change in the reported $\delta^{13}CH_4$ increases linearly. Results obtained from tests carried out throughout the year, for both instruments are noted in Table 2.3, and plotted in Fig. 2.9. The correction equation can be expressed as:

$$[\delta^{13}CH_4]_{CORRECTED} = [\delta^{13}CH_4]_{RAW} - E * C_2H_{6\,CORRECTED} / CH_4 + F \qquad \text{Equation 2-3}$$

where E is the slope of the response function and F is the intercept. E and F are +23.6 ± 0.4 ‰ ppm CH_4 /ppm C_2H_{64} and approximately +0.4±0.2‰ for instrument *CFIDS* 2072 and +23.3 ± 0.7‰ ppm CH_4 /ppm C_2H_6 and approximately -2.4 ±0.4‰ for instrument *CFIDS 2067* respectively. These corrections contain the inherent $\delta^{13}CH_4$ offset of the instrument. When calibrating the $\delta^{13}CH_4$ to a known scale (as described in Sect. 2.5) any instrumental offset will be incorporated within the calibration, therefore the correction equations can be simplified to:

$$[\delta^{13}CH_4]_{CORRECTED} = [\delta^{13}CH_4]_{RAW} - E * C_2H_{6\,CORRECTED} / CH_4. \qquad \text{Equation 2-4}$$

Also highlighted in Fig. 2.9 is the typical measurement range for the majority of ffCH_4 sources related to *dry and wet* natural gas relative to calibrated C_2H_6/CH_4 ratios given on the upper abscissa; whereby *dry* gas refers to natural gas that occurs in the absence of condensate/liquid hydrocarbons (C_2H_6:CH_4 = 1-6%) while *wet* gas typically contains higher concentrations of complex hydrocarbons (C_2H_6:CH_4 >6%) [Yacovitch et al., 2014]. It is clear that within this range the bias on methane isotopic signatures is significant; dry gas will alter the reported $\delta^{13}CH_4$ by 0.8-4‰, while wet gas can cause a shift of up to 13‰ depending on its C_2H_6:CH_4 ratio.

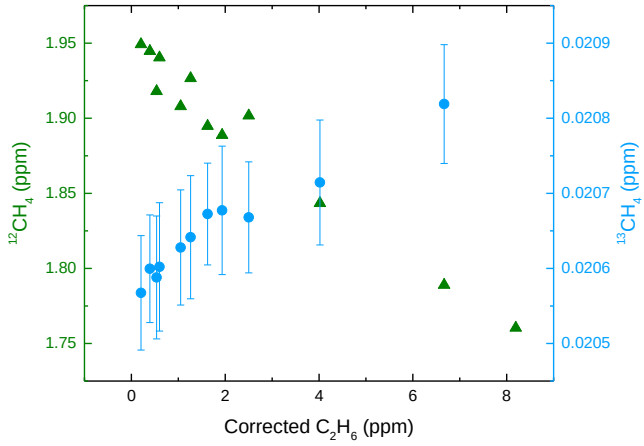

Figure 2.8 During a dilution sequence of ambient gas with C_2H_6, the CH_4 concentration decreases from its nominal concentration 1948.7ppb ± 0.32 ppb as the contribution from C_2H_6 is increased. Thus both $^{12}CH_4$ and $^{13}CH_4$ undergo a similar decrease as the gas is diluted. However what is observed is an increase in the reported value of $^{13}CH_4$, suggesting C_2H_6 interference. The $^{12}CH_4$ axis is plotted to the left in light green, whereas the $^{13}CH_4$ axis is plotted to the right in dark green at a different scale. Error bars represent the standard deviation, the $^{12}CH_4$ markers are larger than their associated error bars.

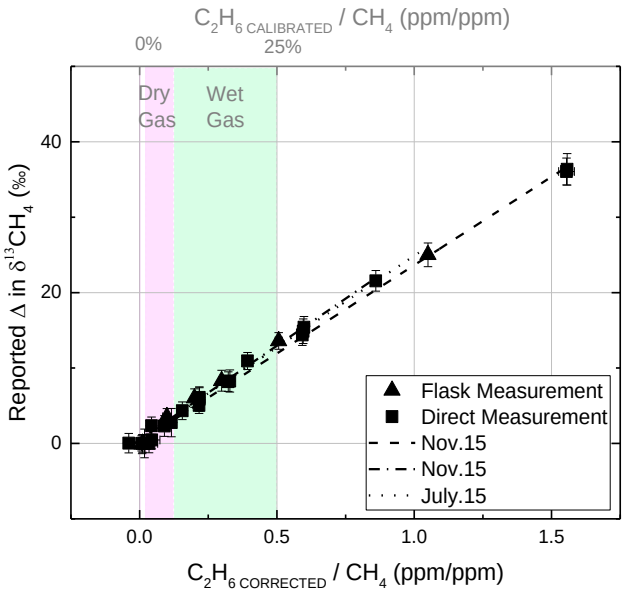

Figure 2.9 The effect of C_2H_6 on reported $\delta^{13}CH_4$. The slopes of reported $\delta^{13}CH_4$ vs the $C_2H_{6\ CORRECTED}$:CH_4 ratio are shown for three tests taken throughout the course of one year. Triangular markers imply whole air sample measurements, while square markers are derived from direct measurements. Error bars indicate the standard deviation. In the presence of C_2H_6 the instrument reports heavier values of $\delta^{13}CH_4$. The typical range of (calibrated) C_2H_6 : CH_4 of dry and wet gas is highlighted in pink and green respectively corresponding to the top axis.

2.4.4 ISOTOPIC CALIBRATION

Full instrument calibrations as described in Sect. 2.4 were performed once in 2014 and 2015. The $\delta^{13}CH_4$ values obtained for the calibration gases by RHUL are measured by IRMS and are therefore not subject to interferences. The calibration gas aliquots were measured with an average standard deviation of 0.03‰. To calibrate $\delta^{13}CH_{4\ CORRECTED}$, the $\delta^{13}CH_{4\ CORRECTED}$ was calculated for each calibration gas and used within the linear regression. The calibrations were linear with R^2>0.99 on both occasions and no change (within our uncertainties) was observed between the two tests. By measuring an ambient air target regularly we later detected a shift in the $\delta^{13}CH_4$ baseline. Two further calibrations were performed in 2016 to assess this incident which confirmed that the offsets of the linear regressions were significantly shifted, while the slopes agreed well with previous calibrations. Therefore to account for a baseline drift it is important to measure a target gas regularly and amend the offset of the calibration equation accordingly.

2.4.5 TYPICAL INSTRUMENTAL PERFORMANCE AND UNCERTAINTIES

In order to characterize the repeatability of the C_2H_6 measured by the CRDS instrument we have measured several targets and monitored the changes of the reported C_2H_6 signal over time. The raw signal is a measurement every 3 seconds, which displays on average a standard deviation of 90 ppb. By aggregating the data to 1 or 30 minute intervals the precision can be improved and a standard deviation of 20 ppb or 8ppb is reached respectively. Furthermore, the 1 minute standard deviation at 52 ppm C_2H_6 is 180 ppb, thus by assuming a linear relationship the typical performance for 1 minute averages is 20 ppb +/- 0.3% of reading.

Of course, there are some substantial uncertainties attributed with the C_2H_6 correction and calibration which need to be accounted for when discussing the uncertainty of the calibrated C_2H_6 concentrations. With regards to the C_2H_6 correction for 1 minute averages, if measuring dried ambient air the propagation of uncertainties are negligible with respect to the raw instrumental precision (20ppb). However, if using 30 minute averages the uncertainty augments from 8ppb to 10ppb. Elevated CH_4, CO_2 and H_2O signals (>5ppm, >1000ppm,> 0.2% respectively) will induce increased C_2H_6 uncertainty regardless of aggregation time. After calibration, the correction factor increases to $2^{1/2}$ times that of the corrected C_2H_6, so at ambient air concentrations calibrated C_2H_6 has an uncertainty of 30ppb.

The repeatability of $\delta^{13}CH_4$ for 1 minute averages on our instrument is a standard deviation of 0.66‰. Again the standard deviation is reduced to 0.29‰ and 0.09‰ by aggregating the raw data for 5 minutes and 30 minutes, respectively. For the correction of $\delta^{13}CH_4$ due to C_2H_6, error propagation of the factors applied in Eq. (4) must be taken into account. Therefore, at ambient concentrations, the uncertainty of a 1min average will increase to 0.9‰.

2.4.6 GENERALISABILITY OF CORRECTIONS AND CALIBRATIONS

The experiments in this study were repeated multiple times and performed on two instruments to better understand how the instrument responses change over time and how they vary between instruments. The C_2H_6 correction and calibration, and $\delta^{13}CH_4$ correction experiments were repeated on *CFIDS 2072* over the course of a year to determine any temporal drifts.

The coefficients of the C_2H_6 correction were examined over a 4 month period. Methane, carbon dioxide and water vapour coefficients for dried gas displayed no noticeable variation over this time frame. Both CH_4 and CO_2 coefficients for undried gas also showed good stability throughout this period, however the undried H_2O coefficient is seen to vary significantly (±0.1 $ppmC_2H_6/\%H_2O$). As discussed previously, the H_2O correction is subject to a hysteresis effect, which makes analysis of its long term variation difficult. As we did not find a clear temporal pattern of the variations we therefore suggest that this coefficient is not likely to be time dependant.

The calibration of C_2H_6 was calculated twice within a 9 month period (see Table 2.2). No variation of the slope of the response function is observed within this time frame. The intercept is prone to drift in time as discussed previously.

The $\delta^{13}CH_4$ correction has been examined three times throughout a 6 month period (see Table 2.3). The variability of the slope observed over 6 months is 1‰ $ppmC_2H_6/ppmCH_4$. Given that the error attribution of each experiment is approximately ± 1‰ $ppmC_2H_6/ ppmCH_4$, this variability is not statistically significant. The intercepts show good agreement with no variation outside the expected uncertainties.

The comparison of both CRDS instruments showed good agreement for all calculated C_2H_6 correction coefficients with the exception of the undried H_2O coefficient at >0.16% H_2O. For this coefficient we calculate a difference of 0.3 $ppmC_2H_6/\%H_2O$ between that of *CFIDS* 2072 and *CFIDS 2067*. The variance may be the consequence of spectrometer differences, a long-term hysteresis effect or due to

differences in their past use up to our tests (mostly dried samples on CFIDS 2072 and mostly undried samples for CFIDS 2067).

The slopes derived for the C_2H_6 calibration of both instruments correspond well, with no significant difference seen between the two. The intercepts differ by approximately 0.6 ppm, thus suggesting distinct difference between intra-instrumental C_2H_6 baselines.

The slopes of the $\delta^{13}CH_4$ correction were found to be in good agreement between the two instruments. Where the instruments differ is with regards to their $\delta^{13}CH_4$ baseline, thus causing the observed disparity in intercept (seen in Table 2.3) of approximately 3‰.

To the best of our knowledge, at this time there is only one published study reporting on a correction due to C_2H_6 interference on an isotopic Picarro analyser. Rella et al., (2015) have studied the interference using a Picarro G2132-i, a high precision CH_4 Isotope-only CRDS analyser which uses similar analysis algorithms and spectral regions as that of the Picarro G2201-i. Rella et al., (2015) obtained C_2H_6 correction parameters of A=0.658 ppm C_2H_6/ ppm H_2O, B=5.5 ± 0.1 x 10^{-3} ppm C_2H_6/ ppm CH_4, C=1.44 ± 0.02 x 10^{-4} ppm C_2H_6/ ppm CO_2 in 2015. Factors B and C for CH_4 and CO_2 respectively agree well with the dried air coefficients attained within this study. The H_2O coefficient, as suggested by Rella et al., (2015) differs to both that of *CFIDS* 2072 and *CFIDS 2067* but confirms the variability of this factor between instruments when measuring undried air samples. Lastly, Rella et al., (2015) report a correction factor for $\delta^{13}CH_4$ of 35‰ ppm CH_4 /ppm C_2H_6 which indicates a different response to C_2H_6 contamination of the different instrument series.

Table 2-2 Summary of C_2H_6 calibration factors calculated for both instruments CFIDS 2072 and 2067.

C_2H_6 Calibration	CFIDS 2072		CFIDS 2067	
	Slope	**Intercept (ppm)**	**Slope**	**Intercept (ppm)**
Feb,15	0.49 ± 0.03	0.00 ± 0.01		
Oct,15	0.51 ± 0.01	-0.06 ± 0.04	0.52 ± 0.01	-0.12 ± 0.01

Table 2-3 The various response functions calculated for the $\delta^{13}CH_4$ correction due to C_2H_6. *Flask measurement.

$\delta^{13}CH_4$ Correction	CFIDS 2072		CFIDS 2067	
	Slope(‰CH_4/C_2H_6)	**Intercept (‰)**	**Slope(‰CH_4/C_2H_6)**	**Intercept (‰)**
July,15	+24 ± 2	0.5 ± 0.6	-	-
Nov,15	+23 ± 1	0.2 ± 0.6	+23 ± 1	-2.3 ± 0.7
Nov,15 *	+24 ± 1	0.6 ± 0.6	+24 ± 2	-2.5 ± 0.8

2.5 Source Identification at a Natural Gas Compressor Station

In order to quantify the effect of C_2H_6 contamination in a real world situation, we have applied the corrections and calibrations discussed in this paper to measurements taken at a natural gas site, with the aim of distinguishing emissions between two natural gas pipelines. In the following section we demonstrate the effect of C_2H_6 interference on $\delta^{13}CH_4$ at a fossil fuel site, as well as discuss the alternative approach of using calibrated C_2H_6:CH_4 ratios to distinguish source signatures, a method which has not been previously tested on a Picarro G2201-i.

2.5.1 Description of field campaign

2.5.1.1 Site description

Located in an industrial park in northern Europe, the campaign took place at a natural gas compressor station in summer 2014. Such stations serve the distribution of natural gas; its key purpose is to keep an ideal pressure throughout the transmission pipelines to allow continuous transport from the production and processing of natural gas to its use. The compressor site visited comprises two major pipelines with their corresponding compressors. The two pipelines carry gas of different origins to the site, where after pressurisation, they are combined for further transmission. The site topography is flat and open with the surrounding area as predominantly farm land and close proximity to a major road. $FFCH_4$ emissions were expected to emanate from various sources on site such as the compressors, methane slip from turbines, and fugitive emissions due to the high pressure of gas [Roscioli et al., 2015]. Other possible

methane sources in the nearby region were identified as traffic and agriculture, including a livestock holding situated less than 500m southwest of the site.

2.5.1.2 Continuous measurements of CH_4, $\delta^{13}CH_4$ & C_2H_6

Two instruments were utilised for continuous measurements throughout the two-week field campaign: a CRDS instrument (*CFIDS 2072*, characterised in detail in previous sections) and an automatic Gas Chromatograph with a Flame Ionization Detector (GC-FID) (Chromatotec, Saint-Antoine, France) measuring VOCs (light fraction C_2-C_6 hydrocarbons), described in detail in Gros et al., (2011). Both were located at a distance of approximately 200m-400m from both the pipelines and compressors.

The air measured by the CRDS instrument was dried consistently to <0.16 % H_2O using a Nafion (Perma Pure LLC, Lakewood, USA). The $\delta^{13}CH_4$ was calibrated using the method described previously in Sect. 2. 20 minute measurements of two calibration gases were made every two days to calibrate the CH_4 and CO_2 data and to track any drift in the isotopes. A C_2H_6 free working gas was measured every 12 hours and used simultaneously as a target gas for the calibration of CH_4 and CO_2, and to track any drift in the C_2H_6 baseline for the calibration of C_2H_6.

The GC-FID was calibrated at the beginning and end of the campaign using a certified standard gas mixture (NPL, National Physics Laboratory, Teddington, UK). The sampling time is a 10-minute average every half an hour; 10 minutes of ambient air is measured after which the following 20 minutes are used to analyse the input.

2.5.1.3 Grab sample measurements of CH_4, $\delta^{13}CH_4$ & C_2H_6 in pure natural gas samples

Grab samples of pure natural gas were taken of both pipelines, with the aim of characterizing the two differing gas supplies. The 0.8L stainless steel flasks were evacuated prior to sampling to a pressure of the order of 10^{-6} mbar, after which they were filled to ambient pressure when sampling. The flasks were measured independently in the laboratory with a manual GC (described in Sect. 2.4) and, after dilution with zero air by the CRDS instrument.

2.5.2 Impact of C_2H_6 on isotopic observations at the field site

To quantify the effect of C_2H_6 interference on $\delta^{13}CH_4$ a total of 16 events were selected from the two-week field campaign, whose criteria was defined as a peak exhibiting both increasing CH_4 concentrations and a change in $\delta^{13}CH_4$ signature for a minimum of 1 hour. Two such events are plotted in Fig. 2.10.

Event 1 represents the majority of events measured during the field campaign, in which CH_4 and C_2H_6 are well correlated. This particular event has a maximum concentration of 11ppm CH_4 and 0.6ppm C_2H_6. On average the selected events have peak concentrations of 5ppm CH_4 and 0.3ppm C_2H_6. The methane isotopic signature was characterized using the Miller-Tans method [Miller & Tans, 2003], in which $\delta^{13}CH_4$* CH_4 values are plotted against CH_4 to calculate the isotopic signature of the methane source in situations where the background is not constant. In order to avoid bias stemming from using Ordinary Least Squared (OLS) regression, the York least squares fitting method was implemented thus taking into account both the X and Y error [York, D. 1968]. All events excluding one were found to have $\delta^{13}CH_4$ signatures characteristic of natural gas, corresponding on average to -40‰. A single event (Event 2 plotted in Fig. 2.10) was detected with a $\delta^{13}CH_4$ signature of -59‰ ± 1.5‰. Such a signature suggests a biogenic source and, due to the south-westerly wind direction throughout the event (where the livestock holding is located), suggests the source is likely to originate from livestock, either as ruminant or manure emissions.

If the data is left uncorrected, sources containing C_2H_6 substantially bias the calculated isotopic signature of CH_4 events. This is demonstrated in Fig. 2.10 where, for Event 1, the slope of points after C_2H_6 correction (in blue) is shifted in comparison to the slope derived from points left uncorrected (in red); signifying a modification of the $\delta^{13}CH_4$ signature. Corrected $\delta^{13}CH_4$ suggests a signature of -40.0‰ ± 0.1‰, while uncorrected values imply -37.8‰ ± 0.08 ‰. When no C_2H_6 is present, i.e. Event 2, there is no disparity between the raw and corrected $\delta^{13}CH_4$ slope, resulting in a $\delta^{13}CH_4$ signature of -59‰ ± 1‰ for both methods. For the 15 natural gas related events, the average shift induced due to uncorrected data is 2‰. Consequently the bias in isotopic signatures due to C_2H_6 means that uncorrected data will always overestimate the source, when a simple two end-member mixing model between is applied.

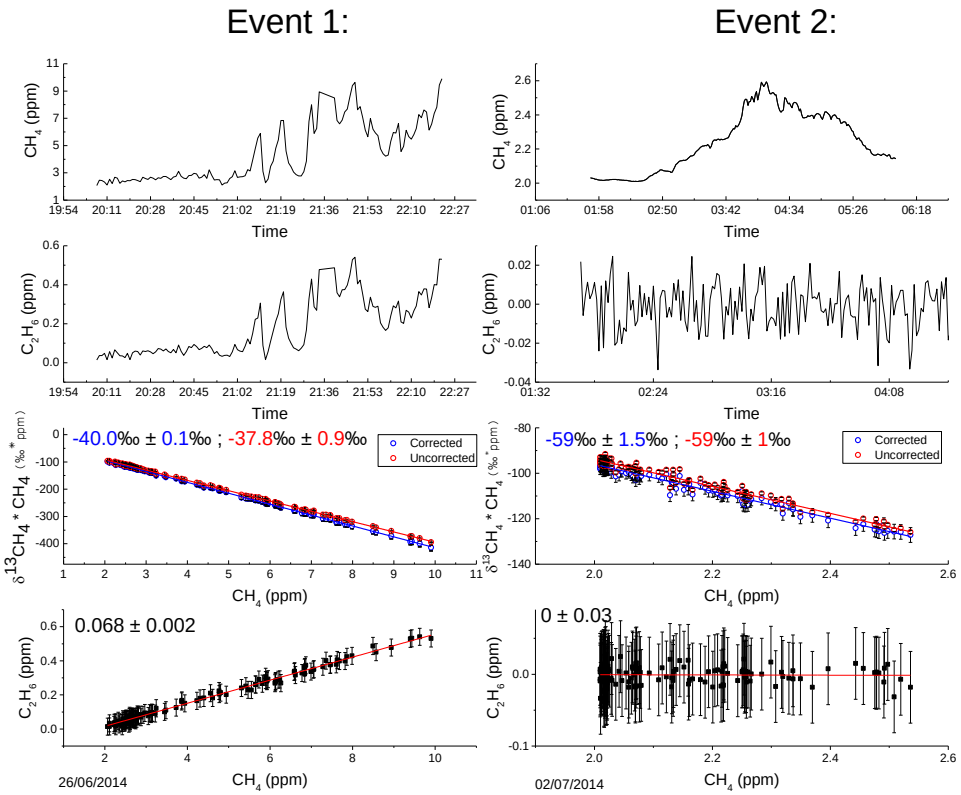

Figure 2.10 Ethane and Methane content of two selected peaks. Methane and Ethane 1 minute averaged time series is shown in the top two panels. Miller-Tans plots of the corresponding peaks are shown in the third panel, blue for the corrected $\delta^{13}CH_4$ due to C_2H_6, and red representing uncorrected $\delta^{13}CH_4$. Event 1 includes elevated C_2H_6 emissions and thus displays a difference between the slope before and after C_2H_6 correction, corresponding to a shift in isotopic signature. Event 2, with no C_2H_6 shows no alteration in slope. The slopes of C_2H_6 vs CH_4 are shown in the bottom panel, signifying the C_2H_6: CH_4 ratio of the emission. Error of both the isotopic and C_2H_6: CH_4 signatures are calculated from the standard error of the slope.

2.5.3 CONTINUOUS FIELD MEASUREMENTS OF ETHANE

As an independent verification of the CRDS performance we compared two time series of C_2H_6 which were measured simultaneously by the CRDS and GC-FID during the natural gas field campaign by using a co-located air inlet. The CRDS data was averaged to identical time stamps as the GC-FID, i.e. a 10-minute average every 30 minutes. From which we calculated a Root Mean Squared Error (RMSE) of 13 ppb. Given the precision of C_2H_6 measured by the CRDS instrument is 10 ppb for 10 minute averages, and the uncertainty on the GC-FID is 15%, we conclude that this is extremely good agreement.

Furthermore, the flask samples, taken on the 4th of July 2014, were measured by the CRDS to have a C_2H_6: CH_4 ratio of 0.074 ± 0.001 ppm C_2H_6/ppm CH_4 and 0.046 ± 0.003 ppm C_2H_6/ppm CH_4 for the gas within Pipeline 1 and Pipeline 2 respectively. That same day gas quality data from the onsite GC recorded a C_2H_6: CH_4 ratio of 0.075 ppm C_2H_6/ppm CH_4 and 0.048 ppm C_2H_6/ppm CH_4 respectively. Although the error associated with the later figures is unknown, the strong agreement between the two verifies our correction and calibration strategy of C_2H_6.

2.5.4 USE OF CONTINUOUS OBSERVATIONS OF C_2H_6: CH_4 BY CRDS

The instruments capability to now measure interference corrected and calibrated C_2H_6 opens the door for using another proxy for source apportionment, namely the C_2H_6:CH_4 ratio [Yacovitch et al., 2014, Roscioli et al., 2015, Smith et al., 2015]. The C_2H_6:CH_4 ratio that characterises each source is determined by the slope of the C_2H_6 to CH_4 relationship. This method was applied to the 16 events identified within the natural gas field campaign, again using the York linear regression method taking into account both X and Y error. Two examples of this method are displayed in the bottom panel of Fig. 2.10. Event 1, representing a natural gas emission has a measured C_2H_6: CH_4 ratio of 0.068 ± 0.002 ppm C_2H_6/ppm CH_4 suggesting a wet gas source. Biogenic events, such as Event 2 are absent of C_2H_6 (within our detection limit) thus resulting in a C_2H_6: CH_4 ratio of 0 ± 0.2 ppm C_2H_6/ppm CH_4. Excluding the biogenic event, on average the 15 natural gas emissions detected have a weighted mean C_2H_6: CH_4 ratio of 0.069 ppm C_2H_6 /ppm CH_4 with an average uncertainty on each event of 0.006 ppm C_2H_6/ppm CH_4. This figure agrees well with the median value for conventional gas ratios measured by Roscioli et al., (2015).

If the C_2H_6 data is left uncorrected and un-calibrated the C_2H_6: CH_4 ratio calculated is significantly shifted by approximately +0.06. The average raw C_2H_6: CH_4 ratio for the 15 natural gas events is 0.132 ± 0.007 ppm C_2H_6/ppm CH_4, while the biogenic events C_2H_6: CH_4 ratio calculated is negative and thus impossible.

2.5.5 COMBINED METHOD FOR CH_4 SOURCE APPORTIONMENT

To distinguish which pipeline the emissions originate from, we compare both the $\delta^{13}CH_4$ signature and the C_2H_6: CH_4 ratio source apportionment methods. The two pipelines were characterised from the whole-air samples taken on July 4th 2014; although the gas within the pipelines is subject to change as incoming gas varies we assume here this did not occur throughout the short duration of the campaign (24th June to the 4th July 2014). The data collected from the aforementioned 16 events is compiled

within Fig. 2.11 which illustrates the distribution of $\delta^{13}CH_4$ signature vs C_2H_6: CH_4 ratios. The results from the flask measurements, i.e. characteristics of Pipeline 1 and 2, are plotted as dashed purple and red lines respectively. Both methods clearly identify the biogenic source, seen as an outlier in the bottom left corner of the plot. Furthermore, both methods are able to distinguish between the two pipelines. The isotopic signatures of the natural gas events (on average 40.2 ‰ ± 0.5‰) are clustered near the isotopic signature of Pipeline 1, which has a $\delta^{13}CH_4$ signature of 40.7 ‰ ± 0.2‰, thus suggesting the majority of the measured methane is an emission from this pipeline. When considering the C_2H_6:CH_4 ratio a similar conclusion may be drawn as the mean C_2H_6:CH_4 ratio is 0.069 ± 0.002 ppm C_2H_6/ppm CH_4, much alike to that of Pipeline 1 at 0.074 ± 0.003. A future study will address the shift in measured events to left of Pipeline 1 in Fig. 2.11 by using additional VOC data from the GC-FID to aid source identification. The *uncorrected* 16 events are also plotted in Fig. 2.11 as circular markers. These are found in the top right hand corner of Fig. 2.11 and do not correspond well with either of the Pipelines, thus re-confirming the importance of the corrections.

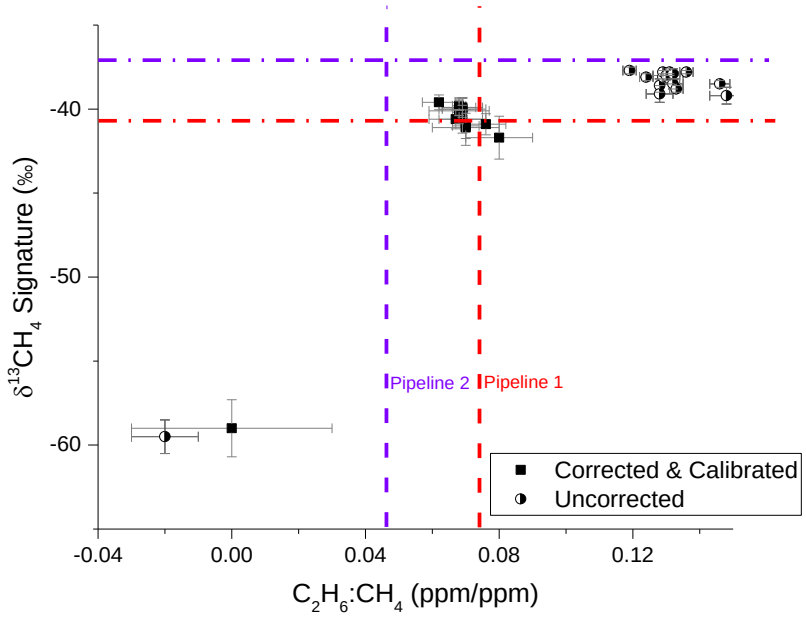

Figure 2.11 Distribution of 16 events according to their C_2H_6: CH_4 ratios and isotopic signature. The red and purple dashed lines signify the characterisation of Pipeline 1 and 2 respectively as measured by the CRDS instrument from flask samples taken on the 4.07.14. For corrected and calibrated data (square markers), both the isotopic signature and C_2H_6: CH_4 ratios identify the biogenic source (bottom-left point) and suggest the natural gas emissions emanate from Pipeline 1. Circular markers represent the uncorrected data which does not agree with the flask sample measurements of Pipelines 1 or 2. The error bars indicate the standard error of the slope calculated from Miller-Tans and C_2H_6 vs CH_4 plots for $\delta^{13}CH_4$ signature and C_2H_6: CH_4 ratio respectively.

2.6 Concluding Remarks

This study focuses on measurements of C_2H_6 contaminated methane sources by a CRDS (Picarro G2201-i), with emphasis on correcting $\delta^{13}CH_4$ and (although not intended for use by standard users) C_2H_6 for cross-interferences before calibration. Our extensive laboratory tests suggest that CRDS instruments of this model are all subject to the similar interferences (as expected as they scan the same spectral lines) and that they can have a significant impact on reported concentrations and isotopic signatures if not accounted for properly, when measuring industrial natural gas sources. For now, we suggest using constant instrument specific correction factors if possible or the ones found in this study (summarised in Fig. 2.12). As our study period only encompasses one year it is clear that the stability of the correction over the full life-time needs to monitored further. To fully exploit the reported C_2H_6 data, we suggest drying gas samples to <0.16% H_2O, calibrating the instrument and frequent measurements of a working gas (or set of working gases) to monitor and correct for the instrumental baseline drift.

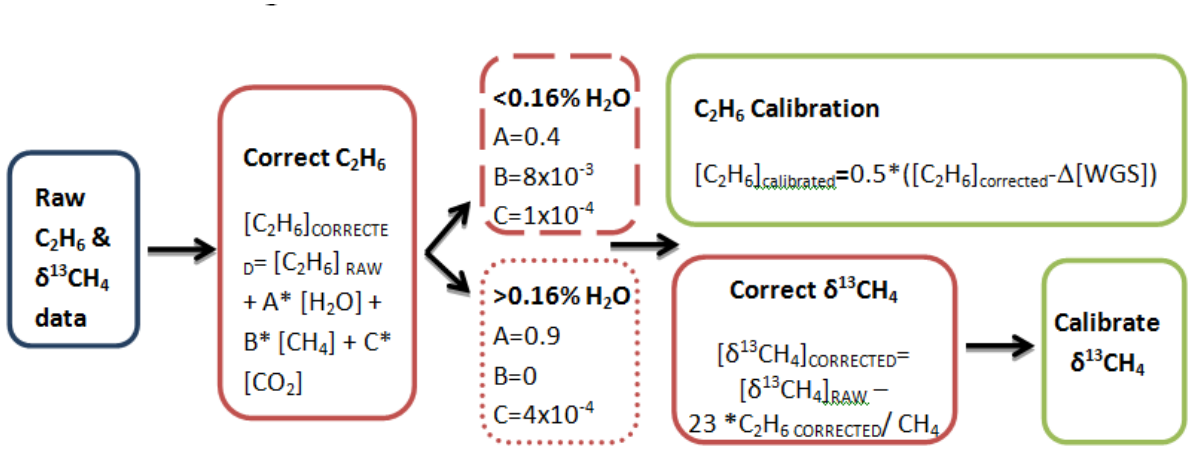

Figure 2.12 Flow chart illustrating the steps and the corresponding equations to calibrate C_2H_6 and $\delta^{13}CH_4$ as determined from this study. The coefficients are the mean of both CRDS instruments tested. We suggest removing H_2O from gas samples prior to analysis.

The results of our field campaign demonstrate the extent of the interferences of C_2H_6 on $\delta^{13}CH_4$ for a real world application and also support the validity or our C_2H_6 correction and calibration through the comparison with an independently calibrated GC-FID. In our case, when measuring wet gas emissions we detected an average shift in isotopic signature of 2.5‰ due to C_2H_6 interference, however the extent of this bias will vary according to the contribution of C_2H_6 therefore affecting each ffCH_4 source to a different degree which can cause problems for source determination. The results reported here are

important for all future work of CRDS in fossil fuel regions (where sources consist of a C_2H_6:CH_4 ratio between 0-1 ppm C_2H_6/ppm CH_4) to be aware of such interferences and correct for them accordingly. Our CRDS instrument is sufficient for measurements of strongly variable C_2H_6 sources, where if using calibrated one minute C_2H_6 data, concentration variations above 150 ppb are required to achieve a signal to noise ratio of 5. Thus for industrial natural gas sites it offers a new opportunity of using continuous C_2H_6:CH_4 observations as a means of source determination independent to $\delta^{13}CH_4$ methods. The recently released G2210-i analyser is dedicated to C_2H_6:CH_4 ratio measurements and as such achieves a higher precision making it suitable for a wider variety of ethane sources.

Finally, we successfully combined both the $\delta^{13}CH_4$ and C_2H_6:CH_4 ratio source apportionment methods. At the natural gas compressor site both methods clearly distinguish biogenic sources from that of natural gas based sources. Combining those two independent methods yields a better finger print of the source and spurious C_2H_6 or $\delta^{13}CH_4$ can be more easily identified. Lastly, by characterising both the $\delta^{13}CH_4$ and C_2H_6:CH_4 ratio of our source, we gain insight into the formation and source region of the gas [Schoell, 1983].

ACKNOWLEDGEMENTS

The authors would like to thank the NPL team for organising the field campaign, in particular the support from Rod Robinson, Fabrizio Innocenti and Andrew Finlayson. We thank our LSCE colleagues: Camille Yver Kwok and Sebastien Ars for assistance during the field campaign, as well as Bernard Bonsang and Dominique Basinee for their technical help and contributions on the GC instruments both in and off the field. We also thank Rebecca Fisher (RHUL) and Dave Lowry for their contributions, especially for measurements of $\delta^{13}CH_4$ for our calibration cylinders under the InGOS' TransNational Access program (TNA-id-666) (http://www.ingos-infrastructure.eu/project-info/workpackages/tna-transnational-access/).. This work was supported by the Climate KIC through the FuME project (http://www.climate-kic.org/projects/fume/) and the funding of the PhD studies of S.A. through education pillar of climate KIC.

Chapter 3 CAN WE SEPARATE INDUSTRIAL CH_4 EMISSION SOURCES FROM ATMOSPHERIC OBSERVATIONS? - A TEST CASE FOR CARBON ISOTOPES, PMF AND ENHANCED APCA.

3.1 INTRODUCTION

Methane is the second most important anthropogenic greenhouse gas, with a global warming potential 28-32 times that of carbon dioxide on a 100-year period, and even greater on shorter timescales [Etminan et al., 2016, Allen 2014]. Anthropogenic methane emissions account for 50-65% of the global CH_4 budget, of which there are a number of contributing sources, the major players being: agriculture (livestock ruminants), oil and gas production and distribution, landfill and wastewater [Saunois et al., 2016]. The EU climate and energy package aims to reduce European greenhouse gas emissions by 20% by 2020 and 80% by 2050, thus bringing anthropogenic methane emissions to the forefront of interests as they offer a large reduction potential without major technological changes [Höglund-Isaksson, 2012]. To effectively implement greenhouse gas reduction strategies, a good understanding of source categories and their contributions is necessary.

Natural gas, of which CH_4 is the principle component, is considered as a transition fuel as countries work towards a cleaner energy future. Nonetheless, potential climate benefits may be offset if there are significant gas leaks in the gas supply chain to the atmosphere. Alvarez et al., [2012] suggest leakage from the natural gas well to delivery system must be < 3.2% for the US to profit from net climate benefits. In 2016, the UK became the largest producer of natural gas in the EU-28 [Eurostat, 2017]. Furthermore, the national atmospheric emissions inventory estimates that over half of the UKs oil and gas related CH_4 emissions are attributed to gas leaks [NAEI inventory available at http://naei.defra.gov.uk/data]. Leaks can occur along the entire distribution network; in the UK, this consists of 23 compressor stations, which pressurise gas through more than 7 600 km of pipelines (National Transmission System, National Grid). However, due to the diffusive nature of gas leakages and few measurements, emissions estimates are highly uncertain.

Often different activities causing anthropogenic CH_4 emissions are co-located within a given region and dedicated techniques are necessary to properly identify contributions of different sources to local concentration enhancements [Roeckmann et al., 2016, Zazzeri et al., 2015, Yacovitch et al., 2014]. Isotopic ratios of carbon ($^{13}C/^{12}C$) and hydrogen (D/H) are commonly used to better understand global and local methane emissions since isotopic signatures vary by source [Lowry et al., 2001, Hiller et al., 2014, Zazzeri et al., 2017]. Isotopic measurements are technically challenging and thus scarcely available, therefore different methods are sometimes required for correct source identification. Another approach is based on analysing multiple co-emitted species. Typically, volatile organic compounds (VOCs) emissions are highly correlated with fossil fuel CH_4 emissions, while also exhibiting source specific emission ratios that allow identifying e.g. oil-associated natural gas, shale gas and coal-bed methane [Helmig et al., 2014, Yacovitch et al., 2014, Roscioli et al., 2015, Assan et al., 2017]. For agriculture and the waste sector, CO_2 is known to be co-produced with CH_4 due to microbial decomposition of organic matter [Madsen et al., 2010, Daelman et al., 2012]. As the source contribution to local CH_4 enhancements can often be quite complex and variable in time, a simple analysis of individual proxy gas to CH_4 ratios might not be sufficient. Studies focussing on pollution from particulate matter (PM), whose sources mix can be equally challenging, often rely on source apportionment models in order to identify and characterise sources. Principle component analysis (PCA) and Positive Matrix Factorisation (PMF) are two of the most commonly used methods for deconvolution of emission sources as they are widely available and require limited knowledge about the number and nature of pollution sources [Viana et al., 2008, Belis et al., 2013], but have not been widely applied to investigate CH_4 sources, yet.

The principles of PCA and PMF receptor models are similar. Source profiles and contributions are calculated on the basis of the analysis of correlations found in the dataset, assuming highly correlated species originate from the same source. Studies comparing the results of different receptor models have found that the number and contributions of sources identified can vary depending on the model used and the characteristics of the data set (number of species measured and observations) [Cesari et al., 2016, Contini et al., 2012, Zhang et al., 2009, Viana et al., 2008, Shrivastava et al., 2007, Hopke et al., 2006]. Publications using simulated data, such as in Chen et al., [2010], Brinkman et al., [2006], Hambre et al., [2011], suggest that, although factor solutions always exist, they are not necessarily unique or correctly representative to the actual sources.

The purpose of this study is understanding the CH_4 and VOC source contributions and its temporal changes at an industrial park by applying and comparing three different source apportionment methods for CH_4 source identification: the commonly used empirical isotopic analysis and the expansion of PCA and PMF models. The aim is also to evaluate strengths and limitations of said techniques for improved CH_4 source apportionment at industrial sites in general. Although the receptor models are commonly used in air pollution studies, they have rarely been implemented for CH_4 sources, thus by systematically optimising the modelling parameters, we include modifications to the standard PCA which improve source separations to better fulfil the goal of CH_4 source identification. The methods are applied to CH_4 and VOC time series data measured at a natural gas transmission (compressor) station. Combining the analysis of in-situ observations with meteorological data and direct samples of pipeline gas to characterize its VOC and isotopic composition we can interpret and understand the estimated profiles of the CH_4 sources throughout the measurement campaign.

3.2 METHODS

3.2.1 DESCRIPTION OF DATASET

3.2.1.1 Natural Gas Compressor station site description

Located in an industrial park in northern Europe, the campaign took place at a natural gas compressor station for two weeks, from the 25th of June to the 3rd of July 2014. The compressor site comprises two major pipelines with their corresponding compressors. The two pipelines carry gas of different origins to the site, where after pressurisation they are combined for further transmission. The site topography is flat and open with the surrounding area as predominantly farm land and close proximity to a major road. An aerial view of the site can be seen in Figure 3.1, where fossil fuel methane ($ffCH_4$) emissions were expected to emanate from 4 zones. The compressors are situated 20 m to the north of the instrument inlet (marked in red in Figure 3.1), high pressure above ground pipelines are found 100-200 m to the north and north west (marked as sources A and B in Figure 3.1) and a flow meter calibration and safety valve testing installation 200 m to the north east (Source C in Figure 3.1). Those regions likely emit CH_4 due to methane slip (compressors) or fugitive emissions from the pipeline systems. Other possible methane sources in the nearby region were identified as traffic and agriculture, including a livestock holding situated less than 500 m south-west of the site.

Figure 3.1 *Aerial view of the natural gas compressor station and the location of the presumed principle natural gas sources from Ars et al. 2017 © Google Maps. Location of sampling inlet is indicated by circular red marker.*

3.2.1.2 Data Collection: Continuous measurements of CH_4, $\delta^{13}CH_4$ & VOCs

Two instruments were utilised for continuous measurements throughout the two-week field campaign: a cavity ring down spectrometer (CRDS) instrument (Picarro G2201-i) measuring CH_4, CO_2, C_2H_6, $\delta^{13}CH_4$, $\delta^{13}CO_2$ and an automatic gas chromatograph with a flame ionization detector (GC-FID) (Chromatotec, Saint-Antoine, France) measuring light fraction C_2-C_6 hydrocarbons. The sampling time for the GC-FID is a 10-minute average every half an hour; 10 minutes of ambient air is collected after which the following 20 minutes are used to analyse this input. The CRDS measures all species multiple times a minute. A synchronised time series of both instruments was achieved by locating the two inlets beside one another on a mast (3 m a.g.l) and averaging the CRDS time series in accordance with the GC by using time stamped measurements (i.e. the CRDS data is averaged every 10 minutes, and every 30 minutes, 20 minutes are discarded corresponding to the GC analysis time). The calibration scheme was chosen to be suitable for a broad range of $\delta^{13}CH_4$ values and high atmospheric concentrations of the key species measured (-24‰ to -66‰ $\delta^{13}CH_4$, 1.8-

3ppm CH_4, 370-500ppm CO_2, 0.3-3ppm C_2H_6) relative to WMO standards for the GHG dry mole fractions, VPDB for $\delta^{13}CH_4$ and NPL standards for VOC mixing ratios. More information on both instruments and the calibration protocols can be found in Assan et al., [2017] and Gros et al., [2011]. For simplicity, we will refer to both the mixing ratios of VOCs and the dry mole fractions for the GHGs interchangeably as 'concentrations' in this manuscript and report them in ppm or ppb, signifying umol/mol or nmol/mol, respectively.

To reduce the impact of missing data, short gaps of less than two hours (i.e. 3 consecutive data points) were linearly interpolated. This time length was chosen as it significantly increased available data for some VOCs without altering their variability. The species used within the source apportionment models were chosen from a selection process in which species with more than 15% of missing data points or more than 20% of values below the detection limit (LOD, calculated as 3-sigma baseline noise, see Table B.3.1 in the Appendix B) were discarded as a reliable correlation/covariance analysis of different species would not have been possible with this data. Three chemical species were rejected: n-Hexane (n-C_6H_{14}), propene (C_3H_6) and Ethylbenzene (C_8H_{10}). In total, for the source apportionment models, the final dataset included 386 observations of 13 chemical species: Methane (CH_4), Ethane (C_2H_6), Propane (C_3H_8), i-Butane (i-C_4H_{10}), n-Butane (n-C_4H_{10}), i-Pentane (i-C_5H_{12}), n-Pentane (n-C_5H_{12}), Ethylene (C_2H_4), Acetylene (C_2H_2), Benzene (C_6H_6), Toluene (C_7H_8), MP Xylenes (C_8H_{10}), and Carbon Dioxide (CO_2).

3.2.1.3 Meteorological data

On-site meteorological observations (wind speed and 2d horizontal wind direction) from a wind mast are available from June 30th to July 8th. To obtain wind data for the missing days, wind fields at 10m height were interpolated from the operational analysis of ECMWF as described in Staufer et al., [2016], to have temporal resolution of 1 hour. We found good agreement (seen in Figure B1 in the Appendix B) with the on-site meteorological measurements; hourly averages of both datasets showed over 75% of wind direction measurements within the same 22.5° direction bins. For reliably measurable wind speeds (above 1m/s), modelled wind speeds agree within 1m/s and 2m/s for 60% and 91% of the time, respectively. The RMS of modelled and observed wind speed is ca. 1m/s. Dominant wind conditions during the two-week measurement period were north and east-north-easterly winds. The mean wind speed was 3.1m/s with minimum and maximum wind speeds of 0.05m/s and 7.5m/s respectively. A windrose plot can be seen in Figure 3.2.

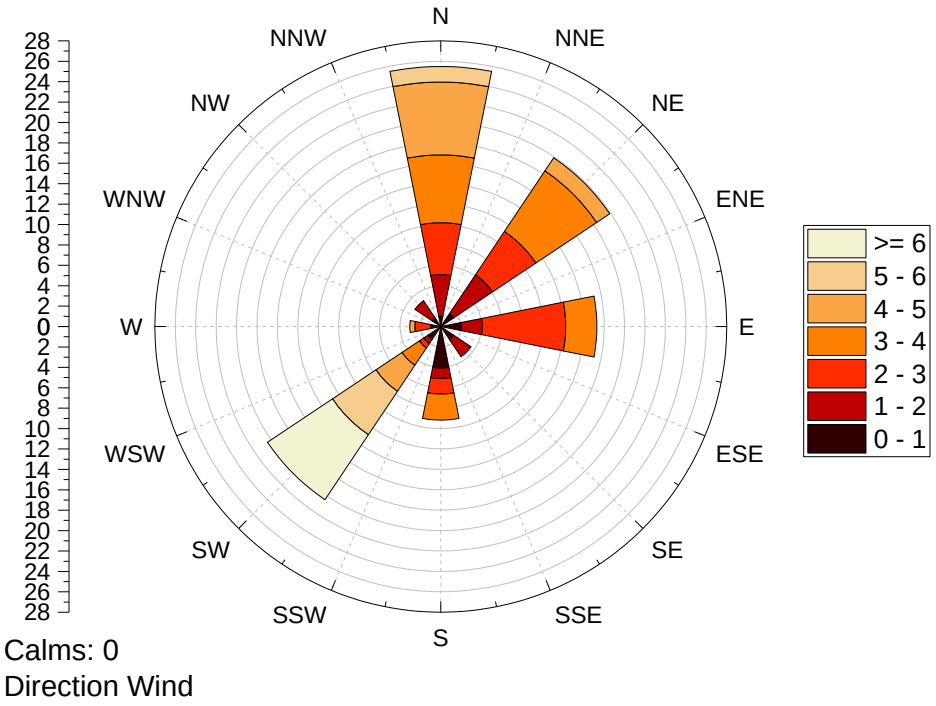

Figure 3.2 *Wind data plotted as a windrose for the period of the 25th of June 2014, to 3rd July 2014. Wind speed is shown by the colour in m s-1, the contribution from a certain wind direction is given on the y-axis, in percent.*

3.2.2 METHODS USED FOR SOURCE APPORTIONMENT

3.2.2.1 Using Methane Isotope

Many methane sources are characterised by specific δ^{13}C-CH_4 ($\delta^{13}CH_4$) signatures, which enable the identification of methane emissions [e.g. Zazzari et al., 2015, 2017]. The isotopic composition is commonly reported in δ notation, where δ is the relative deviation of an isotope ratio R. In our case, R is the ratio of ^{13}C to ^{12}C:

$$\delta^{13}C = \left(\frac{R_{sample}}{R_{standard}} - 1\right) * 1000‰ \qquad \textit{Equation 3-1}$$

Values are expressed in permil (‰) on the Vienna Pee Dee Belemnite (VPDB) scale. In this study, Miller-Tans plots [Miller and Tans, 2003] were used to calculate the CH_4 isotopic source signatures, as this data regression is adapted to identify the source signature in situations where the background of CH_4 and $\delta^{13}CH_4$ are not necessarily constant. The data was analysed through the

implementation of a moving Miller-Tans plot, similar to the moving Keeling plot method of Roeckmann et al., [2016]. For this method, we use 10-minute averaged CRDS data which has not been reduced to GC time-steps in order to capture CH_4 concentration peaks with short term variability. Data within a moving time window (minimum 4 data points) were used to calculate the source isotopic composition if deemed as a significant CH_4 emission period. The criteria used to identify significant emissions were data points with a short change in both CH_4 concentration and $\delta^{13}CH_4$ of greater than 50 ppb and 0.6‰ respectively, which excludes slow concentration variations induced by diurnal vertical mixing. To specifically select well-defined isotopic compositions, only points with increasing CH_4 concentrations and Miller-Tans regressions with $R^2 > 0.9$ were retained. To retrieve uncertainties, a 1000 run Monte Carlo simulation was applied, by randomly adding instrumental noise (calculated as 3 sigma of 10 minute averages in 6-h measurement of a working gas as 1ppb and 0.6‰) to the time series. An example of the identification of a CH_4 peak isotopic signature is demonstrated in Figure 3.3.

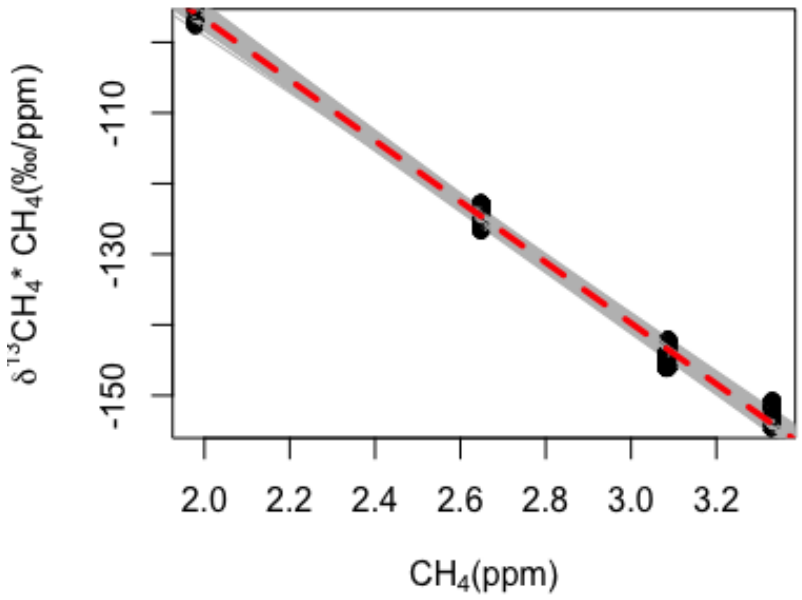

Figure 3.3 *Monte Carlo simulation of Miller-Tans plots to calculate the isotopic signature of a single peak. Grey lines represent each line of fit from 1000 MC runs. The red dashed line is the mean for fits that have R^2 >0.9. The isotopic signature determined from the slope is -41 +/- 1.5 ‰.*

3.2.2.2 PCA and PMF Receptor Models

The fundamental principle of receptor models is mass conservation, and using mass balance analysis to identify and apportion source contributions to observed concentrations. The mass balance equation can be written as:

$$x_{ij} = \sum_{k=1}^{p} g_{ik} f_{kj} + e_{ij} \qquad \textit{Equation3- 2}$$

where x_{ij} is the concentration measurement of the j^{th} species in the i^{th} sample, g_{ik} is the contribution of the k^{th} source to the i^{th} sample (i.e. factor contributions), and f_{kj} is the fraction of the j^{th} species in the k^{th} source (i.e. species profile) and e_{ij} is the residual for each sample/species. Starting from a large number of observations of correlated species, the aim is to explain the variance of the data in terms of a number of independent sources (factors) by solving for factor contributions, *g*, and species profiles, *f*. This general concept has been implemented in different ways.

APCA. Principle component analysis is a data reduction method which uses an eigenvector analysis of a correlation matrix to identify principle components (PCs) (in our case, emission source profiles) which explain the greatest part of the data variance. Principle component analysis has come under some criticism [Hopke, 2015] as it is based purely on mathematical constraints, and thus the PCs do not necessarily have a direct physical meaning [Harris, 1975]. Different approaches have been studied to improve the interpretability and obtain source contributions from PCA; one of the most cited in air pollution literature, and the one used in this work, is Absolute Principle Component Analysis (APCA) described in detail in Thursten and Spengler, [1985] and Bruno et al., [2001]. This method combines PCA with Varimax rotation and multiple linear regression analysis (MLRA) to determine source contributions and profiles. Examples of its applications in air pollution studies can be found in Tauler et al., [2009], Moreno et al., [2009], Viana et al., [2006], and many more.

PMF. Recently, PMF has become more commonly used than PCA in studies focusing on particulate matter (PM), predominantly due to the implementation of a non-negativity constraint resulting in more physically realistic factors which are directly interpretable, and the incorporation of error-estimates to down weight compromised data. It solves the mass balance equation by using a point by point, constrained and weighted least squares minimisation method, first described in Paatero and Tapper, [1994]. Normally there are a number of mathematically equivalent solutions that exist, thus when using PCA or PMF to solve for Equation 3.2 (i.e. cases in which the contributions g_{ik} and number/nature f_{kj} of

sources are unknown) a certain amount of expert knowledge is needed, and subjectivity added when interpreting the solutions.

Sensitivity Studies. As the goal of this study is specifically the source identification and characterisation of CH_4 sources, we examined the sensitivity of the APCA and PMF receptor models to a number of parameters in order to systematically optimise them for this study. The details of the sensitivity study can be found in the Supplementary material, Section 3.5; we briefly describe the key results affecting our practical application of the models here. We found CH_4 factors modelled by APCA deteriorate if species which have little to no correlation with CH_4 are included in the analysis, and that such species which do not add additional information can noticeably increase the uncertainties in the modelled factors. Although the CH_4 factors modelled by PMF are less sensitive to the number of species included than APCA, PMF factor uncertainty can also increase with a higher number of species. APCA was not affected by a reduced length of the time series used (i.e. number of data points), unlike PMF which required over 100 data points to correctly distinguish sources. We found the reconstruction of the principle component by APCA is reliable only when it explains the majority of the data variance. Finally, we found that temporal changes in the CH_4 source emission ratios were better identified by APCA when applying the model to shorter time windows.

Practical application of APCA in this study. Here, APCA was performed using the prcomp(), and varimax() functions in R (package:stats) and implemented with the Guttman-Kaiser rule to select the number of factors retained for Varimax rotation [Cangelosi and Goriely, 2007]. Consequently, only factors well correlated with CH_4 were reconstructed via MLRA. The number of species used within the analysis was subset to: CH_4 with C_2H_6, C_3H_8 n-C_4H_{10}, i-C_4H_{10} for the identification of natural gas sources, and C_6H_6 & C_7H_8 used as tracers for traffic emissions. Receptor modelling techniques have rarely been applied specifically for the identification of different CH_4 emission sources and we thus implement two modifications to APCA to enhance the CH_4 identification potential:

a) Monte Carlo (MC) simulation: a major shortcoming of PCA is its lack of error estimation. We add a MC simulation for uncertainty estimates. The simulation includes randomly added instrumental uncertainty. For species measured by CRDS, the LOD value is applied. For VOCs, 15% of the species concentration is applied. If concentrations are below the LOD, the LOD value is used, (see Table B.3.1 in the Appendix B for information on specific species). This method will be referred to as MC-APCA from here on.

b) 10h moving APCA coupled with Monte Carlo (MC) simulation (MC-mACPA): This method is used to investigate the short-term variability of CH_4 source contributions. Similar to the moving Miller-Tans regression approach for the $\delta^{13}CH_4$ source identification (Section 3.2.2.1), MC-APCA is applied using the method described above to data within a moving time window of 10h (20 data points). The PC was reconstructed for each 10h window.

Practical application of PMF in this study. In this study, PMF was performed using the EPA PMF5.0 software [Norris et al., 2009]. The Multilinear Engine is the underlying program used to solve the PMF problem in EPA PMF and version me2gfP4_1345c4 has been developed by Pentti Paatero at the University of Helsinki and Shelly Eberly at Geometric Tools (http://www.geometrictools.com/). To enable a comparison with the MC-APCA, the same subset of species used in MC-APCA is used for PMF. The signal to noise (S/N) ratio of all species was greater than 2 and therefore weighted as 'strong' following the approach suggested Paatero and Hopke [2003], species specific S/N ratios can be found in the Appendix B.3. The uncertainty matrix was calculated following Norris et al., [2014]. For concentrations below the LOD, the species-specific LOD value is used. The number of factors was determined by combining results from MC-APCA, the analysis of the parameters IM (maximum individual column mean), IS (the maximum individual column standard deviation) obtained from the scaled residual matrix and the physical meaning of the factors obtained. In this case study, 2 to 4 factors were examined to find the optimal PMF solution. Finally, two factors were chosen for the following three reasons: the MC-APCA analysis suggested 2 sources, a higher number of factors resulted in factors which were not rotationally ambiguant and with unrealistic source profiles (even though CH_4 was better fitted), and sensitivity studies show the PMF cannot distinguish two similar NG sources (see Section 3.5). Rotational ambiguity of the PMF factors was investigated between the rotations of 1 to -1. No significant improvements were gained, thus the final solution contained 2 factors, with the standard value 0 rotation. The uncertainties of PMF factors were calculated using Bootstrap and DISP of 100 runs with random seed.

Table 3-1 Summary table specifying the implementation of the 3 identification methods used.

	Isotopic Analysis	PCA Model	PMF Model
Software	R	R (using prcomp() & varimax())	EPA PMF 5.0
Method	Miller-Tans plots	APCA & MLRA	Multilinear Engine
Species Included	CH_4 & $\delta^{13}CH_4$	CH_4, C_2H_6, C_3H_8, n-C_4H_{10}, i-C_4H_{10}, C_6H_6 and C_7H_8	CH_4, C_2H_6, C_3H_8 n-C_4H_{10}, i-C_4H_{10}, C_6H_6 and C_7H_8
Error Estimates	MC of 1000 runs	MC of 100 runs	Bootstrap & DISP of 100 runs
Time Window	Moving (minimum 40min)	Moving 10h & Entire	Entire
Data	10 min averaged (4 points)	30 min averages (20 / 386 points)	30 min averages (386 points)

3.3 Results & Discussions

3.3.1 Observations at the natural gas compressor station

The full record of CH_4 (averaged to GC time-stamps) and other measured species concentration/dry mole fractions measured during the field campaign is shown in Figure 3.4. Methane concentrations vary strongly on the short-term. Typically, concentration peaks last between 30 minutes to 2 hours, and seem driven by strong sources located within proximity of the measurement site and a variable local transport. Concentration enhancements longer than this were occasionally measured and found to occur at night-time. Methane concentrations during peaks range between 3-5ppm, while on average the concentration grows from its minimum of 2 ppm during the afternoon to 2.5 ppm at night. To coherently analyse the temporal variation of the observations, we split the time series into four distinct periods (A to D) marked by dashed lines in Figure 3.4. In period A, from the beginning of the campaign until June 28th, we find episodes with clear concentration enhancements. In period B, less variable concentrations can be observed which lasts until June 30th. During June 30th and 31st, another period of strong concentration enhancements is measured (period C), after which the rest of time series (period D) shows reduced CH_4 variability with minor concentration peaks on July 2nd and 3rd. The majority of CH_4 concentration enhancements (found in periods A and C) correspond to periods of heavier $\delta^{13}CH_4$ values consistent with natural gas emissions, with exception to the period on the 2nd of July in which strong negative contributions are seen, reaching a minimum $\delta^{13}CH_4$ value of -59 ‰. The mean and standard deviation of observed $\delta^{13}CH_4$ is -47 $\pm$ 1 ‰.

From a qualitative inspection of the time series, the figures show a generally good temporal correlation for CH_4 and some VOCs, in particular C_2H_6, i-C_4H_{10}, n-C_4H_{10} and i-C_5H_{12} which all have CH_4 Pearson correlation coefficients ≥ 0.9. Those gases are known to be contained in natural gas (found in the gas stream [Baudic, 2016]) and can be expected to be useful as proxies here for the natural gas contribution to CH_4 time series. Carbon dioxide concentrations are driven predominantly by a strong daily cycle of atmospheric mixing and do not exhibit short-term excursion. We also see significantly lower diurnal variations during periods B and D, as previously found for CH_4. With CO_2 having diffuse biogenic sources in the site vicinity, and CH_4 having a localized source on the compressor station site, we do not expect a tight correlation. The correlation of CH_4 with CO_2 and the other VOCs (e.g. the combustion tracers such as Ethylene, MP Xylenes, Acetylene) is indeed not evident (Pearson's R between 0 and 0.2).

A plot of CH_4 concentration variations with wind speeds and directions is shown in Figure 3.5, revealing that the majority of events with high CH_4 concentrations predominantly originate from the north and north east of the compressor station site. As mentioned in the site description (section 3.2.1.1), the compressor station comprises of two incoming pipelines which transport gas of differing origins to the station. The gas in both pipelines has been sampled, analysed and found to have specific C_2H_6:CH_4 signatures and isotopic signature in $\delta^{13}CH_4$ (see Table 3-2) [Assan et al., 2017]. This can be used to identify if leakages from one pipeline system is predominantly causing the detected CH_4 enhancements. Within this study, we aim to use the isotopic, APCA and PMF source apportionment methods to distinguish between broad categories of CH_4 emissions and also examine the possibility of identifying between very similar sources such as the different gasses arriving in the two pipelines and compare it to the known source profiles.

Table 3-2 Characteristics of gas taken from the two pipelines at the compressor station, from Assan et al. 2017.

Gas source	Isotopic signature (‰)	C_2H_6:CH_4 ratio (ppm/ppm)
Pipeline 1	-40.7 ± 0.2	0.074 ± 0.001
Pipeline 2	-37.7 ± 0.5	0.046 ± 0.003

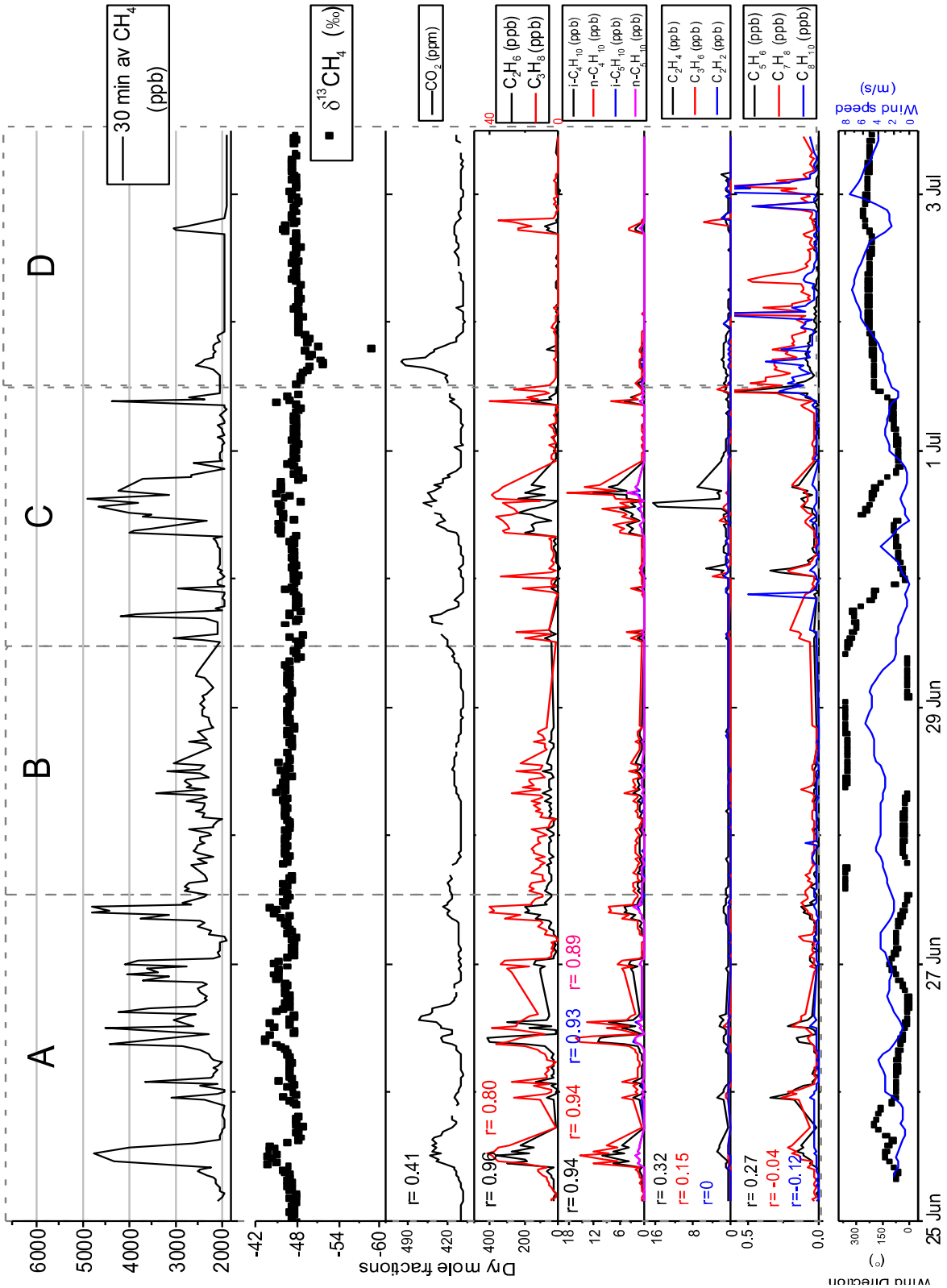

Figure 3.4 Time series of 30min average concentrations of CH_4, $\delta^{13}CH_4$, CO_2, VOCs and wind direction and speed measured at the measurement campaign at the natural gas compressor station. The Pearson correlation coefficient of each species with methane is indicated on each plot.

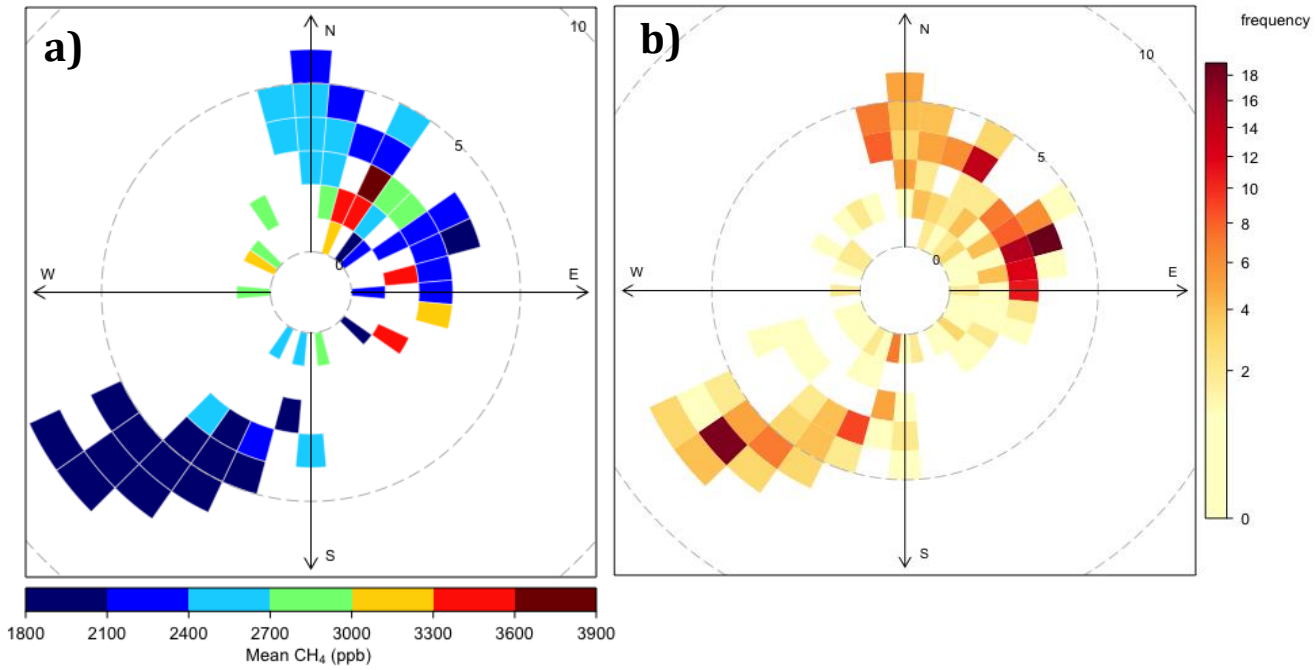

Figure 3.5 a) Pollution rose of mean CH_4 concentrations plotted by wind speed and direction bins. Minimum number of values in each bin is 2.b) Frequency of points in each bin.

3.3.2 Analysing the time-series using isotopic data

To identify the sources of CH_4 from $\delta^{13}CH_4$ analyses, we use the methods outlined in section 3.2.2.1. Twenty events fulfilled the criterions of the moving Miller Tans method, thus 6% of the observed data can reliably be analysed using this method, with typically 1 to 5 significant events per day. The isotopic signatures of those events suggest that the majority of CH_4 concentration peaks originate from natural gas, with 18 of the 20 ranging from -40‰ to -45‰. The temporal variation of $\delta^{13}CH_4$ can be seen at the bottom of Figure 3.6. Throughout period A, the observed isotopic source signature of CH_4 is constant with an average -41.85‰ $\pm$ 0.6‰, strongly suggesting the CH_4 enhancements are due to natural gas emissions from pipeline 1. Throughout period B, the isotopic signatures calculated have much larger standard deviation due to the reduced CH_4 concentration enhancements. This time period corresponds with a change in general wind direction from the previously predominantly North-Easterly winds to North – Westerly winds. For this period, the uncertainties attributed to the isotopic signatures are too large to identify a specific natural gas source as the cause of emissions. The isotopic signatures in period C are well defined; peaks at the start and end of the period identify a gas source much like pipeline 1. The isotopic signature measured on the evening of the 30th June is suggestive of a NG source lighter than

the sampled pipelines. On the 2nd of July, in period D, an isotopic signature of -62 ± 3‰ was calculated, which can be attributed to a local biogenic source, i.e. ruminant emissions from a farm, that are known to be isotopically light and free of C_2H_6 [Assan et al., 2017]. In this singular case, the prevailing wind has a south-westerly direction with high wind speeds of approximately 4m/s. The $\delta^{13}CH_4$ signatures are plotted in a wind rose in Figure 3.7b. Northerly winds resulted in the highest number of isotopic signatures calculated with values between -41 to -43‰. Other wind directions show similar source signatures with exception to winds from a south westerly direction where the biogenic signature is detectable.

3.3.3 Analysing the time-series using modified APCA

Application of MC-APCA in the traditional way (without a moving window) provides an insight into the overall source contributions driving the concentration data. Two distinct sources are identified. The first, accounting for 77.5 ± 0.6 % of the total concentration variance is dominated by CH_4 and NG tracers. The estimated C_2H_6:CH_4 source ratio is 0.0639 ± 5 x10^{-4}, which is in the range reported for wet gas sources [Yacovitch et al., 2014, Roscioli et al., 2015]. The second source, contributing to 66% of the remaining variance, has contributions from predominantly toluene and benzene and a small fraction of CH_4, which rather suggests a traffic source. Maximum and mean absolute CH_4 residuals using this method (shown in Figure 3.8) are approximately 1 ppm and 140 ppb respectively.

A more detailed analysis of the specific time periods is achieved with the 10h-moving MC-mAPCA method (described in Section 3.2.2.2). Results suggest that the number of principal components (PCs) contributing to CH_4 variability and their source characteristics vary depending on the time period analysed. The first PC (PC1) generally explains between 60% to 80% of the total concentration variance. Its temporal variation and that of the C_2H_6:CH_4 source ratio of PC1 are shown in Figure 3.6. Outliers and unstable points with a Δ (C_2H_6:CH_4 ratio) (i.e. C_2H_6:$CH_4^{\ n}$ - C_2H_6:$CH_4^{\ (n-1)}$) of greater than 0.01 were excluded from the results. During period A, the source ratio is very stable, suggesting a natural gas source with a C_2H_6:CH_4 signature of between 0.065 and 0.075 ppm/ppm. Throughout period B, CH_4 enhancements are low. Here we find estimated source signatures to be more variable. However, they continue to suggest a natural gas source similar to that of the two pipelines (C_2H_6:CH_4 signature between 0.04 and 0.08). When comparing the results to the known ratios of the natural gas within the two pipelines (dashed green and pink lines in Figure 3.6), it is clear that emissions on the 26th of June have a ratio corresponding to that of Pipeline 1, but the majority of events seem to be a mixture of the two

pipelines. The data coverage is much larger than that of the isotopic analysis, resulting in a fuller understanding of the changing sources, in particular during periods of low CH_4 concentration enhancements. Overall the isotopes and C_2H_6:CH_4 ratios are in good agreement, suggesting Pipeline 1 as the dominant CH_4 source. On July 2nd, the C_2H_6:CH_4 source ratio decreases to 0; the same period identified by the isotopic signatures as a biogenic source. Nonetheless, there are a number of concentration peaks which are indicative of Pipeline 1 when using isotopic values, but a mix of the two pipelines (60% to 80% for Pipeline 1, 40% to 20% for Pipeline 2) is observed if using source ratio values, for example in the second half of Period A. It is important to note that our analysis is more sensitive to changes in C_2H_6:CH_4 ratio than $\delta^{13}CH_4$ values. The two pipelines are separated by 3‰ and 0.02 ppm/ppm for $\delta^{13}CH_4$ signature and C_2H_6:CH_4 ratio, respectively. Yet the typical uncertainty for calculations of a single time window using the moving Miller-Tans and MC-mAPCA are 1.4‰ and 0.005ppm/ppm, respectively. Thus, a mix of 60% from Pipeline 1 and 40% from Pipeline 2 during a short period would not be easily distinguishable from pure Pipeline 1 using the $\delta^{13}CH_4$ signatures alone, while APCA-based C_2H_6:CH_4 ratios would be sensitive enough. The size of the error bars and the stability of the C_2H_6:CH_4 source ratio from the MC further aid our analysis by giving an idea of the robustness of modelled CH_4 source contributions. For example, during period C, in which the C_2H_6:CH_4 source ratio is changing from dominantly Pipeline 1 to 2 without stabilising suggests the principle component does not model the CH_4 source well. From our sensitivity studies, we find that such characteristics usually occur when there is a second type of CH_4 source explaining a similar portion of the concentration variability as the principle source (see Section 3.5, Figure S3.1). In this case, we assume the second source to be traffic emissions, which heavily impacts VOCs. Results from MC-APCA also indicate that traffic has heightened contributions during this period. The factors modelled using MC-mAPCA have maximum and mean absolute CH_4 residuals of 800 ppb and 134 ppb respectively, indicating CH_4 emissions are better modelled using the 10h moving method than MC-APCA. We find the predominant difference between MC-mAPCA and MC-APCA is the heightened level of detail of PC1 achieved with MC-mAPCA, allowing for the separation between the contributions of Pipelines 1 and 2, information which is not evident from MC-APCA. The pollution-rose (Figure 3.7a) shows the calculated C_2H_6:CH_4 source ratio for given wind direction and speed. The C_2H_6:CH_4 ratio corresponding to Pipeline 1 is found predominantly to originate from the north and north-north-east of the measurement station. Some emissions corresponding to a C_2H_6:CH_4 ratio of Pipeline 2 are suggested in the north-east. However, this sector primarily identifies natural gas emissions as a combination of both pipelines, which could be expected if the CH_4 originated

from the flow testing facility located to the ENE. The stability of the reconstructed C_2H_6:CH_4 source ratio was not influenced by the wind speed.

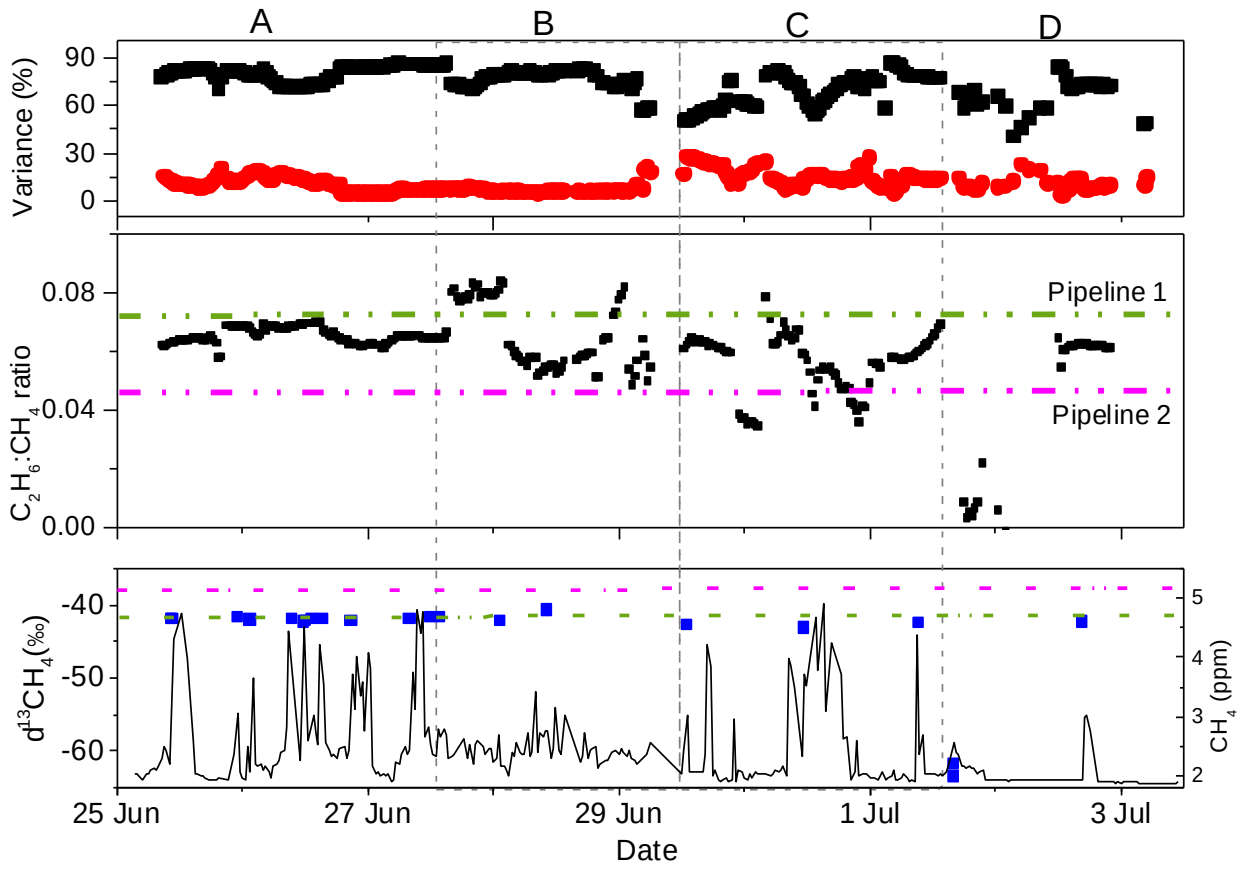

Figure 3.6 Temporal results plot. From top to bottom, a temporal plot of the total concentration variance explained by PC1 (black) and PC2 (red), the reconstructed C_2H_6:CH_4 ratio of PC1 (dotted lines indicated the source signature of gas from pipeline 1 in dark green and pipeline 2 in pink), the isotopic signatures calculated from moving Miller-Tans plots. Error bars are the standard deviation.

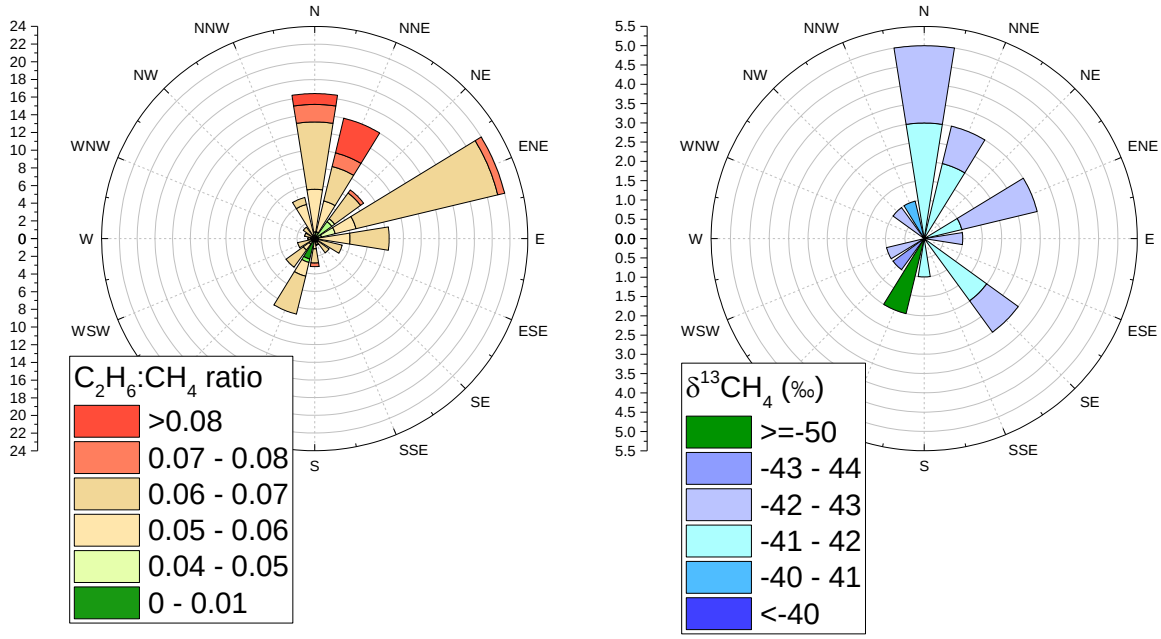

Figure 3.7 Pollution-rose of the reconstructed C_2H_6:CH_4 ratio of PC1 (left) and $\delta^{13}CH_4$ signatures from the moving Miller Tans plot calculations on (right).

3.3.4 Analysing the time-series using PMF

The EPA5.0 PMF model, which is very widely used in air quality studies, does not perform optimally on short time series, (i.e. less than 100 points) but is useful to assess the contribution of sources over the total observed period. Two factors were found as the optimal PMF solution. Factor 1 contributes to 90% of the CH_4 variability. It has a characteristic, stable C_2H_6:CH_4 source ratio of 0.078 (0.072 and 0.079 for the 25th and 75th bootstrap percentiles). This value strongly suggests the source is similar to Pipeline 1. The second factor accounts for the final 10% of CH_4 variability, and is modelled with significant contributions from the traffic trace gases, namely benzene and toluene. The concentration profiles of both factors can be seen in Figures B.2.1 and B.2.2 in the Appendix B. The toluene: benzene ratio is 4.02 (4.00 and 3.63 for the 25th and 27th bootstrap percentiles respectively) indicative of vehicle exhaust emissions [Johansson et al., 2001], much higher than the ratio associated with wood burning emissions [McDonald et al., 2000, Hedberg et al., 2002]. Its associated C_2H_6:CH_4 source ratio has high uncertainties. The base run suggests the ratio is 0.08 (0.058 and 0.066 for the 25th and 75th bootstrap percentiles), which is fairly similar to the first factor and also indicative of a NG source. This implies that the CH_4 component was not clearly separated between the two factors. The bootstrap mapping showed both factors with 0% unmapped. Source apportionment of CH_4 was not strongly affected by the wind direction, however periods with very calm wind speeds (< 1m/s) generally induced higher CH_4 residuals (periods A and C). The factor contributions are shown in Figure 3.8, where Factor 1 and 2 represent the NG and traffic sources, respectively. The CH_4 variability was well fitted with a mean residual of 53ppb and the r^2 of regression for observed vs predicted CH_4 and C_2H_6 greater than 0.9. The scaled residuals of all species ca be seen in Figure B.2.3 in the Appendix B. Examining an input of 3 factors to the EPA PMF model did not result in a robust separation of factors (factors were no longer independent). The temporal variation of factor contributions can be seen in Figure B.2.4 in the Appendix B. We found the traffic factor remained similar, however the CH_4 factor is split into two highly correlated and co-varying factors unlikely to represent the real sources. The result is in agreement with our sensitivity studies which indicated PMF could not distinguish between two sources representing Pipelines 1 and 2. Nonetheless, a major limitation to the application of PMF for this case study is the short time-series (only 386 points), potentially affecting the identification of sources. During periods A and B, Factor 1 and 2 solutions modelled by PMF and MC-APCA are in good agreement, particularly the modelled PMF factors have very low residuals, an average of only 21ppb. In periods C and D there are a number of peaks which are not well characterised by the two sources, specifically the period around the 31st of June where residuals of up to 1.2 ppm are calculated. Notably, this period correlates with a spike in

ethylene concentrations, which can be produced during the heating of natural gas. No other significant correlations of CH_4 and VOCs are seen during periods that less well modelled by PMF and MC-APCA. The first difference in temporal variation between the PMF and MC-APCA modelled factors is seen during period D for Factor 2, in which the PMF attributes concentration enhancements from the biogenic source (as distinguished by MC-mAPCA and moving isotopes) within Factor 2. Periods which show disparity between the modelled factors from PMF and MC-APCA can be used as an indicator for CH_4 contributions from undefined sources.

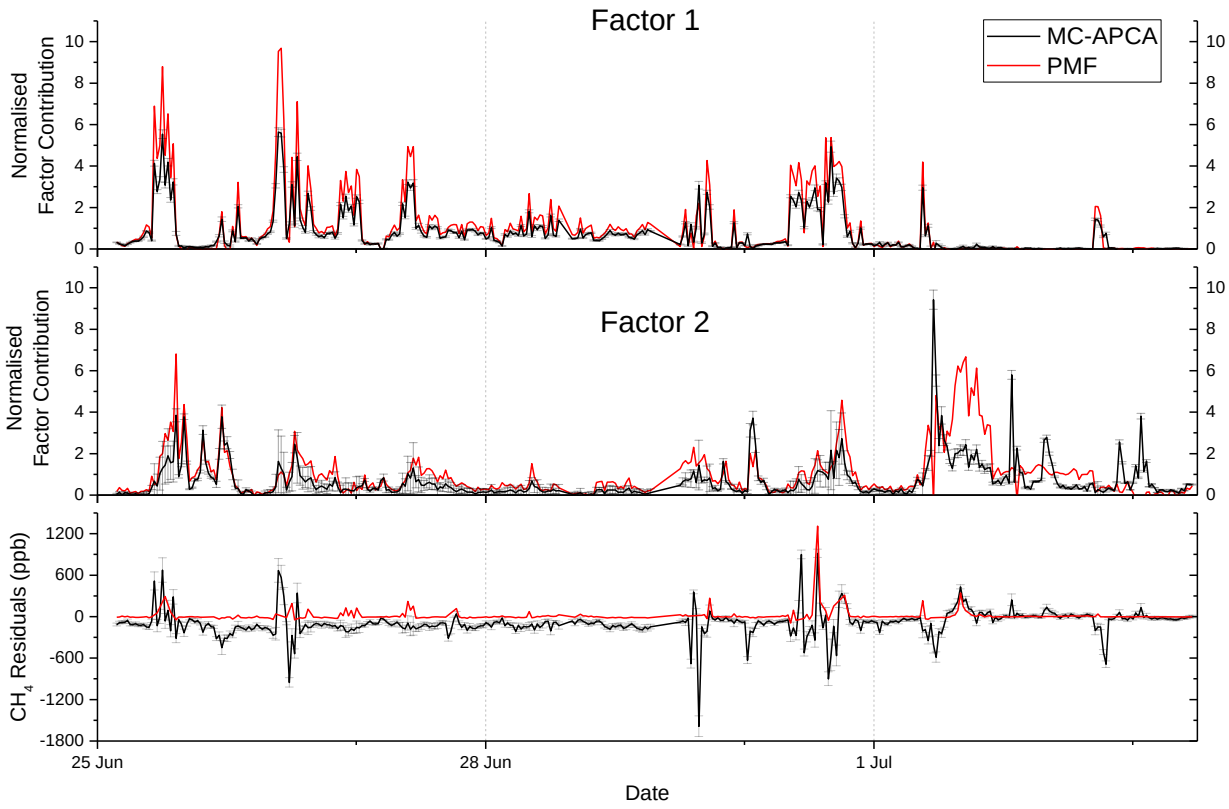

Figure 3.8 Modelled factors from the PMF analysis. Top: A temporal plot of CH_4 residuals. Bottom: Temporal plot of the normalised source contribution from each source. The pure NG source in blue, and the source with traffic emissions in red.

3.4 Conclusions

The source apportionment methods evaluated in this study (isotopic analysis, MC-APCA, MC-mAPCA, PMF) enabled the correct identification of the key sources at the compressor station, in agreement with samples taken from the gas stream, and to identify minor emission sources, traffic and mixed natural gas, from roads and facilities in the vicinity. For the first time, we compared the performance of PCA and PMF receptor models specifically for CH_4 source identification on two-week measurement campaign data from a compressor station site, and include a novel method to implement a 'Monte-Carlo moving APCA' (MC-mAPCA) to distinguish the temporal variance of source contributions.

We found that the methods employed are best suited to different situations. MC-APCA and PMF tools are appropriate for analysis of longer datasets, and may therefore have had reduced functionality when applied to the short time-series here. Both methods identified the same two major sources for CH_4 and VOCs: natural gas and traffic and attributed the majority of CH_4 emissions to a natural gas source. Although the percentage of explained variance and exact source profiles differ slightly, the temporal variation of sources was in good agreement. Our sensitivity studies showed that both MC-APCA and PMF results are sensitive to the number of components included within the analysis and the duration for which each source significantly contributes to the local concentration enhancement. Thus, when using such receptor models for source apportionment, the number and type of gas species considered should be carefully selected, and an understanding of the character of sources (e.g. sporadic high emissions or continuous emissions over a long period) is vital to choose the appropriate model. Regarding the identification of CH_4 sources, all methods (isotopes, MC-APCA, MC-mAPCA and PMF) identify a predominantly natural gas source, but sporadic peaks can only be identified by short term methods, such as the moving isotopic analysis and MC-mAPCA. However, the deviation of PMF and MC-APCA reconstruction during such a sporadic peak indicates that a joint use of PMF and MC-APCA can at least allow detecting such intermittent sources although their source signatures cannot be properly retrieved using these techniques. We find the moving isotopic calculations are very useful here in identifying such short-term sources, however the limited precision means small fluctuations in gas composition, as suggested by the MC-mAPCA, cannot be verified. Furthermore, such calculations require additional instrumentation and strong CH_4 enhancements for stable $\delta^{13}CH_4$ signature calculation which can leave much data un-interpreted. Unfortunately, isotopic observations are not available for all studies, while the use of APCA, mAPCA and PMF can easily be implemented on the same datasets. For a

comprehensive interpretation of longer data sets, the PMF model may be more suitable, however it has difficulties separating sources with similar profiles (such as the two pipelines in our case). Generally, higher residuals are present with increased standard deviation of CH_4, implying that the PMF method has reduced performance with large CH_4 enhancements. Furthermore, as PMF is a ready to use software, it is not flexible to develop the model specifically for CH_4 identification. Application of the MC-APCA model to the entire dataset is best used to distinguish between sources as we find the reconstruction of minor components to be fairly unreliable. The implementation of the monte-carlo approach allows us to better identify situations where classical PCA or APCA solutions are unstable. The limitations of MC-APCA are partially overcome with our implementation of a moving MC-ACPA in which temporal variations of the principle component can be tracked regardless of even changing source profiles.

Overall, we conclude that no single tool is ideal to achieve a fully correct source apportionment for our two-week campaign in a multi-source environment, where major sources were fairly similar, i.e. predominantly from natural gas with intermittent biogenic sources. Thus, a combination of all tools (isotopes, mAPCA, APCA, PMF) and analysing both the short- and long term variations of CH_4 and VOCs is required to fully understand the underlying characteristics of the CH_4 data and for correct identification of all sources.

3.5 SUPPLEMENTAL MATERIALS: SENSITIVITY STUDIES

Major limitations of APCA and PMF models are that a) source interpretation is relatively subjective due to the dependence on the (sub-) set tracer species chosen for the analysis and b) their inability to clearly separate covariant sources [Viana et al., 2008]. Here we test the receptor models on simulated data for an understanding of the limitations associated with each model**.**

S3.1 CREATION OF PSEUDO DATA

To assess the abilities and shortcomings of the receptor models, pseudo data was created to compare APCA and PMF solutions with ground truth. A realistic dataset was created by basing the variability of the pseudo-data time series on the CH_4 concentration time-series measured at a natural gas compressor station ($CH_{4\ obs}$) (see section 3.1). Then VOC concentration time-series for 5 VOCs (C_2H_6, C_3H_8, iC_4H_{10}, nC_4H_{10} and Ethanol) were created using emission factors corresponding to three specific sources (see Table S3.1), using the following equation:

$$VOC_{pseudo,i} = CH_{4\ obs} \cdot [VOC_i:CH_4]_{source\ ratio} \qquad \textit{Equation 3.3}$$

The source ratios chosen for each VOC species reflect realistic emission ratios for a site with 2 natural gas sources and one (intermittent) biogenic source. Natural gas emissions ratios are based on values from Assan et al., [2017]. For the biogenic source, C_2H_6:CH_4 and Ethanol: CH_4 emission ratios are taken from Allen [2016] and Gentner et al., [2014] respectively. The remaining emission ratios are based on flask sample measurements of cow breath measured on a GC. The pseudo dataset was doubled as the PMF model has better performance for longer datasets.

Table S3.1 Source emission ratios used to create pseudo data based on values from Assan et al. [2017].

	SOURCE RATIO (PPM/PPM)				
	C_2H_6/CH_4	C_3H_8/ CH_4	iC_4H_{10}/ CH_4	nC_4H_{10}/ CH_4	Ethanol/ CH_4
SOURCE A (PIPELINE 1)	0.075	0.019	0.0018	0.0029	negligible
SOURCE B (PIPELINE 2)	0.04	0.013	0.0014	0.0025	negligible
SOURCE C (BIOGENIC)	0.008	0.0022	0.0005	0.0002	0.018

S3.2 SENSITIVITY TESTS

In order to develop APCA and PMF models to realise the best possible CH_4 source identification potential, model performance is examined for the impact of:

a) Limited precision and noise (i.e. measurement uncertainties and varying source ratio)
b) Choice of (sub)set of additional VOC species included in the analysis (3-13 species)
c) Duration and types of sources contributing to CH_4 variability (1h-350h sources, biogenic and natural gas sources)
d) The time window applied for APCA/PMF analysis (10h periods or entire dataset)

Impacts of items a), c) and d) were evaluated using pseudo data, described in sections S3.2.1 to S3.2.3. While the impacts of b) were evaluated on data measured during the field campaign at a natural gas compressor station, found in Section S3.2.4.

S3.2.1 Impact of limited precision and noise

The sensitivity of the model solutions to 2 types of unbiased uncertainties were examined, namely: measurement uncertainties and source ratio variability. All measurement techniques have an attributed uncertainty. To recognise the effects that this has on the receptor models, a measurement uncertainty (ε_1) was created for all species as a percentage of their concentration. The variability of source emission ratios was included as ε_2. The method used to create the pseudo data with noise can be seen in equations 3.4 and 3.5.

Measurement Uncertainty (mu): $^{mu}CH_{4\,pseudo} = CH_{4\,obs} + \varepsilon_1{}^{a}$ and $^{mu}VOC_{i,pseudo} = [CH_{4\,obs} \cdot ratio_i] + \varepsilon_1{}^{a}$ *Equation 3.4*

Source Ratio Variability (srv): $^{srv}CH_{4\,pseudo} = CH_{4\,obs} + \varepsilon_1{}^{15\%}$ and $^{srv}VOC_{i\,pseudo} = [CH_{4\,obs} \cdot (ratio_i + \varepsilon_2{}^{a})] + \varepsilon_1{}^{15\%}$ *Equation 3.5*

Where $\varepsilon_1{}^{a} = a \cdot species_{\,pseudo}$, $\varepsilon_2 = a \cdot ratio_i$

Pseudo data was created using the ratios from Source A (see Table S3.1) with **a** as 5%, 15%, 25%, 50% and 100%. For the source ratio variability, a 15% instrumental uncertainty ($\varepsilon_1{}^{15\%}$) (typical uncertainties of concentration for VOCs considered here) was included on top of their respective uncertainties in source ratio ($\varepsilon_2{}^{a}$). For the PCA, uncertainty estimates were retrieved using MC by simulating 1 000 randomly altered 'noisy' datasets for each type of pseudo data. For comparison, the sensitivity of PMF

to these uncertainties was tested on one dataset for each type of pseudo data. Uncertainty estimates were obtained from evaluating the BS, DISP and BS-DISP methods included with the EPA PMF software.

S3.2.2 Duration of source contributing to CH_4 variability

A vital question to be addressed within this study is if the methods can identify intermittent CH_4 sources as well as sources that predominantly contribute to the CH_4 variability. To do this, pseudo datasets were created for Sources A, B and C using Equation 3.4 with 15% instrumental uncertainty ($\varepsilon_1^{15\%}$). Starting with the pseudo time-series of only one source (Source A), the time period of a secondary source (Source B or C, i.e. one that has significantly similar or different source ratios to Source A, respectively) was increased in increments in order to detect the minimum duration (here data points) required for correct source determination of both sources.

This was tested on APCA by applying MC-APCA to a time series in which the contribution from the second source was increased in one hour increments. Uncertainties on the modelled factors were calculated from 100 run MC with 15% instrumental noise applied to all species. The PMF model was applied to 5 pseudo datasets where the period of the second source ranged from 20 to 400 hours. Uncertainties were calculated using BS, DISP and BS-DISP methods, with 15% measurement uncertainty.

S3.2.3 Time window analysed

Field campaign duration can vary from a few days to several weeks, thus influencing the time window of observations. To investigate whether the time window used within APCA or PMF affects the factor solutions, the models were applied to varying time periods of pseudo data. Furthermore, to explore whether the models could distinguish between CH_4 concentration enhancements from two slightly varying gas sources, pseudo data was created using the source ratios of Source A as the predominant CH_4 source, with intermittent methane variability explained by Source B. 15% instrumental error was added to all species.

For APCA, this is analysed through a 'moving' MC-APCA (MC-mAPCA), in which MC-APCA is applied to rolling 10-hour time windows, i.e. for 20 points. For PMF analysis, the time-series was split into sections of minimum 50 points, as suggested in previous studies [Zhang et al., 2009, Chen et al., 2010, Pant and Harrison, 2012].

S3.2.4 Impact of chosen (sub-) set of additional VOCs

As the goal of this study is to improve specifically the identification and characterisation of CH_4 sources, we examine how the number of additional VOC species included in the receptor models affects the modelled CH_4 sources. The number of species included in the MC-APCA and PMF models was increased from only CH_4 and C_2H_6 to all 13 species. 15% instrumental uncertainties were used for the uncertainty estimations, using BS, DISP and BS-DISP for PMF and 1000 MC for APCA.

S3.3 Sensitivity Test Results

S3.3.1 Sensitivity to limited precision and noise

Principle component solutions are affected to different degrees depending on whether the noise added to the pseudo datasets stems from instrumental uncertainties (ε_1) or source ratio uncertainties (ε_2) calculated from Equations 3.4 and 3.5 respectively. We found that the percentage variability explained by the PC (in our case the Source A) was the parameter most influenced by the addition of uncertainties, specifically to ε_2, where an addition of noise of 15% alters the parameter significantly from the reference simulation of 77.22% ± 0.05% to 76.65% ± 0.05%. Instrumental noise additions below 25% were in agreement with reference values. The C_2H_6:CH_4 ratio of the reconstructed PC was found to be less influenced by the addition of ε_1 and ε_2. The addition of ε_1 and ε_2 up to 50% did not shift the reconstructed ratio from the reference value within the standard deviation.

Overall, the PMF shows higher stability in regards to additions of ε_1 and ε_2. Only after the addition of 50% noise does the source apportionment stray from the reference values.

S3.3.2 Sensitivity to duration of source contributing to CH4 variability

Results from the sensitivity study described in Section S3.2.2 found that the minimum duration of a second source (contributing to CH_4 variability) needed for the models to correctly identify both CH_4 sources is dependent on the characteristics of the CH_4 sources.

When introducing a second source (Source C) significantly different to the primary source (Source A), the MC-APCA correctly reconstructs Source A while its variability contributes to approximately 90% or more of the time-series variability. In the case of the pseudo data, this is 300 hours out of a 350 hour

time series. Consequently, for Source C to be correctly reconstructed, it must be present for 340 hours or more, due to the low concentration variability of species in this source. When the sources are found in evenly mixed contributions, the C_2H_6:CH_4 source ratio is no longer representative of either source. This can be seen in Figure S3.1: The left-hand plot shows that whilst Source A is contributing to the most of the concentration variability (> 60%), the C_2H_6:CH_4 source ratio is significantly higher than that of Source A. As the variability of Source C becomes more pronounced, the C_2H_6:CH_4 source ratio is as a mixture of both sources. Substituting Source C with B in the simulation gives similar results. The C_2H_6:CH_4 ratio of either source was correctly calculated when the source represented more than 90% of the dataset. However, when both sources contribute more evenly to the variance, the reconstructed species time series do not well represent the original C_2H_6:CH_4 ratios, seen in the right-hand plot of Figure S3.1. Overall, correct reconstruction of the PC is possible only if it contributes to the majority of the dataset, whilst reconstructions of species time series from the second principle component are rarely correctly attributed.

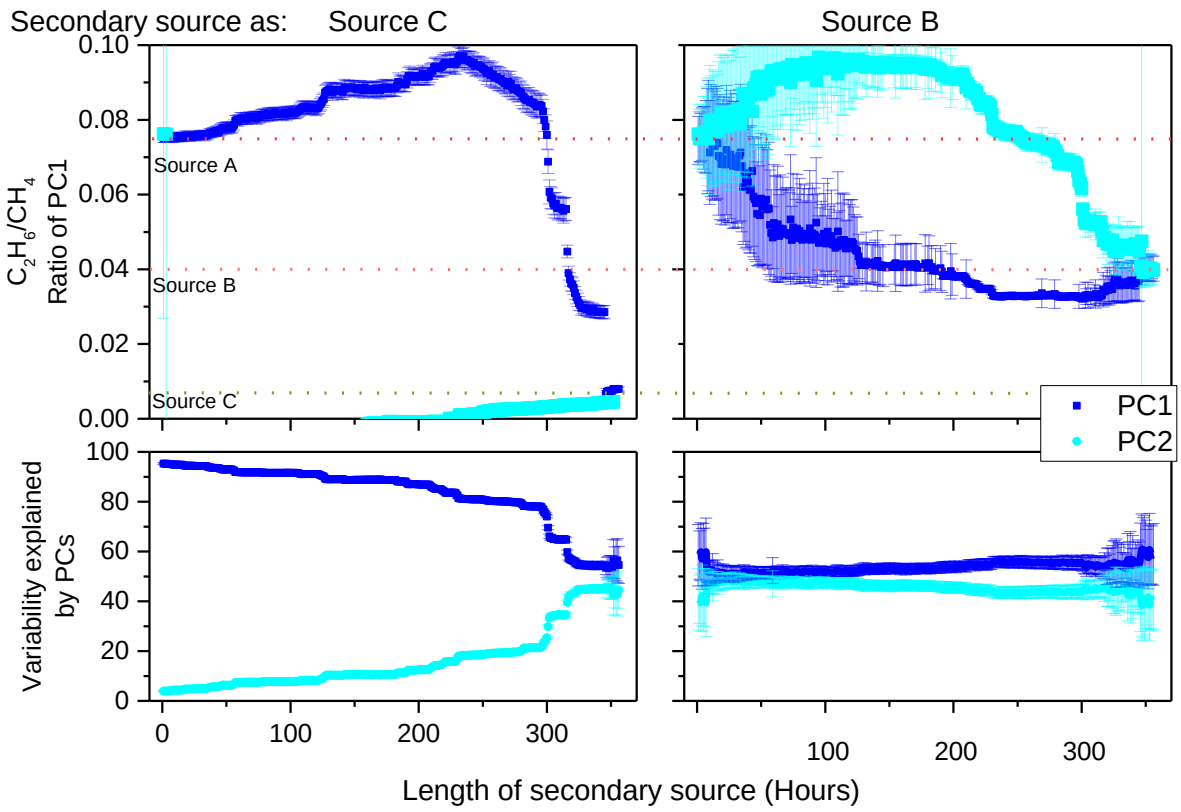

Figure S3.1 The change in the C_2H_6:CH_4 source ratio of PC1 (top), and the variability explained by the principle components 1 and 2 (bottom), as a secondary source is introduced to Source A (Pipeline 1) time-series only. The biogenic (left), and natural gas (right) sources are increased in one hour time-steps. Error bars represent the standard deviation of a 1000 MC simulation with instrumental error of 15% on all species.

For the PMF model, the minimum number of data points required by a second source for the model to correctly distinguish two sources (Biogenic and Pipeline 1, Sources C and A respectively) in the pseudo data was found to be 100 (i.e. 50 hours). The calculated C_2H_6:CH_4 source ratio of the natural gas factor can be seen in Figure S3.2. The number of data points of the biogenic source is increased from 2 to 400 hours, however the correct C_2H_6:CH_4 ratio is measured only when the biogenic source is between 50-300 hours. When substituting the biogenic source with the second NG source (Source B, in red in Figure S3.2) we found the PMF was not able to distinguish between the two NG sources regardless of the time length of the sources.

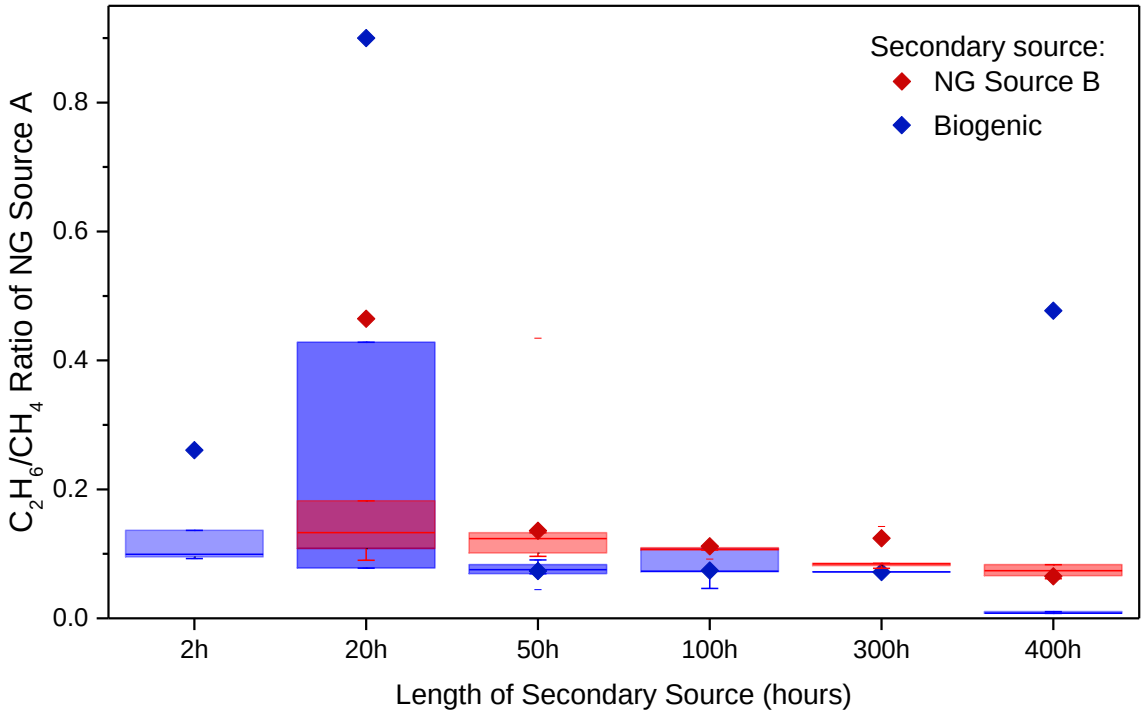

Figure S3.2 The C_2H_6:CH_4 source of the NG source A calculated by PMF as the time of an additional source in the time-series is increased (x-axis.) The original time series is NG source A only and a secondary source is added in varying time steps, a biogenic source in blue, and NG source B in red. Boxes represent the 25th and 75th percentiles from 50 runs, and the diamond markers represent the run identified by PMF as the best solution (lowest Q value).

S3.3.3 Time Period Analysed

The results above suggest that MC-APCA can correctly reconstruct the PC if it explains the majority of the variability (>90% of the data). We find that when using MC-mAPCA it is possible to correctly identify

and characterise individual peaks of the two natural gas sources (see Figure S3.3); a significant improvement to the results achieved with MC-APCA.

Nonetheless, applying the PMF to a time-series split into 100 point (50 hours) sectors does not improve the modelled factors. Mean absolute methane residuals increase by a factor of 10. Confirming that optimal results are achieved by PMF with more data.

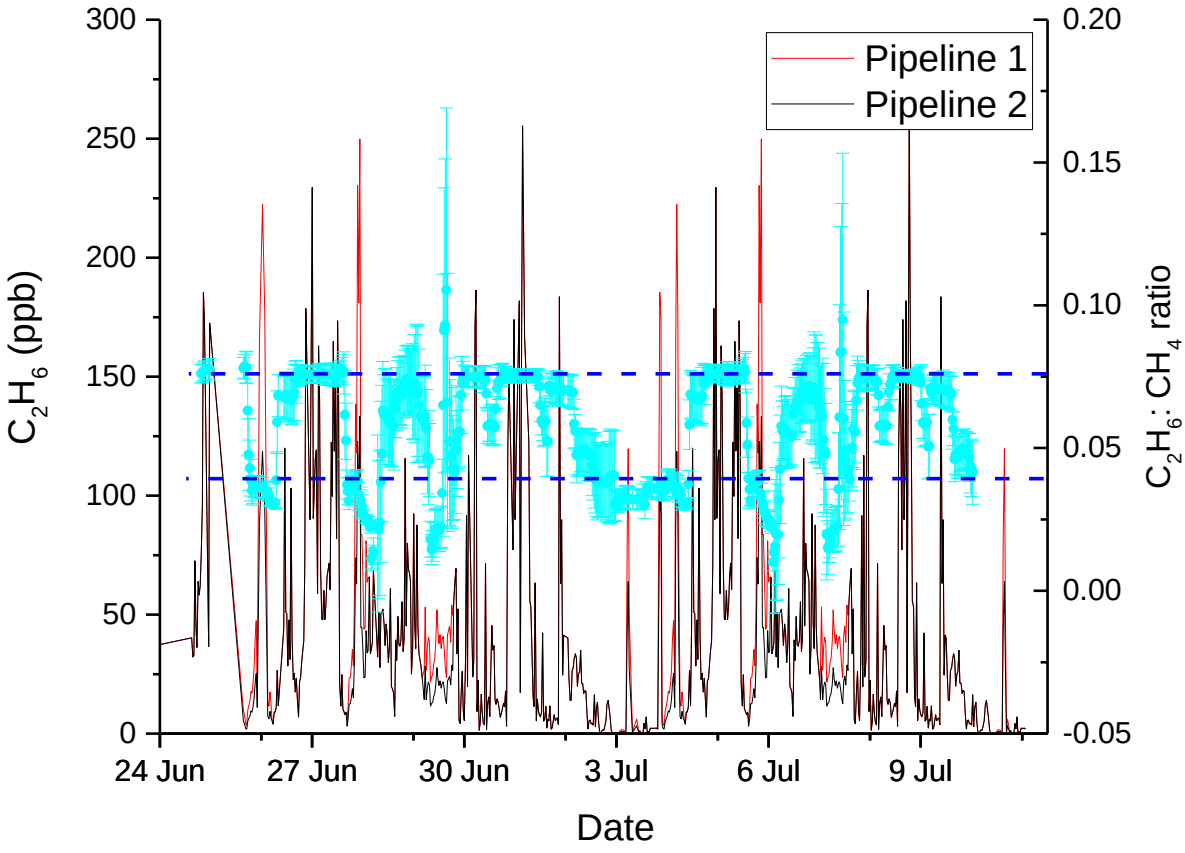

Figure S3.3 Y-axis is the pseudo dataset of C_2H_6 concentration enhancements from Pipeline1 and 2 in red and black, respectively. Light blue markers (right hand y-axis) are the reconstructed C_2H_6:CH_4 ratio of the PC calculated by 10h MC-mACPA. Error bars are the standard deviation from 100 MC simulations. The horizontal dashed lines denote the source signature of pipeline 1 (red) and pipeline 2 (black).

S3.3.4 No. of Variables Included

We find that for both the APCA and PMF models, retaining more species for the analysis does not aid CH_4 attribution and can degrade the modelled CH_4 factors. The MC-APCA tests show that including four CH_4 co-varying species (i.e. other natural gas tracers such as iC_4H_{10}, nC_4H_{10}) results in the best reconstructed CH_4 variability. Increasing the number of NG tracers after this degrades the modelled CH_4

variability. This is probably due to the increase of noise and uncertainties as the number of species augments. The MAD of residuals is reduced from 306 ppb to 137 ppb when using all, or NG related species only respectively. If only NG species are included, CH_4 variability is split between NG components. Nonetheless, when including non-NG related species (e.g. Ethylene, Benzene) only one NG component is detected. Including un-correlated species also results in a reduction of the goodness of fit of modelled CH_4 variability.

The number of species included also affects the PMF modelled factors, residuals increased by a factor of 10 when changing from 3 to 13 species respectively (allocation of 2 and 5 factors respectively). Including species which do not add extra information reduces the goodness of fit primarily due to additional noise and uncertainties which are carried forward to the modelled factors.

Chapter 4 FUGITIVE METHANE SOURCE CHARACTERISATION OF BIOGENIC SOURCES IN THE ILE DE FRANCE REGION.

The fourth chapter of this thesis combines the improved instrumental and data analysis methods for methane source apportionment (the focus of Chapters 2 and 3) and applies them to field measurements of anthropogenic methane emissions from biogenic sources in the Ile de France region. The two major contributors to the biogenic sector are the agriculture (ruminants) and waste (wastewater treatment and landfills) industries. Combined, these aforementioned sources accounted for 74% of anthropogenic methane emissions in France in 2006-2007 according to UNFCCC reporting, and ca. 34% globally for 2000-2012 [Saunois et al. 2016]. As countries are set to reduce greenhouse gas emissions, CH_4 reductions from these sectors will be imperative to reach emission reduction goals. For effective implementation of reduction strategies, CH_4 emissions from these sources, and their temporal changes, must be well understood and characterised. Nonetheless, characterisation of such biogenic sources can be challenging as exact processes are dependent on a number of external factors. For example, in the case of CH_4 emissions from ruminants, the diet, breed, weight etc. will affect the CH_4 emission factor. In the case of wastewater or landfill, CH_4 emissions are known to vary with the type of waste, temperature, treatment processes etc. Furthermore, nation and region specific characterisation of CH_4 sources (and signatures) is rare, thus contributing to large uncertainties in emission factors. Six field campaigns at three major industrial sources are discussed in detail here; an agricultural farm, two wastewater treatment plants and a landfill site were visited for methane measurements. The aim is to characterise ruminant and waste emissions using isotopic analysis, source ratios of co-emitted species and receptor models.

4.1 CHARACTERISING CH_4 EMISSIONS FROM DAIRY FARMING IN ILE-DE-FRANCE

Methane produced by ruminants is estimated to account for half of French CH_4 emissions [Vermorel et al., 2008]. The contributions and emission factors from dairy, beef and growing cattle are known to vary depending on weight, feed, waste management, etc. [Vermorel et al., 2008]. Carbon isotopes can help better identify source contributions when analysing continuous observations e.g. from the French SNO-ICOS (Service National d'Observations – Integrated Carbon Observation System) network and aid inverse modelling estimates. This study aims to facilitate improved understanding and characterisation of

ruminant emissions through the analysis of three measurement campaigns undertaken at an experimental farm in the Ile de France region. Measurements were taken through a mobile campaign with the objective to identify and characterise the on-site CH_4 sources (and their signatures), and 2 'fixed-site' campaigns (in Autumn and Spring) in order to compare emission characteristics between seasons. Results from Chapter 3 indicate that the greatest understanding of emissions from a NG compressor station were achieved through a combination of source apportionment methods. Therefore the same methods (modified for optimal performance) are applied here, combining isotopic and receptor model analysis.

4.1.1 Site Description of the Grignon farm

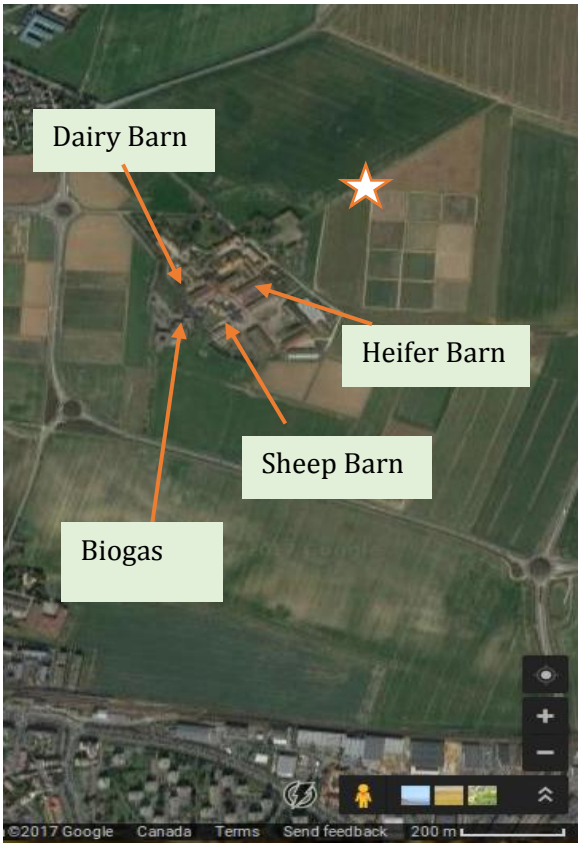

Figure 4.1 Arial image of Grignon farm and surrounding area. The star marks the location of instruments and sample inlet used during the long term measurement campaigns. A small town is approximately 2km South. © Google Maps.

Situated 40km west of Paris, Grignon farm, seen in Figure 4.1, consists of 20 ha of agricultural lands managed by crop rotation of: corn, winter wheat, rapeseed, winter barley and mustard. The croplands surround outbuildings in which ruminants including Holstein Friesian cattle, sheep and goats are housed. Initially, 7 potential CH_4 sources were identified, 4 of which can be seen marked in Figure 4.1. Three barns housing ruminants (productive dairy cattle, non-productive dairy cattle, and sheep), are from here on named Dairy Barn (Image 4.1 and 4.2), Heifer Barn, and Sheep Barn (Image 4.2) respectively. The number of ruminants on the farm varies with time. During the measurement campaigns approximately 166-180 lactating dairy cattle, 12-20 dry cattle, 70-200 non-productive cattle, approximately 600 sheep, and 170 goats were present. The temporal variation of the live weight for each type of ruminant at Grignon Farm is plotted in Figure 4.2. Ruminants in the Dairy Barn are fed different diets to those in the Heifer and Sheep barns. In October and November, productive dairy cows were fed a diet of 31% corn, 19% rapeseed, 18% Lucerne, 12% ground corn, 6% sugar beetroot pulp, 5% hay of Lucerne, 5% barley and 4% other. While the ruminants in the other barns were fed 30% corn, 5% rapeseed, 30% sugar beetroot pulp, 13% hay, and 20% potatoes. During April and May, the diet was changed slightly to 35% corn, 13% rapeseed, 16% Lucerne, 13% ground corn, 9% beetroot pulp, 3% hay of Lucerne, 5% barley, 4% potatoes and 2% other for productive dairy cows and 30% corn, 5% rapeseed, 30% sugar beet pulp, 15% hay and 20% potatoes for ruminants in Heifer and Sheep barns. Overall the C3:C4 plant ratio in each diet does not significantly change between the Autumn and Spring campaign. Dry cattle and a number of young heifers (in total approximately 10-20 cows) are located on pastures surround the farm buildings to the north, west and south. These ruminants feed by grazing on grass biomass. A biogas production unit [Nenufar Biogaz] fuelled from 100% dairy cattle slurry (seen in Image 4.1), and three waste/manure collection points are also found on the farm. Roads border the entire site, a small town is situated 1-2km south of the farm and a recycling centre, including a landfill and wastewater treatment plant, is situated 1.5km to the south-west. The terrain on and around the farm is flat and open.

Following IPCC guidelines, an approximation of the total enteric CH_4 emissions on the farm can be estimated from ruminant weight and IPCC emissions factors. The emission factors for lactating cows, heifers, sheep and goats are 117, 57, 8 and 5 $kgyr^{-1}$ respectively (IPCC, 2007). The emissions in $kgday^{-1}$ during the field campaigns is plotted in Figure 4.2. On average, 104 $kgday^{-1}$ of CH_4 emissions are estimated.

Image 4-1 *Sources are located within close proximity. Dairy Barn, housing containing lactating cows to the left, and the Biogas production unit in the background.*

Image 4-2 (Left) Lactating Holstein Friesian cattle in Dairy Shed 1. (Right) Sheep Shed.

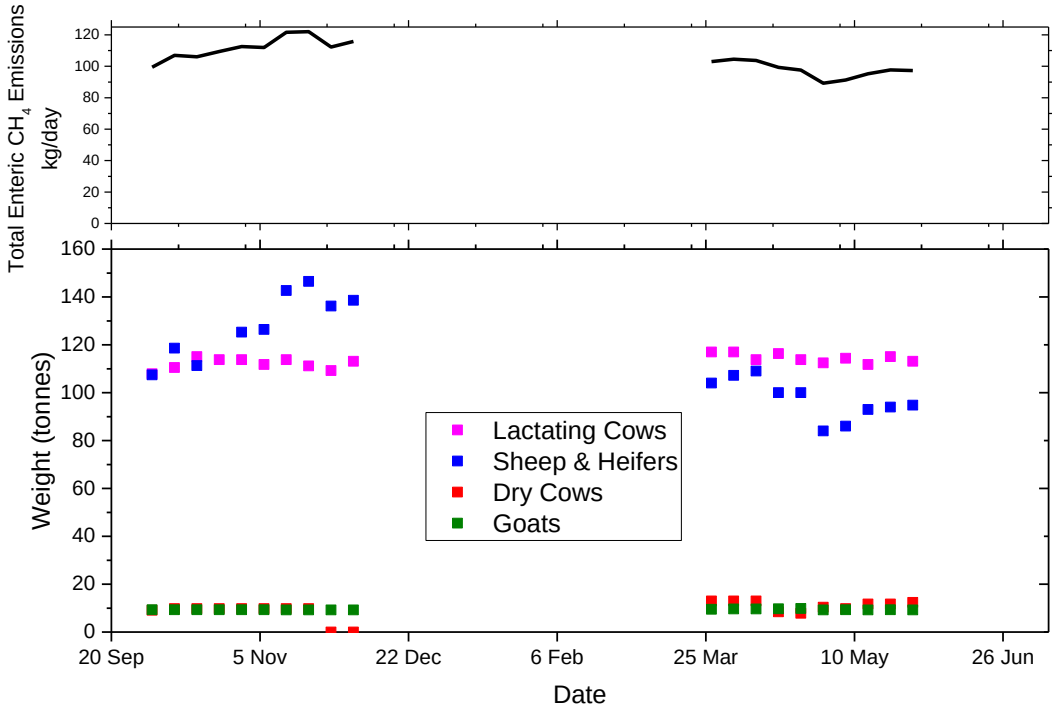

Figure 4-2 (Top) Fluctuation of the expected CH_4 emissions (kg/d) estimated using IPCC Tier 1 method. (Bottom) Weekly measurements of the live weight (metric tonnes) of each ruminant subgroup.

The measurement campaigns at Grignon Farm took place in autumn 2016 (19th Oct - 27th Nov 2016) and spring 2017 (4th April - 2nd of May). Wind data is continuously measured on-site (INRA-Grignon site) from a meteo and flux-tower maintained by ICOS, and can be seen in Image 4.3. Hourly wind speed and direction data at 5m for these two periods is given in Figure 4.3. The predominant wind directions throughout autumn were from the North-East and South West. Generally wind speeds were between 2-6 m/s however speeds up to 14 m/s were recorded. Wind directions during the spring campaign were more evenly distributed across all directions excluding the South and South East however lower wind speeds were recorded, on average between 2-4 m/s with a maximum of 6 m/s.

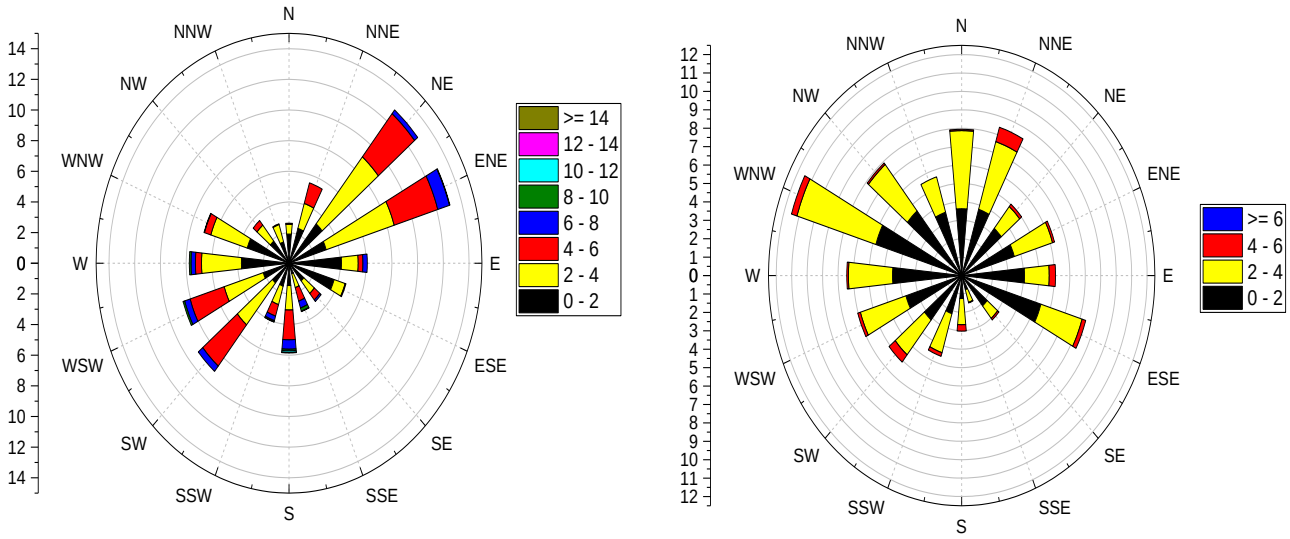

Figure 4-3 Wind Rose for October and November 2016 for the Autumn campaign(left) and April and May for the Spring campaign (right) at Grignon Farm. Frequency is shown on left hand axis as percentage.

Image 4-3 To the left, the building within which the CRDS, and GCs are located during the two long-term measurement campaigns. Instrument inlets are co-located on the roof of the building. The meteo-station and flux tower can be seen on the right-hand side of the image.

4.1.2 Mobile Campaign: 1st May 2017, 9am – Midday

Methods

The purpose of the mobile campaign was to identify the CH_4 sources at Grignon farm to aid source identification during the long-term campaigns and improve the characterisation of ruminant CH_4 sources for emission inventories through high precision isotopic measurements. This objective was reached by installing a CRDS instrument measuring CH_4, CO_2, C_2H_6, and $\delta^{13}CH_4$ (Picarro G2201-I, described in detail in Chapter 2) in a vehicle. The air inlet was fixed to the roof of the car, and ambient air was passed through a Nafion drier (Perma Pure, LLC, Lakewood, USA) followed by magnesium perchloride to ensure the moisture content was consistently < 0.1% H_2O. All power was obtained from a 150Ah lead battery system (Yuasa, Saint-Quentin-Fallavier, France). A picture of the set-up can be seen in Image 4.4. A calibration of all species was performed before and after the mobile campaign spanning -24‰ to -66‰ $\delta^{13}CH_4$, 1.8-3ppm CH_4, 370-500ppm CO_2 and 0.3-3ppm C_2H_6.

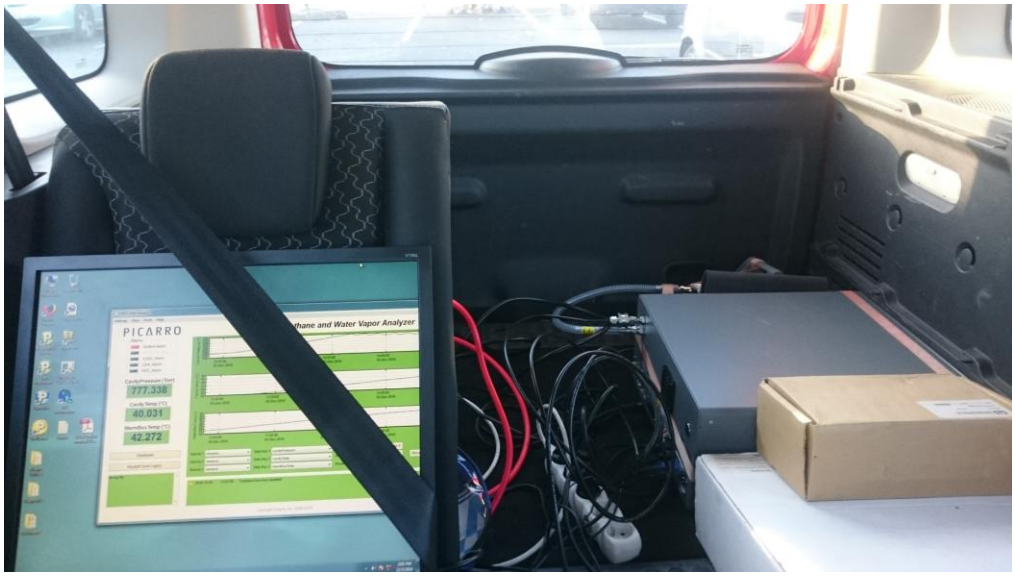

Image 4-4 *Set up for mobile campaign with a Picarro G2201-I.*

The isotopic signatures were calculated for all sources using Miller-Tans plots (see Chapter 3 for details). As a second proxy, the ΔCH_4:ΔCO_2 source signatures (abbreviated to CH_4:CO_2 from here on) were calculated from the slope of the regression of CO_2 and CH_4, again with X and Y errors, much like the method to calculate C_2H_6:CH_4 signatures described in Chapter 2.

Results and Discussion

Highest concentration offsets were measured at the Dairy Barn which at the time housed 173 lactating dairy cows. This barn was passed 3 times; the maximum CH_4 concentration measured was approximately 10ppm (see Figure 4.4). Concentration enhancements from the other ruminant barns were significantly lower. This is expected to be largely explainable by the level of aeration in the barns. The Heifer and Sheep barns are well aerated, thus CH_4 is likely to be instantly diluted whilst the Dairy barn is relatively enclosed and sampling was taken at one of the few openings where air left the barn. The CH_4 emitted from the cattle production system is expected to be approximately 85-90% enteric fermentation and the rest manure [Hindrichsen et al. 2005]. Concentrations measured from liquid and solid manure piles in Grignon were not elevated enough to calculate reliable isotopic signatures.

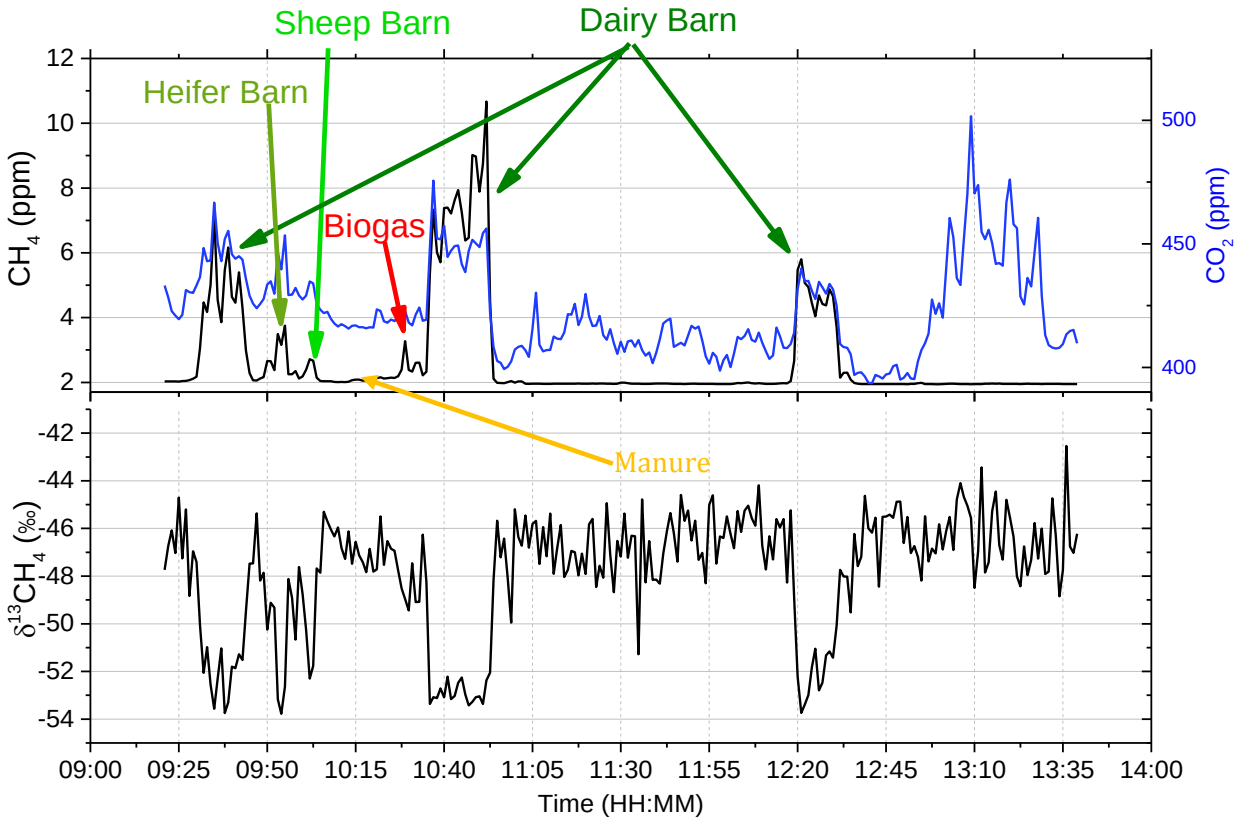

Figure 4-4 Time series of mobile campaign at Grignon Farm. Methane (left axis) and CO_2 (right axis) in top plot, and $\delta^{13}CH_4$ in the bottom plot. The sources identified are annotated with their corresponding measurement times.

The isotopic and CH_4: CO_2 signatures were calculated for the three ruminant barns and the Biogas source, results are displayed in Table 4.1. From the mobile measurement results we find the isotopic signatures of the Dairy Barn, measured as -56.4 $\pm$ 0.7 ‰, is significantly less negative (by approximately 5 ‰) to that of Heifer and Sheep barns (which have the same isotopic signature within the uncertainties), measured as on average -61.5 $\pm$ 1.8 ‰. The isotopic signatures of the Sheep and Heifer barns have a higher uncertainty than the Dairy barn due to low CH_4 concentration enhancements. Methane isotopic signatures of ruminants is known to be affected by their diet [Bilek et al. 2001] as plants can have significantly different $\delta^{13}C$ i.e. -25 ‰ to -29 ‰ for C3 plants and -12 ‰ to -16 ‰ for C4 plants [O'Leary, 1988]. Cattle in the Dairy Barn are fed a 50 %:50 % C3:C4 plant diet, i.e. the feed has a $\delta^{13}C$ of about -19 ‰. Whilst ruminants in the Heifer and Sheep barns have a 70%:30% C3:C4 plant diet, so the feed is estimated to have a $\delta^{13}C$ of ca. -22 ‰. Thus, we expect approximately 3 ‰ difference of respired CH_4, given a constant bacterial fractionation in the rumen [Coleman et al, 1981]. Given the uncertainties associated with our calculations, and possible fluctuations in feed ratio, fermentation rate etc. our measurements are in agreement with the theoretical calculations. Furthermore, the isotopic signatures calculated are similar to results from Levin et al. (1993) which found cattle with 60-80 % C4 diets have $\delta^{13}C$ =-55.6 $\pm$ 1.4 ‰ and C3 only diet as -65.1 $\pm$ 1.7 ‰. The isotopic signature of fugitive emissions from the Biogas plant were measured as -52 $\pm$ 3 ‰, in good agreement with measurements from Levin et al. (1993) which reported -51. 8 $\pm$ 2.8 ‰.

The CH_4: CO_2 signature suggests ruminants in the Heifer and Sheep barns produce more ppm CH_4 per ppm CO_2 than the lactating cattle in the Dairy Barn, signatures are on average 0.067 $\pm$ 0.003 ppm/ppm and 0.143 $\pm$ 0.009 ppm/ppm respectively. Literature of CH_4: CO_2 for dairy cows consistently report ratios similar to these Heifer barn values; Lee et al. (2017) calculate approximately 0.07 ppm/ppm, Bjerg et al. (2011) calculate ratios between 0.05 and 0.08 ppm/ppm, and Rentrop [2007] reports 0.07 ppm/ppm while Haque et al. (2014) measured on average 0.09 ppm/ppm and found that CH_4: CO_2 is not variable with diet composition, but can vary between individual cows. Given that around 180 cows were present in the stable we can assume that the variability of individual animals does not significantly change the mean CH_4:CO_2 ratio. As the CH_4: CO_2 ratio from the Dairy barn is significantly larger than the literature there may be an influence of CH_4 originating from manure. Assuming the CH_4: CO_2 ratio of fresh manure is approximately 1.5 ppm/ppm [Williams, 1992], and that on average the lactating cattle have the same ratio as the heifers (0.068 ppm/ppm), we calculate manure contributes to 5.5% of the CH_4 measured from the Dairy barn. This value is in good agreement with a study by Kinsman et al., (1995) in which

manure emissions were calculated to contribute to 5.8% of CH_4 emissions for a dairy cattle barn. Recalculation of the isotopic signature for pure eructated methane from lactating cattle is therefore -57.3 ‰ (assuming $\delta^{13}C$ of animal waste is -45.5 ‰ [Levin et al. 1992]). As the CH_4: CO_2 signature expresses the efficiency of microbial fermentation into CH_4 [Madsen et al. 2010], combing these two parameters can create a source characterisation plot, as seen in Figure 4.5, which may be crucial when interpreting the results from the two month-long field campaigns at the fixed site.

Table 4-1 Results of source signatures from the mobile field campaign at Grignon Farm

Location	Isotopic Signature (‰)	CH_4 :CO_2 Signature (ppm/ppm)
Dairy Barn	-56.4 ± 0.7	0.143 ± 0.009
Heifer	-63.9 ± 3.5	0.068 ± 0.003
Sheep	-60.6 ± 2.2	0.064 ± 0.004
Biogas	-52 ± 3	0.2 ± 0.2

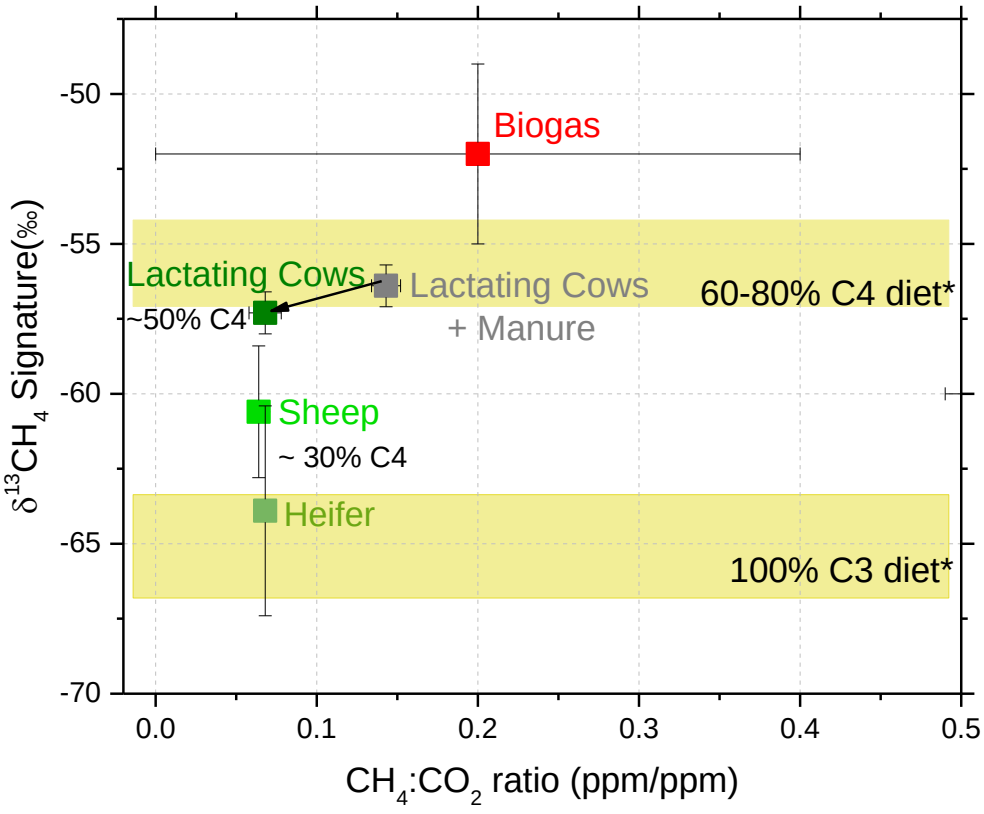

Figure 4-5 *Methane source characterisation plot from mobile campaign at Grignon Farm. $\delta^{13}CH_4$ signature on the y-axis and CH_4: CO_2 source ratios on the x-axis. Highlighted bands are $\delta^{13}CH_4$ results from *Levin et al. (1993)*

4.1.3. Autumn Field Campaign: 19th Oct – 27th Nov 2016

Methods

The objective of longer, fixed-site measurement campaigns was to gain an understanding of the temporal variation of predominant CH_4 sources at Grignon farm. Using source apportionment techniques such as methane isotopic measurements and correlations with VOCs, we attempt to distinguish between CH_4 concentration enhancements from on-site (such as biogas and ruminant sources) and off-site (e.g.traffic) activities.

The following species were measured continuously during the autumn campaign: CH_4, CO_2, C_2H_6, $\delta^{13}CH_4$, and $\delta^{13}CO_2$ using the same CRDS instrument (G2201-i) as in the mobile campaign. To dry the ambient air to <0.1% H_2O a combination of Nafion dryer and magnesium perchlorate was placed before the instrument inlet. Every two days, 20 minute measurements of two calibration gases were made to calibrate CO_2 and CH_4 data and another working gas was measured every 12 hours and used as a target gas. A calibration for isotopic measurements was run prior and post the field campaign and the working gas measurements during the campaign were used to track any drift in the isotope measurements. VOCs were measured using proton transfer reaction mass spectrometry (PTR-MS) and gas chromatography (GC + FID). Calibration of the GC-FID was performed at the beginning of the campaign with a NPL (National Physical Laboratory, Tedington, UK) standard. Calibration of selected compounds was made for PTRMS with a GCU unit and its internal standard (Ionikon, Innsbruck, Austria). A list of the VOCs measured can be seen in Table 1.3. All instruments were installed in the same building (see Image 4.5) approximately 400m from the farm outbuildings. The building is marked by a star in Figure 4.1, and can be seen in Image 4.3 with co-located inlets approximately 4m above ground level.

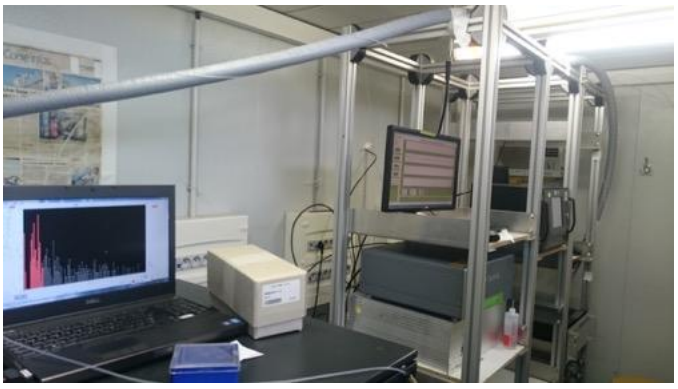

Image 4-5 Inside the instrumental building seen in Image 4, the GC (left) and CRDS instruments (right) can be seen in operation.

Following the successful source apportionment presented in Chapter 3, here the same CH_4 identification methods are implemented: CH_4 isotopic analysis, principle component analysis and positive matrix factorisation. All methods have been discussed extensively in Chapter 3, therefore only certain details, that are specific modifications for this application will be discussed here.

Analysis of continuous $\delta^{13}CH_4$ and CH_4:CO_2 ratio

To calculate the isotopic signatures of CH_4 concentration peaks, the moving Miller-Tans plot method (as described in Chapter 3) was implemented with the criteria of a simultaneous increase of 5 ppb CH_4 or greater, and change in $\delta^{13}CH_4$ greater than 0.7 permil. Only data points corresponding to an increase in CH_4 concentrations were used for the linear regression and only regressions with $r^2 > 0.9$ were accepted. As a complimentary tracer, the CH_4: CO_2 ratio source signatures were simultaneously calculated during the same periods. This tracer ratio was chosen as there is a known correlation in the respiration of ruminants, as confirmed from the mobile field campaign results. The calculated ratios were influenced by the large daily concentration variations present in the CO_2 time series (less present for CH_4), due to regional sources and the daily cycle of atmospheric mixing present. This is evident from Figure 4.4, in which CO_2 concentrations are seen to increase significantly whilst no CH_4 enhancements are measured. For this reason, to allow investigating the signatures of the short-term concentration increases which are due to more local sources, the average diurnal cycle of CO_2 and CH_4 was removed before calculating the ratio. The lower envelope of the diurnal cycles was fitted using a percentile filter with a 20-hour window at the 10^{th} percentile. The uncertainty was estimated as the RMS difference between the resulting time series calculated using the percentile filter or a high pass filter to model the daily cycle. For the calculation of CH_4: CO_2 ratios, regressions with r^2 greater than 0.8 were accepted. The error was estimated from the 1000 run MC simulation.

Receptor Models

Two types of PCA were implemented; MC-APCA and 10h MC-mAPCA for long and short term source apportionment respectively. The subset of species included in the APCA analysis were as follows: CH_4, CO_2, C_2H_6 and C_3H_8. This subset contains only a small selection due to the lack of correlation of CH_4 with the other measured species, and driven by the necessity of CH_4 variability being a major contributor to the principle component. Model details are the same as described in Chapter 3, with the exception of certain modifications to the 10h MC-mAPCA:

a) Only components with a significant contribution from CH_4 (CH_4 contribution > mean contribution of all variables) were used.

b) Only the principle component was reconstructed (sensitivity studies described in the supplementary material of the Chapter 3 demonstrate reconstruction of the 2nd + components are not reliable).
c) Diurnal cycles of CO_2 and CH_4 were removed before analysis (same method as above) in order to facilitate the calculation of the CH_4: CO_2 source ratio of the principle component.

Finally, we apply the PMF receptor model from EPA. Details of this model are also discussed in Chapter 3. The following variables were selected for PMF: CH_4, CO_2, C_2H_6, C_3H_8, Ethylene, Propene, Acetylene, and N-Hexane. Certain variables such as Trans-2-Butene and Cis-2-Butene were excluded from the analysis due to very low concentration enhancements. The dataset was then trimmed further by excluding i-Butane, n-Butane, i-Pentane, n-Pentane and 2-Me-Pentane as these variables were not correlated with CH_4 and their inclusion did not improve the source apportionment of CH_4.

Results & Discussion

Observed concentrations and variability

In total, 40 days of CH_4 measurements were made at Grignon farm in Autumn 2016, 30 of which simultaneously measured 17 VOCs: Ethane, Ethylene, Propane, Propene, i-Butane, n-Butane, Acetylene, Trans-2-Butene, X1.Butene, i-Pentane, n-Pentane, X1.3-Butadiene, Trans-2-Petene, X.1-Penetene, X2.ME-Pentane and n-Hexane. Mean and standard deviation of CH_4 and CO_2 concentrations throughout the campaign were 2.05ppm and 0.18ppm for CH_4 and 431ppm and 20ppm for CO_2 respectively. Maximum concentrations observed for 30 minute averages were 4ppm and 512 ppm for CH_4 and CO_2 respectively. Methane concentrations were not significantly correlated with any of the other measured gases (Pearson's R is less than 0.5) which can also be seen from the time series in Figure 4.6 in which the temporal variation of CH_4 concentration enhancements is not in agreement with the other measured species. Methane concentration peaks are short lived and sporadic with minimal diurnal variation when compared to CO_2.

The highest frequency of data was measured during West and South-Westerly wind directions; the majority of elevated CH_4 concentrations occur during South and particularly South-Westerly winds as shown in the pollution rose in Figure 4.7. The polarplot in Figure 4.7 models the mean CH_4 concentration with respect to wind speed and direction. In agreement with the pollution rose, elevated mean CH_4

enhancements are measured during winds from the South-West at speeds between 0-6m/s. The strongest enhancements occur at lower wind speeds suggesting the CH_4 sources are local.

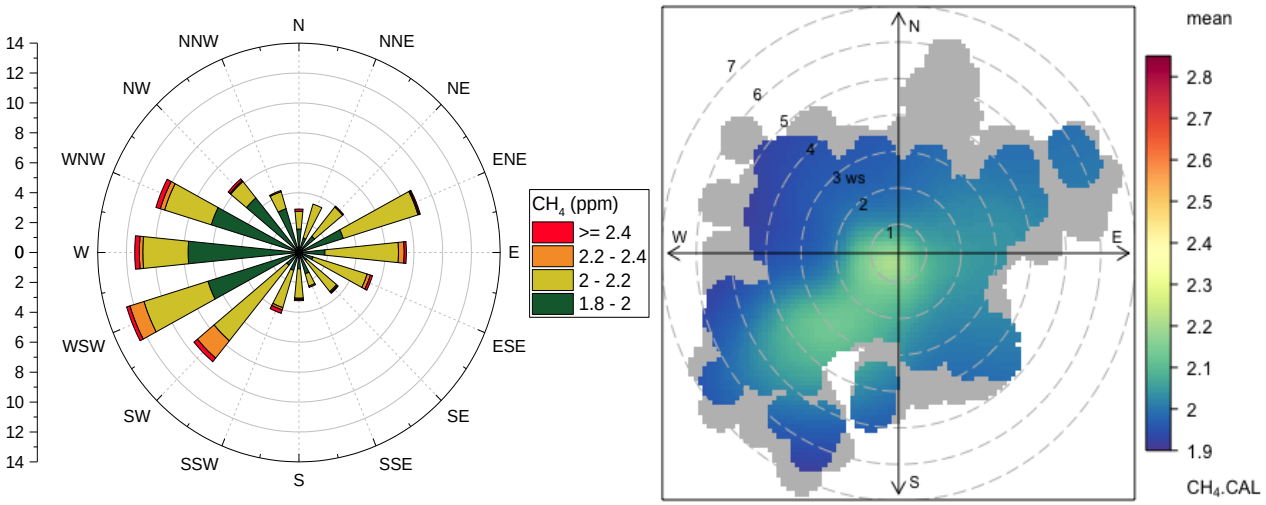

Figure 4.6 (left) Methane excess rose at Grignon during the Autumn 2017 campaign. Y-axis signifies the count. (right) Polar plot of mean CH_4 concentration with respect to wind speed and direction. Coloured bins require 2 or more data points. Grey areas signify single data points.

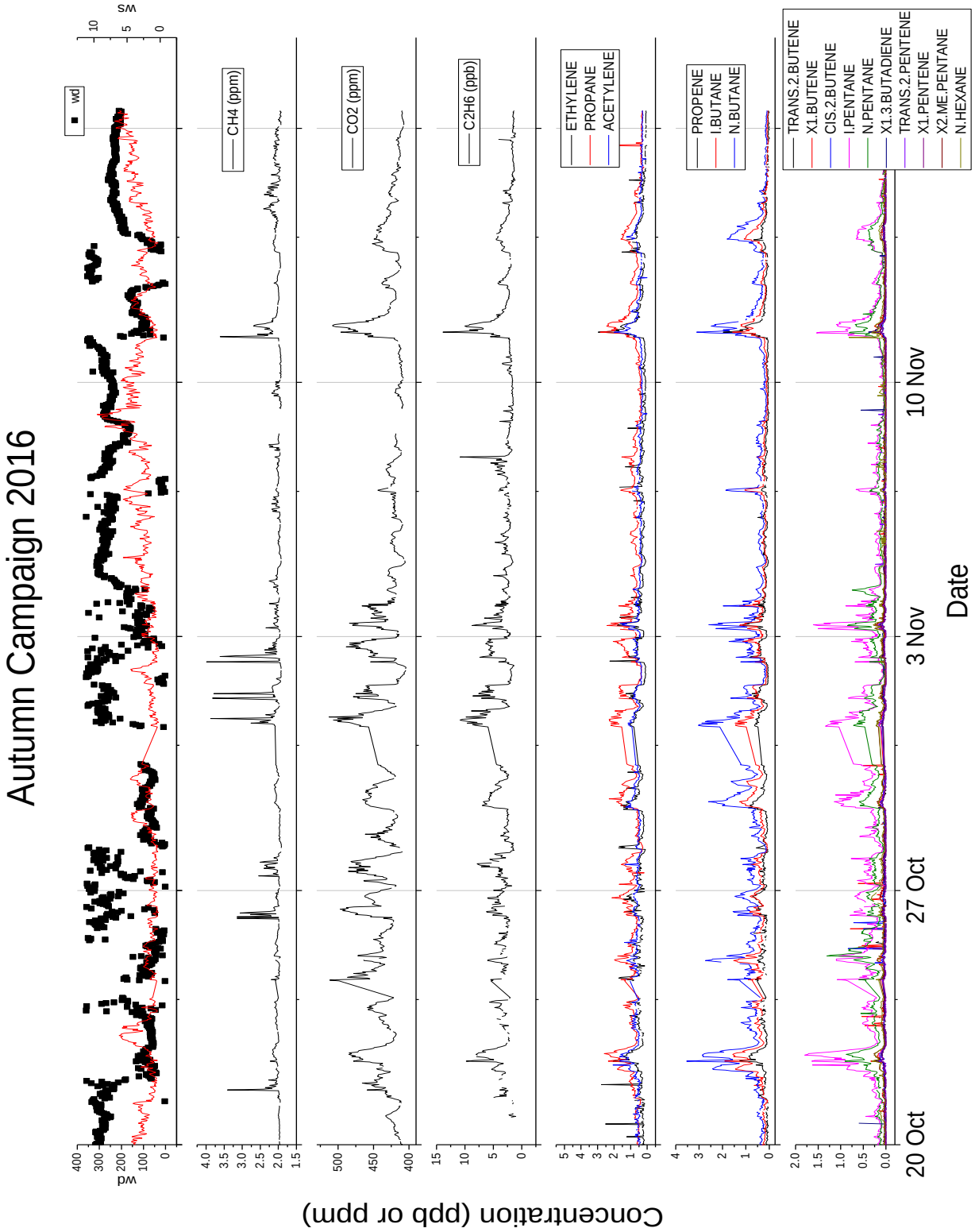

Figure 4.7 Time series data of the variables measured during the Autumn 2017 measurement campaign at Grignon Farm. Wind speed is in m/s. Methane and CO_2 are plotted in ppm units while all other VOCs are plotted in ppb units.

Source Signature measurements: Isotopic & CH_4: CO_2

The time-series of methane isotopic measurements can be seen in Figure 4.8; the mean, standard deviation, minimum and maximum values measured during this period were -47.7 ‰, 0.7 ‰, -54.8 ‰ and -46.4 ‰ respectively. The majority of CH_4 concentration enhancements are correlated with lighter periods of $\delta^{13}CH_4$. The time-series of isotopic signatures calculated from the moving Miller Tans method is plotted in Figure 4.8. In total, 24 isotopic signatures of CH_4 enhancement were calculated, with a mean of -56.5 $\pm$ 5 ‰, strongly suggesting a predominantly biogenic CH_4 source similar to that of the Dairy Barn (lactating cows and manure). Five CH_4 concentration peaks are isotopically similar to the Dairy Barn/lactating cows, whilst two are suggestive of Heifer and Sheep emissions. The majority of values are too uncertain (caused by very low concentration enhancements) to distinguish between such similar biogenic sources. The majority of Miller-Tans plots consist of between 3-5 data points, indicating short lived CH_4 enhancements lasting approximately 30-50 minutes. This is likely due to changing meteorological conditions. Figure 4.9 shows the spread of $\delta^{13}CH_4$ signatures with wind direction. Lightest $\delta^{13}CH_4$ are measured during southerly winds with an average of -65 $\pm$ 2 ‰, whilst the signature is seen to be less negative during winds from the West or North. This can be explained by cattle on pastures to the South and Heifers in the South-West, both of which are expected to have lower $\delta^{13}CH_4$ signatures than the lactating cattle which are located West-South-West of the instruments. One isotopic signature measured on the 12th of November was found to be significantly heavier than the average, with $\delta^{13}CH_4$ of -41$\pm$ 6 ‰. More information is required to identify the methane enhancement is due to manure or possibly a fossil fuel source.

The secondary proxy, the CH_4: CO_2 ratio signatures, were calculated during the same CH_4 enhancement periods and display on average 0.02 $\pm$ 0.02. Such ratios are lower than expected, and do not correlate with the ratios measured at the ruminant barns during the mobile campaign. This can be attributed to strong CO_2 concentration variations from other processes (e.g. uptake or variations in background concentration) which lead to an irregular daily CO_2 cycle. Thus resulting in an imperfect fit of the daily cycle, which prevents the calculation of the ratio based on the excess CO_2 alone.

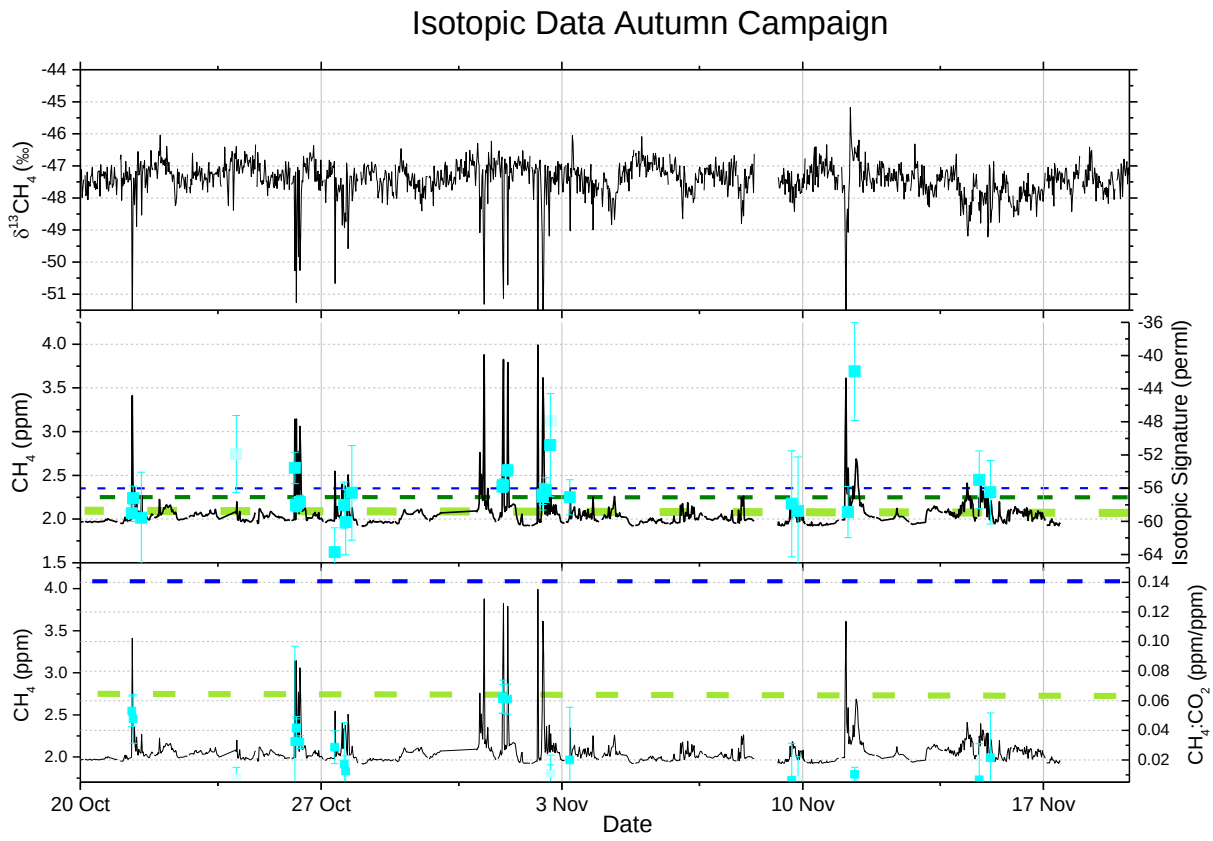

Figure 4.8 Isotopic Data from Autumn Campaign at Grignon. (Top) Time series of CH_4 isotopic measurements during the autumn campaign at Grignon Farm. (Mid) Isotopic signature (right-hand axis, light blue points) superimposed on the CH_4 time series (black) calculated using the moving Miller-Tans method. (Bottom) CH_4: CO_2 ratio of CH_4 concentration enhancements (right-hand axis, light blue points). Dark and light green dashed lines signify the $\delta^{13}CH_4$ signature calculated from the mobile measurement campaign for lactating cows, and the average of Heifer & Sheep emissions respectively. Dark blue signifies Dairy Barn 1 (i.e. lactating cows influenced by manure emissions).

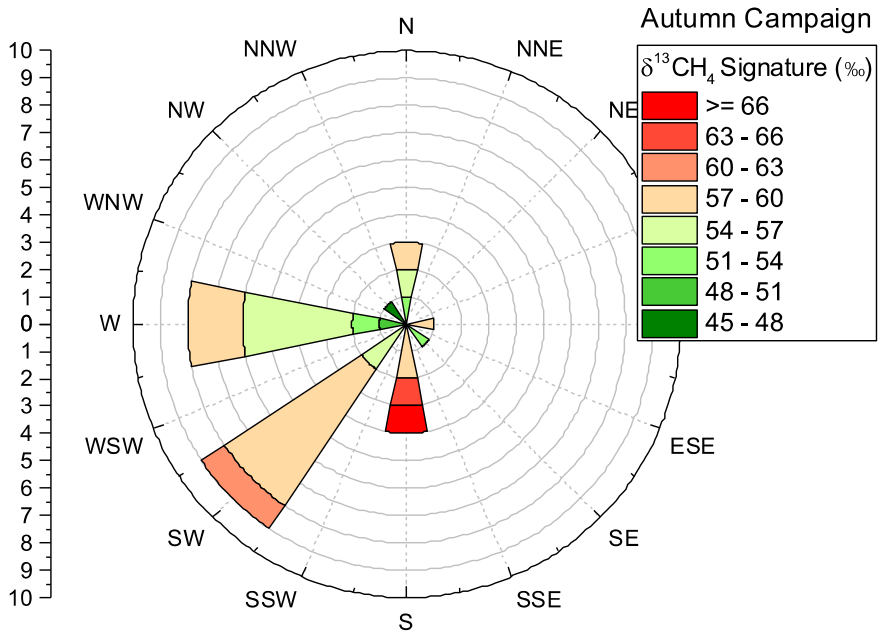

Figure 4.9 Isotopic signatures of CH_4 concentration enhancements calculated from the moving Miller-Tans plots by wind direction.

Analysis using receptor models

The isotopic analysis describes only a portion of the data. From the work described in Chapter 3 it was found that the use of receptor models can aid in describing the characteristics of CH_4 sources, both by using moving APCA to build on the short-term analysis of isotopic data, and long term analysis from APCA and PMF which provides an overview of the predominant CH_4 sources.

APCA

Application of the MC-APCA model on the selected dataset suggests two principle components. The first describes 64% of the total concentration variance, predominantly explaining CO_2, C_2H_6 and C_3H_8, (with some contribution to CH_4) variation. This component describes the daily cycle due to atmospheric mixing and therefore includes all variables. The second component explains 28% of the total concentration variance, and approximately 60% of CH_4 concentration enhancements. Its temporal variation is very well correlated with that of the CH_4 data. This component has little contribution from other species, suggesting that the CH_4 source is not correlated with CO_2, C_2H_6 or C_3H_8.

Short-term variation of the C_2H_6:CH_4 and CH_4:CO_2 ratios calculated from the reconstructed principle component modelled by the 10h MC-mAPCA is plotted in Figure 4.10. Gaps in the ratios occur when CH_4 is not the dominant species explained by the principle component. Furthermore, highly varying ratios or ratios with greater than 100% uncertainties were also omitted. Ratios calculated during periods with no CH_4 concentration enhancements can be particularly high and do not necessarily represent a CH_4 source. Overall, we find much of the CH_4 concentration enhancement periods un-modelled. In particular, the reconstructed CH_4:CO_2 ratio is sparse, which is due to the large uncertainties carried forward from the diurnal cycle fitting. Nonetheless, C_2H_6:CH_4 and CH_4:CO_2 ratios calculated during CH_4 peaks are generally between 0 and 0.02 and 0 and 0.1 respectively. This is as expected from the biogenic CH_4 sources located on the farm.

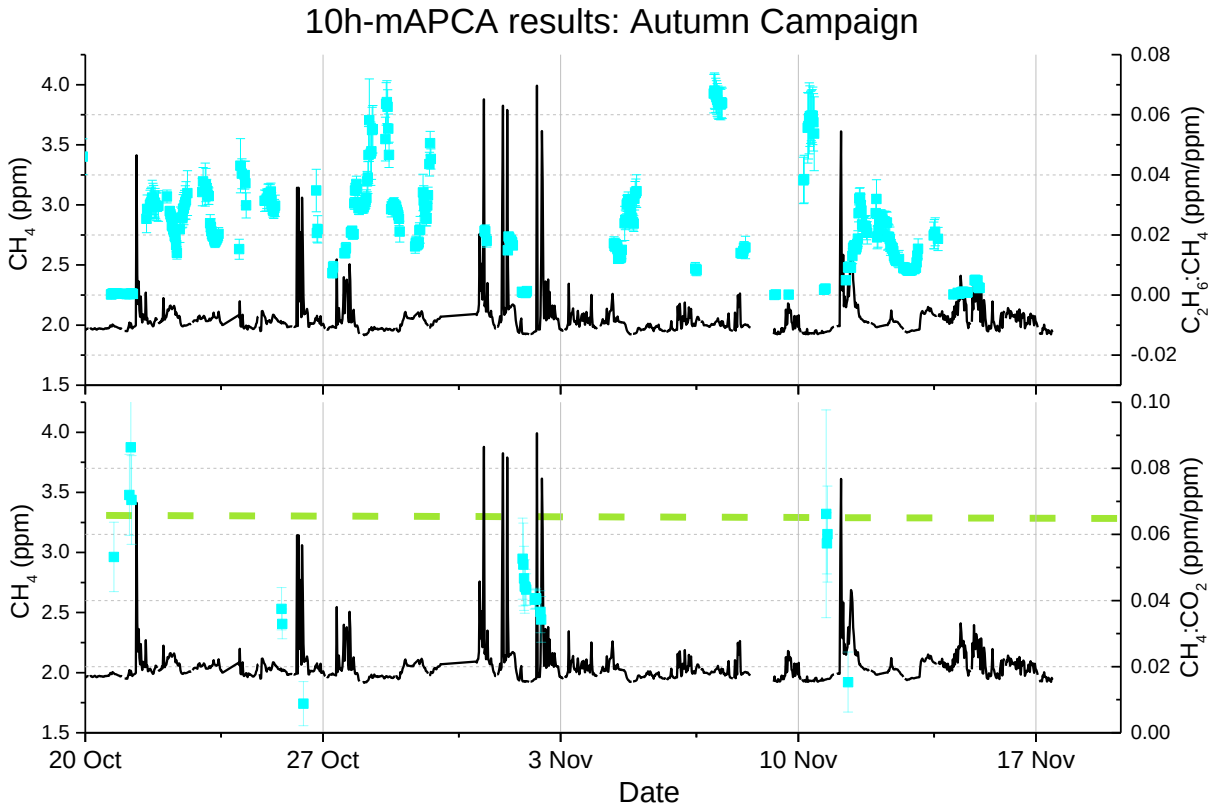

Figure 4.10 10h-mAPCA reconstructed ratios of the Principle Component calculated during the autumn campaign at Grignon Farm. X-axis is the time-series of CH_4. Z-axis is: Top) C_2H_6:CH_4 ratio. Bottom) CH_4: CO_2 ratio. Green dashed line signifies ruminant emissions measured during the mobile field campaign.

PMF

For an initial idea of the number of factors (sources) to include, APCA was applied to the dataset selected for PMF (inclusion of a greater number of species than the MC-APCA datset). Results suggested between 2 to 4 principle components. Applying PMF, 4 factors were found to provide the optimal solution. Ethylene was the component least well modelled; the r^2 of the regression of oberseved vs modelled concentrations was greater than 0.75 for all variables bar ethylene for which r^2 was 0.47.

Carbon dioxide comprised the majority of Factor 1 with small contributions from CH_4, propene, propane, ethylene and ethane. The contribution of CH_4 is associated with large DISP and BS error (uncertainty of concentration ranges between 10^{-1} and 10^{-4} ppm). The temporal variation suggests strongly that this factor is associated with the diurnal cycle at Grignon. Factor 2 describes most VOCs; namely ethane, ethylene, propane and acetylene, thus suggesting contributions from a fossil fuel source. Its temporal variation shows some contributions from a daily cycle with certain more sporadic emission peaks. Here large DISP and BS errors are again associated with CH_4, but more notably with CO_2 whose concentration uncertanty is between 10^{-4} and 1 ppm. Factor 3 is the component attributed to 90% of CH_4 variability

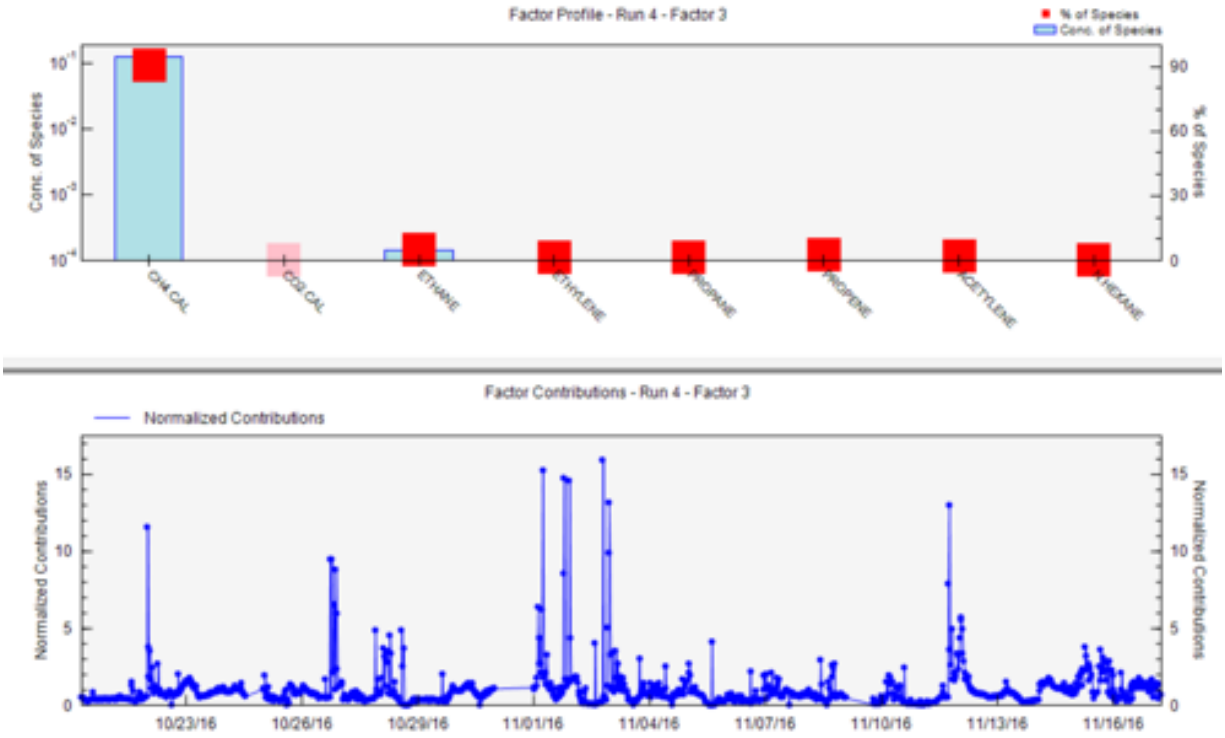

Figure 4.11 PMF results for autumn campaign at Grignon: Factor 2 profile [biogenic CH_4 factor. Top) concentration and percentage of species contributing to the factor. Bottom) temporal variation of normalised contributions of factor.

and does not include significant contributions from other variables. However error estimation for CO_2 is again large suggesting concentrations between 10^{-4} and 10 ppm. Factor 4 describes some CH_4 variability (concentration uncertainty estimation suggests between 10^{-4} and 10^{-2} ppm), but predominantly describes n-hexane with small contributions from other VOCs. Correlation of CH_4 and n-hexane suggests the source is derived from petrol or traffic. The contribution and concentration of each species, for the dominant CH_4 factor (Factor 3) is plotted in Figure 4.11. Factor contributions for Factors 1,2 & 4 can be found in Appendix C. When examining the rotational ambiguity, Factors 1,2 and 4 were found not rotationally ambiguant. To investigate further, Fpeak rotations between -1.0 and 1.5 were applied. A rotation of Fpeak -0.5 significantly improved the rotational ambiguity of the 4 factors. The rotated results suggest CH_4 contributes to 3 factors: Factor 1 (CO_2 factor), 2 (VOC factor) and 3 (biogenic CH_4 factor) contributing to 3%, 32%, and 65% of CH_4 respectively.

4.1.4 Spring Field Campaign: 10th of April until the 1st May 2017

Methods

In order to assess the temporal variation, if any, of the CH_4 sources and source signatures at Grignon farm we conducted a second field campaign during the spring season. Continuous measurements of CH_4, CO_2, C_2H_6, $\delta^{13}CH_4$, and $\delta^{13}CO_2$ using a CRDS instrument (G2201-i) were made. VOCs were measured using PTR-MS and GC-FID. At the time of writing only alkane data measured by the GC-FID is available for analysis, thus the following VOCs are discussed here: C_2H_6, C_3H_8, i-C_4H_{10}, i-C_5H_{12} and n-C_5H_{12}.

The instrument location, set up and calibration was the same as described in the autumn campaign: all instruments installed within the same building (marked by a star in Figure 4.1) and with co-located inlets approximately 4m above ground level.

The methods used to analysis the data gathered during the spring campaign follow the same protocol as those described previously for the Autumn campaign.

Results & Discussion

Observed concentrations and variability

A record of the variables measured during the spring measurement campaign at Grignon Farm in 2017 can be seen in Figure 4.13. Methane shows short term concentration variations, in which peaks can typically reach between 3 to 5 ppm. Carbon dioxide measurements display a strong diurnal cycle throughout the duration of the field campaign, which is not as evident in the CH_4 time series. As with the autumn campaign, there is no evident temporal correlation between CH_4 and the other measured gases; Pearsons R correlation coefficient is below 0.5 for all gases. The alkanes included in the analysis are often used as tracers for fossil fuel emissions, thus suggesting the CH_4 concentration enhancements measured on site are not strongly correlated with such a source.

The highest frequency of measurements were recorded during north and north-westerly winds. From these directions, low CH_4 concentration enhancements were recorded, on average between 1.8-2.1 ppm. Highest CH_4 concentrations were measured during south-westerly wind directions, as can be seen in the pollution rose in Figure 4.12. A more complete understanding of the distribution of CH_4 sources can be gained from the polarplot in Figure 4.12 in which mean CH_4 concentration is plotted according to wind speed and direction. The plot indicates a methane 'hotspot' located in close proximity, southwest of the measurement station. Thus suggesting the farm outbuildings are the main source of CH_4 emissions.

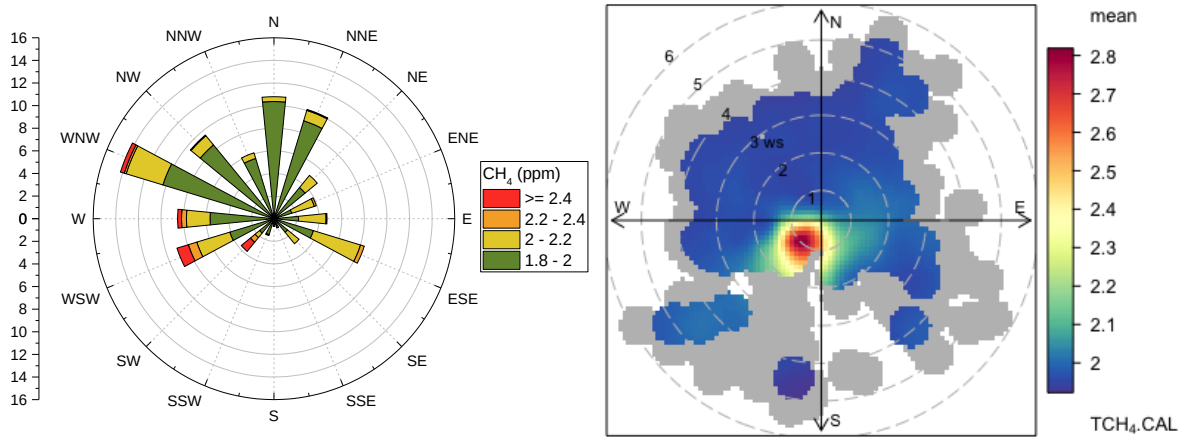

Figure 4.12 (left) Methane pollution rose for spring campaign at Grignon. X-hand axis is the count. (right) Polar plot of mean CH_4 concentration with respect to wind speed and direction. Each bin has 2 or more data points, grey bins have only one data point.

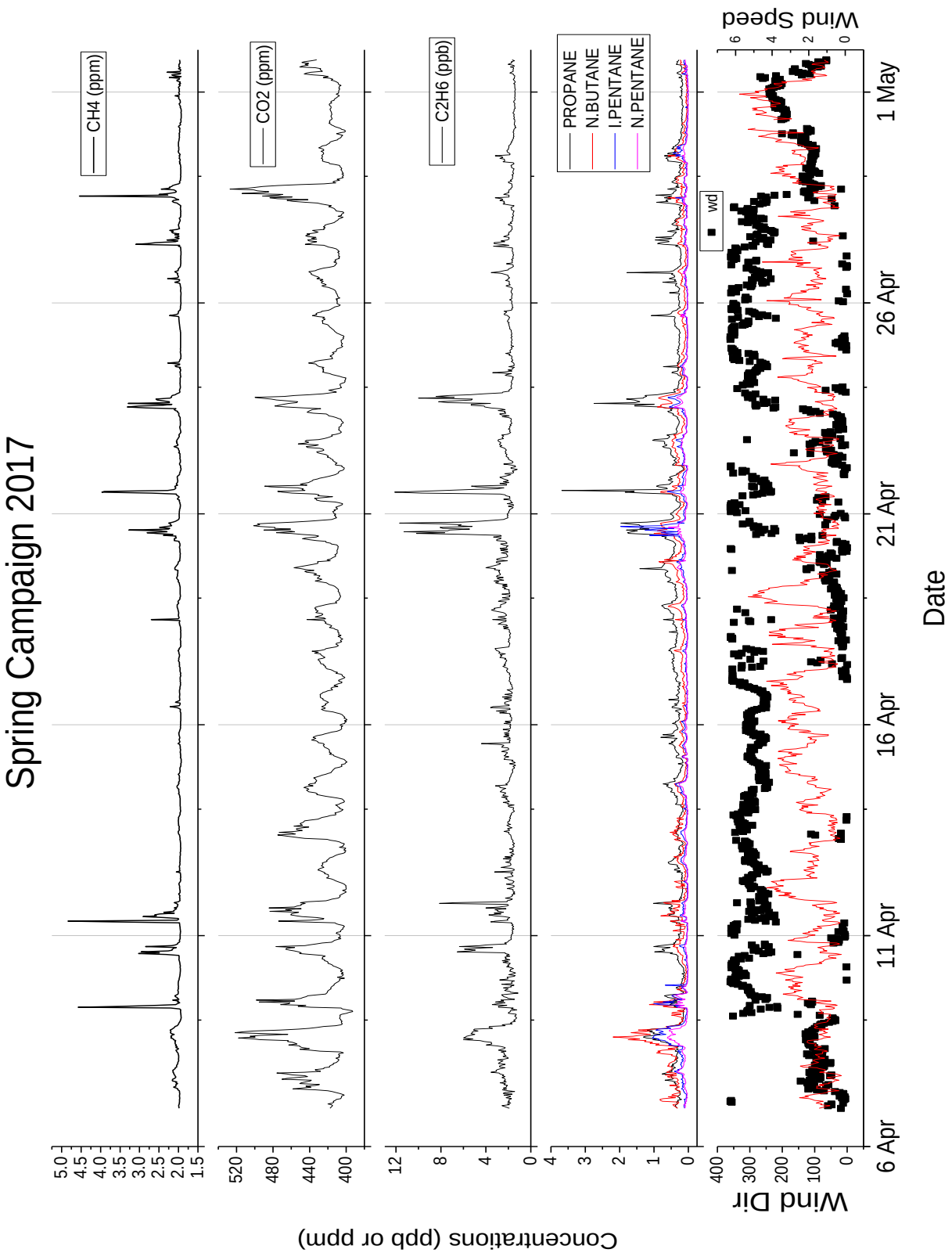

Figure 4.13 Temporal concentration data of the species measured during the spring measurement campaign at Grignon Farm. From top to bottom: CH_4, CO_2, C_2H_6, VOCs (Propane, n-Butane, i-Butane, i-Pentane, n-Pentane) and wind direction (black) and speed in m/s (red, z-axis).

Source signature measurements: Isotopic & CH4:CO2

The temporal variation of $\delta^{13}CH_4$ is plotted in Figure 4.14 (top). Negative changes in the isotopic data are correlated with peaks of CH_4 concentrations, the largest change in $\delta^{13}CH_4$ was measured on the 11th of April in which $\delta^{13}CH_4$ dropped from background levels of -48 ‰ to -55 ‰. The $\delta^{13}CH_4$ signatures of the CH_4 concentration peaks calculated from the moving Miller-Tans plot method are plotted alongside the CH_4 concentration time series in Figure 4.14 (middle). In total, 35 $\delta^{13}CH_4$ signatures were calculated. The average and standard deviation is -60 ‰ and 4 ‰ respectively. All of the $\delta^{13}CH_4$ signatures calculated are suggestive of biogenic sources. Overall a larger number of CH_4 enhancements are isotopically more similar to the heifers and sheep than lactating cows. Throughout the spring campaign a number of the $\delta^{13}CH_4$ signatures calculated are lighter than that measured for ruminants during the mobile campaign. A particular outlier, the peak on the 21st of April, has a $\delta^{13}CH_4$ signature of -70.9 $\pm$ 2.9 ‰. Although significantly lower than the mobile campaign measurements, we suggest the source is cattle on pastures

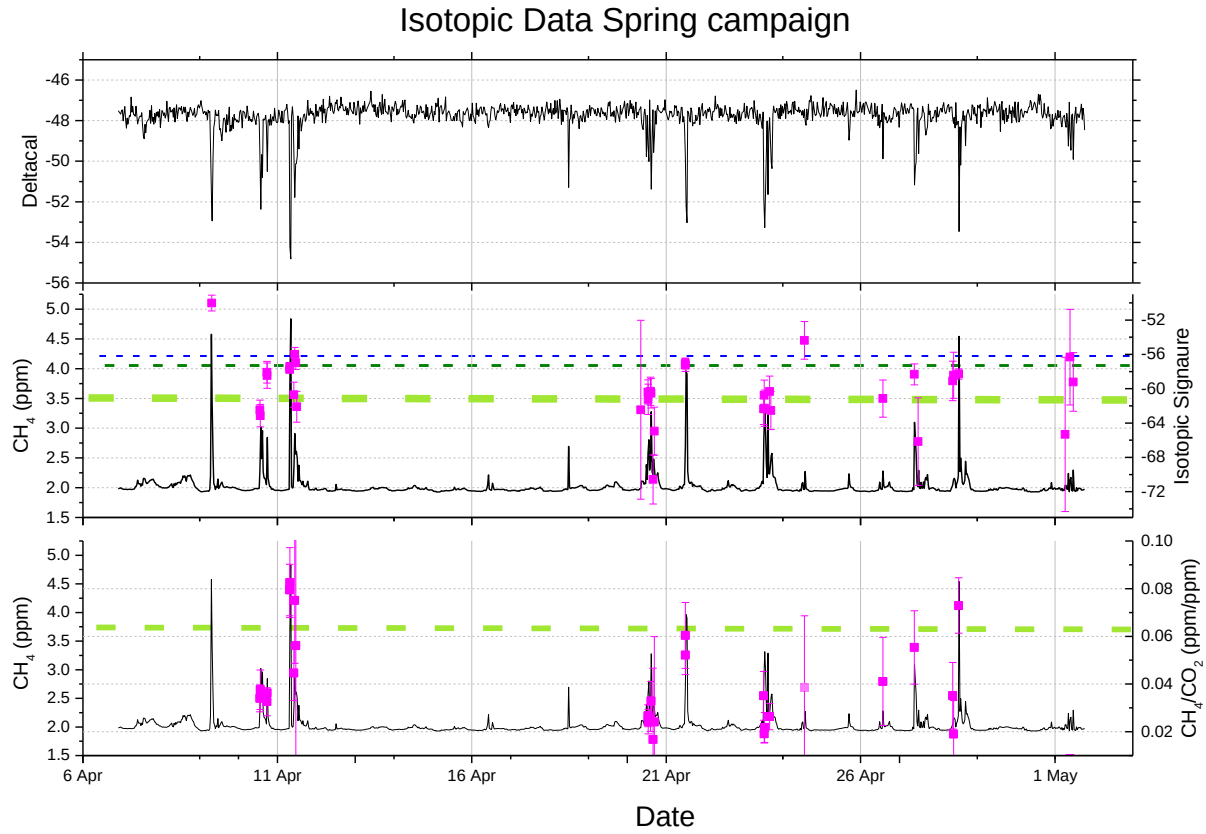

Figure 4.14 Isotopic data measured during the spring Grignon field campaign. From top to bottom, the time series of $\delta^{13}CH_4$, the time series of CH_4 with corresponding $\delta^{13}CH_4$ signatures (right hand axis) calculated from moving Miller-Tans plots, and the time series of CH_4 with corresponding CH_4:CO_2 source ratio (right hand axis). Green horizontal lines are measured values for biogenic sources (Heifers in light green, lactating cows in dark green. Blue dashed line signifies the manure contaminated measurement.

(diet as 100% C3, thus lighter $\delta^{13}CH_4$ is expected) or possibly liquid manure (reported as -73.9 $\pm$ 0.3 ‰ by Levin et al. (1993)) as wind speeds were less than 2m/s indicating a local source from the WSW. In general, between 3 to 5 points were used in the regression, i.e. short lived methane peaks of between 30 to 50 minutes. In Figure 4.15, the calculated $\delta^{13}CH_4$ signatures are plotted with respect to wind direction. This plot explains that more negative biogenic CH_4 source signatures are measured during winds from the southwest than west. We expect this to be due to the location of ruminants as explained above in the autumn campaign.

There are 30 CH_4:CO_2 signatures calculated for the same time period and are plotted at the bottom of Figure 4.15. Here the results are less affected by diurnal CO_2 as it is more regular during this season thus allowing for a better fit and removal from the CO_2 time series using the percentile filter. The majority of CH_4:CO_2 ratios are between 0.02 and 0.08, with a minimum of 0 $\pm$ 0.005 and a maximum 0.08 $\pm$ 0.01. The results suggest a source similar to that of ruminants (plotted as the light green dashed line in Figure 4.15). Haque et al., (2013) and Kinsman (1995) found that CH_4:CO_2 ratios can vary throughout the day, which many explain some of the CH_4:CO_2 ratio variability.

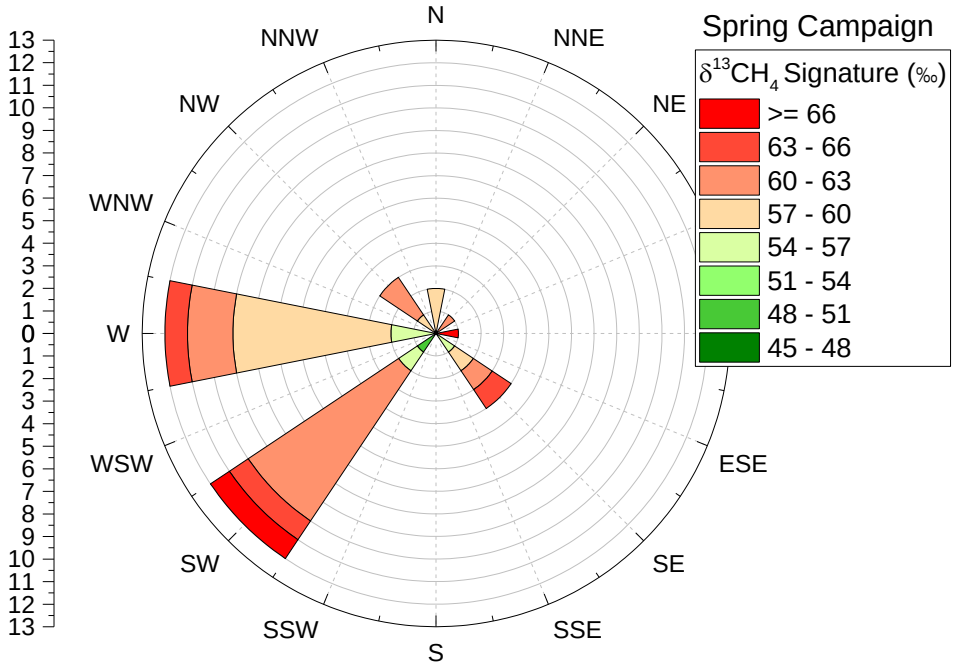

Figure 4.15 Variation of $\delta^{13}CH_4$ signatures with respect to wind direction. X-axis represents count number.

Analysis using Receptor models

APCA:

For consistency with the autumn 2016 campaign, the same subset of variables were selected for the APCA analysis of the Spring 2017 campaign. The application of MC-APCA modelled two dominant components; all species contribute to the first component which accounts for 67% of the total variability, while the second component contributions are derived predominantly from CH_4 and accounts for 16% of the total concentration variability. The reconstruction of these two components is plotted in Figure 4.16. The principle component (plotted in black), has a clear diurnal cycle and may be considered as the component describing the variation of VOC, CO_2 and CH_4 concentrations due to atmospheric mixing and changes in the boundary layer height. This suggests sources of CH_4, CO_2, C_2H_6 and C_3H_8 are located within proximity but do not necessarily originate from the same source. The second component (plotted in red in Figure 4.16), describes a similar temporal variation to that of the CH_4 concentrations, and describes 55% of CH_4 concentration enhancements, very similar to the 60% calculated for the autumn campaign.

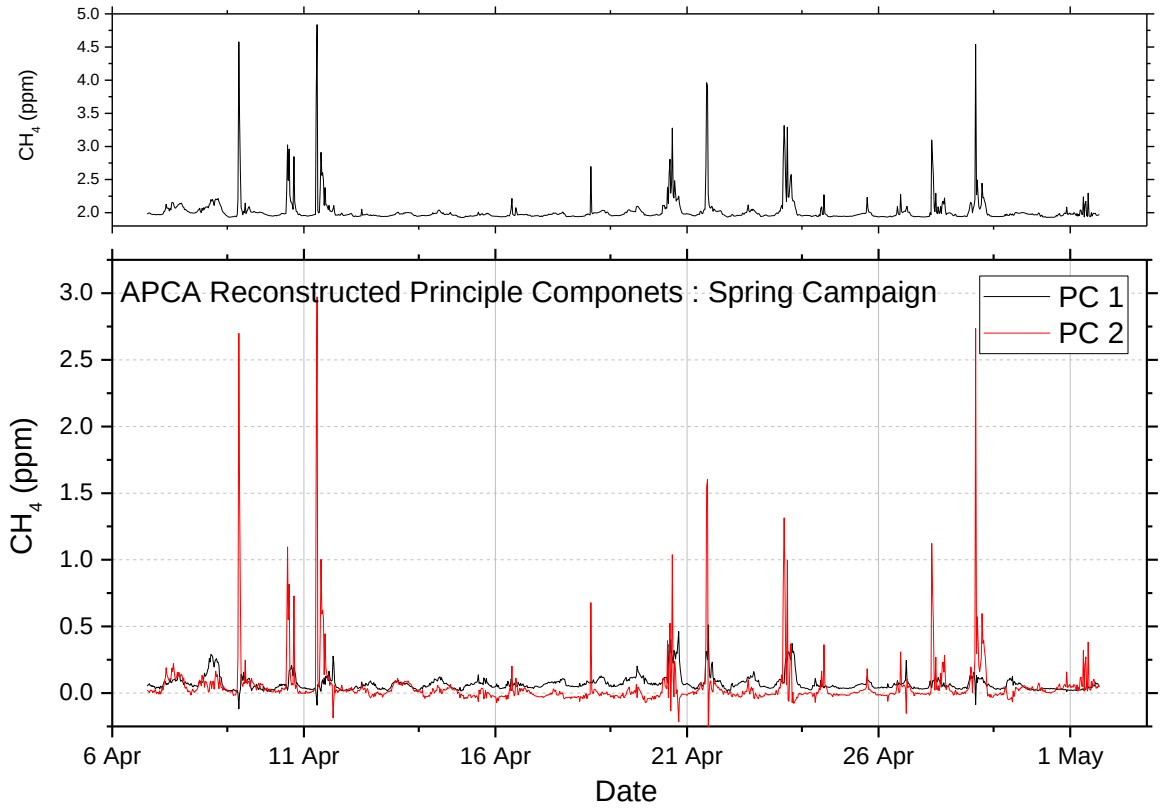

Figure 4.16 Temporal variation of (Top) Methane variability (Bottom) Reconstructed components modelled by MC-APCA. The principle component (PC 1) in black, and the second component (PC 2) in red.

By using the source ratios calculated from 10h MC-mAPCA, the short-term variation of sources during the spring campaign is visible. The temporal variation of the reconstructed C_2H_6:CH_4 ratio of PC1 is plotted in Figure 4.17. Its application was more successful than the autumn campaign, although a number of periods still lack data as CH_4 was not a dominant species present in the principle component during such 10-h time windows. On average the C_2H_6:CH_4 ratio is 0.01 $\pm$ 0.01, again implying a predominantly biogenic source. Periods with C_2H_6:CH_4 ratio greater than 0.02, and the majority of periods for which calculation of the CH_4:CO_2 ratio was possible, occurs when CH_4 concentration enhancements are minimal and therefore should not be interpreted as CH_4 sources. One CH_4 peak which stands out occurs on the 23rd of April. It corresponds with peak concentrations of propane, and I & n butane and has a C_2H_6:CH_4 ratio of 0.03 ppm/ppm. Periods for which the calculation of CH_4:CO_2 ratios were possible are infrequent due to large uncertainties on the data points.

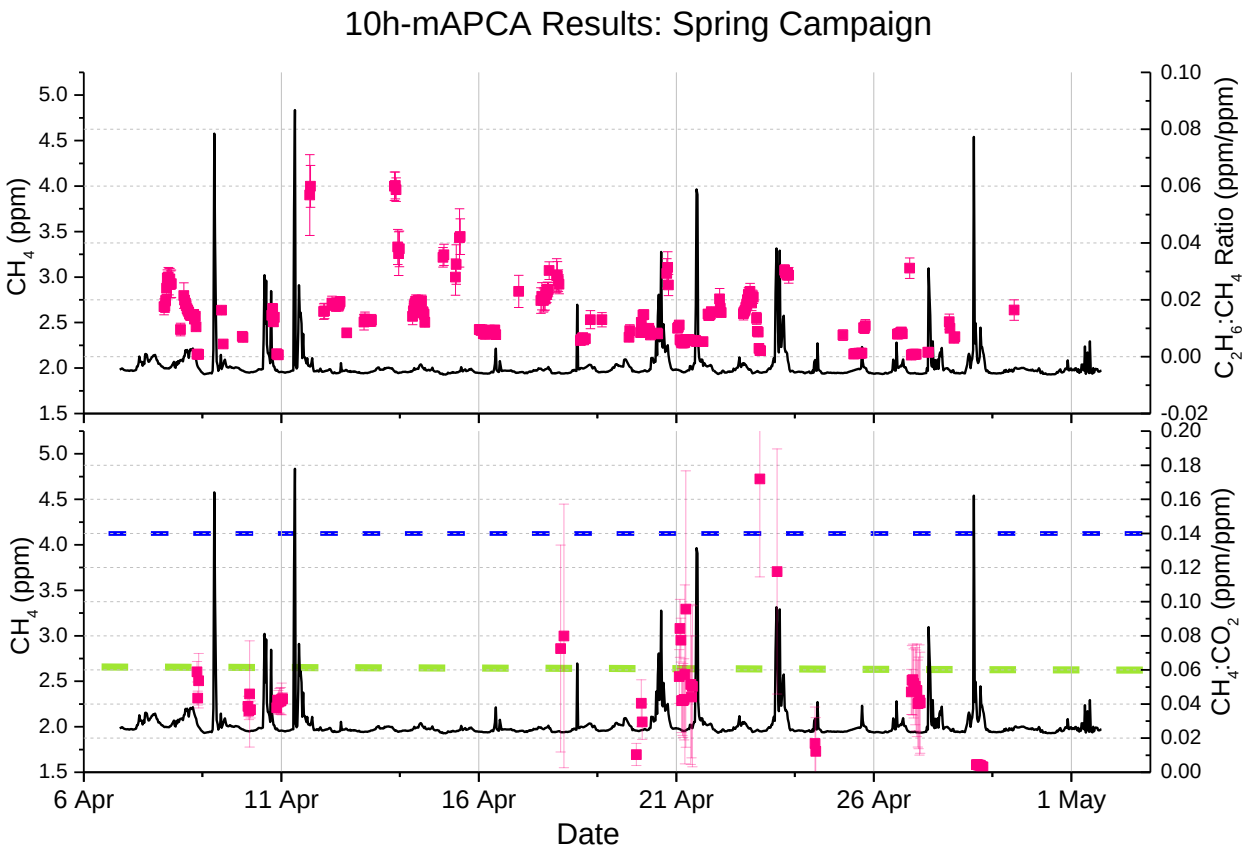

Figure 4.17 10h MC-mAPCA results for the spring campaign. Temporal variation of CH_4 plotted in black on x-axis. Z-axis: (Top) Modelled C_2H_6:CH_4 and (Bottom) CH_4: CO_2 source ratios of the principle component. Points with high uncertainty are plotted with higher transparency.

PMF

Positive matrix factorisation was applied to the spring campaign with 7 variables: CH_4, CO_2, C_2H_6, C_3H_8, i-C_4H_{10} and i & n-C_5H_{12}. These were chosen as they were the available measurements at the time of writing and displayed the most significant concentration enhancements. Principle component analysis suggested between 1 to 3 principle components to describe up to 89% of the concentration variability. Using PMF the optimal fit was achieved with a 3-factor solution. This is one factor less than the autumn campaign due to the absence of n-hexane in the input species. Factor 1 predominantly explains the variance of alkanes (contributions are >90% for all VOCs), and approximately 30% of CO_2 variance. The CH_4 contribution is modelled as negligible in the base run, however DISP and BS error suggest concentrations of CH_4 and CO_2 are not stable for this factor; concentrations vary by a factor of 10^{-2} to 10^{-4} and 10^{1} to 10^{-4} for CH_4 and CO_2 respectively. The contribution of alkanes to this factor implies a fossil fuel source, however the diurnal variability underlying its variation suggests the source does not necessarily originate from the farm. Factor 2 accounts for approximately 83% of CH_4 concentrations, and has little to no contributions from other variables. The temporal variation is in agreement to the CH_4 concentrations measured on site, correlation of the two datasets has an r^2 greater than 0.9. Errors for this factor are predominantly in regards to the CO_2 concentrations, ranging from 10^{0} to 10^{-4}. As this factor has no correlations with the measured VOCs, and due to our previous analysis using APCA and isotopic measurements we can allocate this factor as the biogenic CH_4 source. The largest contributor to Factor 3 is CO_2, (73% of CO_2) with small contributions from CH_4 (DISP and BS error suggest between 10^{-2} and 10^{-4}), C_2H_6 and C_3H_8. The temporal variation is diurnal. The contribution and concentration of each species, including the temporal variation of the CH_4 only factor (Factor 2) is plotted in Figure 4.18. Contributions of Factors 1 & 3 are shown in Appendix C. Factors 1 and 3 show some rotational ambiguity (to be expected as they both exhibit a periodic daily cycle), which was examined through Fpeak rotations of -0.5 to 1.5. Improved rotational ambiguity was achieved with Fpeak rotations of -0.5 and -1 in which CH_4 contributed to all factors; Factor 1 (fossil fuel factor),2 (biogenic CH_4 factor) and 3(diurnal factor) by 22%, 67% and 9% respectively.

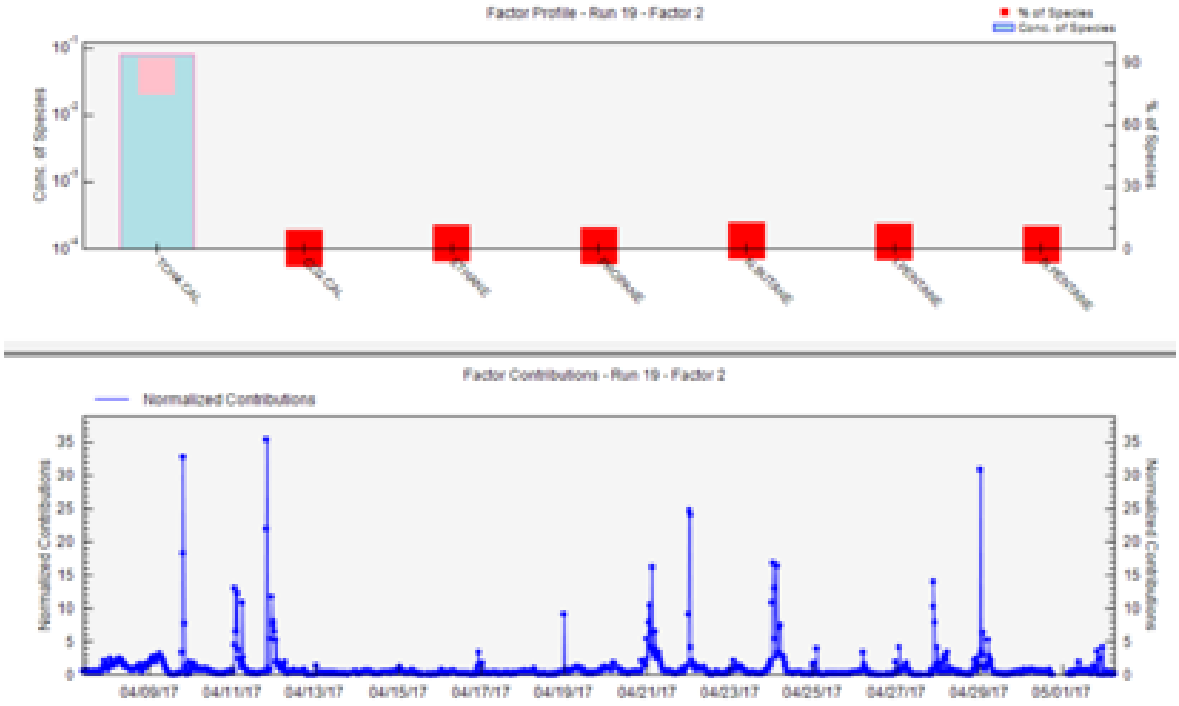

Figure 4.18 Factor 2 profile [CH_4–only factor]. (Top) concentration and percentage of species contributing to the factor. (Bottom) Temporal variation of normalised contributions of factor.

4.1.5 Comparison of Autumn & Spring campaigns

Overall, the characteristics of the variables measured during both fixed-site campaigns were very similar. Methane enhancements were more variable during the spring campaign where 10-minute averaged data shows maximum concentration peaks of 10.5ppm, in comparison to 5.8 ppm during autumn. Methane concentrations during both campaigns exhibit a small daily cycle, although more pronounced during the spring; on average reaching a maximum and minimum of 2.15ppm and 1.95 ppm and 2.06ppm and 2.00ppm for the spring and autumn campaigns respectively. Furthermore, when comparing Figures 4.7 and 4.12, the local source is more clearly identified in spring given the high mean CH_4 enhancements originating southwest of the measurement station. Calculating the expected CH_4 emissions using IPCC Tier 1 emission factor data, total emissions should be less during spring as the average live weight of ruminants is significantly decreased (see top of Figure 4.2). Thus, the higher CH_4 enhancements measured are most likely due to changes in meteorological conditions; in particular wind speeds which were significantly lower during the spring campaign. Daily, hourly and weekly averages for

both campaigns are compared in Figure 4.19. A prominent feature in the daily cycle is a large methane concentration peak at approximately 6 pm measured during both campaigns. To evaluate whether this concentration peak originates from onsite activities or the transport and mixing in the atmosphere, the CH_4 daily cycle was compared to that of radon (measured from the ICOS measurement tower in Saclay). No anomalous variations were detected in the radon data. Furthermore, there is no correlation with wind data, thus suggesting that the CH_4 concentration peak is due to a periodic activity at the farm. Food is distributed once per day between 6am and 8am, with enough to last until the following day. Bilek et al. (2001) found that that CH_4 concentrations of cattle increased 1-2 hours after feeding followed by a sharp decline. Therefore, the evening peak may be linked to a peak in food consumption; heifers and other ruminants are expected to eat throughout the day however the dairy cattle are particularly hungry after milking periods which last from 5.30am to 8am and 3pm to 6pm.

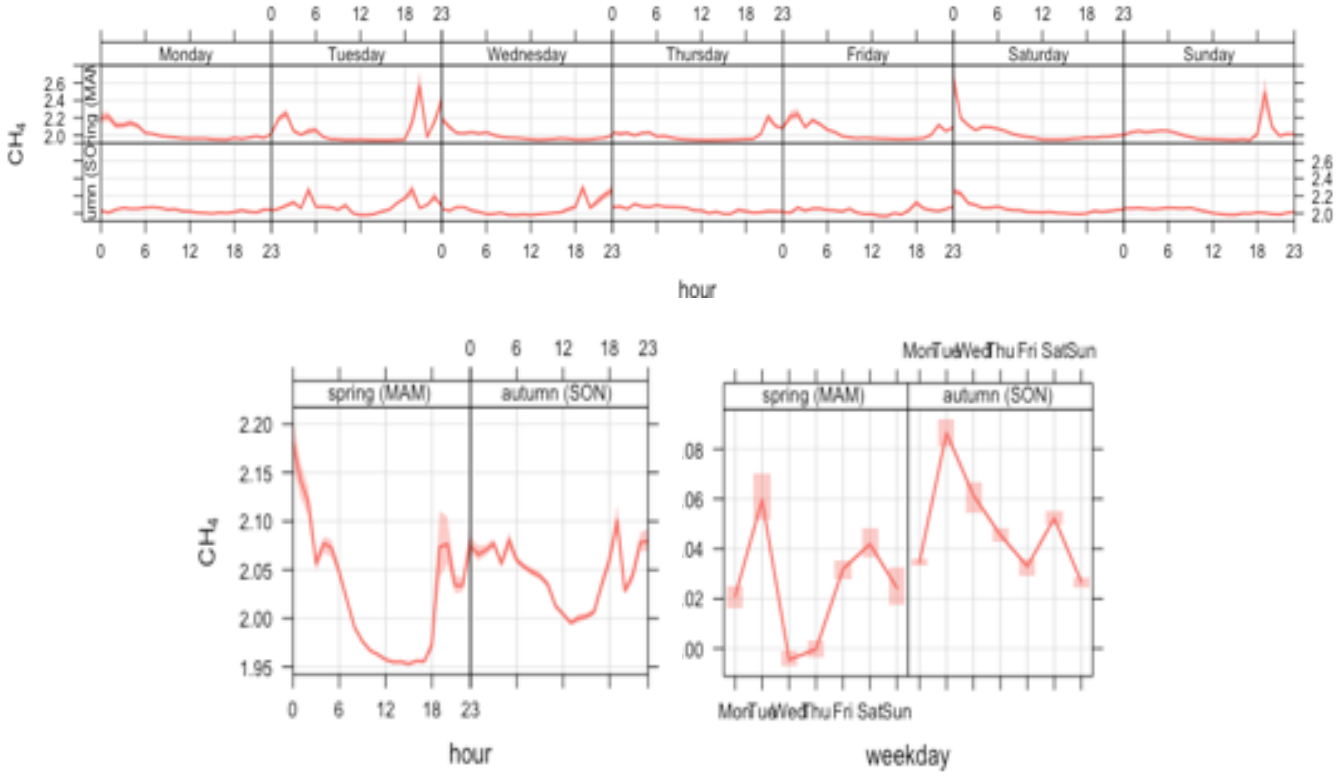

Figure 4.19 Hourly, daily and weekly temporal variation of mean CH_4 concentration for the spring and autumn Grignon campaigns. Shaded regions represent 95% confidence interval in mean.

Source signature observations: Isotopic & CH_4:CO_2 ratio

Within the uncertainties, the mean $\delta^{13}CH_4$ signature does not change between the autumn to spring campaigns. Overall, the $\delta^{13}CH_4$ signatures calculated are within the range measured during the mobile field campaign. Moreover, $\delta^{13}CH_4$ signatures have been measured to vary by up to 10 ‰ over a 24-hour period (dependant on feeding times and substrate availability) [Bilek et al. (2001)]. At Grignon farm, feed is available throughout the day, thus we expect variation to a lesser extent over the 24-hour period. Using the CH_4: CO_2 source ratio as a second proxy, the characterised CH_4 peaks are plotted in Figure 4.20. The majority of points are clustered to the left of the plot. Source ratios calculated from the autumn campaign are less robust as it was difficult to fit the diurnal CO_2 cycle, likely due to the large influence of CO_2 respiration from the ecosystem in winter. Characteristics of spring sources correspond to the lactating cows, and isotopically to sheep and heifers as well. In autumn, isotopically, sources are strongly correlated to the lactating cows. A number of points found in the top left hand of the plot have significantly heavier $\delta^{13}CH_4$ signatures which are expected to be associated with biogas emissions.

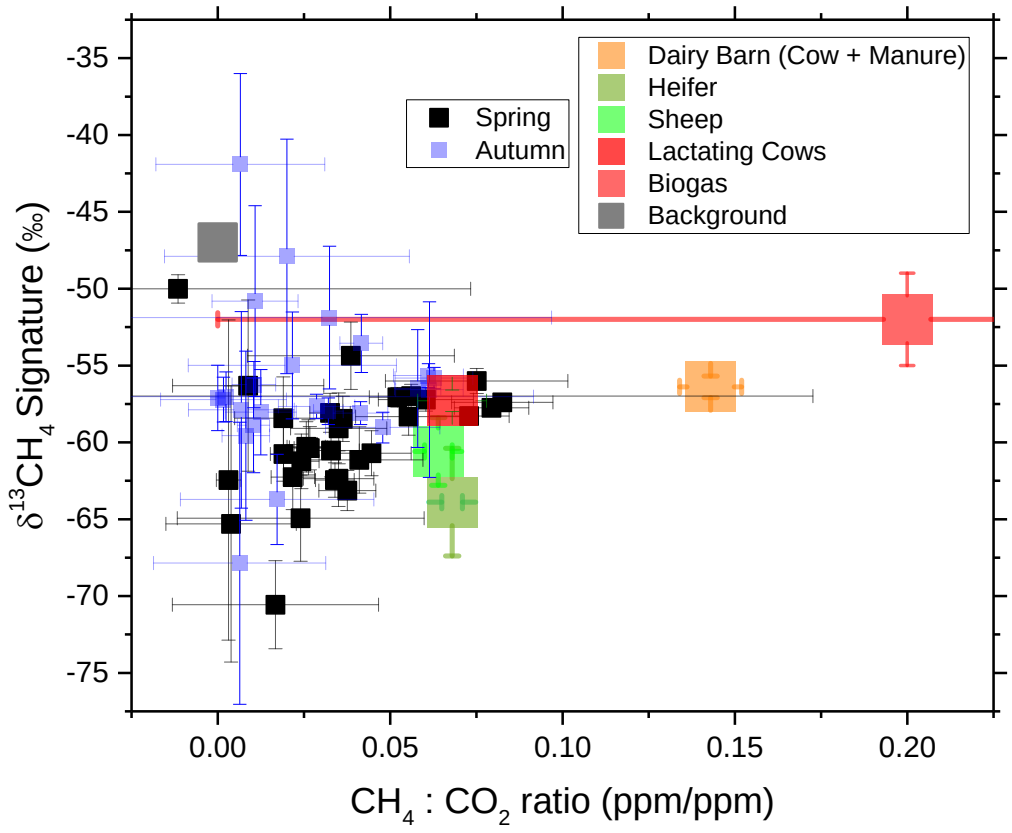

Figure 4.20 Methane source characterisation plot. $\delta^{13}CH_4$ signature on the y-axis and CH_4: CO_2 ratios on the x-axis. Methane concentration peaks are plotted in dark and light blue for the spring and autumn campaign respectively.

Receptor models

The factors calculated by the two receptor models were in very good agreement for both the spring and autumn campaigns. MC-APCA calculates a CH_4 only component explaining between 50-60% of the total CH_4 variability while for the PMF this is 66%. Large uncertainties are associated with CH_4 contributions to the fossil fuel PMF factors for both campaigns. Results from the short-term variation of CH_4 sources modelled by MC-mAPCA found the method to be sub-optimal for a measurement site in which CH_4 is not correlated with other variables, resulting in missing data for most of CH_4 concentration enhancements.

4.1.6 GRIGNON FARM CONCLUSION

Measured values of $\delta^{13}CH_4$ signatures of ruminants, as influenced by diet type, is scarce in many countries. Through the use of a mobile measurement method, this study identified characteristic $\delta^{13}CH_4$ signatures of dairy cattle for the Ile de France region as -57.3 $\pm$ 0.7 ‰ and -61.5 $\pm$ 1.8 ‰ for a 50% or 30% C4 plant diet respectively. We found good agreement with values published previously in literature; from cattle in Germany (Levin et al. 1992), Japan (Bilek et al., 2001) and Switzerland (Klevenhusen et al., 2010), see Figure 4.21. The effect of the C3:C4 plant ratio in cattle diet is visible in the $\delta^{13}CH_4$ signatures. Given the CH_4 eructated from cows is dependent on the diet of C3:C4 plants, where maize (the C4 plant component in the feed) has a $\delta^{13}CH_4$ = -13 ‰, and C3 plants have on average $\delta^{13}CH_4$ = -27 ‰ [Vogel, 1980], the isotopic fractionation taking place in the ruminants can be calculated using the following formula:

$$\alpha_{COW/DIET} = (\delta^{13}CH_4^{Cow} + 1000) / (\delta^{13}CH_4^{Diet} + 1000) \qquad \text{Equation 4-1}$$

The fractionation factor for lactating cows is calculated as $\alpha_{COW/DIET}$ = 0.9622 $\pm$ 0.001, and $\alpha_{COW/DIET}$ = 0.958 $\pm$ 0.003 for heifers. Uncertainties are derived from the maximum and minimum fractionation factors using 5% feed uncertainty (highlighted yellow in Figure 4.21), and isotopic signature uncertainty for lactating cows and heifers respectively (highlighted red in Figure 4.21). The fractionation factor calculated for heifers is in good agreement to the cited literature (above) and the lactating cow signature after correction for manure. Indicating fractionation is constant with regards to diet and cattle type within the uncertainties. Consequently, the fractionation factor can be used to estimate the $\delta^{13}CH_4$ signature of ruminant emissions for a given C3:C4 diet, or vice versa.

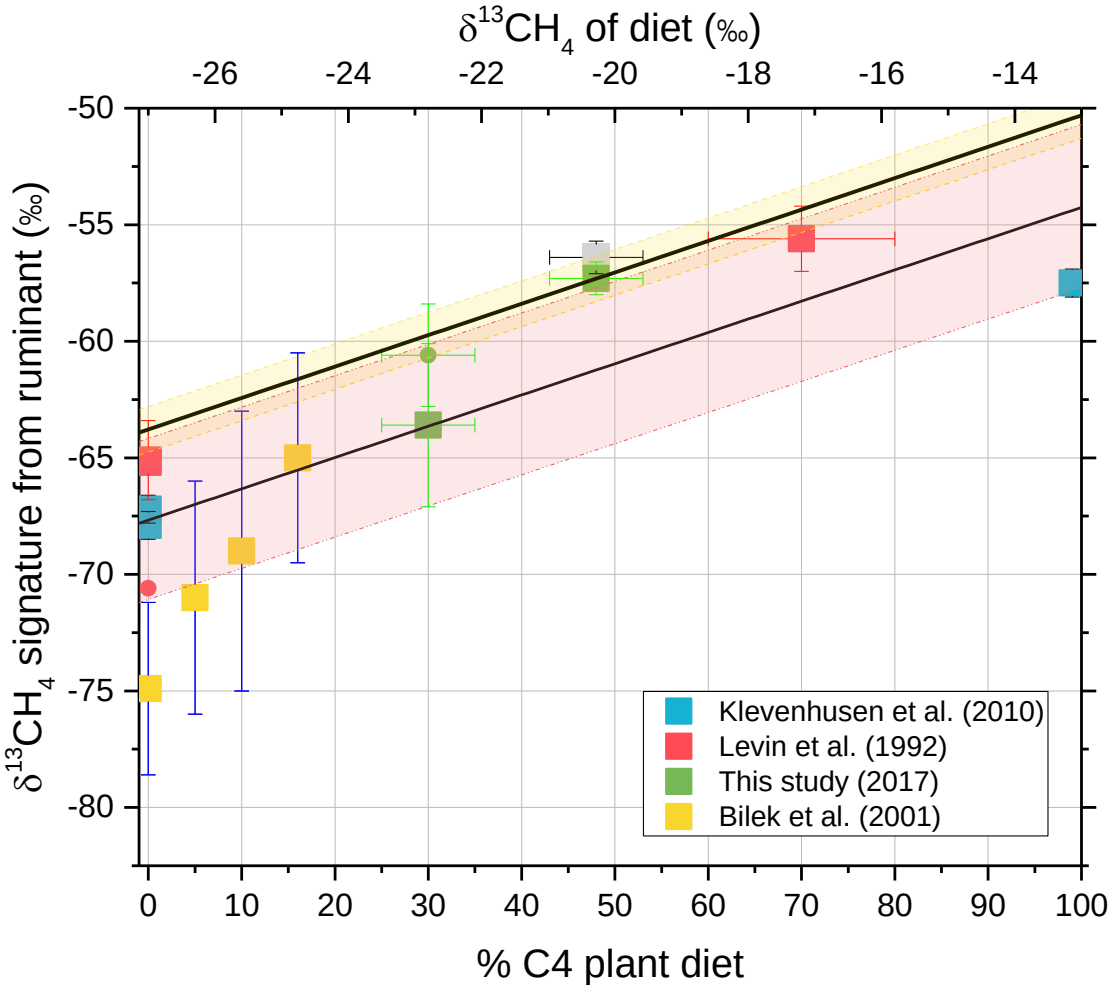

Figure 4.21 Comparison of $\delta^{13}CH_4$ signatures from ruminants depending on their diet measured in this study and literature. Square markers represent cattle, while circular markers represent sheep.

Furthermore, the calculated values for CH_4: CO_2 source ratio can be useful to estimate CH_4 production if other parameters are unknown by using the equation below:

CH_4 produced (l/day) = a(b-d)* (c-e) Equation 4-2

Where a is CO_2 produced by the animal (l/day), and b is the concentration of CH_4 in the air mix, c is the concentration of CO_2 in the air mix, and d and e are the concentrations of CH_4 and CO_2 in background air. [Madsen et al., 2010]. Such a method enables an easy alternative/comparison to calculations using IPCC emission factors.

The moving analysis (MC-mAPCA) detect and identify specific CH_4 concentration enhancement events, long term techniques such as the PMF and MC-APCA on the other hand determine the source contributions of the whole signal, and therefore also attribute a background CH_4 source.

This study found isotopic analysis to provide the greatest insight into emission characteristics for our fixed field campaigns, as typical CH_4 emissions were short lived and strongly enhanced compared to background concentrations. The CH_4: CO_2 ratio is less reliable as it is easily influenced by daily cycles of concentration data. It is not recommend to use short term analysis with m-APCA at such a site, due to minimal VOC and CH_4 source correlation. Finally, CH_4 source contributions were found to be well calculated using PMF and APCA receptor models however in the case of this measurement campaign, isotopic analysis was necessary for detailed CH_4 source identification.

4.2. CH_4 EMISSIONS FROM THE WASTE MANAGEMENT SECTOR

Methane emissions due to anaerobic decomposition of organic waste from waste management accounted for ca. 4% of the global GHG emissions in 2010 [UNEP, 2012]. Approximately half of which originate from municipal solid waste (MSW) landfills and half from waste water treatment (WWT) [JRC, and PBL, 2012]. According to UNFCCC reports for 2001-2006 the contribution from the waste sector to total annual emissions in France is even higher, estimated at 14% [Bergamaschi et al. 2010]. Waste management is therefore a major factor contributing to anthropogenic CH_4 emissions. However, such emissions depend on a number of factors including temperature and production process resulting in significant uncertainties in emission factors. This work aids future regional CH_4 source apportionment studies by characterizing the CH_4 source signature at 3 waste management sites in the Ile de France region; two waste water treatment plants and one landfill.

4.2.1 Waste Water Treatment Facility: St Thibault-des-Vignes

Site description

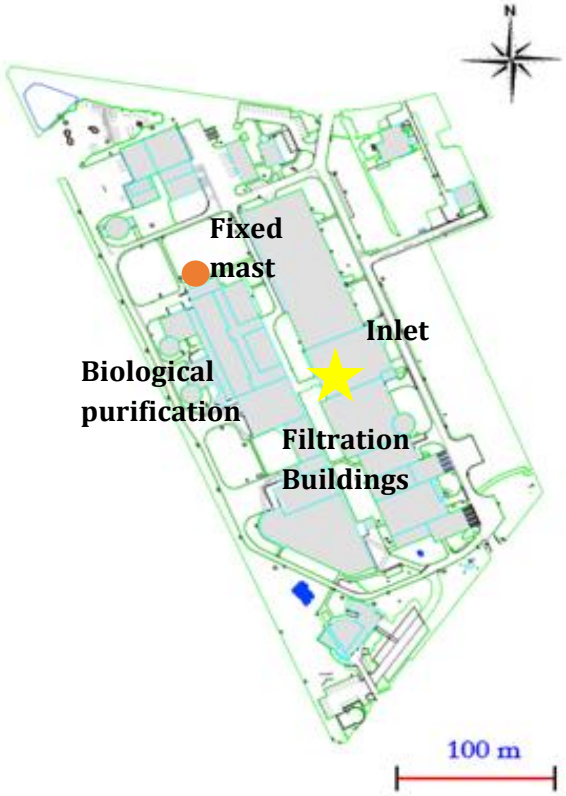

Figure 4.22 St Thibault–des-Vignes WWT site map. Inlet location is marked by a yellow star.

This measurement campaign took place from the 21st July to 6th August 2015 at the St Thibault-des-Vignes waste water treatment site, situated to the west of Paris. The plant treats approximately 38,500 m^3day^{-1}, serving a population equivalent to 400,000. Its operation is conventional, meaning that filtration and sedimentation of particles is followed by aerobic biological treatment. As air is continuously pumped and stirred into the sludge, anaerobic digestion is expected to be minimum and CO_2 is the major waste gas produced from this process. Detailed information of on-site processes is included in the Appendix C. After treatment, the plant discharges the treated water into the Marne river to the north. The site was located in an industrial area with an incinerator facility to the north and major highways to the west and south. A scale map of the site is shown above in Figure 4.22.

A fixed mast with two wind sensor packages (11.9m and 3.4m) was located in an open area on the northwest of the site. Wind measurements started on the 28th of July. Data from the fixed mast upper sensor is used throughout this study. During the measurement period, the predominant wind direction was from the west and southwest with low wind speeds as shown in the wind rose below, Figure 4.23.

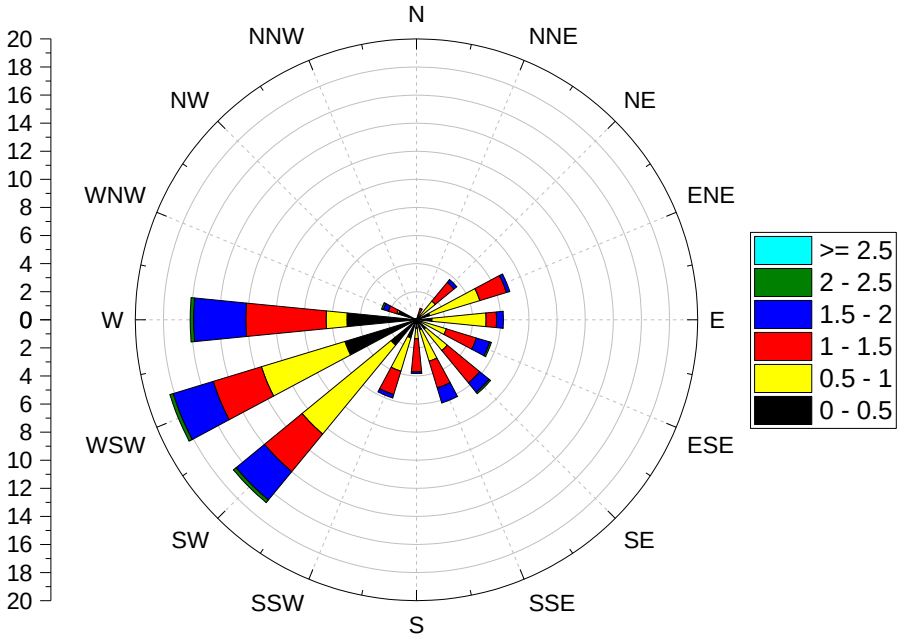

Figure 4.23 *Wind rose from wind data at St Thibault WWTfacility from the 28th of July to the 5th of August. Wind speed is in m/s. Percentage frequency is shown on the y-axis.*

Methods

The CRDS instrument was deployed from the 22nd of July until the 5th of August 2015, for continuous measurements of CH_4, CO_2, C_2H_6, and $\delta^{13}CH_4$. The same set up and calibration scheme as described for the Grignon Farm field campaign was used here (Image 4.6). Here, VOCs were not measured as strong correlations between VOCs and CH_4 were not expected (suggested from measurements performed at the WWF Cergy Pontoise, see Section 4.2.2).

The instrument was located within the filtration building, with the inlet placed on the roof of the building, marked by a star in Figure 4.22.

Methane source identification was analysed using the moving Miller–Tans method. For this field campaign, CH_4 enhancements were particularly low so the requirements for identification of a concentration peak were adjusted to a 3ppb increase in CH_4 and a change in $\delta^{13}CH_4$ of greater than 0.5‰.

Image 4-6 : (Left) Set-up of CRDS instrument with calibration and target gases located within the filtration building. (Right) location of inlet on the roof of the building, image faces north.

Results and Discussion

The time series of CH_4, CO_2, and $\delta^{13}CH_4$ is plotted in Figure 4.24. Measurements up to the 3rd of August are used in this analysis, after which $\delta^{13}CH_4$ measurements are seen to drift substantially and were therefore discarded from the final dataset. The CRDS continuously measured for 13 days, 9 days of which are available with simultaneous wind data. 10-minute averaged mean, maximum and minimum CH_4 concentrations are 2.01ppm, 2.84ppm, and 1.88ppm respectively and 402.3ppm, 447.6ppm and 384.0ppm for CO_2. Only small variations were measured in the CH_4 isotopes. CH_4 concentrations were found to be similar, on average, for all wind directions. This can be seen in Figure 4.25 which plots the relationship between mean CH_4 concentration and wind speed and direction data. This plot illustrates that the highest concentrations are measured at low speeds, surrounding the instrument inlet, thus indicating that the CH_4 source is local. No significant remote sources are observed in the data. Our results are in good agreement with measurements by NPL from a second CRDS instrument measuring in intervals at 13 locations surrounding the site. Figure 4.26 plots the concentration roses for each

measurement location confirming that the CH_4 source is centrally located on the site, surrounding our instrument location. The daily cycle of CH_4 is not very well defined, suggesting a distinct emission source within the site. In contrast, CO_2 has a clear diurnal variation peaking at approximately 4am at 410ppm, and dropping lowest at midday to approximately 390ppm. This indicates the lack of a distinct CO_2 emission source within the site. The highest concentrations are measured during periods of very low wind speed which is indicative of stable atmospheric conditions with very little dispersion of local sources (stagnant conditions). During the campaign, 11 CH_4 concentration peaks occurred that met the requirements of the moving Miller-Tans method. On average the CH_4 peaks have a $\delta^{13}CH_4$ signature of -55 $\pm$ 3 ‰. Although uncertainties are large due low CH_4 concentration enhancements, these values are in good agreement with previous studies. For example, Levin et al. (1999) calculate an isotopic signature of -55.4 $\pm$ 1.4 ‰ for waste emissions in Germany, and Lowry et al. (2001) derive an average signature for WWT of -57 $\pm$ 3 ‰ from a compilation of 13 studies.

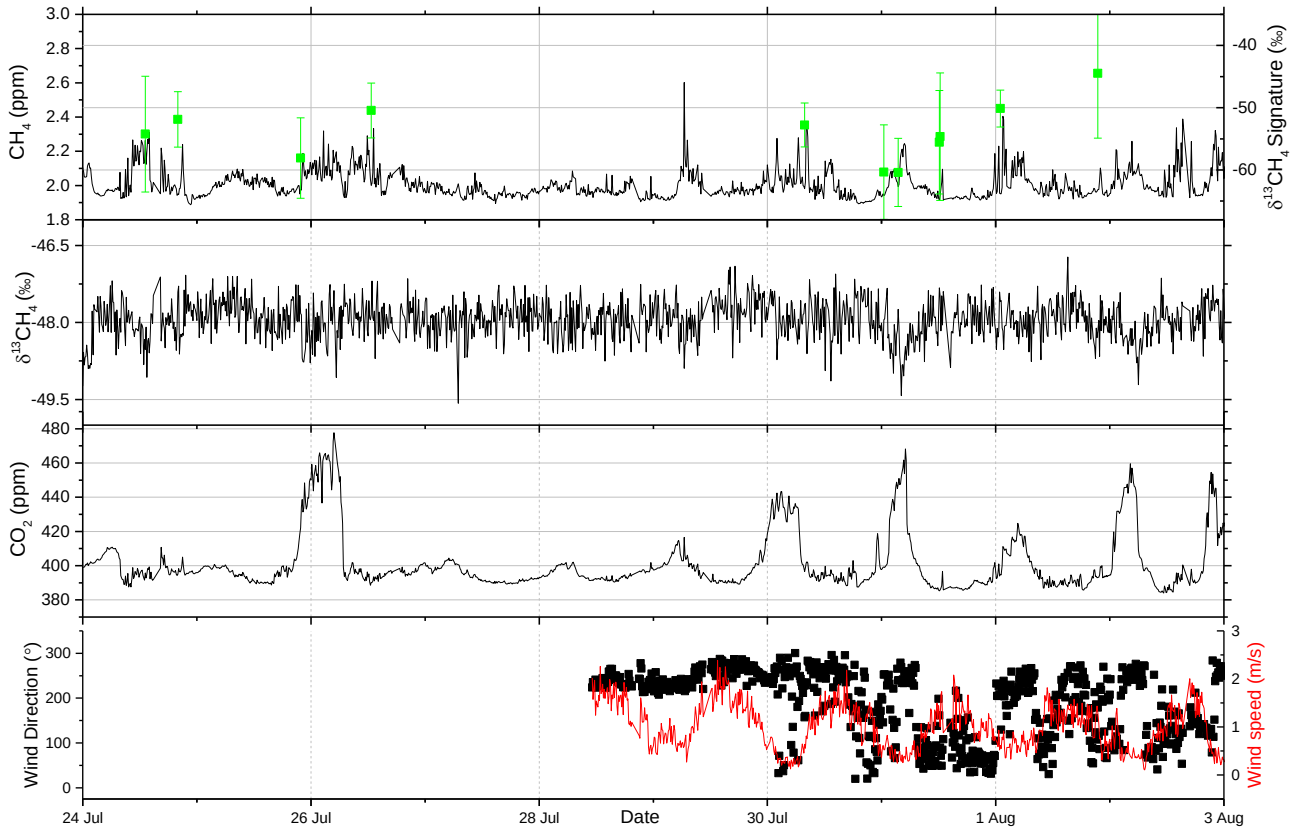

Figure 4.24 Continuous observations of CH_4, CO_2, $\delta^{13}CH_4$ and metrological data at St Thibault WWT plant during the measurement campaign. Isotopic signatures are calculated from moving Miller-Tans and plotted as green points corresponding to top z-axis.

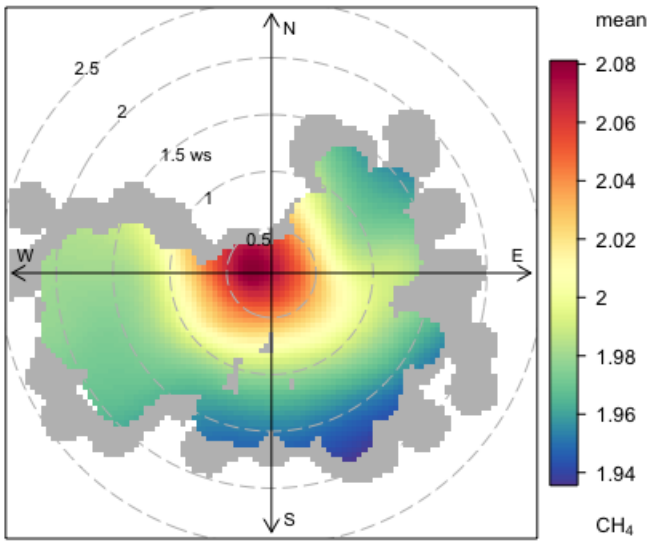

Figure 4.26 Methane concentration rose for measurements at inlet. Concentration in ppm.

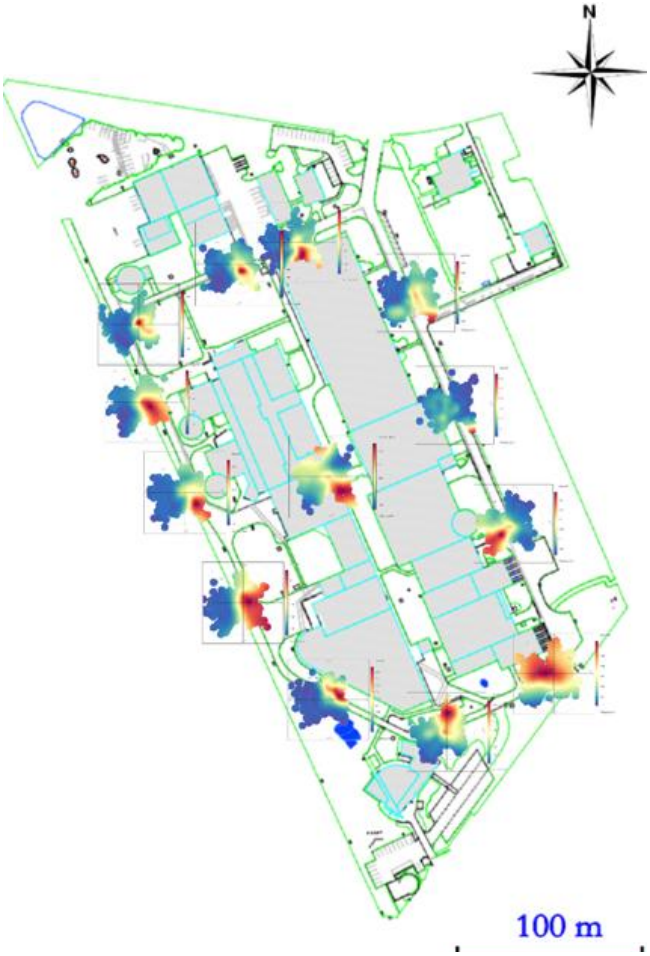

Figure 4.25 Methane concentration roses for measurements by NPL at 13 locations surrounding the WWT facility.

4.2.2 Waste Water Treatment Facility: Cergy Pontoise

Site Description

This measurement campaign took place between the 24th October and 7st November 2014, near the town of Cergy Pontoise, north-west of Paris. The plant treats approximately 34,225 m^3day^{-1}, and implements anaerobic digestion. Initial processes of separation and filtration of organic waste are similar to St Thibault, however the sludge is processed in digesters anaerobically in order to produce CH_4 which is captured and stored for later use or flaring. All relevant buildings are annotated in Figure 4.27. The site is located on the edge of a town, with a river along the western edge, woodland along the southern and eastern edges, and trees lining the northern edge of the site.

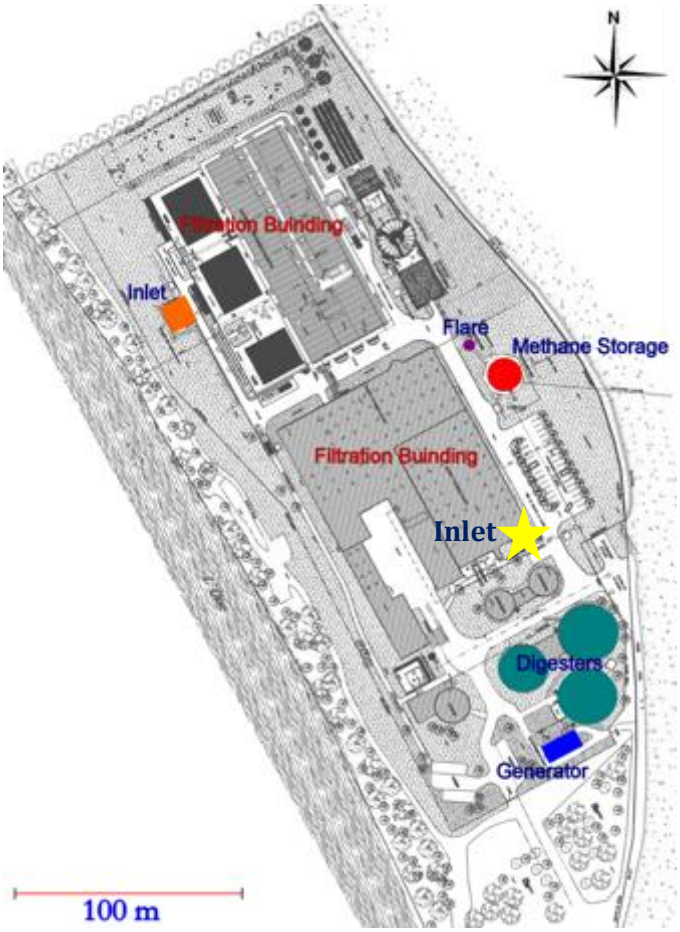

Figure 4.27 Cergy Pointoise WWT site map

A fixed mast with wind sensor packages was located in an open area NW of the site, near the inlet as shown in Figure 4.27. Wind measurements were recorded every minute at a height of 2m. The wind direction was predominantly from the south-east over the course of the campaign with low wind speeds. The corresponding windrose is plotted in Figure 4.28.

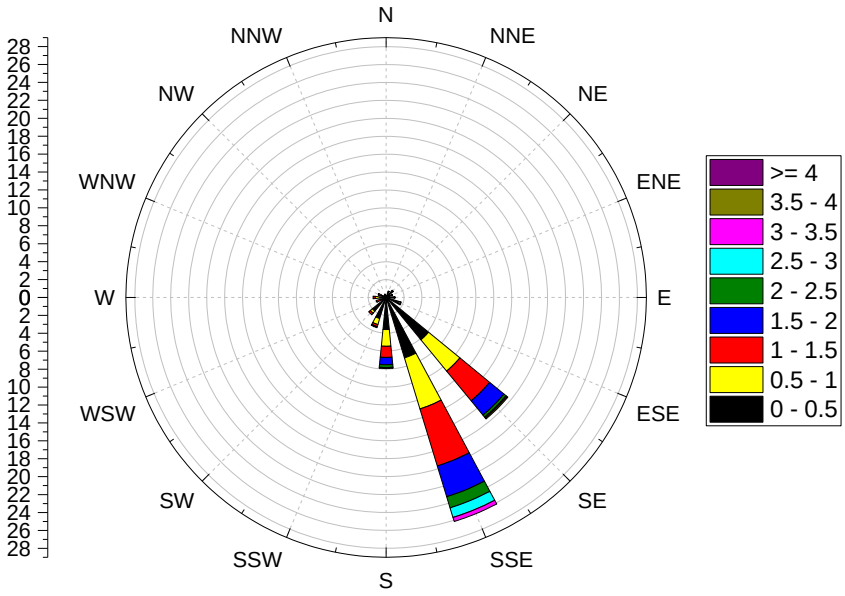

Figure 4.28 Windrose for the duration of the Cergy-Pointoise WWT campaign. Count is shown on the y-axis. Wind speeds are measured in m/s.

Methods

As with previous campaigns, the same CRDS instrument was used for continuous measurements using the set up and calibration schemes previously described. During this campaign, three kinds of VOC measurements were performed: on-line (using portable GC-FID systems) and off-line through sampling of air in dedicated flasks (with later analysis at the laboratory using GC-FID). Sampling of air in 2h-integrated cartridges (filled with Tenax) were analysed at the laboratory with GC-MS in order to investigate halo-carbonated VOCs. All instruments were located in the filtration building to the south-east of the site. Sampling lines of both instruments were co-located on the roof of the building, approximately 10m above ground level. The location can be seen as a star in Figure 4.27.

The moving Miller-Tans isotopic analysis method was used for identification of CH_4 sources. The same method and requirements as described for the Grignon Farm field campaign were used here.

Results & Discussion

Continuous measurements using CRDS were made from the 25th of October until the 6th of November 2014, resulting in 13 days of measurements. The time-series of 10-minute average concentrations of CH_4, CO_2 and $\delta^{13}CH_4$ are plotted in Figure 4.29. Extremely high concentrations of CH_4 were measured throughout the measurement campaign, with a mean of 5.1 ppm. The maximum concentration was measured on the 29th of October as 11.3 ppm, whilst the minimum concentration of 2.2ppm is a value well above background concentrations for the Ile de France region (measured as 1.95 ppm-2.1 ppm at the SNO-ICOS station in Saclay in Gif sur Yvette). Mean, maximum and minimum CO_2 concentrations during the campaign were measured as 711.4 ppm, 1144.5 ppm and 419.5 ppm respectively. Concentration enhancements of both species show a similar diurnal cycle, and were found to have good correlation, with Pearsons R of 0.85. This indicates that besides experiencing similar atmospheric mixing, the emissions can be expected to be co-located due to a similar production processes (microbial activity). The isotope observation revealed a clear anti-correlation of $\delta^{13}CH_4$ with CH_4 concentration enhancements, in which the local source is strongly discriminated from the atmospheric background, as can be seen in Figure 4.29.

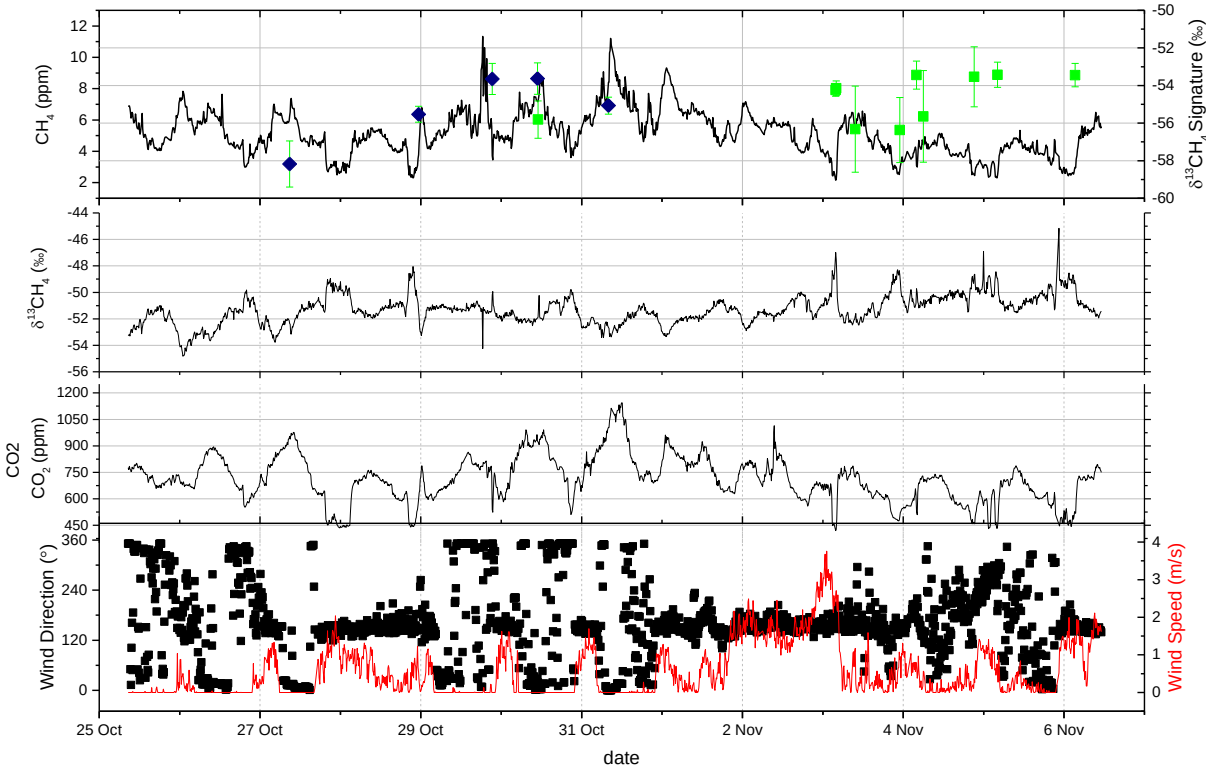

Figure 4.29 Continuous observations of CH_4, CO_2, $\delta^{13}CH_4$ and metrological data at Cergy Pointoise WWT during the measurement campaign. Green points are the periods for which isotopic signature was calculated. Blue points are periods for which both the isotopic signature and CH_4:CO_2 ratio was calculated.

No significant correlations were observed between the measured VOCs and CH_4. As the results of the Grignon Farm campaign analysis suggest that receptor models do not aid CH_4 source apportionment at a site with such characteristics, VOC concentrations were not analysed further here.

Due to meteorological conditions, the data coverage encompasses predominantly the south and south-east of the WWT plant. The largest CH_4 concentration enhancements were detected directly south of the inlet, indentifying the digesters and generators as the major detectable CH_4 sources. The distribution of mean CH_4 concentration with respect to wind direction and speed, as plotted in Figure 4.30.

In total, 16 CH_4 concentration peaks were calculated using the moving Miller-Tans method. On average the peaks lasted 70 minutes, and had a mean $\delta^{13}CH_4$ signature of -55 $\pm$ 1 ‰. This is in agreement with the signatures calculated at St Thibault WWT plant and literature. A CH_4 concentration peak measured on the 3rd of November at 7am has a significantly lighter $\delta^{13}CH_4$ of -65 $\pm$ 5 ‰. Such a signature is typically measured from enteric fermentation or animal waste and cannot be explained by the surrounding sources.

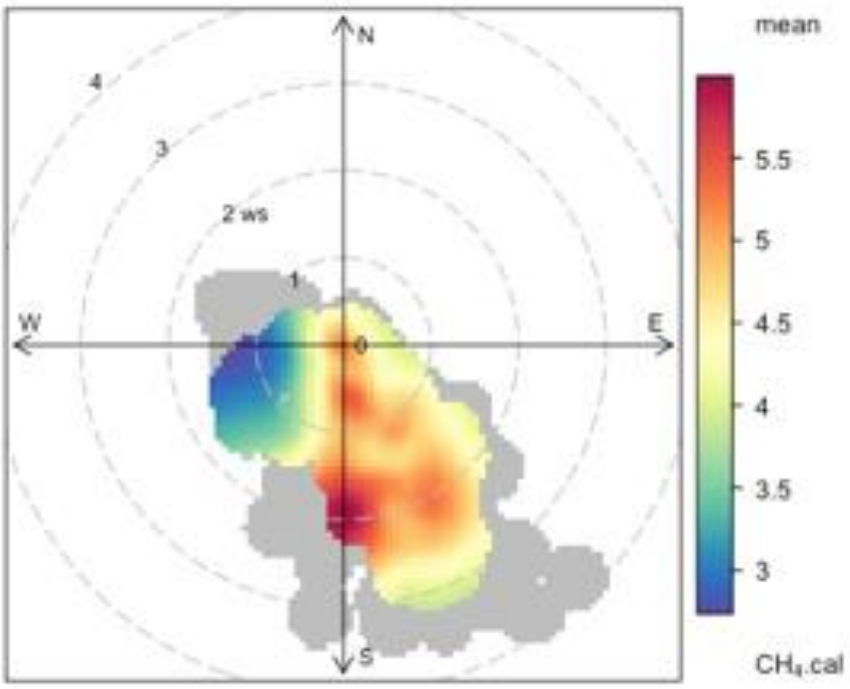

Figure 4.30 Mean CH_4 concentrations (ppm) with respect to wind speed and direction.

Figure 4.31 shows the isotopic signatures with respect to wind direction. Isotopic signatures are found to be heavier when winds originate from the south, ranging between -53 to -55 ‰, and lighter when winds originate from the north, measured between -55 to -58 ‰. This suggests that CH_4 emitted from the digesters is isotopically different to CH_4 emissions emitted from the filtration system.

The CH_4: CO_2 source ratio was calculated for 5 concentration peaks, plotted as blue markers in Figure 4.29. The average ratio is 0.022 ppm/ppm. In a comparison study of 35 Australian WWT plants, de Haas et al. [2009] report CH_4: CO_2 emission ratios of ca. 0.09 ppm/ppm for anaerobic treatment processes and ca. 0.28 ppm/ppm for sites with co-generators. This study uses an emission model that assumes a 1% leakage rate from the digester system. Measurements of CH_4 at a WWT plant with anaerobic digesters (Kralingseveer) indicate annual emissions of 109.2 tCH_4, while CO_2 annual emissions (estimated based on CH_4 consumption), are 1500 tCO_2 [Daelman et al. 2012]; corresponding to an emission ratio of 0.046ppm/ppm. Emissions from other Dutch WWT plants are reported as 38.4 tCH_4/5820 tCO_2 (Kortenoord) and 29.2 tCH_4/3458 tCO_2 (Papendrecht), which correspond to ratios of 0.016ppm/ppm and 0.021ppm/ppm respectively [Daelman et al. 2012]. The observed range at Cergy Pontoise of 0.0086 $\pm$ 0.0004 ppm/ppm to 0.031 $\pm$ 0.002 ppm/ppm is significantly closer to these studies, which might indicate that emission model reported factors cannot be directly compared to observed ratios e.g. due to over or underestimation of emission factors in some WWT plant emission models.

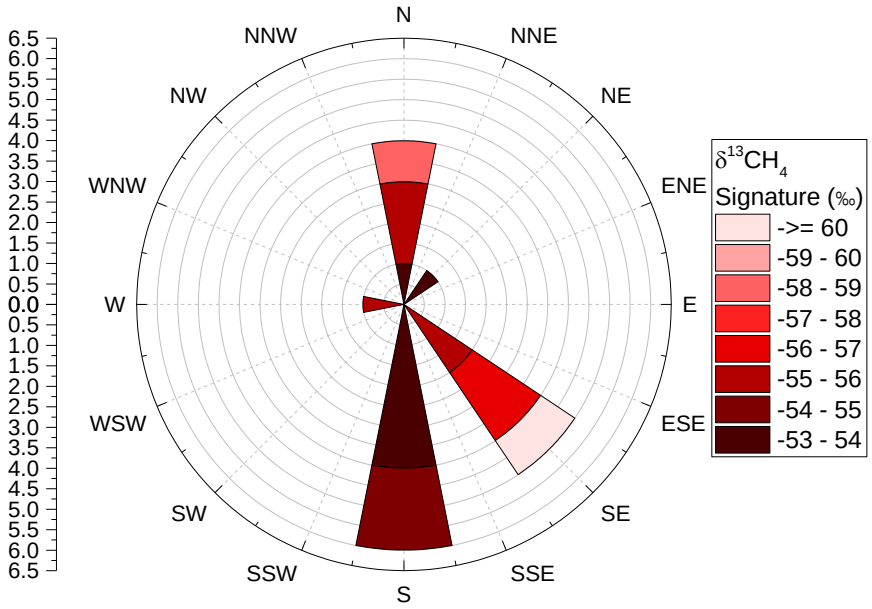

Figure 4.31 Isotopic signature with respect to wind direction. Y-axis is the count.

Comparison

The two WWT plants analysed in this Chapter are relatively similar in size and region, however certain key characteristics differ. The initial processing of waste for both facilities is the same, but sludge treatment at St Thibault is aerobic, while anaerobic digestion is applied to sludge at the Cergy-Pointoise site, where CH_4 is produced and stored onsite. The results from St. Thibault suggest that water treated at aerobic WWT plants still undergoes some anaerobic digestion processes, as clear (although low) CH_4 concentration enhancements were measured surrounding the filtration buildings. Methane enhancements were also measured surrounding the filtration buildings at Cergy-Pointoise, however there the digesters were identified as the predominant CH_4 source. Measurements from Cergy-Pointoise showed a much stronger correlation of CH_4 and CO_2 in comparison to that of St Thibault; Pearsons R of 0.85 and 0.57 respectively. This is in agreement with what would be expected from concentration enhancements driven predominantly by anaerobic digestion process at Cergy-Pointoise in which CH_4 and CO_2 are produced in unison, illustrated in Eq. 4.3. Whilst in St Thibault the dominant process is aerobic digestion, converting organic material into CO_2, without production of CH_4 as shown in Eq. 4.4.

$$2CH_2O \rightarrow CO_2 + CH_4 \qquad \text{Equation 4-3}$$

$$CH_2O + O_2 \rightarrow CO_2 + H_2O \qquad \text{Equation 4-4}$$

The large difference in the overall concentration enhancements (both from CO_2 and CH_4) is likely further intensified by the different metrological conditions i.e. particularly stable conditions during the Cergy-Pointoise campaign, thus allowing for concentration build-up. Furthermore, the building design has surely contributed as well. At St Thibault the filtration systems are well enclosed resulting in little air exchange to ambient air, while at Cergy-Pointoise the filtration buildings had many openings, thus greatly increasing fugitive emissions. We find the mean isotopic signature of CH_4 enhancement periods to be in agreement for both WTT plants, indicating that the anaerobic digestion processes, intentional and unintentional, are similar at both sites.

4.2.3 LANDFILL: BUTTE BELLOT

Site Description

The investigated landfill ("Buttes-Bellot") is located in the Ile-de-France region, about 35 km from Paris. It is situated in a predominantly agricultural area and surrounded (at a distance of approximately 1 km) by a number of small residential areas and industrial sites. In its vicinity is a second, fully covered landfill ("La Ferme") that has ceased operations. Major roads are situated south and west of the Buttes-Bellot site, while agricultural paths can be found surrounding the site (limited access to the north), as can be seen in Figure 4.32.

Figure 4.32 Overview of experimental area of Buttes Bellot mobile measurement campaign. © Google Maps

Methods

The objective of this measurement campaign was to complete an inventory of isotopic measurements of anthropogenic CH_4 emission sources in the Ile de France region. A mobile measurement campaign set-up as described for Grignon Farm (see Chapter 4.1.2) was implemented here. The campaign took place on the 2nd of December 2016, with stable weather conditions, information for which can be found in Table 4.2. $\delta^{13}CH_4$ source signatures are calculated using Miller-Tans plots as previously described.

Table 4-2 *Weather conditions on 2.12.2016*

Variable (unit)	Typical value (during measurement)	Range of value (min/max)
Temperature (°C)	5	0/5
Air Pressure (mbar)	1024	1023/1028
Wind speed (m/s)	2.7	1.8/4.4
Wind direction (degrees) (coming from the direction)	NNE	ENE/NNE
Rain (mm)	0	0

Results & Discussion

The plumes measured down-wind of the site typically reached CH_4 concentrations of 10ppm. They are clearly associated with the emissions of the Buttes-Bellot site given the prevailing winds and lack of other major sources in the region upwind of our observations (16h15-17h00 and 17h15-18h00). Figure 4.33 plots the 8 plume crossings that were measured downwind of the Buttes-Bellot site. Increases in CH_4 concentration are clearly correlated with lighter periods of $\delta^{13}CH_4$. During measurements on the roads west of Buttes-Bellot (between 17h00 and 17h15), i.e. downwind of the closed landfill, no significant plumes were measured, indicating that it does not contribute to CH_4 concentration enhancements in the area. During the plume measurements on the agricultural road south of the landfill, CH_4 concentrations range from 2ppm to 12ppm and atmospheric $\delta^{13}CH_4$ values range from -43 ‰ to -57 ‰.

Miller-Tans fits were used to derive the $\delta^{13}CH_4$ signature using the data from all 8 plume crossings combined as only one unique source was identified. For this landfill, a signature of -60.0 $\pm$ 1.3 ‰ was calculated. Although isotopically light, this signature is comparable with literature; -59 $\pm$ 2 ‰ for European landfills were found by Bergamaschi et al. (1998), -54 ‰ for winter measurements in Florida by Chanton et al. (2000) and -51 ‰ by Lowry et al. (2001) from U.K. landfills. For Buttes-Bellot, a CH_4: CO_2 ratio of 0.55 $\pm$ 0.06 ppm/ppm was calculated. This is in agreement with the reported ratio of 0.42-0.53 ppm/ppm calculated by Sonderfield et al. (2017) for the active region of a landfill site in the U.K. Such a ratio is representative of waste decomposition under aerobic conditions.

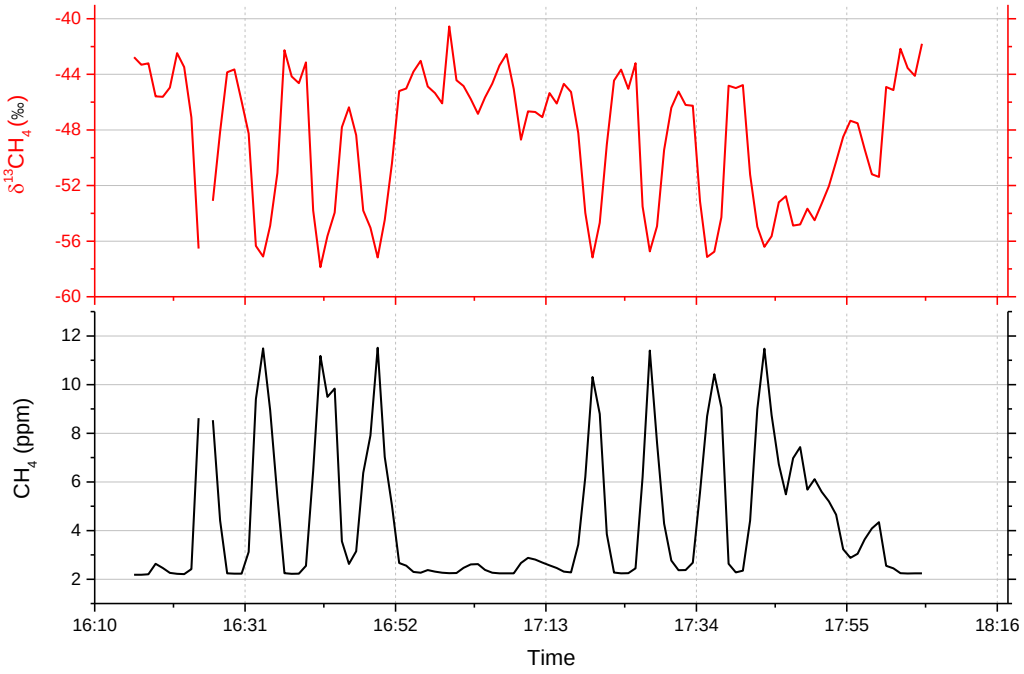

Figure 4.33 Time-series of $\delta^{13}CH_4$ measured downwind of the active landfill (Buttes –Bullot) using mobile measurements.

4.2.4 Waste Management Conclusion

Isotopic analysis was implemented at 3 biogenic methane field campaigns in order to identify and characterise waste management methane sources. Although the Cergy-Pointoise and St Thibault WWT plants treat incoming waste using different processes (anaerobic and aerobic digestion respectively) no difference in the isotopic characterisation of methane was measured. The results are in good agreement with literature as a $\delta^{13}CH_4$ of -55 ‰ was measured at both sites. The isotopic signature of landfill emissions measured during a mobile campaign is isotopically lighter than the wastewater emissions at -60 ‰, and also in good agreement with literature of measurements of European landfills.

4.3 CONCLUSION

Three major source categories contributing to anthropogenic methane emissions have been successfully categorised in the Ile de France region; namely ruminant, wastewater and landfill sources. Mobile campaigns were found to be the most useful for the precise characterisation of ruminant source signatures. For example, the isotopic source signatures of lactating cows, heifers, sheep and biogas range from -57 ‰ to -63 ‰ which is in good agreement with theoretical estimates based on C3:C4 plant diets and previous work in other regions. Fractionation in the rumen was found to be constant (within uncertainties) with regards to diet and breed, facilitating a robust way to estimate $\delta^{13}CH_4$ values of cattle from C3:C4 diet. The long-term field campaigns in spring and autumn demonstrate that the temporal variation of CH_4 source signatures on the farm is not significant, and that ruminant emissions explain the majority of CH_4 emissions with little to no contribution from other sources. Characterisation of CH_4 emissions from two WWT plants indicates that the isotopic signature of facilities using aerobic processes is not distinguishable (within uncertainties) to those using anaerobic digesters. On average -55 ‰ was calculated for both WWTP sites. Lastly, CH_4 emissions from landfill were investigated and measured to have a signature of -60 ‰.

Overall for such biogenic sources, little to no correlation of CH_4 with the 'light' VOCs was measured in this study. For this reason, receptor models are not suitable to solve these biogenic source apportionment problems, in contrast to their demonstrated value at industrial sites (see Chapter 3). Instead it was found that CH_4: CO_2 source ratios could be a good second proxy to aid identification. Using a combination of both these methods it was possible to identify 5% manure emissions in the sample of gas from the Dairy barn. Furthermore, as the CH_4: CO_2 source ratio for wastewater and landfill were measured to be significantly different, this proxy has the potential to improve source apportionment of these two sources which can be isotopically very similar. Nonetheless, this method can also be prone to high uncertainties if the CO_2 concentrations are being emitted from multiple sources, or the time series contains strong daily CO_2 cycles.

Chapter 5 THESIS CONCLUSIONS & OUTLOOKS

The emissions of CH_4 are uncertain because they proceed from complex processes like microbial decomposition and leaks in natural gas extraction and distribution systems that are particularly difficult to characterize. Future emission reductions can be implemented more efficiently through a thorough quantification and understanding of current anthropogenic methane sources. This PhD thesis combines new instrumental and analytical developments as well as methods based on time-series analysis of CH_4 concentration measurements in the vicinity of localized anthropogenic sources. It presents improved methane source identification methods at local scales, as well as their application to field campaign measurements, at sites with different source and emission characteristics. As stable isotopic analysis is key to partitioning sources on local and global scales [Zazzeri et al., 2017, Nisbet et al, 2016], this thesis also increases the availability of CH_4 source isotopic signatures in Europe for future work in this field.

As cavity ring-down spectrometers become common deployment for CH_4 site scale measurements [e.g. Yvon-Lewis et al., 2011, Lopez et al. 2017], the problem of biases resulting from unknown laser absorption interference [Rella et al., 2015], in particular at industrial locations when gas concentrations are far above ambient, is more problematic. While the biases due to abundant gasses such as H_2O, Ar, O_2, have been well characterised [Rella et al., 2015, Nara et al., 2012], other gases, such as C_2H_6 (a secondary component in natural gas), have not. During this thesis, extensive laboratory analysis characterised the biases in $\delta^{13}CH_4$ measurements due to C_2H_6 contaminated air from a CRDS G2201i Picarro instrument that measures the absorption spectrum of both species with interference between them. The derived correction and calibration factors enable unbiased measurements of both $\delta^{13}CH_4$ and C_2H_6, thus offering the opportunity to combine continuous measurements of $\delta^{13}CH_4$ and C_2H_6:CH_4 ratio to improve source characterisation, in particular for the oil and gas upstream sector where CH_4 is mixed with C_2H_6 in natural gas. As awareness and correction of this interference is important to all past and future CRDS work in fossil fuel environments, the laboratory tests are described in detail for others to calculate instrument specific correction factors, or if not possible, to use the ones in this study. These findings facilitate complementary C_2H_6:CH_4 characterisation with the G2201i Picarro, assisting future studies to improve spatial and temporal understanding of fossil fuel sources. Improvements to this work include the validation of the long-term stability of the proposed corrections, and a comparison with a greater number of instruments to determine their homogeneity. Further research should also be conducted into the characterisation of $\delta^{13}CH_4$ biases due to elevated concentrations of Ammonia (NH_3)

[Rella et al., 2015], a gas emitted largely from livestock manure with reported mean NH_3 concentrations of 3-8ppm for cattle houses in Europe [Ngwabie et al., 2009, Groot Koerkamp et al., 1998].

A large factor contributing to uncertainties associated with CH_4 emissions and source signatures, is the lack of available methods to discriminate between the different production processes and co-located CH_4 sources. In this thesis, a variety of source apportionment techniques were investigated and developed to specifically improve CH_4 source apportionment, with the goal of distinguishing emissions from different systems at a NG site. As simultaneous CH_4 and co-emitted VOC data were available at this site, Principle component analysis (PCA) and Positive Matrix Factorisation (PMF) receptor models were investigated. Significant extensions were made to the classical PCA; Monte Carlo Absolute PCA 'MC-APCA' and Monte Carlo moving Absolute PCA 'MC-mAPCA' were found to be more suitable for this application. This work determined MC-APCA and PMF to be most appropriate for the analysis of long-term temporal variation of the dominant sources. Overall, both techniques agreed on the contribution (within 12%) of different CH_4 sources but could not be used to identify sporadic peaks or to separate the relative contributions of sources with very similar characteristics (such as two types of natural gas). Reduced subjectivity was possible when PMF and MC-APCA techniques were combined. Techniques such as the moving Miller-Tans method for isotopic identification and MC-mAPCA were found to give an insight into the short-term variability of source composition. Offering the potential to identify CH_4 enhancements from sporadic sources and differentiate small fluctuations in source (in our case NG) composition. Overall, the best method to identify CH_4 sources from ambient, local measurements strongly depends on the characteristics of said source. By implementing sensitivity studies, it was possible to judge the abilities of PMF and APCA tools and determine their sensitivities to model parameters. The campaign investigated here was predominantly single sourced, and focussed on the identification of two gas streams, thus it required very sensitive analysis. In such a case, it was found that a combination of techniques provided the greatest information on the characteristics of CH_4 sources and gives confidence in the results. As no additional measurements are required, existing PMF studies can be easily enhanced with the inclusion of MC-APCA or MC-mAPCA. Further research could be done into a comparison and evaluation of the performance of these source apportionment methods when applied in a more multi-source environment, such as an urban site.

Source contributions to local CH_4 enhancements can often be complex and variable. This, in combination with the limited number of studies reporting on source characteristics contributes to large uncertainties. Thereby affecting regional to global emission estimates when using isotopic data or co-emitted tracer:CH_4 ratios to constrain CH_4 sources [Tyler et al., 2007, Mikaloff Fletcher et al., 2004, Schwietzke et al., 2014]. The signatures and temporal variability of 3 biogenic CH_4 sources (agricultural, waste water, and landfill) were successfully investigated in the Ile-de-France region using the source apportionment techniques developed. Three campaigns were conducted at the Grignon agricultural farm of which the mobile campaign was most useful to identify isotopic (-57 ‰ to -63 ‰) and CO_2:CH_4 (~ 0.06 ppm/ppm) signatures of ruminants. Using both signatures improved source apportionment, and allowed identification of manure contaminated signals. Consequently, the measurements indicate that the rumen fractionation is independent of diet and breed, facilitating a robust way to estimate the $\delta^{13}CH_4$ signatures of cattle using only their C3:C4 diets. Two wastewater treatment plants had the same mean $\delta^{13}CH_4$ source signature of -55 $\pm$ 3 ‰. That of an active landfill was found to be significantly more depleted at -60 $\pm$ 1 ‰. We find that these biogenic sources have little correlation with VOCs and receptor model analysis was shown not suitable for such datasets. Furthermore, as emission enhancements were very low during some of the long-term campaigns, the isotopic and ratio analysis could not be successfully applied for large portions of the dataset. Although the CO_2:CH_4 ratio of these sources has the potential to significantly aid source apportionment, it was a challenge to calculate from ambient measurements as CO_2 was often influenced by other sources. This issue could be resolved by the use of $\delta^{13}CO_2$ signatures as a second proxy in future. Nonetheless, these 3 major source categories were well characterised for the Ile de France region. The values measured are similar but not always identical to other literature (see Table 5.1). It is therefore suggested these values be used for future emission estimates for this region, and/or specific CH_4 processes. There is still the requirement for more frequent measurements of $\delta^{13}CH_4$ sources to assess their variability. In regards to the ruminant study in this thesis; as some of our $\delta^{13}CH_4$ values have high uncertainty, an improved understanding would be gained with higher precision signatures and frequent measurements to find if isotopic or CH_4: CO_2 ratio signatures change throughout the day (as suggested by Bilek et al., 2001) or possibly year. Furthermore, $\delta^{13}CH_4$ signatures for manure emissions of ruminants is scarce in literature. The detection of manure contributions would be more certain if $\delta^{13}CH_4$ signatures were better characterised with regards to time and feed.

Table 5-1 Summary of isotopic source signatures for methane sources in Western Europe, and the values from this thesis.

Methane Source	*European $\delta^{13}CH_4$ (‰)*	*Reference*	**This Study (France, ‰)**
Wastewater	-54 (Germany) -53 ± 3 (U.K)	(Levin at al. 1999) (Zazzeri., 2015)	**-55 ± 3**
Landfill	-60.3 ± 2.3 (Germany) -50.8 to -52.6 (U.K.) -58 ± 3 (U.K) -57.4 ± 1.7 (Netherlands)	(Bergamaschi et al. 1998) (Lowry et al., 2001) (Zazzeri, 2015) (Bergmaschi et al., 1999)	**-60 ± 1**
Cattle, (100% C3 Diet)	-65.1 ± 1.7 (Germany) -67.6 ± 1 (Switzerland)	(Levin et al 1999) (Klevenhusen et al, 2010)	**-63.9 ± 3.5 (70% C3)**
Cattle, (100% C4 Diet)	-56.5 ± 1 (Switzerland)	(Klevenhusen et al. 2010)	**-57.3 ± 0.7 (50% C4)**
Sheep (C3 diet)	-70.6 (Germany)	(Levin et al 1999)	**-60.6 ± 2.2 (70% C3)**

As present day research attempts to reduce source emission uncertainties and quantify emissions that are relevant for regulations as well as international agreements, large efforts are being made towards the understanding and accuracy of $\delta^{13}CH_4$ measurements. Projects which aim to identify and evaluate methane emissions using mobile measurements, isotopes and modelling will greatly increase the temporal and spatial understanding of $\delta^{13}CH_4$ signatures in Europe. A number of findings from this thesis can be useful for such future studies including; improved calibration strategies for $\delta^{13}CH_4$ on CRDS, improved CH_4 specific source apportionment methods for different sites, and the first coverage of $\delta^{13}CH_4$ signatures for the Ile-de-France region.

Chapter 6 REFERENCES

Alexe, M., Bergamaschi, P., Segers, A., Detmers, R., Butz, A., Hasekamp, O., Guerlet, S., Parker, R., Boesch, H., Frankenberg, C., Scheepmaker, R. A., Dlugokencky, E., Sweeney, C., Wofsy, S. C., and Kort, E. A.: Inverse modelling of products from GOSAT and SCIAMACHY, Atmos.Chem.Phys., 15, 113–133, doi:10.5194/acp-15-113-2015, 2015.

Allen, D. T. Methane emissions from natural gas production and use: reconciling bottom-up and top-down measurements. Current Opinion in Chemical Engineering, 5, 78-83. (2014).

Alvarez, R.A., Pacala, S.W., Winebrake, J.J., Chameides, W.L. and Hamburg, S.P., 2012. Greater focus needed on methane leakage from natural gas infrastructure. Proceedings of the National Academy of Sciences, 109(17), pp.6435-6440.

Ars, S. Caracterisation des emissions de methane a l'echelle locale a l'aide d'une method d'inversion statistique basee sur u n modele gaussien parametre avec les donnees d'un gaz traceur. PhD Thesis, Universite Paris-Saclay.(2017)

Assan, S., Baudic, A., Guemri, A., Ciais, P., Gros, V. and Vogel, F.R., 2017. Characterization of interferences to in situ observations of δ 13 CH 4 and C 2 H 6 when using a cavity ring-down spectrometer at industrial sites. Atmospheric Measurement Techniques, 10(6), p.2077.

Belis, C.A., Karagulian, F., Larsen, B.R. and Hopke, P.K., 2013. Critical review and meta-analysis of ambient particulate matter source apportionment using receptor models in Europe. Atmospheric Environment, 69, pp.94-108.

Bergamaschi, P., C. Lubina, R. Königstedt, H. Fischer, A. C. Veltkamp, and O. Zwaagstra. "Stable isotopic signatures ($\delta^{13}C$, δD) of methane from European landfill sites." *Journal of Geophysical Research: Atmospheres* 103, no. D7 (1998): 8251-8265.

Bergamaschi, Peter, Maarten Krol, Jan Fokke Meirink, Frank Dentener, Arjo Segers, John van Aardenne, Suvi Monni et al. "Inverse modeling of European CH4 emissions 2001–2006." *Journal of Geophysical Research: Atmospheres* 115, no. D22 (2010).

Bilek, R. S., S. C. Tyler, M. Kurihara, and K. Yagi. "Investigation of cattle methane production and emission over a 24-hour period using measurements of $\delta^{13}C$ and δD of emitted CH4 and rumen water." *Journal of Geophysical Research: Atmospheres* 106, no. D14 (2001): 15405-15413.

Bjerg, Bjarne, Guoqiang Zhang, Jørgen Madsen, and Hans B. Rom. "Methane emission from naturally ventilated livestock buildings can be determined from gas concentration measurements." *Environmental monitoring and assessment* 184, no. 10 (2012): 5989-6000.

Brandt, Adam R., et al. "Methane leaks from North American natural gas systems." *Science* 343.6172 (2014): 733-735.

Brinkman, G., Vance, G., Hannigan, M.P. and Milford, J.B., 2006. Use of synthetic data to evaluate positive matrix factorization as a source apportionment tool for PM2. 5 exposure data. Environmental science & technology, 40(6), pp.1892-1901.

Bonsang B., and Kanakidou,M. Nonmethane hydrocarbon measurements during the FIELDVOC 1994 experiment, Chemosphere, Global Change Science, 3, 259-273. (2001).

Caulton, Dana R., Paul B. Shepson, Renee L. Santoro, Jed P. Sparks, Robert W. Howarth, Anthony R. Ingraffea, Maria OL Cambaliza et al. "Toward a better understanding and quantification of methane emissions from shale gas development." *Proceedings of the National Academy of Sciences* 111, no. 17 (2014): 6237-6242.

Cangelosi, Richard, and Alain Goriely. "Component retention in principal component analysis with application to cDNA microarray data." *Biology direct* 2, no. 1 (2007): 2.

Cesari, D., Amato, F., Pandolfi, M., Alastuey, A., Querol, X. and Contini, D., 2016. An inter-comparison of PM10 source apportionment using PCA and PMF receptor models in three European sites. Environmental Science and Pollution Research, 23(15), pp.15133-15148.

Chai, Xiaoli, David J. Tonjes, and Devinder Mahajan. "Methane emissions as energy reservoir: Context, scope, causes and mitigation strategies." *Progress in Energy and Combustion Science* 56 (2016): 33-70.

Chanton, Jeffrey, and Karen Liptay. "Seasonal variation in methane oxidation in a landfill cover soil as determined by an in situ stable isotope technique." *Global Biogeochemical Cycles* 14, no. 1 (2000): 51-60.

Chen, L.W.A., Lowenthal, D.H., Watson, J.G., Koracin, D., Kumar, N., Knipping, E.M., Wheeler, N., Craig, K. and Reid, S., 2010. Toward effective source apportionment using positive matrix factorization: Experiments with simulated PM2. 5 data. *Journal of the Air & Waste Management Association*, *60*(1), pp.43-54.

Coleman, Dennis D., J. Bruno Risatti, and Martin Schoell. "Fractionation of carbon and hydrogen isotopes by methane-oxidizing bacteria." *Geochimica et Cosmochimica Acta* 45, no. 7 (1981): 1033-1037.

Contini, D., Belosi, F., Gambaro, A., Cesari, D., Stortini, A.M. and Bove, M.C., 2012. Comparison of PM10 concentrations and metal content in three different sites of the Venice Lagoon: an analysis of possible aerosol sources. Journal of Environmental Sciences, 24(11), pp.1954-1965.

Daelman, Matthijs RJ, Ellen M. van Voorthuizen, Udo GJM van Dongen, Eveline IP Volcke, and Mark CM van Loosdrecht. "Methane emission during municipal wastewater treatment." *Water research* 46, no. 11 (2012): 3657-3670.

de Haas, David, Jeff Foley, and Paul Lant. "Energy and greenhouse footprints of wastewater treatment plants in south-east Queensland." *Australian Water Association, Melbourne* (2009).

Denman, K., Brasseur, G., Chidthaisong, A., Ciais, P., Cox, P. M., Dickinson, R. E., Hauglustaine, D., Heinze, C., Holland, E., Jacob, D., Lohmann, U., Ramachandran, S., da Silva Dias, P. L., C., W. S., and Zhang, X. (2007). Couplings Between Changes in the Climate System and Biogeochemistry. In Solomon, S., Qin, D., Manning, M., Chen, Z., Marquis, M., Averyt, K., Tignor, M., and Miller, H., editors, *Climate Change 2007: The Physical Science Basis. Contribution of Working Group I to the Fourth Assessment Report of the Intergovernmental Panel on Climate Change*. Cambridge University Press, Cambridge, United Kingdom and New York, NY, USA.

Ding, Luyu, Wei Cao, Zhengxiang Shi, Baoming Li, Chaoyuan Wang, Guoqiang Zhang, and Simon Kristensen. "Carbon dioxide and methane emissions from the scale model of open dairy lots." *Journal of the Air & Waste Management Association* 66, no. 7 (2016): 715-725.

Dlugokencky, Ed. "Trends in atmospheric methane." *Global Greenhouse Gas Reference Network* (2016).

*Dlugokencky, Ed, NOAA/ESRL (*www.esrl.noaa.gov/gmd/ccgg/trends_ch4/)

Hindrichsen, I. K., H. R. Wettstein, A. Machmüller, B. Jörg, and M. Kreuzer. "Effect of the carbohydrate composition of feed concentratates on methane emission from dairy cows and their slurry." *Environmental monitoring and assessment* 107, no. 1 (2005): 329-350.

Höglund-Isaksson, L. Global anthropogenic methane emissions 2005–2030: technical mitigation potentials and costs. Atmospheric Chemistry and Physics, 12(19), 9079-9096. (2012).

Etminan, M., G. Myhre, E. J. Highwood and K. P. Shine (2016), Radiative forcing of carbon dioxide, methane, and nitrous oxide: A significant revision of the methane radiative forcing, Geophys. Res.Lett,43.

Eurostat:(http://ec.europa.eu/eurostat/statisticsexplained/index.php/Natural_gas_consumption_statistics) (2017)

Fisher, R., Lowry, D., Wilkin, O., Sriskantharajah, S. and Nisbet, G. High- precision, automated stable isotope analysis of atmospheric methane and carbon dioxide using continuous-flow isotope-ratio mass spectrometery. Rapid communications in mass spectrometry, 20(2), 200-208. (2006)

Gilman, J. B., Lerner, B. M., Kuster, W. C., & De Gouw, J. A. Source signature of volatile organic compounds from oil and natural gas operations in northeastern Colorado. Environmental science & technology, 47(3), 1297-1305. (2013).

Gros**,** V. , Gaimoz,C., Herrmann,F., Custer,T., Williams,J., Bonsang,B., Sauvage,S., Locoge,N., d'Argouges,O., Sarda-Estève,R., and Sciare,J. Volatile Organic Compounds Sources in Paris in spring 2007. Part I: qualitative analysis, Environmental Chemistry, 8, 74-90. (2011).

Haque, Md Najmul, Cecile Cornou, and Jørgen Madsen. "Estimation of methane emission using the CO 2 method from dairy cows fed concentrate with different carbohydrate compositions in automatic milking system." *Livestock Science* 164 (2014): 57-66.

Hausmann, Petra, Ralf Sussmann, and Dan Smale. "Contribution of oil and natural gas production to renewed increase in atmospheric methane (2007–2014): top–down estimate from ethane and methane column observations." *Atmospheric Chemistry and Physics* 16.5 (2016): 3227-3244.

Hein, R., Crutzen, P. J., and Heimann, M.: An inverse modeling approach to investigate the global atmospheric methane cycle, Global Biogeochem. Cy., 11, 43–76, 1997.

Helmig, Detlev, C. R. Thompson, Jason Evans, P. Boylan, J. Hueber, and J-H. Park. "Highly elevated atmospheric levels of volatile organic compounds in the Uintah Basin, Utah." *Environmental Science & Technology* 48, no. 9 (2014): 4707-4715.

Hiller, R. V., Bretscher, D., DelSontro, T., Diem, T., Eugster, W., Henneberger, , R. Henneberger, S. Hobi, E. Hodson, D. Imer, M. Kreuzer, T. Künzle, L. Merbold, P. A. Niklaus, B. Rihm, A. Schellenberger[1], M. H. Schroth, C. J. Schubert, H. Siegrist, J. Stieger, N. Buchmann, and D. Brunner. Anthropogenic and natural methane fluxes in Switzerland synthesized within a spatially explicit inventory. Biogeosciences, 11(7), 1941-1959. (2014).

Höglund-Isaksson, L. Global anthropogenic methane emissions 2005–2030: technical mitigation potentials and costs. Atmospheric Chemistry and Physics, 12(19), 9079-9096. (2012).

Hopke, P.K., 2015. It is time to drop principal components analysis as a "receptor model". *Journal of Atmospheric Chemistry*, *72*(2), pp.127-128.

Hopke, P.K., Ito, K., Mar, T., Christensen, W.F., Eatough, D.J., Henry, R.C., Kim, E., Laden, F., Lall, R., Larson, T.V. and Liu, H., 2006. PM source apportionment and health effects: 1. Intercomparison of source apportionment results. Journal of Exposure Science and Environmental Epidemiology, 16(3), p.275.

Howarth, Robert W., Renee Santoro, and Anthony Ingraffea. "Methane and the greenhouse-gas footprint of natural gas from shale formations." *Climatic Change* 106, no. 4 (2011): 679.

IPCC: Climate Change 2007: the physical Science Basis. Contribution of Working Group I to the Fourth Assement Report of the Intergovernmantal Panel on Climate Change, Cambridge University Press, Cambridge, United Kingdom and New York, NY , USA, 2007.

IPCC: Climate Change 2013: the physical Science Basis. Contribution of Working Group I to the Fith Assement Report of the Intergovernmantal Panel on Climate Change, Cambridge University Press, Cambridge, United Kingdom and New York, NY , USA, 2013.

Jackson, R. B., Down, A., Phillips, N. G., Ackley, R. C., Cook, C. W., Plata, D. L., & Zhao, K. Natural gas pipeline leaks across Washington, DC. Environmental science & technology, 48(3), 2051-2058. (2014)

JRC, 2012. European Commission, Joint Research Centre (JRC)/Netherland Environmental Assessment Agency (PBL). Emission Database for Global Atmospheric Research (EDGAR): edgar.jrc.ec.europa.eu

Kang, Mary, et al. "Identification and characterization of high methane-emitting abandoned oil and gas wells." *Proceedings of the National Academy of Sciences* 113.48 (2016): 13636-13641

Kirschke, Stefanie, Philippe Bousquet, Philippe Ciais, Marielle Saunois, Josep G. Canadell, Edward J. Dlugokencky, Peter Bergamaschi et al. "Three decades of global methane sources and sinks." *Nature Geoscience* 6, no. 10 (2013): 813-823.

Kinsman, R., F. D. Sauer, H. A. Jackson, and M. S. Wolynetz. "Methane and carbon dioxide emissions from dairy cows in full lactation monitored over a six-month period." *Journal of Dairy Science* 78, no. 12 (1995): 2760-2766.

Klevenhusen, F., Stefano M. Bernasconi, Michael Kreuzer, and Carla R. Soliva. "Experimental validation of the Intergovernmental Panel on Climate Change default values for ruminant-derived methane and its carbon-isotope signature." *Animal Production Science* 50, no. 3 (2010): 159-167.

Koerkamp, PWG Groot, J. H. M. Metz, G. H. Uenk, V. R. Phillips, M. R. Holden, R. W. Sneath, J. L. Short et al. "Concentrations and emissions of ammonia in livestock buildings in Northern Europe." *Journal of Agricultural Engineering Research* 70, no. 1 (1998): 79-95.

Koss, A. R., J. de Gouw, C. Warneke, J. B. Gilman, B. M. Lerner, M. Graus, B. Yuan et al. "Photochemical aging of volatile organic compounds associated with oil and natural gas extraction in the Uintah Basin, UT, during a wintertime ozone formation event." *Atmospheric Chemistry and Physics* 15, no. 10 (2015): 5727-5741.

Lamb, B. K., McManus, J. B., Shorter, J. H., Kolb, C. E., Mosher, B., Harriss, R. C., Allwine,E., Blaha, D., Howard,T., Guenther,A., Lott, R. A., Siverson,R., Westburg, H., Zimmerman,P. Development of atmospheric tracer methods to measure methane emissions from natural gas facilities and urban areas. Environmental science & technology, 29(6), 1468-1479. (1995).

Lassey, Keith R. "Livestock methane emission and its perspective in the global methane cycle." *Australian Journal of Experimental Agriculture* 48, no. 2 (2008): 114-118.

Laurent, O et al. "Icos ATC Metrology Lab: Metrological performance assessment of GHG analyzers." Atmospheric Measurement Techniques 8.10 (2015): 4075-4082. Poster session presented at: 18th WMO/IAWA Meeting on Carbon Dioxide, Other Greenhouse Gases, and Related Measurement Techniques (GGMT). Sep 13-17. 2015; California, CA.

Levin, Ingeborg, Peter Bergamaschi, Helmut Dörr, and Dorothea Trapp. "Stable isotopic signature of methane from major sources in Germany." *Chemosphere* 26, no. 1-4 (1993): 161-177.

Lee, Mark A., Allison Todd, Mark A. Sutton, Mizeck GG Chagunda, David J. Roberts, and Robert M. Rees. "A time-series of methane and carbon dioxide production from dairy cows during a period of dietary transition." *Cogent Environmental Science* 3, no. 1 (2017): 1385693.

Lowry, D., Holmes, C. W., Rata, N. D., O'Brien, P., & Nisbet, E. G. London methane emissions: Use of diurnal changes in concentration and $\delta^{13}C$ to identify urban sources and verify inventories. Journal of Geophysical Research: Atmospheres, 106(D7), 7427-7448. (2001).

Lopez, M., O. A. Sherwood, E. J. Dlugokencky, R. Kessler, L. Giroux, and D. E. J. Worthy. "Isotopic signatures of anthropogenic CH4 sources in Alberta, Canada." *Atmospheric Environment* 164 (2017): 280-288.

Madsen, Jørgen, Bjarne Schmidt Bjerg, Torben Hvelplund, Martin Riis Weisbjerg, and Peter Lund. "Methane and carbon dioxide ratio in excreted air for quantification of the methane production from ruminants." *Livestock Science* 129, no. 1 (2010): 223-227.

Malowany, K., Stix, J., Van Pelt, A., & Lucic, G. H 2 S interference on CO 2 isotopic measurements using a Picarro G1101-i cavity ring-down spectrometer. Atmospheric Measurement Techniques, 8(10), 4075-4082. (2015).

Miller, J.B., and Tans, P.P. "Calculating isotopic fractionation from atmospheric measurements at various scales." Tellus B 55.2 (2003): 207-214. (2003).

Mikaloff Fletcher, Sara E., Pieter P. Tans, Lori M. Bruhwiler, John B. Miller, and Martin Heimann. "CH4 sources estimated from atmospheric observations of CH4 and its 13C/12C isotopic ratios: 1. Inverse modeling of source processes." *Global Biogeochemical Cycles* 18, no. 4 (2004).

Moreno, N., Viana, M., Pandolfi, M., Alastuey, A., Querol, X., Chinchón, S., Pinto, J.F., Torres, F., Díez, J.M. and Saéz, J., 2009. Determination of direct and fugitive PM emissions in a Mediterranean harbour by means of classic and novel tracer methods. Journal of environmental management, 91(1), pp.133-141

Mønster, Jacob G., Jerker Samuelsson, Peter Kjeldsen, Chris W. Rella, and Charlotte Scheutz. "Quantifying methane emission from fugitive sources by combining tracer release and downwind measurements–a sensitivity analysis based on multiple field surveys." *Waste Management* 34, no. 8 (2014): 1416-1428.

Mønster, Jacob, Charlotte Scheutz, and Peter Kjeldsen. "Quantifying greenhouse gas emissions from waste treatment facilities." PhD diss., PhD thesis, DTU Environment, Kgs. Lyngby, 2014.

Myhre, Gunnar, et al. "Anthropogenic and natural radiative forcing." *Climate change* 423 (2013): 658-740.

Norris, G., Vedantham, R. and Wade, K., 2008. EPA Positive Matrix Factorization (PMF) 3.0-Fundamentals & User Guide. US Environmental Protections Agency EPA 600. R-08/108. Available: http://www. epa. gov/heasd/products/pmf/EPA PMF 3.0 User Guide v16_092208_final. pdf

Norris, G.A., Duvall, R., Brown, S.G. and Bai, S., 2014. EPA Positive Matrix Factorization (PMF) 5.0 fundamentals and User Guide Prepared for the US Environmental Protection Agency Office of Research and Development, Washington, DC. DC EPA/600/R-14/108.

Nara, H., H. Tanimoto, Y. Tohjima, H. Mukai, Y. Nojiri, K. Katsumata, and C. W. Rella. "Effect of air composition (N2, O2, Ar, and H2O) on CO2 and CH4 measurement by wavelength-scanned cavity ring-down spectroscopy: calibration and measurement strategy." *Atmospheric Measurement Techniques* 5, no. 11 (2012): 2689.

National Atmospheric Emissions Inventories: (http://naei.defra.gov.uk/)

Nisbet, E. G., E. J. Dlugokencky, M. R. Manning, D. Lowry, R. E. Fisher, J. L. France, S. E. Michel et al. "Rising atmospheric methane: 2007–2014 growth and isotopic shift." *Global Biogeochemical Cycles* 30, no. 9 (2016): 1356-1370.

Nisbet, E. G., Dlugokencky, E. J., and Bousquet, P.: Methane on the Rise-Again, Science, 343, 493–495, doi:10.1126/science.1247828, 2014

Ngwabie, N. M., K-H. Jeppsson, S. Nimmermark, C. Swensson, and G. Gustafsson. "Multi-location measurements of greenhouse gases and emission rates of methane and ammonia from a naturally-ventilated barn for dairy cows." *Biosystems Engineering*103, no. 1 (2009): 68-77.

O'Leary, Marion H. "Carbon isotopes in photosynthesis." *Bioscience* 38, no. 5 (1988): 328-336.

Paatero, P., and Tapper, U.: Positive matrix factorization: a non-negative factor model with optimal utilization of error estimates of data values, Environmetrics, 5, 111- 126, 1994.

Pandey, S., Houweling, S., Krol, M., Aben, I., Chevallier, F., Dlu- gokencky, E. J., Gatti, L. V., Gloor, E., Miller, J. B., Detmers, R., Machida.: Inverse modeling of GOSAT- retrieved ratios of total 2009 and 2010, Atmos. Chem. Phys., 16, 5043–5062, doi:10.5194/acp-16-5043- 2016, 2016.

Patra, P. K., Saeki, T., Dlugokencky, E. J., Ishijima, K., Umezawa, T., Ito, A., Aoki, S., Morimoto, S., Kort, E. A., Crotwell, A., Ravikumar, K., and Nakazawa, T.: Regional methane emission estimation based on observed atmospheric concen- trations (2002–2012), J. Meteorol. Soc. Jpn., 94, 85–107, doi:10.2151/jmsj.2016-006, 2016.

Penman, James, D.Kruger, I.E. Galbally, T.Hiraishi, B.Nyenzi, S.Emmanuel, L.Buendia et al. “Good practise guidance and uncertainty management in national greenhouse gas inventories.” (2000)

Pétron, Gabrielle, Anna Karion, Colm Sweeney, Benjamin R. Miller, Stephen A. Montzka, Gregory J. Frost, Michael Trainer et al. "A new look at methane and nonmethane hydrocarbon emissions from oil and natural gas operations in the Colorado Denver-Julesburg Basin." *Journal of Geophysical Research: Atmospheres* 119, no. 11 (2014): 6836-6852.

Phillips, N. G., Ackley, R., Crosson, E. R., Down, A., Hutyra, L. R., Brondfield, M., Karr,J.D., Zhao, K., Jackson, R. B. Mapping urban pipeline leaks: Methane leaks across Boston. Environmental pollution, 173, 1-4. (2013).

Pratt, Chris, Adrian S. Walcroft, Julie Deslippe, and Kevin R. Tate. "CH 4/CO 2 ratios indicate highly efficient methane oxidation by a pumice landfill cover-soil." *Waste management* 33, no. 2 (2013): 412-419.

Quay, Paul, John Stutsman, David Wilbur, Amy Snover, Ed Dlugokencky, and Tom Brown. "The isotopic composition of atmospheric methane." *Global Biogeochemical Cycles* 13, no. 2 (1999): 445-461.

R Core Team (2016). R: A language and environment for statistical computing. R Foundation for Statistical Computing, Vienna, Austria. URL https://www.R-project.org/.

Rentrop, M., 2007, Untersuchung natürlicher und anthropogener Quellen und Senken von Treibhausgasen im Rahmen von CarboSchools. State Examination Thesis, Ruprecht-Karls Universitaet, Heidelberg, Germany

Röckmann, T., Eyer, S., Veen, C.V.D., Popa, M.E., Tuzson, B., Monteil, G., Houweling, S., Harris, E., Brunner, D., Fischer, H. and Zazzeri, G., 2016. In situ observations of the isotopic composition of methane at the Cabauw tall tower site. Atmospheric chemistry and physics, 16(16), pp.10469-10487.

Rella, C. W., J. Hoffnagle, Y. He, and S. Tajima. "Local-and regional-scale measurements of CH 4, δ 13 CH 4, and C 2 H 6 in the Uintah Basin using a mobile stable isotope analyzer." *Atmospheric Measurement Techniques* 8, no. 10 (2015): 4539-4559.

Roscioli, J. R., Yacovitch, T. I., Floerchinger, C., Mitchell, A. L., Tkacik, D. S., Subramanian, Martinez, D. M., Vaughn, T. L., Williams, L., Zimmerle, D., Robinson, A. L., Herndon, S. C., & Marchese, A. J. Measurements of methane emissions from natural gas gathering facilities and processing plants: measurement methods. Atmospheric Measurement Techniques, 8(5), 2017-2035. (2015).

Saunois, M., Bousquet, P., Poulter, B., Peregon, A., Ciais, P., Canadell, J.G., Dlugokencky, E.J., Etiope, G., Bastviken, D., Houweling, S. and Janssens-Maenhout, G., 2016. The global methane budget 2000-2012. Earth System Science Data, 8(2), p.697.

Schneising, Oliver, John P. Burrows, Russell R. Dickerson, Michael Buchwitz, Maximilian Reuter, and Heinrich Bovensmann. "Remote sensing of fugitive methane emissions from oil and gas production in North American tight geologic formations." *Earth's Future* 2, no. 10 (2014): 548-558.

Schoell, M. Genetic characterization of natural gases. AAPG bulletin, 67(12), 2225-2238. (1983).

Schwietzke, Stefan, W. Michael Griffin, H. Scott Matthews, and Lori MP Bruhwiler. "Natural gas fugitive emissions rates constrained by global atmospheric methane and ethane." *Environmental science & technology* 48, no. 14 (2014): 7714-7722.

Shrivastava, Manish K., R. Subramanian, Wolfgang F. Rogge, and Allen L. Robinson. "Sources of organic aerosol: Positive matrix factorization of molecular marker data and comparison of results from different source apportionment models." *Atmospheric Environment* 41, no. 40 (2007): 9353-9369.

Smith, M. L., Kort, E. A., Karion, A., Sweeney, C., Herndon, S. C., & Yacovitch, T. I. Airborne ethane observations in the Barnett shale: Quantification of ethane flux and attribution of methane emissions. Environmental science & technology, 49(13), 8158-8166. (2015).

Smith, Pete, Davis Reay, and Andre Van Amstel, eds. *Methane and Climate Change*. Routledge, 2010.

So, K. L., and T. Wang. "C 3–C 12 non-methane hydrocarbons in subtropical Hong Kong: spatial–temporal variations, source–receptor relationships and photochemical reactivity." *Science of the Total Environment* 328, no. 1 (2004): 161-174.

Sonderfeld, Hannah, Hartmut Bösch, Antoine PR Jeanjean, Stuart N. Riddick, Allen Grant, Sébastien Ars, Stewart Davies et al. "CH4 emission estimates from an active landfill site inferred from a combined approach of CFD modelling and in situ FTIR measurements." *Atmospheric Measurement Techniques, available online* 3 (2017).

Staufer, J., Broquet, G., Bréon, F.M., Puygrenier, V., Chevallier, F., Xueref-Rémy, I., Dieudonné, E., Lopez, M., Schmidt, M., Ramonet, M. and Perrussel, O., 2016. The first 1-year-long estimate of the Paris region fossil fuel CO 2 emissions based on atmospheric inversion. Atmospheric Chemistry and Physics, 16(22), pp.14703-14726.

Stevens, C. M., & Engelkemeir, A. Stable carbon isotopic composition of methane from some natural and anthropogenic sources. Journal of Geophysical Research: Atmospheres, 93(D1), 725-733. (1988).

Subramanian, R., Williams, L. L., Vaughn, T. L., Zimmerle, D., Roscioli, J. R., Herndon, S. C., Yacovitch, T.L., Floerchinger, C., Tkacik, D.S., Mitchell, A.L., Sullivan, M. R., Dallmann, T.R., & Robinson, A.L. Methane emissions from natural gas compressor stations in the transmission and storage sector: Measurements and comparisons with the EPA greenhouse gas reporting program protocol. Environmental science & technology, 49(5), 3252-3261. (2015).

Tauler, R., Viana, M., Querol, X., Alastuey, A., Flight, R.M., Wentzell, P.D. and Hopke, P.K., 2009. Comparison of the results obtained by four receptor modelling methods in aerosol source apportionment studies. Atmospheric Environment, 43(26), pp.3989-3997.

Thurston, G.D. and Spengler, J.D., 1985. A quantitative assessment of source contributions to inhalable particulate matter pollution in metropolitan Boston. Atmospheric Environment (1967), 19(1), pp.9-25.

Tyler, Stanley C., Andrew L. Rice, and Henry O. Ajie. "Stable isotope ratios in atmospheric CH4: Implications for seasonal sources and sinks." *Journal of Geophysical Research: Atmospheres* 112, no. D3 (2007).

UNEP 2012: The Emissions Gap Report 2012, United Nations Environment Program, Nairobi. Found here (http://staging.unep.org/pdf/2012gapreport.pdf)

U.S. Environmental Protection Agency's (U.S. EPA's). (2011) Global Anthropogenic Emissions of Non-CO2 Greenhouse Gases: 1990–2030. EPA 430-D-11-003

U.S Environmental Protection Agency. "Inventory of U.S Greenhouse Gas Emissions and Sinks: 1990-2014." EPA 430-R-16-002 (2016): Annex 7. Found online here: https://www3.epa.gov/climatechange/Downloads/ghgemissions/US-GHG-Inventory-2016-Annex-7-Uncertainty.pdf

Vermorel, Michel, J. Pierre Jouany, Maguy Eugene, Daniel Sauvant, Jean Noblet, and Jean-Yves Dourmad. 'Evaluation quantitative des emissions de methane enterique par les animaux d'elevage en 2007 en France." *INRA Prod. Anim 21*, no 5 (2008): 403-418

Viana, M., Querol, X., Alastuey, A., Gil, J.I. and Menéndez, M., 2006. Identification of PM sources by principal component analysis (PCA) coupled with wind direction data. Chemosphere, 65(11), pp.2411-2418.

Viana, M., Pandolfi, M., Minguillón, M.C., Querol, X., Alastuey, A., Monfort, E. and Celades, I., 2008. Inter-comparison of receptor models for PM source apportionment: case study in an industrial area. Atmospheric Environment, 42(16), pp.3820-3832.

Viana, M., Kuhlbusch, T.A.J., Querol, X., Alastuey, A., Harrison, R.M., Hopke, P.K., Winiwarter, W., Vallius, M., Szidat, S., Prévôt, A.S.H. and Hueglin, C., 2008. Source apportionment of particulate matter in Europe: a review of methods and results. Journal of aerosol science, 39(10), pp.827-849.

Vogel, F. R., Huang, L., Ernst, D., Giroux, L., Racki, S., & Worthy, D. E. J. Evaluation of a cavity ring-down spectrometer for in situ observations of 13 CO 2. Atmospheric Measurement Techniques, 6(2), 301-308. (2013).

Vogel, Johann C. "Fractionation of the carbon isotopes during photosynthesis." In *Fractionation of the Carbon Isotopes during Photosynthesis*, pp. 5-29. Springer, Berlin, Heidelberg, 1980.

Warneke, C., F. Geiger, P. M. Edwards, W. Dube, G. Pétron, J. Kofler, A. Zahn et al. "Volatile organic compound emissions from the oil and natural gas industry in the Uintah Basin, Utah: oil and gas well pad emissions compared to ambient air composition." *Atmos. Chem. Phys* 14, no. 10977 (2014): e10988.

Warneke, C., et al. "VOC identification and inter-comparison from laboratory biomass burning using PTR-MS and PIT-MS." *International Journal of Mass Spectrometry* 303.1 (2011): 6-14.

Williams, D. J. "Methane emissions from manure of free-range dairy cows." *Chemosphere* 26, no. 1-4 (1993): 179-187.

Wolf, Julie, Ghassem R. Asrar, and Tristram O. West. "Revised methane emissions factors and spatially distributed annual carbon fluxes for global livestock." *Carbon Balance and Management* 12, no. 1 (2017): 16.

Yacovitch, T. I., Herndon, S. C., Roscioli, J. R., Floerchinger, C., McGovern, R. M., Agnese, M., Pétron, G., Kofler, J., Sweeney, C., Karion, A., Conley, S. A., Kort, E. A., Nähle,L., Fischer, M., Hildebrandt,L., Koeth,J.,

McManus, J. B., Nelson, D. D., Zahniser, M. S., & Kolb. C. E. Demonstration of an ethane spectrometer for methane source identification. Environmental science & technology, 48(14), 8028-8034. (2014).

Yacovitch, T. I., Herndon, S. C., Pétron, G., Kofler, J., Lyon, D., Zahniser, M. S., & Kolb, C. E. Mobile laboratory observations of methane emissions in the Barnett Shale region. Environmental science & technology, 49(13), 7889-7895. (2015).

York, D. Least squares fitting of a straight line with correlated errors. Earth and Planetary Science Letters 5, (1969), 320-324. (1968).

Yvon-Lewis, S. A., Hu, L., & Kessler, J. Methane flux to the atmosphere from the Deepwater Horizon oil disaster. Geophysical Research Letters, 38(1). (2011).

Yver Kwok, C. E., D. Müller, Christopher Caldow, B. Lebègue, J. G. Monster, C. W. Rella, C. Scheutz et al. "Methane emission estimates using chamber and tracer release experiments for a municipal waste water treatment plant." (2015): 2853.

Zazzeri, G., Methane Emission in UK: Deciphering Regional Sources with Mobile Measurements and Isotopic Characterisation. Thesis. Royal Holloway, University of London.

Zazzeri, G., Lowry, D., Fisher, R.E., France, J.L., Lanoisellé, M., Grimmond, C.S.B. and Nisbet, E.G., 2017. Evaluating methane inventories by isotopic analysis in the London region. Scientific Reports, 7.

Zazzeri, G., Lowry, D., Fisher, R.E., France, J.L., Lanoisellé, M. and Nisbet, E.G., 2015. Plume mapping and isotopic characterisation of anthropogenic methane sources. Atmospheric Environment, 110, pp.151-162.

Zhang, YuanXun, Rebecca J. Sheesley, Min-Suk Bae, and James J. Schauer. "Sensitivity of a molecular marker based positive matrix factorization model to the number of receptor observations." *Atmospheric Environment* 43, no. 32 (2009): 4951-4958.

APPENDIX A: CHAPTER 2 SUPPLEMENTARY MATERIAL

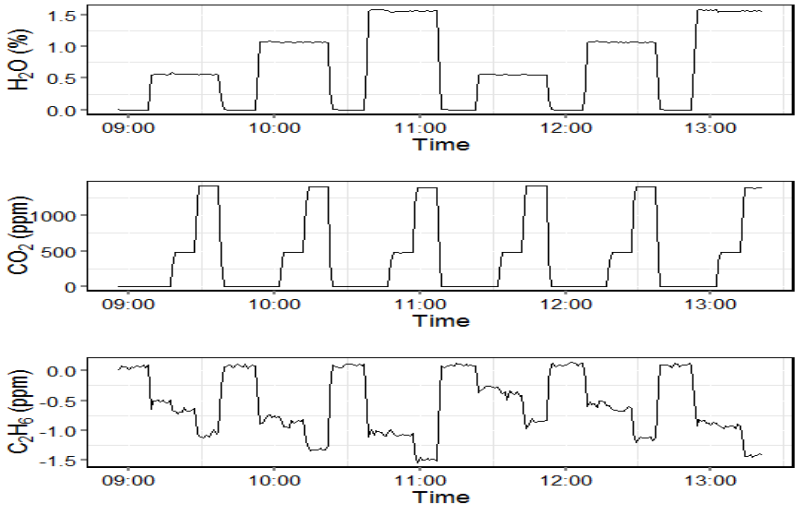

Figure S2.1: Time series of CO_2 interference experiment at varying H_2O concentrations. As H_2O and CO_2 are altered, the reported C_2H_6 is expected to be constant given there is no C_2H_6 input. However due to interference the corresponding shifts of reported C_2H_6 are evident

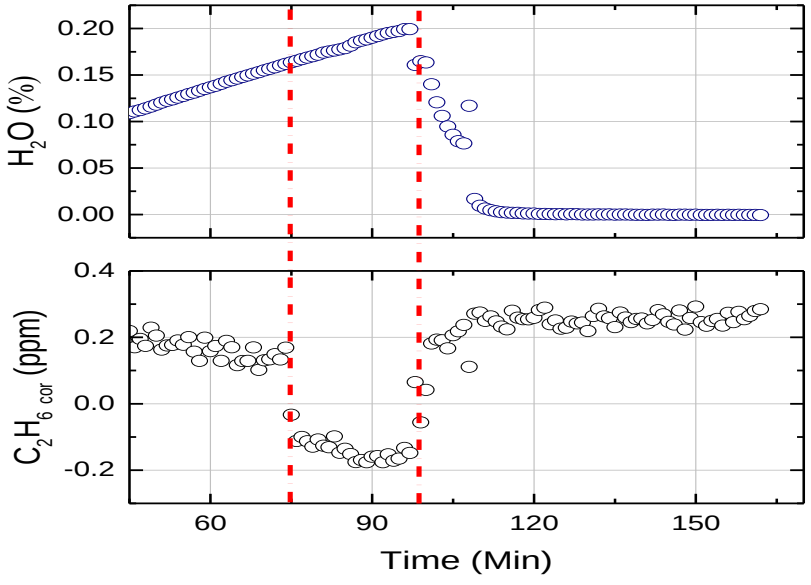

Figure S2.2: Time series of the discontinuity for instrument CFIDS 2067, the H_2O content is increased and decreased crossing the 0.16% H_2O threshold twice. The point at which 0.16% H_2O humidity is reached is marked by red dashed lines. The discontinuity is present when moving from dry to wet air, and inversely from wet to dry air.

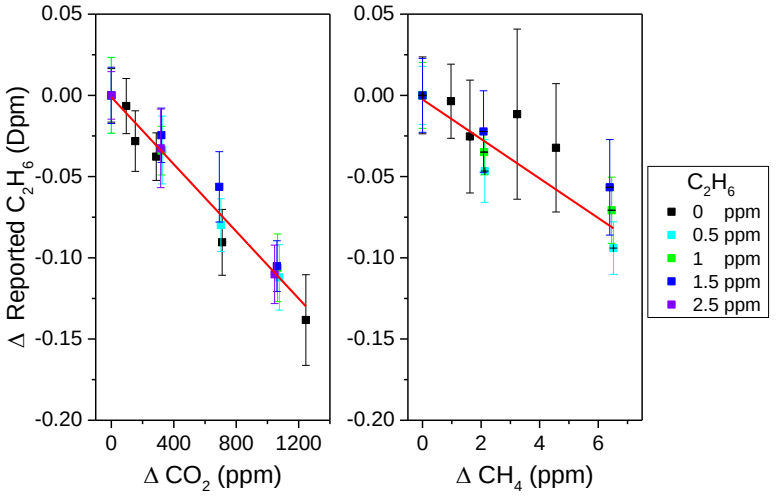

Figure S2.3: Relationship between the reported C_2H_6 and concentration changes of CO_2 (left) and CH_4 (right) at 5 C_2H_6 concentrations for instrument CFIDS 2072. The concentration change (from background levels) of the targeted gas is plotted on the x-axis, while the change in reported C_2H_6 is plotted on the y-axis. Markers represent a 20 minute average, with error bars denoting the standard deviation. For each dilution series, C_2H_6 concentration was kept constant at different concentrations, represented by the coloured markers. The CH_4 correction was examined up to 1.5 ppm C_2H_6 to sustain a C_2H_6:CH_4 ratio <1, well above the upper range expected from natural gas sources. At all C_2H_6 concentrations examined, for both ΔCO_2 and ΔCH_4, the response function agreed within the uncertainties to that calculated at 0 ppm C_2H_6. The red line represents the linear fit taking into account both X and Y error; Pearson's R is -0.99 and -0.89 for concentration changes of both CO_2 and CH_4 respectively.

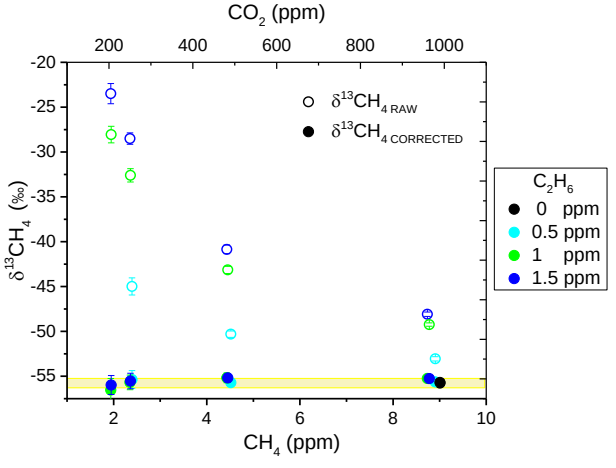

Figure S2.4: Isotopic signal (raw and corrected) from the CRDS for varying mixtures of CH4, CO2 and C2H6 at ~0% H2O. The top and bottom x-axis represent the CO2, and CH4 concentration respectively. The y-axis represents the methane isotopic signal before and after correction, shown by empty and filled markers respectively. For each dilution series, CO2 and CH4 were altered while C2H6 concentration was kept constant at different concentrations (ppm), represented by the coloured markers. The raw δ^{13}CH4 signal is subject to large biases, while the corrected δ^{13}CH4 maintains the standard value, -55.7 +/- 0.2 (highlighted in yellow).

APPENDIX B: CHAPTER 3 SUPPLEMENTARY MATERIAL

B.1 Comparison of ECMWF wind fields with onsite meteorological data.

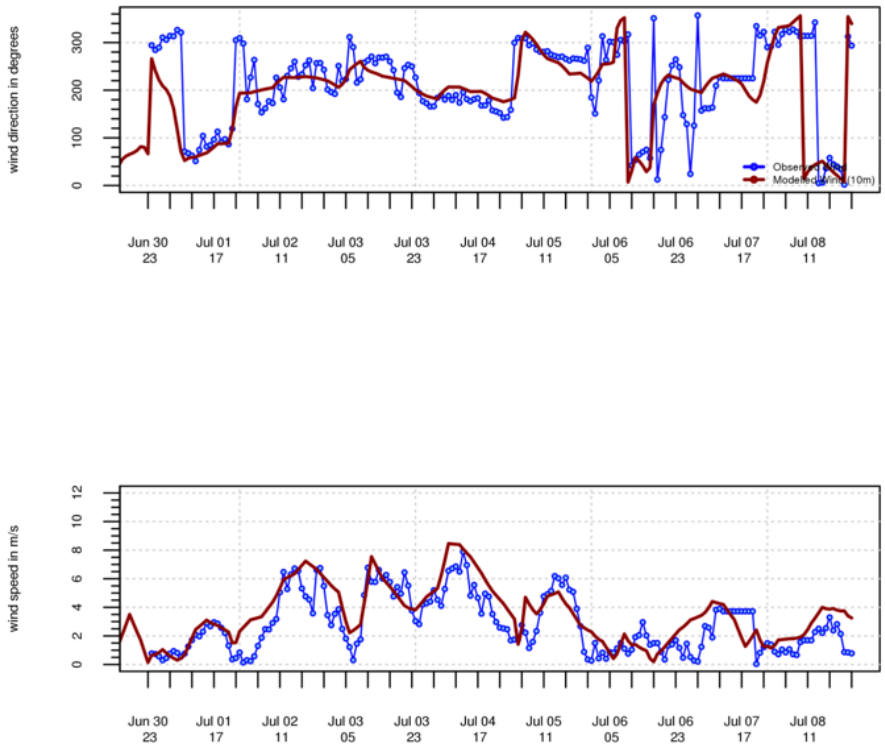

Figure B.1: Interpolated ECMWF wind fields (red line) comparison with measurements from onsite meteorological station (blue points) for the 30th June until 8th July.

B.2 Positive Matrix Factorisation Factor Profiles

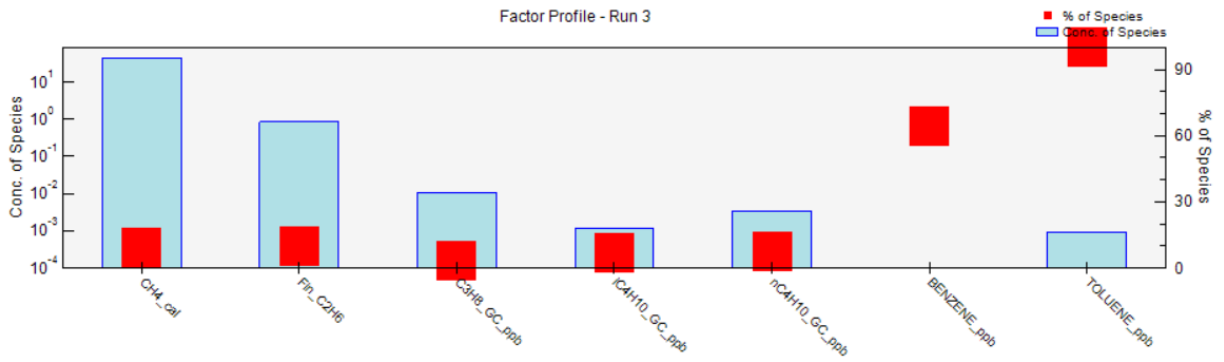

Figure B.2.1. Factor profile from PMF analysis for the factor representing traffic emissions (factor 2).

Figure B.2.2: Factor profile from PMF analysis for the factor representing natural gas emissions (factor 1).

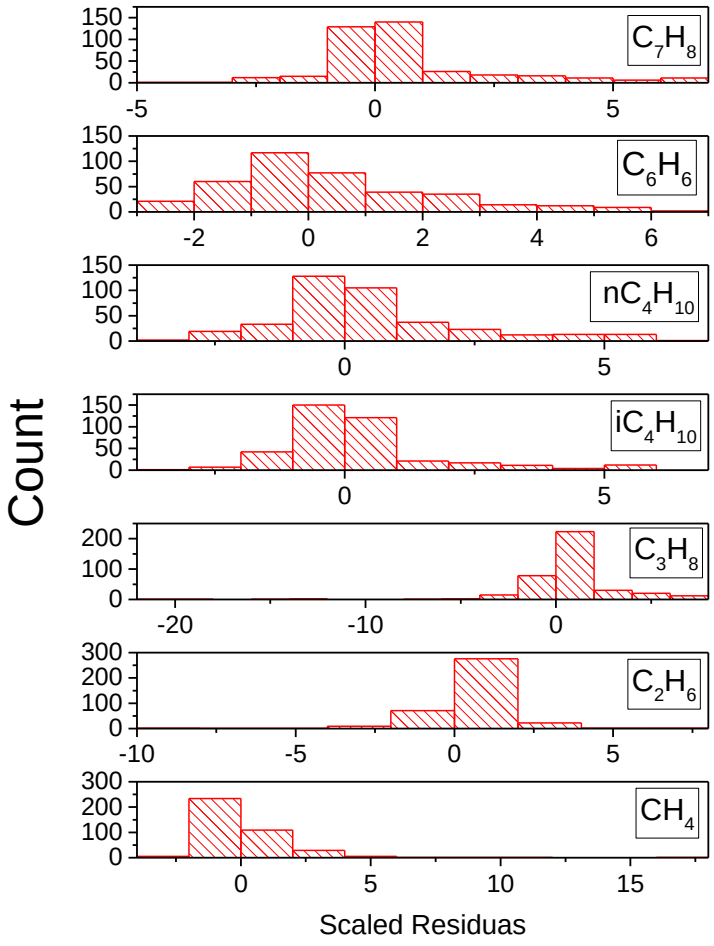

Figure B.2.3: Histogram of the scaled residuals from PMF analysis.

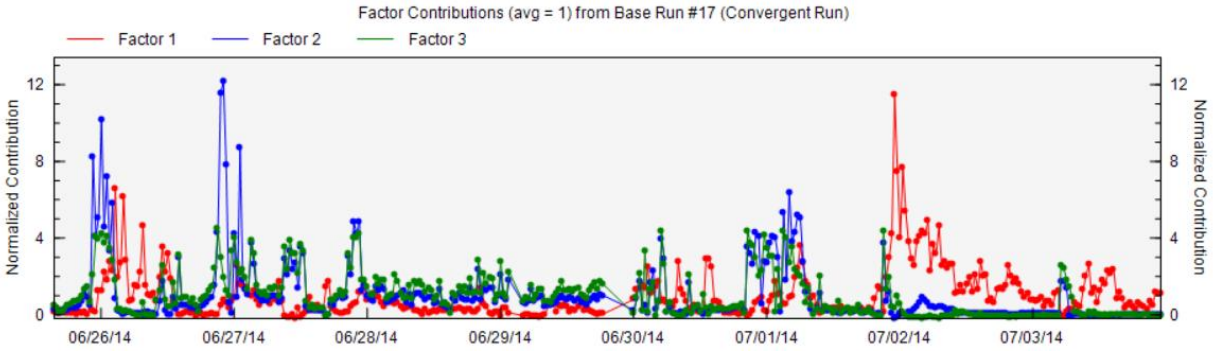

Figure B.2.4: Factor contributions from PMF analysis when defining three factors. Here factors 2 and 3 are not clearly separated and co-vary significantly

B.3. Instrumental Uncertainties

Table B.3.1: Species specific LOD values used throughout the study and % instrumental uncertainty. Instrumental uncertainties of CH_4 & CO_2 are overestimated in comparison to Picarro specifications for a G2201-I Analyser [https://www.picarro.com/products_solutions/isotope_analyzers/13c_for_ch4_co2] and were used in the PMF analysis only.

Species	**CH_4** (ppb)	**CO 2** (ppm)	**C_2H_6** (ppb)	**C_3H_8** (ppb)	**iC_4H_{10}** (ppb)	**nC_4H_{10}** (ppb)	**i /n C_5H_{12}** (ppb)	**nC_6H_{14}** (ppb)	**C_2H_4** (ppb)	**C_3H_6** (ppb)	**C_2H_2** (ppb)	**C_6H_6** (ppb)	**C_7H_8** (ppb)	**C_8H_{10}** (ppb)
LOD	1	0.1	0.075	0.075	0.05	0.05	0.05	0.025	0.075	0.15	0.15	0.015	0.015	0.015
Instrumental uncertainty	1%	1%	15%	15%	15%	15%	15%	15%	15%	15%	15%	15%	15%	15%

*Table B.3.2. Signal/Noise ratio of selected species in PMF analysis. *Although toluene has a S/N ratio below 2, it was categorised as 'strong' for the PMF analysis after empirical tests showed no significant improvement in the modelling of the species when altering its weighting or increasing the analytical uncertainty.*

Species	*Signal/Noise*
CH_4	*9.5*
C_2H_6	*5.3*
C_3H_8	*5.2*
iC_4H_{10}	*4.3*
nC_4H_{10}	*4.8*
C_7H_8	*1.8**
C_6H_6	*3.3*

APPENDIX C: CHAPTER 4 SUPPLEMENTARY MATERIAL

S4.1. PMF Factor Results for Autumn Grignon Campaign.

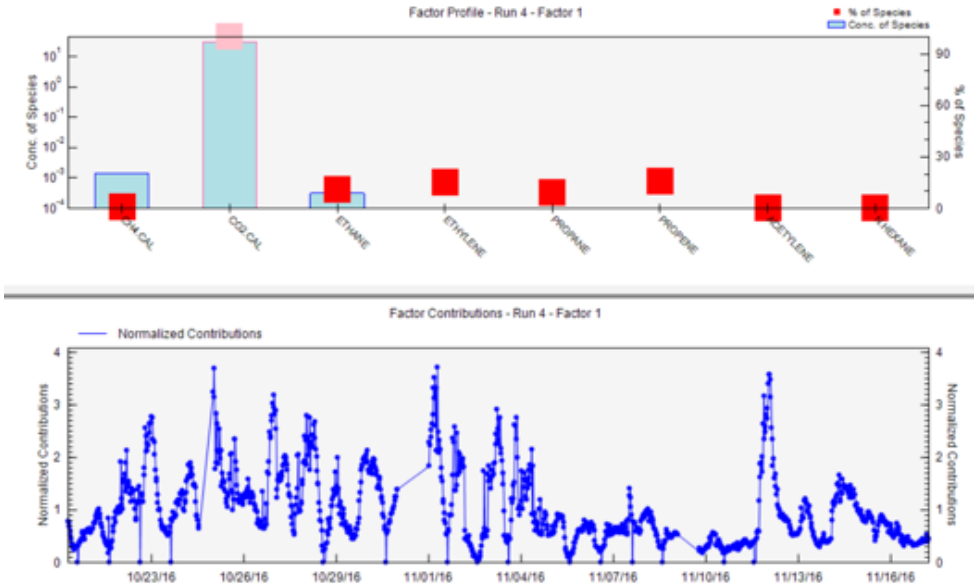

Figure S.4.1.1: Factor 1 profile [CO_2 diurnal factor], (top) concentration and % of species contributing to the factor (bottom) temporal variation of normalised contributions of factor.

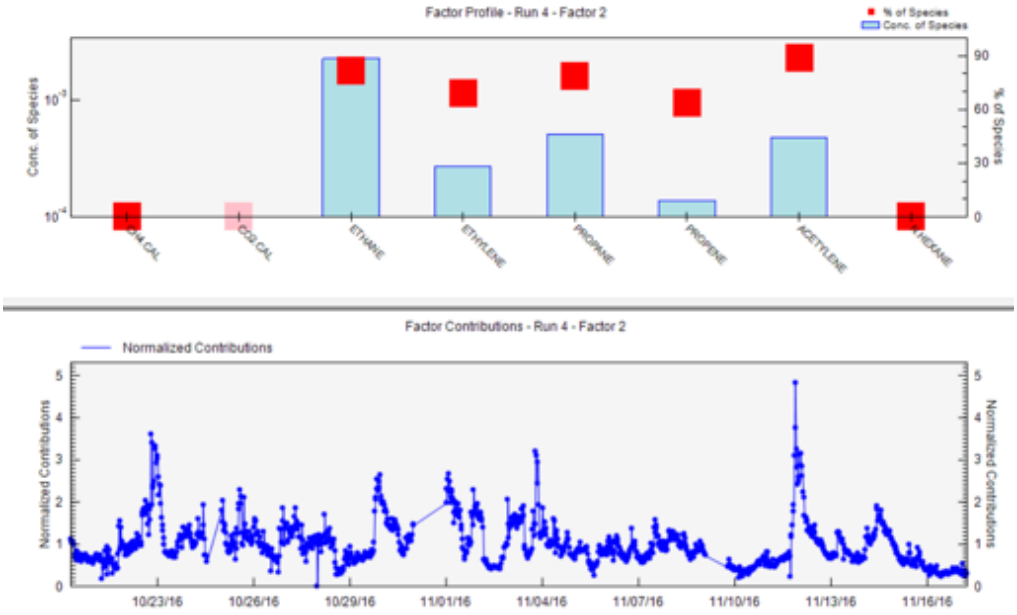

Figure S.4.1.2: Factor 2 profile [fossil fuel factor], (top) concentration and % of species contributing to the factor (bottom) temporal variation of normalised contributions of factor.

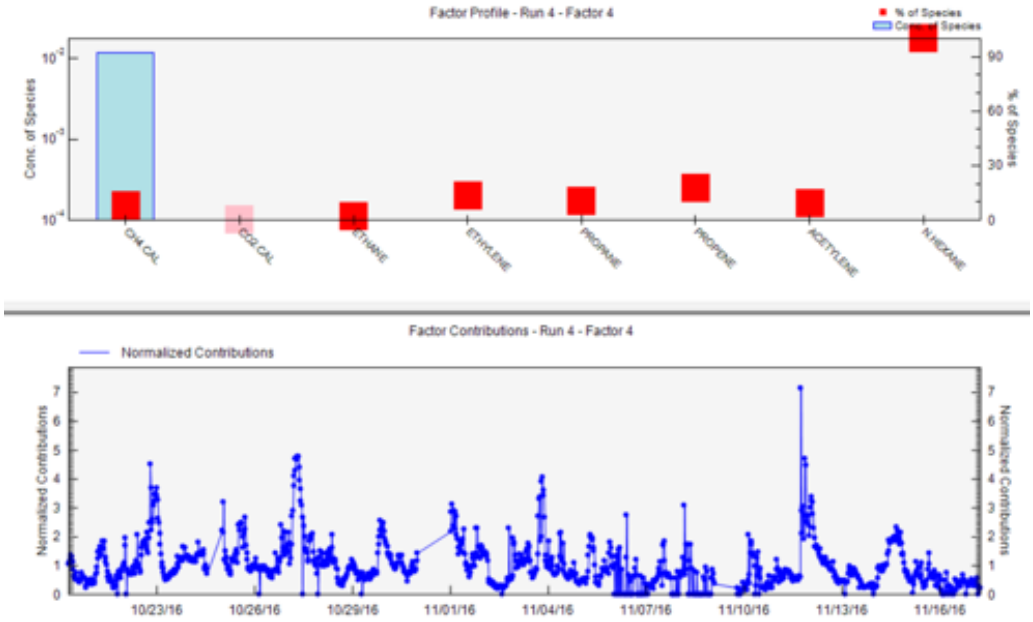

Figure S.4.1.3: Factor 4 profile [Traffic/petroleum factor], (top) concentration and % of species contributing to the factor (bottom) temporal variation of normalised contributions of factor.

S4.2. Information on number of ruminants and diet at Grignon farm for the Autumn 2016, and Spring 2017 measurement campaigns.

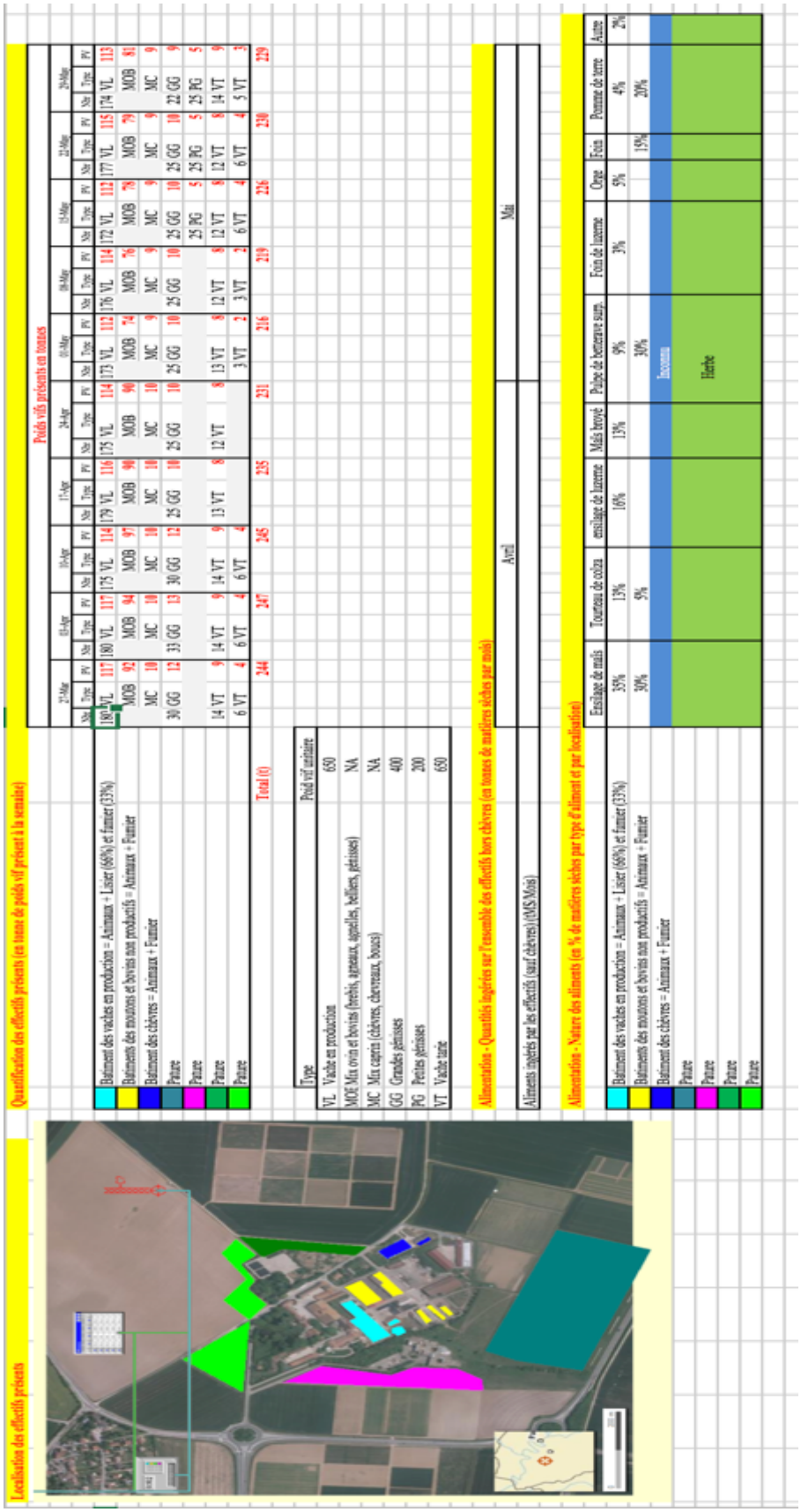

S4.3: PMF Factor Results for Spring Grignon Campaign

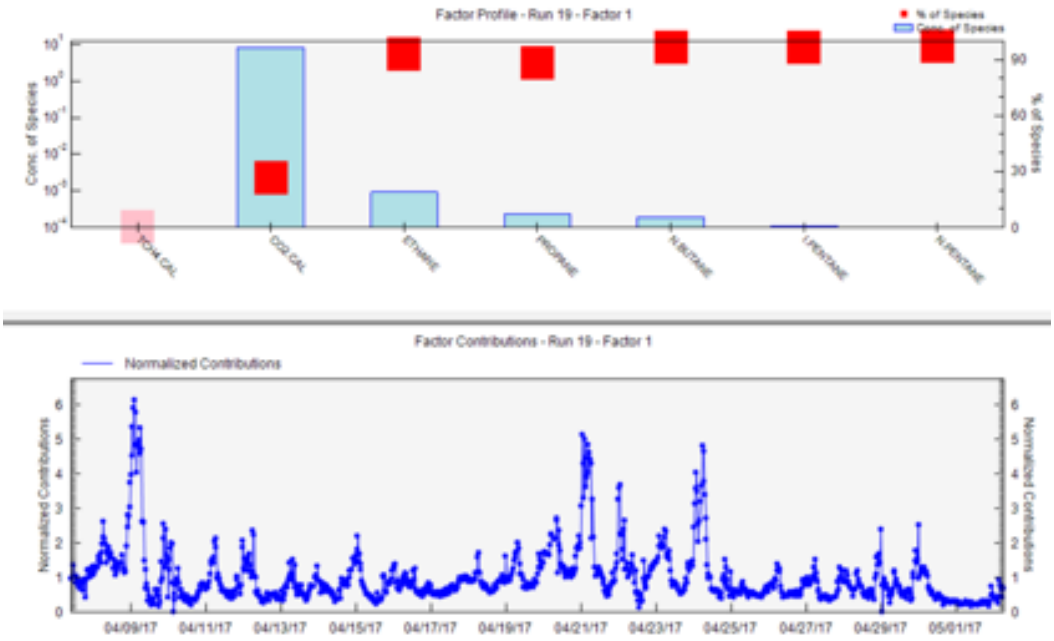

Figure S.4.1.4: Factor 1 profile [fossil fuel factor], (top) concentration and % of species contributing to the factor (bottom) temporal variation of normalised contributions of factor.

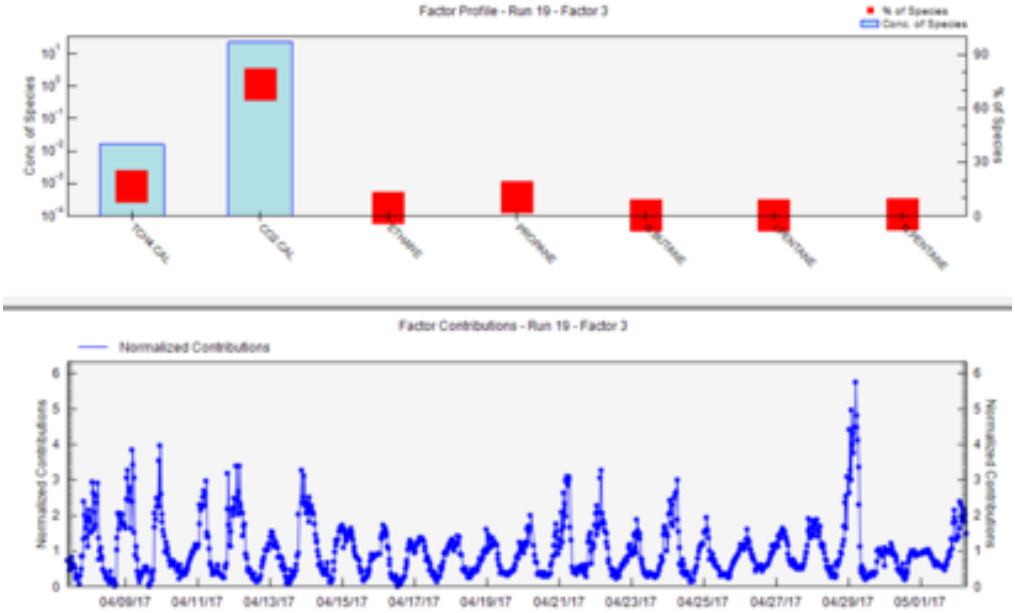

Figure S.4.1.5: Factor 3 profile,, (top) concentration and % of species contributing to the factor (bottom) temporal variation of normalised contributions of factor.